CEMENT-BASED SOLIDIFICATION OF FERRO-ALLOY SOLID WASTES

A thesis submitted to the

UNIVERSITY OF CAPE TOWN

in fulfillment of the requirements

for the degree of

DOCTOR OF PHILOSOPHY

by

BRETT COHEN BSc (Chem Eng) (UCT)

Department of Chemical Engineering

University of Cape Town

Rondebosch 7701

SOUTH AFRICA

October 1997

neutralisation of liquid effluent streams, were chosen for study. The solidified products were studied from both a physical and chemical standpoint.

A literature review presents a background to cement-based S/S, cement hydration behaviour and mechanisms by which metals could be contained in S/S products, based on proposals by other workers. Cr and Zn were of particular interest in this work due to high levels being found in the wastes and the different mechanisms by which they have been found to interact with cement.

Preliminary experiments identified conditions which were conducive to the effective setting of the monolith. Three operational variables were chosen as having significance in determining the quality of the resultant S/S product, namely water to solids ratio, cement content and curing time. Effective setting of the cement-waste product was found to require a preliminary wash of the untreated dust to remove much of this soluble chromium and other salts. It was identified furthermore that the solids required higher amounts of water for mixing than would be required for hardened cement pastes and concretes.

A number of fundamental tools was used to analyse the resultant product. These included Scanning Electron Microscopy (SEM) which was used to characterise the morphology of the S/S product, Energy Dispersive X-Ray Spectrometry (EDS) to characterise the chemical composition of the products formed during cement hydration, X-Ray mapping which identifies the spread of chemical components across a surface, X-Ray Diffraction (XRD) to characterise crystalline structures in the material and permeability and pore size characterisations.

The results of these characterisations found the S/S product to be highly porous and amorphous structures in which the solid wastes were bound together by the products of cement hydration. The chemical nature of these hydration products was found to be significantly different to those found in a hardened cement paste.

Based on the results of the fundamental characterisations and literature reports, a physico-chemical model was proposed for the S/S product. Particular attention was given to the fate of chromium - in both Cr (III) and Cr (VI) forms - and zinc for reasons mentioned above.

In the further development of this model, both the mechanical strength of- and chemical release from- the products were characterised. An understanding of the strength of the solid and the dissipation of energy during fracture provide a fundamental indication of the extent and nature of bonding within the product. Strength properties of agglomerated solids are of importance when determining their performance in load-bearing applications, including their behaviour in landfills - their ability to support additional product and over burden, the weight of earth moving equipment, and geological movement.

In the context of this work, the strength of the S/S products is explored via a number of strength characterisation tests. A macroscopic strength parameter is identified by Indirect Tensile Testing (ITT). The results of this test are compared to those obtained via Linear Elastic Fracture Mechanics (LEFM) techniques. The latter were techniques were used to obtain information about mechanisms of failure and infer how agglomerate structure was affected by composition of the S/S products and curing conditions. Comments were offered on the "process zone" concept ahead of the crack tip. Yield strengths which quantify the limit at which elastic (reversible) yielding gives way to plastic (permanent) deformation, were also measured and discussed.

LEFM techniques are favoured over macroscopic tests such as the ITT traditionally used in assessing S/S products in that they provide a more accurate measure of strength and supply information as to the mechanical processes which occur during fracture. A relationship between the macroscopic and LEFM strength measurements is identified. This relationship allows for the prediction of the more sensitive strength parameter from ITT results which are easier and quicker to determine.

The removal of metals or other species from S/S products is via liquid phase transport through- and out of- the solid is known as leaching. Steps in this removal process include mobilization of components not already in the liquid phase, movement via diffusion through the pore network of the solid (intra-particle diffusion), diffusion from the surface of the monolith into the bulk leaching solution and movement away from the solid in the bulk liquid solution.

Four distinct reasons for carrying out leach tests on the S/S products were highlighted in the scope of this work:

(i) To assess the effectiveness of the S/S products in metals retention.
(ii) To provide information as to containment mechanisms of metals in S/S matrices.
(iii) To predict the long-term leaching behaviour of, and the mechanisms controlling leaching from, S/S products. This is included under the general term 'leach modelling'.
(iv) To compare different combinations of operational variables and thus to find an optimal treatment strategy

These aims are not unrelated but the complexity of the S/S products makes it impossible to define a single laboratory-scale test procedure which can achieve all three simultaneously.

Due to the relationship between ultimate strength and the extent of cement hydration, and the effect of cement setting on retention, it was proposed that strength of the products should provide an indication of the effectiveness of containment of the metals within the composite.

In this work batch extractions were used to provide chemical characterisation of the S/S products using a variety of leaching media. Responses in various test conditions provide useful information as to the mechanisms of containment and release from such products.

The results of these tests indicated that only a small percentage of the total Cr contained in the S/S product is releasable, in either the soluble Cr(VI) or the Cr(III) form, the solubility of the latter being dependant on pH of the leaching medium. Zn release was also found to be a strong function of pH. The remaining Cr, along with approximately half of the Zn and two thirds of the K in the solid were retained as a stable species in the original dust particle.

Batch tests do not give any information as to which of the above physical processes control the rate of leaching from the S/S products. To determine the rate of leaching from the S/S products and identify which mechanisms are rate limiting in the leaching process, kinetic leaching tests were used. Release of constituents from the solids were measured as a function of time, and the

results fitted to a variety of mathematical models in an attempt to establish which of the mechanisms are rate limiting.

In the case of high pH leachants found in distilled water leaches, no Zn or Cr(III) was detected in the leachate. In an acidic environment both of these metals are mobilized. In acidic leachants, release of Zn and Cr could be described by diffusion. Leaching of Cr in distilled water showed that Cr leaching (all of which was found to be Cr(VI)) tends towards an equilibrium value, assumed to be that solubilized in the pores. Acetic acid was found to cause breakdown of the solid structure resulting in both a higher rate and extent of leaching than was observed for distilled water. Acid attack resulted in the formation of a distinct leach front where the acid has penetrated the solid. pH plays a significant role in the release of Zn and Cr(III) from the S/S products.

Column tests over 160 days showed that the S/S products had sufficient buffering capacity to raise the pH of a simulated acid rain solution to the natural pH of the S/S products. In such tests an initial high rate of release of Cr was observed. This decreased during the time of the test, and asymptotes to zero over a much longer time period. Similar trends were seen for K, Na and Ca.

In the final sections of the thesis, the S/S products were examined using a modified factorial design technique, the Central Composite Rotational Design. Operational variables chosen were water to solids ratio, cement content and curing time. The effect of these on leach resistance (for certain metal species) and mechanical strength of the resultant products was studied. It was shown that the CCRD provides a rigorous account of solidified product behaviour and does so with a reduced requirement for experimental testing. With the aid of this experimental design an inverse relationship between strength and leach resistance of the critical constituents was demonstrated. This was shown to be of value in practical implementation of the technology.

Using the results of the chemical and physical tests, a conclusive model for the cement-solidified ferro-alloy wastes was established, conclusions were drawn and recommendations for directions for further work were made.

Acknowledgements

To my supervisor, Dr. Jim Petrie, for making this thesis possible, and for advice and input throughout the course of this work.

To the Foundation for Research and Development (FRD) for funding during the course of this project.

To members of the Department of Chemical Engineering, with special mention of Mrs. Leslie Petrik, Mr. Martin Harris and Dr. Dee Bradshaw, for their assistance, input and for making this a fine place to work. To Mrs. Suzana Vasic for her many, many hard hours of analytical work.

To staff at the Electron Microscope Unit at UCT, and especially Dane Gerneke for his encouragement, support and endless patience during training on the electron microscope.

To Dr. Richard Paxton (Richard Paxton Associates), Prof. Mark Alexander and Dr. James MacKechnie (Department of Civil Engineering, UCT) and Prof. James Willis (Department of Geology, UCT) for their input.

For assistance with obtaining materials, to Doug Bolt and Sten Johannsen of CJV.

To members of "The Greenhouse" Environmental Process Engineering Group at UCT, both past and present, for both their friendship and advice.

To Nic, for love, listening and support, and to my friends, especially Paula, Tim and Jen for being there.

And finally to my family, who are the best people around.

Table of Contents

List of Figures

List of Tables

Nomenclature

A	Superficial cross sectional area of sample (m^2)
A_o	Initial contaminant concentration in specimen (mg)
a	Crack length (mm)
$\bar{a}$	Effective crack length ($a + \Delta a$) (mm)
Δa	Increment to notch length for agglomerates (mm)
B	Width of test specimen (m)
B_l	Permeability coefficient (cm/s)
c	Concentration (mg/l) or (mg/g)
C_o	Initial concentration (mg/l)
C_{im}	Concentration of contaminant in solid which is immobile (mg/g)
C_{mo}	Concentration of contaminant in solid which is mobile (mg/g)
D	Sample diameter (m)
d	Particle diameter (m)
D_e	effective diffusion coefficient (cm^2/s)
D_m	Molecular diffusivity (cm^2/s)
D_{obs}	Observed diffusivity (cm^2/s)
E	Young's modulus of Elasticity (N/m^2)
g	Acceleration due to gravity (9.81 m/s^2)
G_c	Energy absorbed per unit area of crack, toughness or critical strain energy release rate (J/m^2)
G_{ci}	Energy absorbed per unit area of crack to initiate fracture (J/m^2)
G_{cp}	Energy absorbed per unit area of crack in propagating the crack (J/m^2)
H	Tensile strength of a single bond
H	Brinell Hardness
k	Coefficient of permeability (m/s)
K_d	Linear adsorption/desorption coefficient
K_I	Stress intensity factor ($kN/m^{-3/2}$)
K_{IC}	Critical stress intensity factor ($kN/m^{-3/2}$)
L	Length of sample/ path length (m)
M_0	Mass of contaminant in sample at time t=0 (mg)
M_t	Cumulative mass of contaminant leached at time t (mg)
m	number of leaching periods
P	pressure at end of test (Pa)
P_m	Load per unit thickness (kN/m)
P_o	pressure at beginning of test (kPa)
ΔP	Pressure drop/gradient (Pa)
R	Universal gas constant (8,314 J/mol K)
r_p	Radius of the plastic zone (m)
R_s	Indenter radius for spherical penetration tests (cm)
S	surface area of a specimen (cm^2)
s	Distance between supports in a triple point bending test (cm)
S_l	Fractional saturation
t	Time for pressure to decrease from P_o to P (s)
T_n	Time to the middle of the leaching period (s)

t_n	Time to end of leaching period (s)
T_n	Principal tensile stress
Δt_n	Duration of the leaching period (s)
u	Apparent linear flow rate (Pa/s)
U	Energy required to initiate fracture
U^{el}	Stored elastic energy (J)
u	Linear flow rate through a solid (m/s)
V_a	Volume of air under pressure (m^3)
V	Volume of the specimen (cm^3)
W	Height of test specimen (m)
WD	Work done (J)
X	Path length (cm)
Y	Polynomial function introduced to account for surface geometries in the triple point bend test

β	Constant
γ	Penetration depth of spherical plunger (mm)
γ_s	Surface tension
ε	Strain
ε_f	Voidage fraction
θ_o	Absolute temperature (K)
θl	Semi-angle of liquid ring
σ	Stress (N/m^2)
σ_f	Failure stress (MN/m^2)
σ_t	Tensile strength (MN/m^2)
σ_{ys}	Yield strength (MN/m^2)
ϕ	Calibration factor
ω	Molecular mass of permeating air (kg/mol)
ν	Poisson's ratio

List of Acronyms

AA	Atomic Adsorption
ANSI	American National Standards Institute
CCRD	Central Composite Rotational Design
CSIR	Council for Scientific and Industrial Research
DCR	Dispersion by Chemical Reaction
DWAF	Department of Water Affairs and Forestry
EDS	Energy Dispersive X-Ray Spectroscopy
EE	Equilibrium Extraction
hcp	Hardened cement paste
ITS	Indirect Tensile Strength
ITT	Indirect Tensile Testing
LEFM	Linear Elastic Fracture Mechanics
MIP	Mercury Intrusion Porosimetry
NKLT	Non-Agitated Kinetic Leach Test
OPC	Ordinary Portland Cement
PPC	Pretoria Portland Cement
SCE	Sequential Chemical Extraction Test
SEM	Scanning Electron Microscope/Micrograph
S/S	Solidification/Stabilization
TCLP	Toxicity Characteristic Leaching Procedure
UCS	Unconfined Compressive Strength
UCT	University of Cape Town
ULP	Uniform Leach Procedure
UV	Ultra violet
US EPA	United States Environmental Protection Agency
XRD	X-Ray Diffraction
w/c	Water to Cement Ratio
w/s ratio	Water to Solids Ratio

Cement Chemistry Notation

A	Aluminium
C	Calcium
C_3A	Tricalcium aluminate
CH	Calcium hydroxide
C_2S	Dicalcium silicate
C_3S	Tricalcium silicate
C-S-H or CSH	Calcium silicate hydrate gel
F	Iron
H	Water
S	Silcia
$\overline{S}$	Sulphate

1.

Introduction

1.1 Hazardous Waste Production and Disposal in South Africa

The issues surrounding production and disposal of hazardous wastes are becoming significant both internationally and in South Africa. Public and legislative pressures are driving industry to look more critically at production and disposal options for its wastes, and more specifically hazardous wastes, than it has in the past. The definition of what constitutes a hazardous waste varies; generally the term 'hazardous' indicates "..chemical reactivity, or toxic, explosive, corrosive or other characteristics which cause, or are likely to cause, danger to health or to the environment, whether alone or in contact with other waste" [DWAF (1994)].

Where it is impractical to reduce waste production or reuse waste products from a process, attention must be given to treatment and disposal to ensure that long-term potential environmental impacts of the waste are limited. A number of different options are available for the treatment of wastes to achieve the aim of reducing their potential environmental impact. These include incineration (land-based or marine), disposal to sea and landfill. Physical, chemical or biological treatment may be carried out with subsequent landfill of the residual. [Sollars and Perry (1989)]. Although total destruction of the waste or conversion to a form which is non-toxic and immobile is the most desirable ultimate goal in terms of environmental impacts, in reality the choice of disposal or treatment option will be governed by available treatment technologies and facilities, economic factors and current legislation.

The Department of Water Affairs and Forestry (DWAF) (1994) lays out the objectives of treatment and disposal of hazardous wastes within the South African context. These are:

(i) to ensure that certain classes of waste are not disposed of without pretreatment
(ii) to ensure the safe disposal of hazardous wastes by ensuring that different classes of wastes are treated and disposed of appropriately
(iii) to avoid detrimental effects both in the short- and the long-term to humankind and the environment

DWAF (1994) provides a classification system for waste products and treatment and disposal requirements for different categories of waste. In DWAF (1994) it is seen that the ultimate fate of the majority of hazardous wastes in South Africa is consignment to landfill, with or without some degree of pretreatment.

The fate of waste consigned to landfill must be carefully considered. The potential exists for the infiltration of aqueous and non-aqueous fluids into the landfill, resulting in mobilization and transport of chemical constituents out of the landfill and into the surrounding environment. Subsurface transport can be responsible for the extensive movement of contaminants through the soil environment, resulting in far-reaching contamination effects [Hemond and Fechner (1994)].

Mobilization of contaminants may be extremely slow. Although in the past responsibility for long-term environmental impacts of such mobilization was not held by the disposing organization, legislation is moving towards ensuring that the person or people disposing of the waste retain responsibility for long-term environmental stability.

1.2 The Ferroalloy Industry and Hazardous Waste Production

Figure 1-1 shows the contributions of various industrial sectors to the total waste production in South Africa, while Figure 1-2 shows the contributions to hazardous waste production [Western Cape Environmental Monitoring Group (1993)]. It is identified that the Minerals Beneficiation industry is the largest contributor to both the total and hazardous waste production streams. The industry as a whole, and in particular the ferroalloy industry, due to extensive growth in the

industry and the associated increase in waste production, has come under pressure to look more critically at its production of- and disposal options for- its waste.

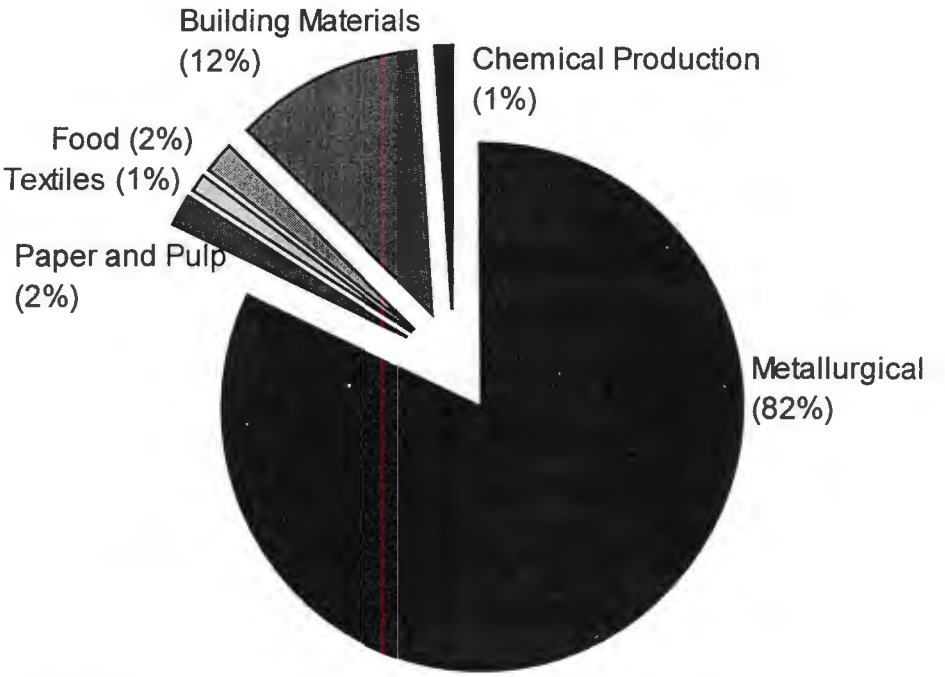

Figure 1-1 - Contributors to the Total Waste Stream in South Africa

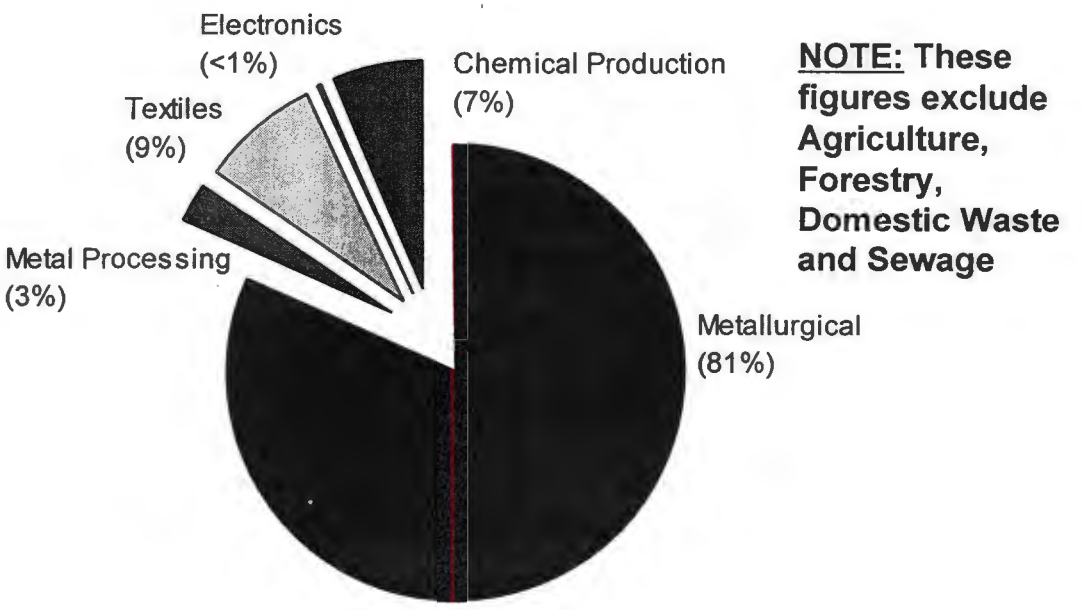

Figure 1-2 - Contributors to the Hazardous Waste Stream in South Africa

Based on the growth in production and the need for waste treatment solutions, the ferroalloy industry and in particular ferrochromium production is of particular interest in this study. In the pyrometallurgical treatment of ores, raw material handling, screening, melting of the ores, the direct reduction shaft furnace, desulphurisation of coal used for processing, the Electric Arc Furnace and the recycling of waste streams within the plant are some of the process steps which give rise to the production of wastes [CSIR (1994)].

According to the DWAF guidelines, a large proportion of the total waste produced in the ferroalloy industry falls into Class 6 or 'Toxic and Infectious Substances', primarily due to the high heavy metal content. Pyrometallurgical treatment is the treatment of choice for waste products from the ferro-alloy industry which contain more than 15% zinc. Whilst return of the wastes to the process with minor bleeds to avoid buildup of zinc is feasible, in the South African context facilities are not currently available for pyrometallurgical treatment of the ultimate wastes from the processes. Hydrometallurgical treatment, such as acid leaching, followed by consignment to landfill provides a potentially practical alternative [von Blottnitz (1994)].

The residuals of hydrometallurgical processing often still contain high levels of potentially mobile hazardous metals. They cannot, therefore, be consigned directly to landfill without ensuring the metals will be effectively retained. Some type of pre-landfill treatment must be undertaken. When investigating available pre-landfill waste treatment technologies for their effectiveness in metal retention, a number of requirements need to be met. Firstly, the treatment should be efficient in permanently reducing the potential hazard of the waste by either physical or chemical mechanisms or both. The processes must be simple to implement in practice and must be economically viable.

In US EPA (1980) four primary objectives of waste treatment prior to ultimate disposal are identified:

(i) improvement of the handling and physical characteristics of the waste,

(ii) a decrease in the surface area across which contaminant transport can occur,

(iii) limiting the solubility of the contaminants

(iv) detoxification of toxic constituents.

1.3 Solidification/Stabilization as a Waste Treatment Option

One group of technologies which satisfies the above requirements is known as Solidification/Stabilization (S/S). The terms Solidification and Stabilization (S/S) refer to technologies in which selected materials are added to a waste in order to render the waste less hazardous, or less capable of introducing itself into the environment [Conner (1986)]. The terms Solidification and Stabilization are often used together. It is necessary, however, to distinguish between the two processes by which treatment is achieved:

> *Solidification* is used to describe processes which improve the physical and handling characteristics of the waste by producing a granular or monolithic solid end product. Reduction of toxicity is achieved primarily by reducing the surface area over which transfer of contaminants to the environment can occur. Solidification may or may not involve chemical bonding between toxic constituents of the waste and the solidification agent.
>
> *Stabilization* describes processes which reduce the solubility or mobility of the toxic components of the waste or convert the waste to a more chemically stable form. Stabilization can be achieved in a number of ways. The mobility of the toxic components can be reduced by encapsulation into a solid structure. Chemical detoxification of the contaminants can be achieved by chemical reaction to less toxic forms or by biological processes. Adsorbents are sometimes added to reduce mobility. Lime can be added to a heavy metal sludge to precipitate out the metals as hydroxides. Stabilization does not necessarily imply a solid end product [Cullinane et al (1986)].

A number of treatment processes fall under the general definition of S/S. Table 1-1 provides a comparison of some such treatment technologies.

Table 1-1 - A Comparison of Commonly Used S/S Processes (based on Arniella and Blythe (1990), Boelsing (1988), Wiles (1988), Cullinane et al (1986). Malone and Larson (1983))

Process	Principles behind operation	Advantages	Disadvantages
Cement-based	Cement is mixed into the waste. This sets and subsequent waste containment is as a result of both physical and chemical incorporation into the product and chemical alteration of the waste constituents.	Wide availability of raw materials Low cost of materials and equipment Strong physical barrier under adverse conditions Low variability in compositions of raw materials Well-known setting reactions Some knowledge exists on immobilisation of metals	Sensitivity of products to impurities at high levels High porosity of S/S treated waste Cement addition results in bulk increases of waste volume Although process appears simple, implementation must be closely monitored to ensure success
Pozzolans	Materials with self-setting properties are added to the waste which set in a similar fashion to cement. Pozzolans are often waste products themselves.	Cheap, uses other waste products (e.g. flyash) as the treatment agents	Not as durable as Portland cement Interferences of wastes with setting reactions as for cement
Vitrification	Wastes are mixed with molten borosilicate glass in a furnace. When the mixture cools the waste is trapped within the glass	Effective for a wide variety of wastes, including radioactive wastes	High temperatures required may lead to volatilization of organics and emission of toxic fumes. High equipment and processing costs
Thermoplastic micro-encapsulation	Wastes are blended with melted asphalt, bitumen, sulphur, polyethylene or wax. As binder cools waste is "buried" in the matrix of binder material.	Good for toxic, soluble and radioactive wastes not readily treated by other processes. Leachability is one hundredth to one thousands of similar cemented wastes.	High temperatures, specialised equipment and pretreatments required lead to extremely high processing costs.

Table 1-1 - (continued)

Macro-encapsulation	Wastes are incorporated into a binder, drum or insoluble jacket	Wastes are completely isolated from entering the environment	High material, energy and labour requirements Durabilities of jackets must be completely known
Dispersion by Chemical Reaction (DCR)	Calcium oxide is added to a waste product onto which organics absorb. This reacts with water to form $Ca(OH)_2$ which then reacts further with CO_2 from the atmosphere to form limestone, a relatively natural, hard, impervious and insoluble product	Effective for the treatment of organics The limestone product is a natural component of the environment	No control over the reactions can be maintained, and subsequent evaluation of the product is difficult.
Pretreatment additives	These are sometimes added to the wastes prior to treatment to enhance the effectiveness of the treatment process. Examples include lime, ferrous sulphate, activated carbon, silicates and zeolites. Often used in conjunction with other treatment agents	Decrease mobility of soluble constituents Reduce effects of certain setting inhibitors	May be effective for one waste constituent but have the opposite effect for a different constituent Result in bulk increases of the wastes
Proprietary Processes such as Hazcon, Seal-O-Safe, Soliditech	A proprietary treatment agent is mixed into waste, often in situ, and allowed to set	Waste contractors implementing processes usually experienced in implementation of processes	Often implemented with little consideration given to waste type, thus potential exists for waste-binder incompatabilities and potential failure

S/S processes were implemented initially with little regard being given to the mechanisms associated with containment of the waste in the end product. To assess compatibility of waste-treatment agent combinations, and to predict the long term mobilization of contaminants from the S/S product, it is essential that interactions which may occur between waste and treatment agents are identified and understood.

1.4 The Potential for Failure of S/S Products

'Failure' of an S/S product denotes both physical breakdown of the solid product and the release of toxic constituents into the surroundings. Long-term physical breakdown of the monolithic end product can occur as a result of the static head of other material above the solid, movement of machinery over the site and ground movement. In a landfill the potential exists for the permeation of water through the solid, with subsequent mobilisation and leaching of components integral to the solidified product. The extent of physical breakdown will therefore be dependent on both the physical integrity of the structure and indirectly on the permeability of the product. The release of toxic components of the waste will occur when waste constituents are mobilised by liquid passing through the solid, carrying these constituents into the groundwater systems. Leaching will thus be dependent on the extent to which water can pass through the solid mass (i.e. the permeability), the solubility of the constituents or leachability in the permeating liquid, and the potential for chemical conversion of insoluble constituents into soluble products in the liquid.

Prior to implementation of the technology, therefore, evaluation of the resultant products is necessary to ensure effective containment of the waste constituents therein.

1.5 Evaluation of the S/S Process Prior to Implementation and the Need for an Improved Understanding of the Nature of the Product

To satisfy the demands for quick and easy assessment of S/S products prior to large-scale implementation of the technology, laboratory tests have been used widely to provide information on the appropriateness of waste/binder combinations. Such laboratory-scale evaluations have

consisted traditionally of three categories of tests, namely (i) *Batch leach tests* which provide a once-off measure of the waste components which are leachable under specific laboratory conditions, (ii) *Permeability tests* which indicate the potential for permeation of water through the solid with subsequent removal of hazardous constituents and (iii) *Structural strength tests* which provide a measure of the physical strength of the S/S product and are often used to serve as an indication of bearing capacity of a waste in a landfill site [Culllinane et al (1986)].

The problem with such 'appropriateness tests' is that they give no indication of the mechanisms by which waste constituents are contained in the S/S end product, and cannot be used to predict either the nature of interactions occurring in the S/S matrix, or the long-term stability of a S/S product.

The mechanisms of waste immobilisation, the interferences of the wastes on binder setting, and the mechanisms of physical and chemical breakdown of the S/S products are often not properly understood prior to implementation of the technology. The lack of such information can lead to the technology being implemented with no assurance of the long-term stability of the S/S product. Although pilot-scale studies are often used to try and predict long-term stabilities, these are both expensive and time-consuming, and have little extrapolative value. A complete understanding of the fundamental physical and chemical structure of the S/S waste product is thus essential in predicting its long-term stability. An understanding of waste/ binder interactions on both a physical and chemical level is necessary to provide a fundamental model of the product.

1.6 S/S in the Context of this Project

This thesis provides a report of research work which was performed to provide an understanding of the interactions and breakdown mechanisms associated with cement-based S/S treatment of solid inorganic waste products. The specific focus is on waste products from the ferro-alloy industry whose importance has been discussed previously. Research in the field of S/S from the early 1980's has been directed at gaining an understanding of the containment of liquid wastes and slurries by cement-based S/S. The work which has been published to date is limited in scope and often vague and inconsistent. [Cocke and Mollah (1993),

Shively et al (1985), Poon et al (1985a,1985b)]. Very little research work has been directed at understanding the cement-based S/S of solid wastes.

1.7 Motivation and Aims of the Project

The motivation for the research work presented in this thesis is to expand the currently existing knowledge base of both the physical and chemical microstructure of the products formed when solid wastes have been solidified with cement, and to identify, characterise and, where possible, quantify, the nature of the physical and chemical structure and, subsequently, the mechanisms and kinetics associated with the long term physical and chemical breakdown of the solidified products.

In this thesis a physico-chemical model of the solidified ferro-alloy waste product is proposed. Based on this model, it is hypothesised that a correlation exists between the physical structure and the chemical behaviour of the product. The work reported in this thesis aims to confirm the accuracy of the physico-chemical model in describing the S/S products and thereafter to explore the proposed hypothesis.

A number of specific aims are identified within this context:

(a) To provide a review of the wide range of literature relevant to the sciences of both cement-based S/S and the fracture mechanics of materials. In this way the thesis is contextualized in terms of work being conducted elsewhere.

(b) To evaluate the mechanisms involved in the fracture of the S/S products using both traditional strength measurement techniques and via Linear Elastic Fracture Mechanics (LEFM) tools. These characterisations contribute to an understanding of the physical structure of the product, and mechanisms involved in the physical breakdown thereof at a microscopic level.

(c) To attempt to identify where various metal species are located within the S/S product. This contributes to understanding the chemical structure of the product.

(d) To identify the variables in the preparation of the S/S mixture which affect the strength and containment properties of the end product, and to quantify the effects of changing these variables on strength and containment. An understanding of the effect of these variables contributes to knowledge on containment and breakdown mechanisms in the S/S products.

(e) To assess critically the validity of the commonly used S/S characterisation procedures, and discuss their applicability in the context of this work

(f) To characterise the mechanisms and kinetics associated with leaching from the S/S products, and to use this data to understand both containment mechanisms of the wastes within the S/S products and the long-term breakdown thereof. Correlation of leaching data with the results of strength testing (point (b)) will indicate the validity of the hypothesis mentioned previously.

Once a complete understanding of the physical and chemical structure of the S/S product is obtained, consideration is given to further implementation of the technology. Areas which are considered in this context include:

(a) identification of factors which could result in the long-term failure of the S/S product, and whether or not these are of significance in making decisions regarding the use of the technology.

(b) investigation of the use of a factorial design tool in the optimization of operational variables involved in S/S processes. The aim of this work is to be able to reduce the number of tests required to evaluate the S/S products prior to implementation of the technology.

(c) to use the information gained during the course of this work, along with a physical model of industrial landfills, to provide information on the engineering of field-scale S/S operations.

After reading this thesis the reader should have both an indepth understanding of the physical and chemical nature of waste products from the ferro-alloy industry which have been solidified using cement, and some knowledge of practical aspects of large-scale implementation of the technology.

1.8 Layout of the Thesis

The thesis is divided into the following chapters:

(i) A review of literature surrounding cement chemistry and the interactions between various waste constituents and cement follows in Chapter 2. The chemistry of chromium and zinc is highlighted to be of particular interest in this study.

(ii) In Chapter 3 the wastes used in the study are characterised and a description of the sample preparation procedure is presented.

(iii) A physical and chemical characterisation of the wastes using fundamental characterisation tools such as Scanning Electron Microscopy/Energy Dispersive X-Ray Spectroscopy (SEM/EDS), X-Ray Diffraction (XRD), Mercury Intrusion Porosimetry (MIP) and Permeability testing is presented in Chapter 4. Based on the results of these tests and the literature review of Chapter 2, the physico-chemical model of the S/S products is presented.

(iv) The physical model is explored further in a discussion of the strength properties and fracture mechanisms of the S/S products in Chapter 5. Information is drawn from both literature and the results of Chapter 4 to provide support for results and aid in interpretation thereof.

(v) An investigation into the leaching behaviour of the S/S products in a variety of leaching tests is presented in Chapters 6 and 7. In Chapter 6 once-off extraction tests are used to further the understanding of chemical containment mechanisms within the S/S products, while results of kinetic tests presented in Chapter 7 indicate the time dependency and mechanisms of the leaching processes. Through the results of these two chapters the chemical model of the product is further developed.

(vi) In Chapter 8 the use of factorial design in S/S technology is investigated. The aim of the factorial design is both to minimize the number of laboratory tests required for the characterisations presented in previous chapters and to provide an effective tool to optimize operational parameters which affect the performance of the S/S process. Considerations surrounding the large-scale implementation of the S/S processes are also presented in Chapter 8.

(vii) Finally, in Chapter 9 the results are summarized, the accuracy of the proposed model in describing the S/S product is discussed and directions for future work are suggested.

2.

Review Of Background Literature

2.1 Introduction

In Chapter 1 the potential for using cement-based Solidification/ Stabilization (S/S) technology in the treatment of metal-containing wastes from the ferrochrome industry was identified. This current Chapter provides a summary of available literature surrounding Solidification/ Stabilization (S/S) technologies. It aims to provide the reader with a background to cement-based S/S, which may be used in the understanding and interpretation of the results presented in this thesis. Cement hydration chemistry is discussed to provide an understanding of the physical and chemical behaviour of cement within cement-based S/S products. Physical and chemical factors which affect hydration are discussed. A summary of work reported in literature on the retention of metals and other waste constituents in cementitious products is presented. The chemistry of chromium and zinc, the two primary metals of interest in this study, and their likely significance in terms of S/S treatment, are examined in detail. An attempt is made throughout this chapter to highlight inconsistencies and shortcomings in work reported in the literature and in this way identify specific points which need to be addressed in this thesis.

2.2 Cement

The term cement may be applied broadly to any material which binds together parts to form a whole. In this work the word 'cement' will be used to refer to normal or Ordinary Portland Cement (OPC) - that which is most commonly used in the construction industry. The composition of OPC is discussed in section 2.2.2 below.

2.2.1 Definitions

The following definitions are presented:

Hardened Cement Paste (hcp) is a mixture of cement and water which has set to form a solid

Aggregate is any inert material added to cement with the purpose of providing an increase in strength and volume

Mortar is a mixture of cement, water and fine (9.5 mm to 150μm) aggregate

Concrete is a mixture of cement, water, fine aggregate and coarse (large-sized) aggregates [Popovics (1982)].

2.2.2 Types of Portland Cement

Portland cement is manufactured by firing a charge of limestone and clay or other silicate materials at high temperatures. The result is a clinker which is ground to a fine powder [US EPA (1980)]. Five types of cement are manufactured:

Type I : Ordinary Portland cement which is used widely in the construction industry;

Type II: A low alumina content for use in the presence of moderate concentrations of sulphates;

Type III: Develops a high early strength for use where rapid set is required;

Type IV: Has a low heat of hydration and is used for large mass concrete work;

Type V: Is a high alumina cement which is used in the presence of high sulphate concentrations (greater than 1500 mg/kg).

Table 2-1 lists the primary components of Ordinary Portland Cement (OPC), along with the cement chemistry notations for these components. Also seen in Table 2-1 are typical compositions of South African OPC [PCI (1986)].

Table 2-1 - Composition of OPC (all values in % by mass)

Component	Cement Chemistry Notation	PPC Riebeek West	Typical Composition
Dicalcium silicate	C_2S	15.0	20-40
Tricalcium silicate	C_3S	64.4	35-55
Tricalcium aluminates	C_3A	4.1	5-12
Alumino-ferric phase	C_4AF	10.7	5-10
Gypsum		4.0	4-7

Ordinary Portland Cement (type I or OPC) manufactured by PPC's Riebeek West plant, South Africa, was used in this study. In Table 2-1 a composition analysis of the cement produced by this plant on 5 April 1994 is presented [van Niekerk (1994)]. The composition of cement will vary widely depending on the source of the raw material. Particle sizes of clinkers usually lie in the range of 5-25μm [Glasser (1993)]. Gypsum is added to cement in order to prevent flash setting caused by tricalcium aluminate.

In cement chemistry the following notation is commonly used:

Chemical Formula	Cement chemistry Notation	Chemical Formula	Cement chemistry Notation
CaO	C	MgO	M
SiO_2	S	Na_2O	N
Al_2O_3	A	K_2O	K
Fe_2O_3	F	H_2O	H
SO_4^{2-}	$\overline{S}$		

This cement chemistry notation is used in the course of this work.

2.2.3 Chemistry of Cement Hydration

The development of cement strength upon contact with water is associated with the precipitation of a number of hydration products of low solubility in the pores between the cement particles. These form a cohesive matrix which binds the residual cement and any other material present into a solid. The steps associated with the setting of the cement are discussed in section 2.2.4.

The reactions which occur when cement comes into contact with water have been extensively studied [Sujata and Jennings (1992), Double (1983), Grudemo (1979), Double and Hellawell (1977)]. Variability in cement composition, composition of mixing waters and setting conditions make it difficult to predict, quantitatively, the relative proportions of the various cement hydration products present in the product. Furthermore, factors including the presence

of aggregates and various chemical species in the setting environment will affect hydration. Only a qualitative understanding of the types of cement hydration products is therefore possible. The discussion which follows is based primarily on Double (1983).

Figure 2-1 presents the main reactions which occur when cement and water come into contact. The reactions shown do not occur independently, and appreciable fine-scale mixing of the hydrate occurs, particularly in the colloidal gel product.

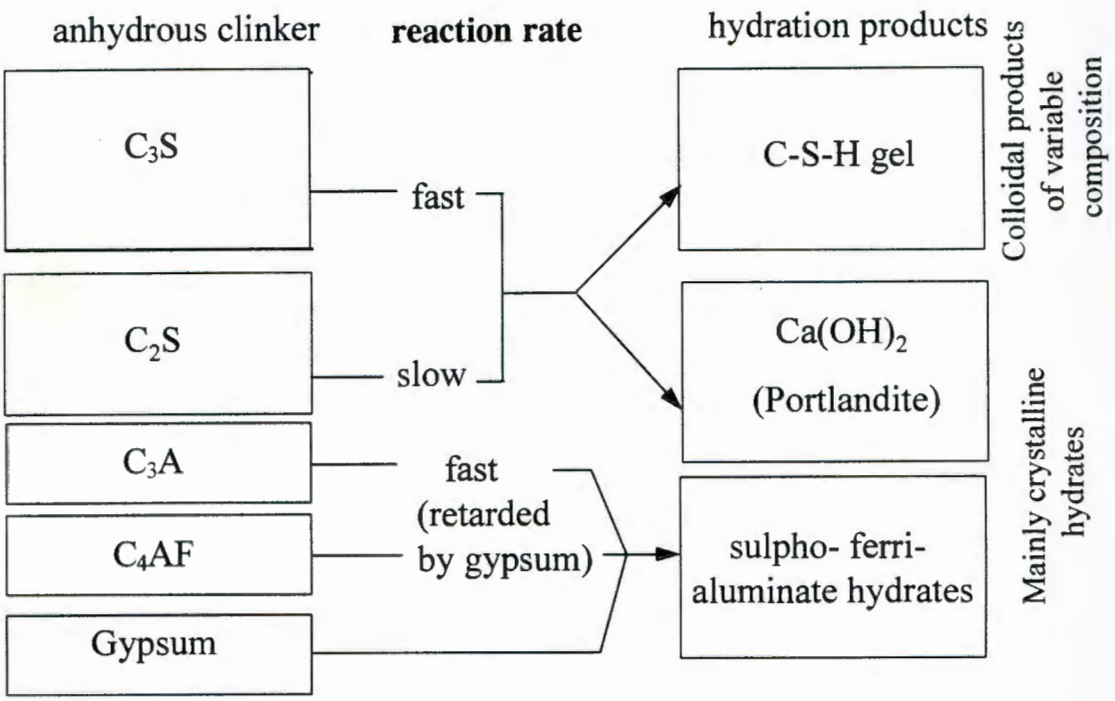

Figure 2-1 - Schematic representation of cement setting reactions (based on Double (1983))

Tricalcium silicate and dicalcium silicate are the dominant components in cement, the primary hydration product being a calcium silicate hydrate (C-S-H or CSH) gel. These hydration products provide the main source of strength in cement and concretes. The gel consists of calcium oxides and silicone oxides and may also include aluminium, iron, sulphur and alkalis as impurities. In normal cements the Ca:Si ratio in the gel is ~ 1.7 (determined by SEM/EDS analysis). Structurally, CSH gel is an agglomeration of colloidal, (mostly amorphous) particles of indefinite shape and variable composition of less than 50 nm in size. Both the composition and morphology of the gel will vary depending on the composition of the cement, the water to cement ratio in the original sample and the time of curing [Double (1983)].

Other components of cement (mainly aluminate phases) affect the setting kinetics but contribute very little to overall strength. Products of hydration of the tricalcium aluminates which have been detected by X-Ray Diffraction (XRD) are ettringite ($C_3A.3C\overline{S}.32H$) and calcium mono-sulphoaluminate ($C_3A.C\overline{S}.12H$). Little is known about the hydration of C_4AF, although it is proposed that solid solutions analogous to those from C_3A are formed, with iron substituting for some of the alumina.

Calcium hydroxide is a by-product of the hydration (see Figure 2-1). Initially it is solubilized in the pore solutions, resulting in a highly alkaline pore environment. The Ca:Si ratio in the pore solution is typically to the order of $(10^2\text{-}10^3)$:1 [Double (1983)]. As hydration proceeds, growth of $Ca(OH)_2$ or crystalline Portlandite platelets occurs via nucleation centres in the pore spaces. This process is discussed in section 2.2.4. Calcium hydroxide may react with free Al_2O_3 or SiO_2 from other materials such as fly ash to form further cement-like products (see section 2.2.7).

During hydration there is an increase in the volume of total solids. The crystalline hydrates grow into the water filled spaces in the cement microstructure. C-S-H gel forms about 60% of the hydration products. Calcium hydroxide contributes a further 20% by volume. The remaining volume of set cement consists of calcium sulphoaluminate and aluminoferrite hydrate phases.

2.2.4 Mechanism of Cement Hydration

A number of analytical techniques have been used to establish the sequence of steps occurring during cement hydration. The discussion presented here is based on Double (1983), Grudemo (1979) and Double and Helawell (1977).

Calorimetric techniques have shown a release of heat of over 30W/kg lasting for the first 10 minutes after initial contact of cement with water [Double (1983)]. This is associated with the hydration of free lime and the dissolution of other impurities from the cement.

Hydration of the cement itself has been shown to be a two stage process. A sharp drop in the released heat follows this initial heat evolution, in a period known as the dormant or induction

In cement-based Solidification/Stabilization, cement is mixed with a waste product. The effect of the waste product on the resultant mixture depends on the form of a waste. In the case of a liquid waste, chemical effects may come into play. The presence of a solid waste will result in chemical and/or physical effects on hydration and the resultant product. In sections 2.2.6, 2.2.7 and 2.4 which follow, a discussion is presented of physical and chemical factors which affect the properties of cement and cementitious products.

2.2.6 Process Variables and Aggregate Properties affecting Product Quality

A number of process variables affect the properties of hardened cement and cementitious products such as the S/S products of interest in this work. Properties of cements and concretes which are significant include strength and resistance to acid attack and weathering. For S/S products, the retention of the wastes within the cementitious product is of interest. Variables which may be controlled during mixing of cement and cementitious products, and their effect on product properties, are discussed in the following sections.

(i) Water Addition and Humidity

The significance of the amount of mixing water on cement hydration is as follows. Sufficient water should be present for stoichiometric reaction with cement clinker in accordance with the equations of Figure 2-1. In practice this is not usually a limiting factor, since more water is required for the formation of a workable paste than is stoichiometrically required for reaction [PCI(1986)].

When a solid is mixed with water, the spaces between the particles in the solid will be a function of, among other factors, the amount of water in the mixture. In a freshly mixed cement paste, the amount of mixing water will thus determine the volume of the pore space not filled by solid. Cement hydration was seen in section 2.2.3 to result in an increase in the total volume of solid material. If too little water is present in the fresh mixture there will be insufficient space for the hydration products to grow during hydration, causing premature retardation of hydration as a result of spatial limitations. This will not necessarily imply a weaker product: the closeness of the cement grains may result in stronger bonds between the particles. An excess of water

results in pores which will not ultimately be filled with hydration product and consequently a weaker and more permeable end product will be formed. At very high water contents segregation of mix constituents may occur before set can be achieved.

The 'optimal' water to cement (w/c) ratio for hardened cement pastes, calculated as giving sufficient water and pore space for hydration, without leaving unfilled pores, has been found experimentally to be of the order of 0.38 [PCI (1986)]. When aggregates are added more water may be required to obtain workable mixtures. This is discussed further in (iii) below.

In the treatment of liquid wastes and slurries it is desirable to achieve the highest possible waste loading for economic reasons. This will imply high w/c ratios, resulting in products of inferior strengths, reduced tolerance to changing ambient conditions and high permeabilities in accordance with the discussion in the previous paragraph. A compromise therefore has to be made between the economic benefits of a high w/c ratio and resultant inferior product quality.

In addition to controlling the water in the fresh paste, it is important to ensure that evaporation of water from the fresh paste does not occur during initial curing, leaving insufficient water for cement hydration. Dehydration in the time between mixing and placement in the site sometimes makes placement and compaction difficult to achieve [PCI(1986)]. Cement and concrete are often covered by plastic sheets during initial curing to retard the evaporation process. In laboratory-scale testing, products are often cured in humidified chambers.

(ii) Quality of the Mixing Water

As has been noted already, a number of salts, metals and anions can significantly alter the rate and chemistry of the hydration reactions. This effect is explored in section 2.3.

(iii) Shape, Surface Texture and Size of Aggregates

These three properties of solids present in a cementitious mixture affect both the water required to achieve workable pastes as discussed in (i) above and ultimate strength of the cementitious product.

Spherical, cubical or chunky shapes produce concrete with lower water demands than elongated or flaky particles. The effect of surface texture on water demand is not as significant as that of shape, but rough textures increase the water demand due to greater surface area [PCI (1986)].

In determining the effect of surface texture and shape on the strength of the hardened cement-aggregate mixture, the 'bond characteristics' of the cement-aggregate combination are of significance. The term 'bond characteristics' of an aggregate encompasses "..surface texture, the extent to which the cement can penetrate into pores or surface depressions, the angularity of the planes of fracture, the friability of the surface and the presence or absence of loosely bonded or friable coatings" [PCI (1986)].

The effect of particle size is as follows: Aggregate particles passing through a 200 mesh (75 μm) may coat larger particles and weaken the bonds between the particles and the cement [US EPA (1980)]. Furthermore, the viscosity of a suspension changes with particle size. The presence of finer particles will result in the formation of a more viscous mixture and hence cements with finer aggregates will require increased water additions to allow for the formation of workable pastes [Wiles (1988), PCI (1986)]. In section (i) above it was identified that excessive water contents may lead to the formation of products with lower strengths. Malone et al (1983) recommend that, when mixing concrete, not more than 3% of the total aggregate should be less than 75 μm.

In the following chapters of this thesis it is seen that the waste products of interest in this work are fine solids (<1 μm). From the discussion presented above, this high content of fines is suggested to be significant in determining the water requirements in mixing of the cementitious products and the strength of the resultant cementitious product. This is explored throughout the course of this present work.

(iv) Temperature

Retarded setting of cement occurs below 0°C while setting is accelerated at temperatures above 30°C [Wiles (1988)]. PCI (1986) suggest that higher temperatures inhibit hardening at later ages. In PCI (1986) it is shown that a 10°C change in curing temperature causes a 1% change in

the ultimate compressive strength of concrete. Based on this observation it is suggested that minor fluctuations in normal ambient temperature which will be expected in the laboratory environment in the scope of this current work will have an insignificant effect on the ultimate strength of the cementitious products being studied.

(v) Other Factors

Extensive mixing after the gel formation stage may destroy the resulting gels and result in a weaker end product [Wiles (1988)]. Furthermore, inefficient mixing of a S/S mix may result in "pockets" of waste which are not actively going to benefit from treatment by the cement.

During mixing, air bubbles can become entrapped in the mixture. If this air is not removed from the mixture it will be entrapped in the hardened cementitious product forming cavities or flaws in the product. The presence of flaws can result in a significant reduction in the strength of a material in a load-bearing application. The effect of flaws on the strength properties of solids is discussed in detail in Chapter 5. Air removal may be achieved by mechanical processes such as compaction [PCI (1986)].

2.2.7 Additives to Cement

A number of additives are used in both the cement industry and in S/S processes to improve product performance. 'Improved performance' implies a product with higher strength, accelerated or retarded setting, improved chemical resistance, lower permeabilities or better waste retention capabilities.

Pozzolans such as fly ash, silica fume, blast furnace slag, and calcinated shales and clays are waste products with large amounts of fine-grained, noncrystalline reactive silica and alumina. These elements react with the calcium hydroxide produced by the cement hydration reactions to form further calcium silicate hydrates which add to the strength of the end product. Further growth of hydrate products results in a reduction in the continuity of the pores within the cement matrix which may reduce permeability and improve the strength of the product. Pozzolans also act effectively as sorbents for wastes and have been shown to reduce the

leaching of metals [Cullinane et al (1986)]. Furthermore, some pozzolans are waste products within themselves, and their use in both cement and S/S applications is advantageous in that a waste product is substituted for a portion of the more expensive cement.

Some of the possible reactions which involve the free silica and alumina from pozzolans are as follows [US EPA (1987)]:

$$Ca(OH)_2 + Si \xrightarrow{H_2O} Ca_xSi_y(H_2O)_z \quad \text{(C-S-H of varying stoichiometry)}$$

$$Ca(OH)_2 + Al \xrightarrow{H_2O} Ca_xAl_y(H_2O)_z \quad \text{(hexagonal and cubic aluminate hydrates)}$$

$$Ca(OH)_2 + Al + Si \xrightarrow{H_2O} Ca_xAl_ySi_z(H_2O)_w \quad \text{(hydrogarnets)}$$

Should sulphate be present in the mixture, the formation of ettringite (hydrated calcium aluminosulphate) and derivatives may also occur as follows:

$$Ca(OH)_2 + SO_4 + Al \xrightarrow{H_2O} Ca_xAl_y(CaSO_4)_z(H_2O)_w$$

The pozzolanic reactions are slow and will carry on as long as calcium hydroxide is released by the reacting cement, and as long as free silica and alumina are available for reaction.

Sulfides, carbonates, silicates and phosphates are sometimes added in S/S treatments to react with metals to form complexes of reduced solubility. Metals that exist in more than one valence state can be converted from a highly soluble to a less soluble valence state. Where respeciation is not effective, various co-precipitation and redox reactions are sometimes employed. The problem with using redox agents for solubility reduction is two-fold. This process becomes expensive if other reducible species are present in the waste which will increase the amount of reducing agent required to reduce the toxic species.

Soluble silicates improve setting and reduce the interference of metals by binding the contaminants. Three phases of reaction have been identified when soluble silicates are added to cement in the presence of metal ions. The initial rapid reaction is between the soluble silicates

and the polyvalent metal ions to give insoluble metal silicates. This is followed by a slower reaction between the silicate and the cement to form a gel. Finally the cement hydration proceeds as before. It is thought that Ca^{2+} reacts with SiO_3^{2-} to give a CS gel which accelerates the cement setting and increases the water demand of the hydration reactions. This is beneficial in that less water remains in the pores after hydration. In support of this suggestion, it has been observed experimentally that there is less CH after hydration when silicate has been added over the cases where there is no silicate present [Poon et al (1985b)].

Clays are often used to absorb liquid and bind with specific cations and anions. Emulsifiers and surfactants allow for incorporation of immiscible organic liquids into the matrix and lime is used to raise the pH and reaction temperature which improves setting [Cullinane et al (1986)].

A number of proprietary additives are currently available which are claimed to improve setting, reduce the effect of the wastes on the setting reactions and physically or chemically alter wastes in some way. Such additives are not explored further here.

2.3 The Chemistry of Chromium and Zinc

Prior to understanding the processes associated with the containment of metals in the S/S product, an understanding of the chemistry of the individual metals is essential. A summary is presented here for the two primary metals of interest in this study, namely chromium and zinc. This section is followed by a discussion in section 2.4 of literature observations on the effect of metals, anions and organic species on cement hydration.

2.3.1 Chromium

Chromium can exist in a number of oxidation states, ranging from -2 to +6, with the +2, +3 and +6 states being the most important and are those expected to be found in wastes investigated as part of this present study. The radii of Cr(III) and Cr(VI) are 0.052 nm and 0.064 nm respectively.

(i) Cr(III)

Chromium in the +3 oxidation state will exist as the Cr(III) ion in solutions of pH lower than 3. In solutions of pH > 3, $Cr(OH)_3$ is formed, which is almost insoluble in the pH range of 5 to 9 - about 10^{-7} M between pH 6 and pH 11.5. The solubility equilibrium is reached slowly - 6 days in the low pH ranges and even longer at pH values of above 12. At pH values of between 9 and 11 the solubility of Cr(III) increases and the Cr(III) exists as $Cr(OH)_4^-$. As $Cr(OH)_3$ solid ages agglomeration occurs to form a more crystalline structure. The older the solid, the lower the solubility in acid. Solubility of Cr(III) as a function of pH is presented in Figure 2-2 [Rai et al (1987)].

Cr(III) has been shown to precipitate with a number of metal cations in solution. If Fe(III) is present, Cr(III) and Fe(III) may co-precipitate into a matrix of $[Fe,Cr](OH)_3$. This matrix is stable and the reaction forms the basis for an effective method for scavenging Cr(III) from solution. Cr(III) is also known to adsorb strongly to mineral iron and manganese. Adsorption is stable and desorption is slow. Adsorption increases with increasing pH. Competing ions in a solution will decrease adsorption due to increased charge densities.

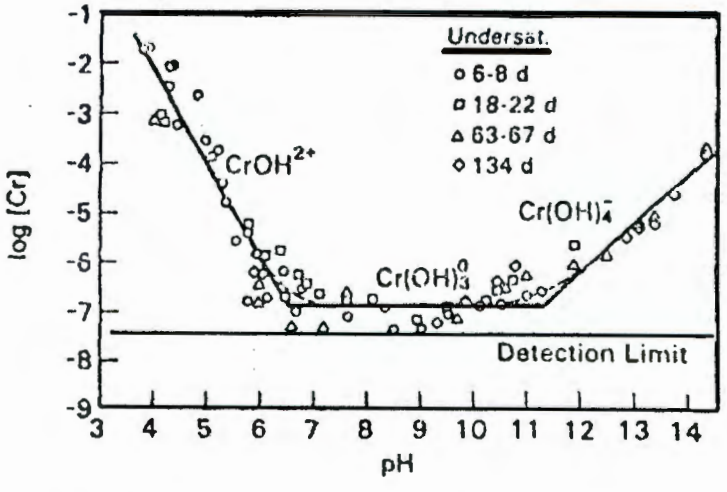

Figure 2-2 - Cr(III) Solubility as a function of pH [Rai et al (1987)]

Cr(III) has been shown to form thousands of aqueous organic and inorganic complexes, a full discussion of which is not relevant here.

(ii) Cr(VI)

Cr(VI) exists in solution as chromic acid (H_2CrO_4). The solid form of Cr(VI) is the anhydride CrO_3, which has a solubility of 6.25 mol/l. The dissolution and hydrolysis reactions are proposed to be:

$$CrO_3 + H_2O \rightarrow H_2CrO_4 \quad (pH < 0.6)$$
$$H_2CrO_4 \rightarrow HCrO_4^- + H^+ \quad (pH > 0.75)$$
$$HCrO_4^- \rightarrow CrO_4^{2-} + H^+ \quad (pH > 6.45).$$

In acidic solutions and at total Cr(VI) concentrations of above 0.01 M, $HCrO_4^-$ dimerizes to di-chromate as follows:

$$2HCrO_4^- \rightarrow Cr_2O_7^{2-} + H_2O.$$

Ligand-free Cr(VI) is not known, and few other complexes other than those described above have been identified.

Metal chromates fall into three categories with regard to the solubility. High solubility chromates (> 1 M) include sodium and potassium chromates and sodium and calcium dichromates. Intermediate soluble complexes (0.1 to 1 M) include calcium chromate and potassium di-chromate. Zinc, lead and barium chromates fall into the low solubility category (< 0.01 M). $PbCrO_4$. PbO is totally insoluble. Chromates are strong oxidizing agents especially of organics. Their adsorptive behaviour is low compared to Cr(III), and they adsorb more readily at low pH values.

(iii) Cr(III) - Cr(VI) interconversions

The conversion of Cr(III) to Cr(VI) and vice versa is of great significance in cement-based S/S. Firstly, Cr(III) is the preferable oxidation state for treatment: it can be precipitated out in the pore solution by the high pH environment and is the less toxic oxidation state. Secondly, it is proposed here that conversion of Cr(III) to Cr(VI) may occur in the highly alkaline pore

solution, causing what appears to be a benign product to start releasing the mobile Cr(VI) over long periods of time.

Above a pH of 2, Cr(III) can be oxidized to Cr(VI) in the presence of oxygen or stronger oxidizing agents. The half reactions are given as follows:

$$Cr_2O_7^{2-} + 14H^+ + 6e^- \rightarrow 2Cr^{3+} + 7H_2O \quad (pH < 3)$$
$$HCrO_4^- + 6H^+ + 3e^- \rightarrow Cr(OH)^{2+} + 3H_2O \quad (pH\ 4 - 6)$$
$$CrO_4^{2-} + 5H^+ + 3e^- \rightarrow Cr(OH)_3^0 + H_2O \quad (pH\ 5 - 9)$$
$$CrO_4^{2-} + 4H^+ + 3e^- \rightarrow Cr(OH)_4^- \quad (pH > 10).$$

The oxidation of Cr(III) by O_2 is feasible but is kinetically limited. The half-life based on first order kinetics is to the order of 2 to 9 years [Saleh et al (1989)]. The oxidation of Cr(III) by MnO_2 has a half-life to the order of 2 to 3.5 years with low concentrations of MnO_2. The half-life will vary widely depending on the concentration of the MnO_2. Oxidation is more favourable at pH 3 than at pH 7 to 9 [Saleh et al (1989), Eary and Rai (1987), Bartlett and James (1979)].

Cr(VI) can be reduced to Cr(III) by Fe(II) [Rai et al (1987), Baes and Mesner (1976)].

2.3.2 Zinc

Hydroxides of Zn are precipitated from solutions of salts by addition of bases. Of all the oxides and hydroxides, $Zn(OH)_2$ is the most stable form. The solubility of $Zn(OH)_2$ is a strong function of pH (see Figure 2-3). As is the case for chromium, the hydroxide is amphoteric with solubility reaching a minimum at a pH of about 9.

$Zn(OH)_2$ readily dissolves in an excess of alkali bases to give zincate ions and solid zincates such as $NaZn(OH)_3$ and $Na_2[Zn(OH)_4]$ which can be crystallized from concentrated solutions.

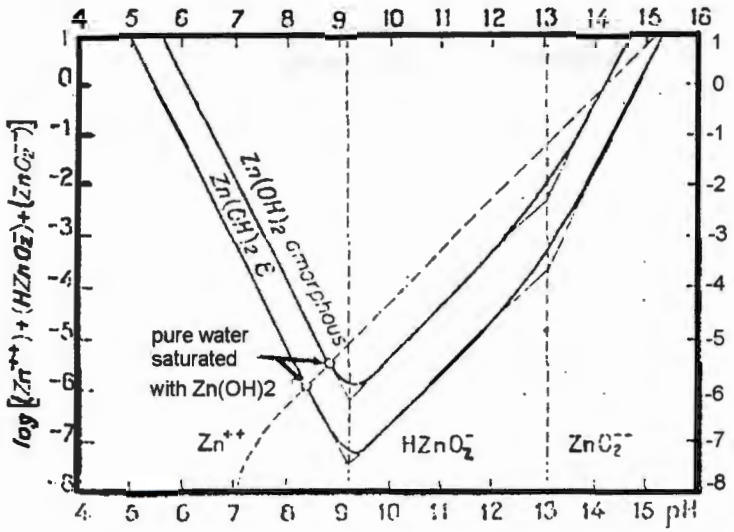

Figure 2-3 - Zn solubility as a function of pH [Pourbaix (1966)]

2.3.3 Comments on the relationship between Solubility and pH

A number of metals display a relationship between solubility and pH as has been discussed above for Cr(III) and Zn(II). Depending on the oxidation state and type of the metal, the species may be amphoteric (displaying a minimum solubility at an intermediate pH, with solubility increasing above and below this pH) or may show a steady decrease or increase in solubility with pH. Solubility-pH relationships for Ca and Mg are shown in Figure 2-4 and Figure 2-5 and respectively. These figures are referred in the course of this thesis.

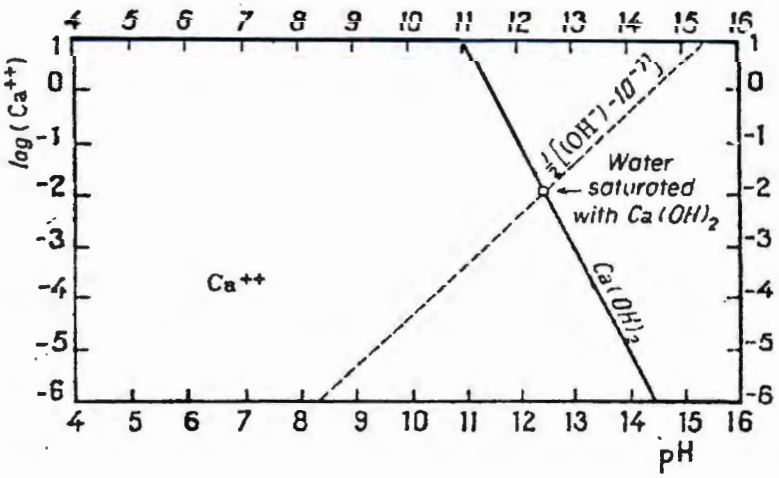

Figure 2-4 - Solubility-pH behaviour for Ca [Pourbaix (1966)]

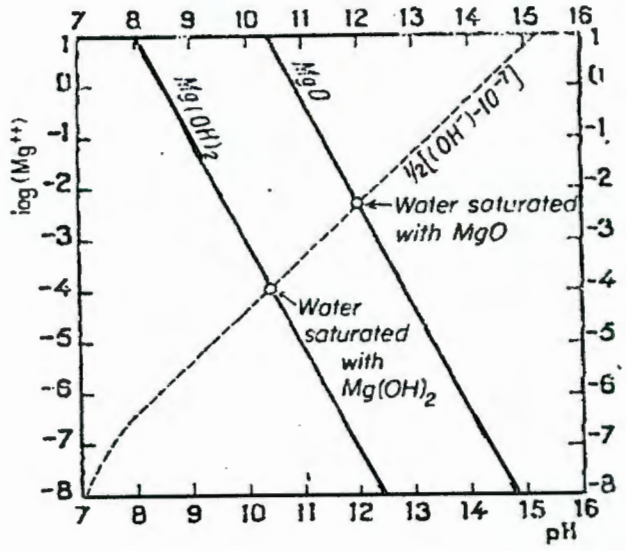

Figure 2-5 - Solubility-pH behaviour for Mg [Pourbaix (1966)]

It is important to recognise that such curves were established for pure systems - a specific metal in contact with a solution (usually deionized water). Metal solubility is dramatically altered by the presence of other ions in solution due to factors such as common ion effects and the formation of more or less soluble complexes with other ions. The complexity of the system being studied in this thesis makes prediction of individual ion solubilities difficult, but general trends are highlighted in interpreting results in further chapters of this work.

2.4 Interactions Between Various Wastes Constituents and Cement

A number of studies are reported in literature concerning the effect of the chemistry of both mixing waters and aggregates on cement hydration. A summary of results reported in open literature are presented here.

2.4.1 Effect of Metals on Setting of Cement

Calorimetry has been used to provide an indication of the accelerating or decelerating effect of metal ions on cement hydration. Using chloride and nitrate salts, the following sequence was determined for cations [Double (1983)]:

$\frac{1}{2}Ca^{2+} > \frac{1}{2}Ni^{2+} > \frac{1}{2}Ba^{2+}, \frac{1}{2}Mg^{2+} > Fe^{3+}, \frac{1}{2}Co^{2+} > La^{3+} >> NH_4^+, K^+ > Li^+ > Na^+ > \frac{1}{2}Cu^{2+} > \frac{1}{2}Zn^{2+} > \frac{1}{2}Pb^{2+}$

← acceleration deceleration →

The following order was established for the effect of anions

$Cl^-, Br^- > SO_4^{2-}, SCN^- > F^-, I^- > NO_3^- > ClO_4^-$

← acceleration

2.4.2 Other Chemical Compounds Which Affect Setting

Other chemical compounds which retard cement setting include calcium sulphate, borates, carbohydrates [Cullinane et al (1986)] and sodium salts of phosphate, iodate and sulfide [US EPA (1980)]. Acidic or acid producing materials such as sulphides react with carbonates (which may originate from acid rain falling on the cementitious structure) and hydroxides which leads to breakdown of cement after setting [Cullinane et al (1986)].

Certain substances such as sodium and potassium silicates, however, have been shown to accelerate setting. Bricka and Jones (1989) showed that sodium hydroxide reduces the strength of cement, while sodium sulphate has little impact on the strength. Sodium arsenate reduces the 14 day compressive strength of a solidified product [Shively et al (1986)]. The effect of a chemical will often be related to the amount of the substance present.

2.4.3 Mechanisms of Containment of Metals by Cement

Cement-based S/S has been most successful in the treatment of heavy metal sludges, with less success being achieved in the case of organic wastes [Montgomery et al (1991)]. Interactions of metals and cement is complex, and chemical interactions are not fully understood. Recently reported work presented in open literature has focused on attempting to characterise such interactions. A summary of results from this open literature is presented in this section.

It is identified that, although cement-based S/S has been used for treatment of liquid and solid wastes, the characterisation studies of waste-cement interactions presented in literature and which are summarized here have been carried out on metal-containing solutions or slurries with solids contents of less than 20%. In such cases the effect of the waste on cement hydration will be due primarily to chemical effects, and physical effects will be limited. This current work focuses on the treatment of metal-containing wastes which have high solids contents (over 50% w/w). In accordance with the discussion presented in this chapter thus far, the physical presence of the solid 'aggregate' will affect properties of the S/S product. Very little work reported in open literature investigates the combined effect of physical and chemical interactions between cement and waste in the S/S process.

Mollah et al (1992) propose that the interaction between metals wastes and cement may involve exchange processes on the surface of the cement particles with the subsequent release of H^+ ions or other cations and the subsequent adsorption and or complexation of a M^+ ion with the CSH. No indication is given here of the source of the H^+ ions - it is suggested in the current work that they originate from dissociation of water molecules from the CSH.

Crystalline calcium silicate hydrates from cement hydration are variable in composition. Such variable compounds are referred to as "solid solutions". The term "diadochy" is commonly used to describe the ability of different ions to occupy the same lattice position in the crystal matrix [Malone and Larson (1983)].

Malone et al (1983), however, report work done using X-ray diffraction (XRD) techniques to check whether new crystalline structures were formed when a fine-grained metal hydroxide electroplating sludge containing As, Cd, Cr, Cu, Fe, Hg, Ni, Pb, Cl and CN was solidified using cement and pozzolans. No change in lattice spacing was observed over uncontaminated cement and it was proposed that no new chemical structures were formed. Microscopic examination of their samples showed that the metals existed in the end product as amorphous metal hydroxides and were retained as such in the pores of the solid end product. A similar observation was reported by Poon et al (1985b).

The iron content, as well as the ratio of Fe(II) to Fe(III), has been shown to reduce the solubility of Cd, Cr, Hg, As, Pb and Cu in solutions by co-precipitation. A ratio of the Fe(II) to Fe(III) of 1:1 has been shown to lead to optimum solubility reduction [Wiles and Lyn Apel (1985)].

Few studies have been carried out on retention of anions in S/S products. Work which has been done has identified that anionic metals are not stabilized as effectively as cationic ones [Shively et al (1986), US EPA (1980)]. The anionic metals will, at best, form a few insoluble salts whose retention is limited. Retention of anionic species is not explored further in this thesis.

For the purposes of this project, zinc and chromium have been selected for detailed study. The reason for this choice is twofold. Firstly, as is revealed in the next sections, literature would suggest that the two metals are contained in different ways in the cement-based S/S product. Secondly, as will be seen in the following chapters, both Zn and Cr are present in the wastes in high concentrations. These metal species have intrinsic value in their own right, both in terms of recovery, and their potentially adverse environmental impact. The mechanisms of their retention in S/S products proposed by studies in literature are described in detail here.

(i) Chromium

A number of studies have been reported in which analytical tools such as SEM/EDX, TEM, FTIR and XRD have been used to attempt to establish the location of various chromium species within cement-based S/S products. Whilst there is active debate over the exact mechanism of chromium retention, it is worthwhile recounting some literature findings which have relevance for this work.

The most widely supported view is that trivalent chromium can be chemically incorporated into all of the cement hydration products described previously, primarily substituting for silica in CSH [Mollah et al (1992), Ivey et al (1990)]. In the work of Mollah et al (1992), FTIR analysis of a Cr-doped cement indicated that chromium is incorporated either into the CSH structure by substitution of Cr(III) for Si(IV), or that chromium affected the polymerisation of silicates (and therefore the crystal structure of the end product) by reaction or adsorption of the chromium onto Portland cement particles. In the case of substitution for Si(IV), no suggestion is made as

to the how the charge balance is achieved: as has been stated previously in this Chapter, the composition of CSH is variable, and it must be assumed that other changes in the CSH structure occur simultaneously to the substitution to make up for the difference of one electron between Cr(III) and Si(IV).

Heimann et al (1990) suggested that Cr(III) associates solely with regions of high calcium content (such as calcium hydroxide and calcium nitrate) in the form of calcium-chromium crystalline precipitates, and that the retention of chromium is not associated directly with CSH formation. This would agree with the results of Malone (1983) presented in section 2.4.3.

A further view is held by Kindness et al (1994), who indicate that Cr(III) associates with the calcium aluminate hydrate phases, as opposed to the silicate phases, by substituting for Al in the hydration products.

It is clear, therefore, that no definite conclusions can be made as to the fate of Cr(III) in cement products. It does, however, appear that there is potential for some direct incorporation of Cr (III) into the products of cement setting, from where its subsequent mobility and leach resistance will be governed by the stability of this solid in its surroundings.

Depending on the pH of the pore solution, the remaining Cr(III) which is not incorporated into the cement product will either remain soluble or precipitate as a metal hydroxide.

A discussion of Cr(III) solubility as a function of pH was presented in section 2.3.1. Figure 2-2 presents the solubility curve for Cr(III) [Rai et al (1987)]. Although the actual solubilities of a species is highly dependant on a number of factors including other species in solution, age of solution and ambient conditions, the shape of the curve is what is significant. At both low and high pHs, the solubility increases. At a pH of 10.5, found later on to be typical of that of the pore solution of S/S products such as the ones under investigation in this work, the solubility of Cr(III) is seen to be at a minimum. Thus most of the Cr (III) will be expected to be present in the pores as insoluble hydroxides. That remaining in solution has the potential to diffuse out of the pores and be removed by any fluid permeating through the solid matrix.

A drop in pH will result in increased solubility and therefore increase the potential for removal of the metals from the solid. A drop in pH can occur as a result of a number of factors. The presence of metal nitrates in the S/S product, especially copper, has been found to cause a drop in the pH of the leachant during a leaching test, which affected the amount of cadmium and nickel released from a solidified heavy metal sludge [Tashiro et al (1977)]. Organics present in the waste can have a similar effect. On a macroscopic level, a reduction in pH in a landfill may occur as an effect of acidic rainfall deposition on the surface of a waste deposit.

Some workers have reported the potential for Cr(VI), in the form of CrO_4^{2-}, to be taken up by substitution for sulphates during the formation of ettringite - the hydration product formed by the reaction of tricalcium aluminate with sulphates. This appears to hold in laboratory simulations where the formation of pure ettringites has been studied in the absence of other cement constituents [Poelmann et al (1993), Glasser (1993)]. In the case of real cements the presence of Cr(III) inhibits the formation of ettringite, and therefore in cases where both Cr(III) and Cr(VI) are added to a cement mixture no incorporation of Cr(VI) by the solid products is expected [Kindness et al (1994), Ivey et al (1993)]. Since Cr(VI) is highly soluble over the entire pH range, it is expected to be found solubilized in the pore solution. Release from the S/S product will therefore be as a result of diffusion out of the product [Kindness et al (1994), Jacobs (1992), Zamorani et al (1988)].

(ii) Zinc

Cocke et al (1992) showed that zinc from solution adsorbs onto the surface of cement particles and cement hydration products and inhibits silicate polymerisation. Since the surface of the cement hydration products has a negative charge [Mollah et al (1992)], adsorption of zinc cations is feasible. Other authors have indicated that this effect may only be temporary. Claudio and Pedro (1990) showed that zinc retards the setting of cement, but has no long term effects on the quality of the end products. Cullinane et al (1987) found, however, that the mechanical strength of the final product depends on the concentration of zinc in the dopant solution: low levels of zinc result in strength increases, while higher levels of zinc have the opposite effect.

Apart from that adsorbed to solid surfaces, some zinc is found also in the pore solution as zinc hydroxide, in either soluble or precipitated form. As in the case of Cr(III), Zn(II) is amphoteric. At a pH of 10.5, typical of the pore solutions, the solubility of amorphous $Zn(OH)_2$ is low (see Figure 2-3). Poon, Peters et al (1985) point out the importance of calcium hydroxide in the stabilization of zinc. Calcium and potassium hydroxides, formed during cement hydration, are released into the pore solution and result in a highly alkaline environment. Cocke and Mollah (1993) suggest that calcium and zinc may combine to form calcium zincate complexes such as $CaZn_2(OH)_6.2H_2O$. The mechanisms of formation of such complexes is not clear.

In a study by Poon, Clarke et al (1985) mercury intrusion porosimetry (MIP) results showed an increase in pore volume and sizes when zinc was added to cement. This was attributed to extensive growth of ettringite crystals associated with the accelerated hydration of tricalcium aluminate, revealed by scanning electron microscopy (SEM) and X-ray diffraction (XRD). Although the porosity was high, the leachability of zinc was low and the release of zinc in a dynamic leach test was shown to be independent of time. This indicated that permeability was not an important factor in leaching and that the reduction in zinc mobility was as a result of chemical stabilization - reduced species solubility associated with the high pH values found in cement products. Furthermore, XRD and SEM showed no crystalline zinc silicate.

Other metals display amphoteric behaviour similar to that shown for Cr(III) and Zn(II), with the pH of minimum solubility depending on the metal species. Retention of many metals in S/S products is as a result of low hydroxide solubility at the pH of the pore solution. Dissolution and subsequent release of metal hydroxides from the S/S product can result if the pH of the pore solution drops.

2.4.4 Organic Compounds

Although organic wastes are not relevant in the context of this study a brief discussion of organics and S/S is presented for the reader's benefit. Cement-based S/S has been less successful in the treatment of organic wastes than in the treatment of inorganic wastes. This may be due to interference in the hydration of the cement particles. Sollars and Perry (1989)

report that wastes cannot be solidified successfully without additives if organics are present in concentrations of more than 1 to 2 %.

There is some scope for the use of *organic* S/S binders for the treatment of organic wastes. Telles et al (1984) discuss a study in which radioactive ion exchange resins were encapsulated in types of plastics. This is done using thermoplastic techniques as mentioned in Table 1.1. Furthermore, treatment of tributyl phosphate, carbon tetrachloride and tetrachloroethylene has been successfully achieved using polythene. Asphalt showed less promise in treatment of these wastes.

Immobilization of organics by S/S can be achieved by effecting reactions which will alter or destroy the organic compound, or by physical processes such as adsorbtion (using sorbents such as fly ash and activated carbon) and encapsulation. Hydrolysis, oxidation, reduction, compound formation and fixation onto an insoluble substrate are the most important reactions when considering the containment of organics [Conner (1993)]. Organic materials are unlikely to complex chemically with the cement products and are therefore contained primarily by physical entrapment in the pores of the cement [Wiles (1988)]. Any chemical bonds which do occur are weak and readily reversible [Weitzman (1990)].

Oils, grease, sugars, ethylene glycol, p-bromophenol and other organics are known to interfere in the setting of cements [De Percin (1989), Pojasek (1989), Bricka and Jones (1989), Cullinane et al (1987)]. In the case of oils and grease, retarded setting occurs as a result of coating of the surfaces of the cement particles by the oil. This retards the hydration process and thereby impedes the setting of the cement [Cocke (1990)].

In the study conducted by Cullinane et al (1987), it was found that the reduction in the strength of the product by oil and grease was significant, while trichloroethylene and hexachlorobenzene had little effect on the strength. Bricka and Jones (1985) found that although the latter two components had little effect on the end-product strengths, their presence in a solidified waste increased the leaching behaviour of metals also present in the waste. This was due to the decrease in pH of the leachate and the consequent dissolution of the metal hydroxides, which are insoluble at high pH values.

Phenols in the waste have been shown to reduce strength and durability of cementitious products [Bricka and Jones (1985)]. Adipic acid decreases the end compressive strength of the product. Methanol, benzene and xylene retard the setting of cement and have been found to lead to higher rates of leaching of other toxic components [Wiles (1988)].

Portland cement has been shown to be unsuitable for the solidification of radioactive ion exchange resins in ratios greater than 10% (resin to cement on a weight basis). The resins are hygroscopic and tend to swell, causing cracking of the cement [Telles et al (1984)].

Another problem with the S/S of organics is the possibility of release of volatile and semi-volatile components into the atmosphere during transport and processing. This effect will be intensified if the waste's temperature increases during the mixing and setting of the cement [Weitzman (1990)].

2.4.5 Sulphates

Wastes containing high levels of sulphates have been found to have adverse effects on the success of an S/S operation. Sulphates undergo rapid reaction with tricalcium aluminate to form crystals of hydrated calcium aluminosulphate (ettringite). This occupies a much higher volume than the original calcium aluminate hydrates. Should ettringite form during the early stages of cement setting, therefore, the volume increases will not be a problem and the crystals will be incorporated into the cement matrix. Once the cement has set, however, the formation of ettringite can cause cracking and spalling due to the associated volume increase.

Type II and V Portland cements are made to be sulphate resistant. Arniella and Blythe (1990) recommend the use of type I Portland cement for wastes containing less than 150 ppm of sulphates and sulphides.

Some researchers [Bricka and Jones (1985), USEPA (1980)] have reported that the addition of pozzolans such as fly ash can reduce the effect of sulphate attack on the final product. This is

due to the fact that pozzolans consume calcium hydroxide during setting as described previously.

Bricka and Jones found that addition of sulphate to samples had little effect on leaching of metals from a cement matrix. The sulphate, however, leaches out readily due to its high solubility.

2.5 Summary

This review has provided the reader with an understanding of the chemistry and mechanisms associated with the hydration of cement. A discussion of the mechanisms and chemistry of retention of metal species in cement-based S/S products has been presented.

The complexity of the interactions which can occur between metals and cement, and metals with each other has been identified. In flue dusts from the ferrochromium industry, metals present include mercury, zinc, cadmium, chromium, boron, lead, arsenic, magnesium, manganese, sodium, potassium and antimony [Kornelius and Boegman (1994)]. When one considers the interactions between waste dusts and the cement, consideration must therefore be given to the system as a whole.

Although some work is reported in open literature on the S/S of liquid wastes and slurries containing low solids contents, it was identified that little work has been reported on the cement-based S/S of wastes containing a large amount of solid materials. In the former, chemical interactions will be of significance, while in the latter both physical and chemical interactions will affect the quality of the end product. A need exists for complete characterisation of the solid wastes treated with cement prior to implementation of S/S as a treatment option.

3.

Wastes Used in the Study, Results of Preliminary Investigations and Sample Preparation

This chapter provides a description of the waste products under investigation in this study. The waste products are identified as being potentially hazardous due to the presence and leachability of various toxic species, primarily metal ions. None of the wastes can be consigned directly to landfill without some form of pre-treatment. The procedure for making of samples and the ranges of operational variables used in this study are also presented here. This chapter is intended to serve as a reference when reading further sections of the thesis.

3.1 The Wastes Products of Interest in this Study

In Chapter 1 the contribution of the minerals extraction and beneficiation industry to the total and hazardous waste streams in South Africa was identified. Both government legislation and public pressure are causing industry to look more carefully at the reprocessing and treatment of its wastes. In the context of the current study, the ferroalloy industry was highlighted as being of interest due to the extensive growth of the industry in South Africa and the associated increase in the production of wastes.

A number of process steps in carbon- and stainless- steel production arise in the production of wastes. Many of these wastes are precluded from direct disposal to landfill due to high levels of mobile heavy metals. Cement-based Solidification/ Stabilization has been identified as being potentially feasible as a pre-landfill treatment option which aims to ensure the long-term immobilization of such heavy metal species [Petrie and Paxton (1995)].

In this current study of the S/S of wastes from ferrochromium production, two solid waste products were chosen as being representative of those produced in the industry. These are:

(i) a Ferrochromium Smelter Dust which is representative of wastes produced during the pyrometallurgical reduction of ores. This waste is designated throughout this work as FeCr Dust, and

(ii) a metal hydroxide-containing precipitate from a wastewater stream originating during the surface treatment of products. This waste is designated as ETP filter cake.

As is demonstrated in the sections which follow, these two wastes are fundamentally different in both their physical and chemical characteristics. In Chapter 2 it was shown that both physical and chemical characteristics of aggregates and wastes affect the properties of the ultimate product. An understanding of the effects of these two different wastes on the properties of S/S products, to be developed through this thesis, will assist in the prediction of the properties of other solidified waste products which are similar in chemistry and physical structure to the two wastes investigated here.

3.1.1 Ferrochromium Smelter Dust (FeCr Dust)

(i) Origin

Various steps in pyrometallurgical processing of ferrochromium ores give rise to fine dust products which are collected from the air by filter systems. Von Blottnitz (1994) provides a brief discussion of the three mechanisms of formation of dusts in the Ferrochrome industry. These are:

(i) dusting of fine solids added to the furnaces in the form of fluxes and slag formers,
(ii) atomization of the liquid phase, followed by partial oxidation during cooling and subsequent conversion from liquid to solid, and
(iii) fuming or evaporation of volatile metals with subsequent condensation, sometimes onto other dust products.

Such dusts are usually extremely fine and contain high levels of metals and other inorganic elements. The FeCr Dust, examined in this work, is one such dust originating in the ferrochromium smelter.

(ii) Physical Description

The FeCr Dust is fine, with a large proportion of the particles being less than one micron. A particle size distribution for the dust, determined by a Malvern laser particle sizer, appears in Figure 3-1. The majority of the particles are less than 0.36μm, with 12% of the particles being less than 60nm in diameter. The dust is gunmetal grey in colour, highly mobile in air, settles rapidly in water and has a specific gravity of 2.63.

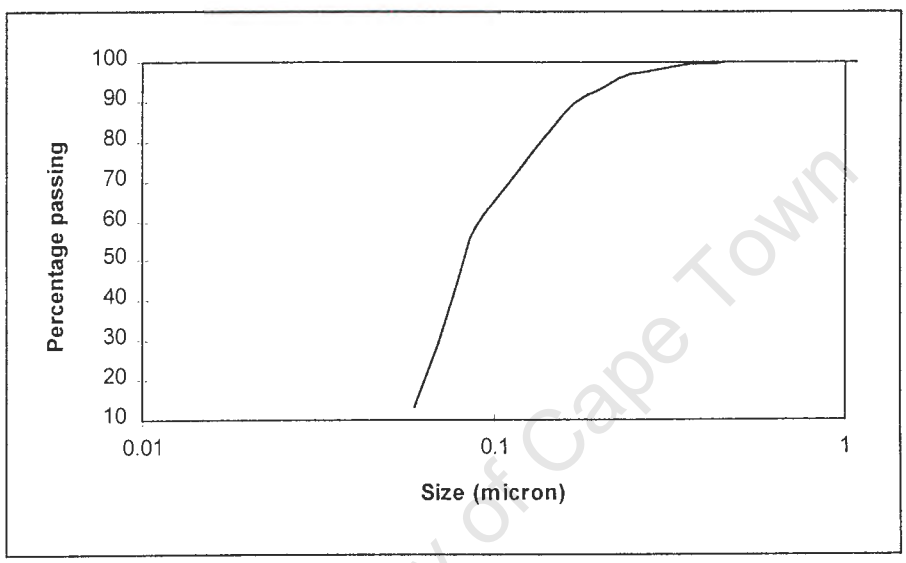

Figure 3-1 - Particle Size Distribution of the FeCr Dust

Figure 3-2 presents a scanning electron micrograph (SEM) of the FeCr Dust.

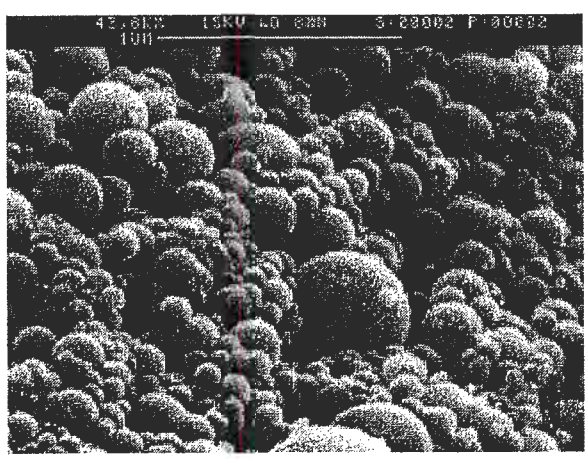

Figure 3-2 - Scanning Electron Micrograph of the FeCr Dust

It can be seen that the particles are spherical, and visual observation indicates that the majority of the particle sizes are between 30 and 200 nm in diameter, confirming Figure 3-1. Further SEM observation showed that the spheres cluster readily into agglomerates of between approximately 1 and 100 μm. This is attributed to static charging. When this dust is slurried with water, however, this static interaction is suggested to no longer be of significance.

(iii) Chemical Characterisation

The results of four different chemical characterization steps are presented in Table 3-1. A fusion digest (see Appendix A1) was used to determine the overall composition of the material. The Toxicity Characteristics Leaching Procedure (TCLP) test is a batch leach test often used to determine the constituents of a waste leachable under specific laboratory conditions and hence classify the waste as hazardous or non-hazardous. A full discussion of the TCLP and its shortcomings appears in Chapter 6. In addition to the fusion and TCLP data, the constituents mobilized by agitation in distilled water for one hour and the TCLP characterisation of this washed material are reported. The significance of the washing step is discussed in section 3.2.1 below.

The TCLP specifies maximum levels in the leachate from a waste, above which the waste must either be consigned to a class I or hazardous landfill site, or treated prior to disposal. These maximum limits are presented in Appendix A2. The specified level for Cr is 5 ppm, while no limit is set for Zn. For comparison, however, the maximum permissible Zn concentration in drinking water is 5 ppm [Eaton (1993)]. These dusts thus require either disposal to hazardous landfill, or further treatment prior to disposal.

A comparison of the TCLP leachate concentrations for the washed and unwashed dusts and the wash water composition shows that washing the dust for an hour removes approximately 20% of the mobile Cr and approximately half of the mobile Zn, Ca, Mg and Mn. It was also observed to reduce the amount of mobile K.

Table 3-1 - Chemical Characterisation of the FeCr Dust

Element	Mass % in dust	Conc in TCLP leachate of raw dust (ppm)	Conc in wash water after 1 hour (ppm)	Conc in TCLP of washed dust (ppm)
pH		4.5	6.4	4.5
Total Cr	2.5	35.3	20.9	27.6
Cr(VI)	-	19.9	14.2	9.0
Cr(III)	-	15.4	6.7	18.6
Fe	0.6	1	nd	nd
Mn	0.3	12	7.2	6.6
Zn	7.1	1109	920	595
Pb	0.1	0.1	0	0.1
Cd	3.0 g/t	0.1	0.15	nm
K	4.7	632	641	61
Mg	1.0	434	404	238
Na	7.89	nm	nm	nm
S	1.95	nm	nm	nm
Cl	4.20	nm	nm	nm
Al	1.89	nm	nm	nm
Ca	0.2	65.5	55.1	27.3

nm - not measured

nd - not detected

Ferrochromium smelter dust products have been established to consist of a core of, among other constituents, silica, alumina, calcium, magnesium and chromites around which are found a rim of condensed volatile species such as K, Zn, Cr(VI) and Mg [Gencor (1996)]. It is expected that it is constituents of this 'volatile layer' which are removed during the washing and TCLP steps.

A comparison of the TCLP carried out on the washed and unwashed dusts reveals the following in terms of Cr and Zn. The washing step of 1 hour removes less Cr(VI) than does the TCLP over 18 hours. The dissolution of Cr(VI) would be expected to be rapid and hence kinetic effects would not initially be expected to play a role in determining the amount of Cr(VI) leached in these two steps. The reason for the observation is the following. As

mentioned above, Cr(VI) is expected to be contained in a condensed layer of volatile species around the dust core. The dissolution of this layer, which is required to expose the Cr(VI) to the leachant solution, will be kinetically controlled, explaining the differences in Cr(VI) leached. The TCLP of the washed dusts shows less Cr(VI) leached than in that on the unwashed dusts. This is due to the Cr(VI) removed during the washing step.

Zn is expected to be contained with Cr(VI) in the outer layer surrounding the dust particles. In the pH of both the TCLP leachates and the water wash, the solubility of $Zn(OH)_2$ is not expected to be limiting. The explanation presented for Cr(VI) is expected to hold in the case of Zn leaching in the three tests.

As was identified in Chapter 2, Cr(VI), Cr(III) and Zn are expected to be contained in different ways in S/S products. The high levels in the dusts and the different mechanisms by which they are contained in S/S products (see Chapter 2) motivated their choice for study in this work.

3.1.2 Metal Hydroxide Filter Cakes (ETP)

(i) Origin of the Filter Cakes

Liquid effluent from stainless steel surface treatment operations contains significant quantities of heavy metals. Although the preferable fate of such streams would be reprocessing, this is not always economically viable. Common practice suggests that acidic effluent be neutralized by a source of free lime. In this way metal species are recovered by ionic precipitation as solids. Water reclamation and recycling options first require removal of heavy metals by such ionic precipitation, followed by effective desalination of the water. The focus of this section of the study was the heavy metal precipitate from such streams, which is commonly sent to landfill if the economic return of reprocessing is not attractive.

Two wastewater streams typical of those from stainless steel producing operations were simulated. Compositions of these two streams are presented in Table 3-2 below. The high concentrations of both anions and cations clearly preclude this stream from discharge directly to public sewer systems and thus neutralization and subsequent removal of metals from this stream by precipitation was warranted. Filter cake material was produced by controlled neutralization using calcium hydroxide. Since solubility of Cr(VI) is high over the entire pH range (see

Chapter 2), it was necessary to reduce Cr(VI) to Cr(III) in order to effectively remove Cr by precipitation. To this effect $Fe(SO)_4$ was added as a reduction agent during the neutralization. A full record of the precipitation procedure can be found in Department of Chemical Engineering (1995).

Table 3-2 - Compositions of the simulated wastewater solutions

Species	Stream 1 (mg/l)	Stream 2 (mg/l)
Fe^{2+}	369	332
Fe^{3+}	872	2190
Ni	176	359
Cr (III)	120	108
Cr (VI)	224	603
Na	1041	1059
K	19	17
Mg	188	183
Ca	245	227
SiO_2	51	49
F	770	3077
Cl	333	334
SO_4	6174	5846
NO_3	2464	9625
CO_3	177	171

The primary differences between the two streams are in the Fe^{3+}, Cr(VI), F^- and NO_3^- concentrations. Prediction of how these concentration differences will affect the rate of precipitation, compositions of the precipitates and particle sizes within the precipitates from the different streams is difficult for a complex system such as this - precipitation mechanisms and kinetics are still not fully understood [Dustan (1997)].

One qualitative comment which may be made about the difference in Fe^{3+} between the two streams is the following. Fe^{3+} is expected to precipitate as $Fe(OH)_3$. Both cationic and anionic species have the potential to adsorb to metal oxides, with cationic adsorption increasing with

increased pH and anionic adsorption decreasing with increasing pH. The effect of other ionic species in solution on adsorption equilibria warrants a study of its own, but it is acknowledged here that the increased Fe^{3+} concentration in solution in stream 2 over stream 1 will result in an increased amount of precipitated $Fe(OH)_3$ onto which metal adsorption can occur. Cr(VI) is expected to be found as the chromate, CrO_4^{2-}, species in high pH solutions (see Chapter 2) and adsorption of Cr(VI) (in the form of CrO_4^{2-}) to the $Fe(OH)_3$ surface is plausible.

(ii) Physical Characterisation of the Filter Cakes

The filter cakes from this treatment step consisted of a fine-grained metal hydroxide. The consistency and colour resembled that of a light brown clay-like material. Unfortunately at the time of testing the equipment used to determine the particle size distributions for the FeCr Dust was not available and hence no accurate particle size distributions could be obtained. Equipment which was available, however, indicated particle sizes to be less than 1 μm, and the material appeared to the eye to be even finer than FeCr Dust products. The water content of the cakes lay between 43% and 51% (w/w).

(iii) Chemical Characterisation of the Filter Cakes

Table 3-3 below provides chemical analyses of the filter cakes and the filtrate from the neutralization process, the latter which is expected to be similar in composition to the water remaining entrained in the filter cake.

No Cr(VI) was found by UV spectroscopy to be contained in the filtrate solutions and hence Cr in the filtrates is expected to all be Cr(III). This would suggest that either the Cr(VI) has all been reduced to Cr(III) by the ferrous sulphate added to the system, or that Cr(VI) is adsorbed to the solid surfaces as discussed previously.

Anions expected to be part of the filter cake are hydroxides, sulphates, chloride and fluoride ions. As has already been mentioned, Fe^{2+} and Fe^{3+} would be expected to precipitate with OH^- ions. Ca would be expected to form $Ca(SO)_4$. Remaining sulphate and chloride ions would be found solubilized in the pore solution.

Table 3-3 - Compositions of the Filter Cakes and Filtrate

Species	Cake 1		Cake 2	
	Solid (%)	Filtrate (mg/l)	Solid (%)	Filtrate (mg/l)
Total Fe	13.2	0.04	13.3	0.13
Ni	1.19	1.57	0.98	0.82
Total Cr	3.6	0.08	2.7	1.37
Mg	0.18	199	0.16	221
Ca	22.3	910	24.0	1510
Si	0.76	0.2	0.78	0

No TCLP characterization was carried out on this filter cake material. It is expected, however, that the acidic leachant used in the TCLP would cause resolubilization of some of the precipitated metal species in the solid. Based on the potential mobility of metals in acidic environments, S/S was deemed to be necessary prior to consignment landfill.

3.2 Results of Preliminary Investigations and Sample Preparation

Prior to commencing a rigorous experimental programme it was necessary to assess, on a qualitative basis, factors which affect the solidification process and to develop a procedure for preparation and curing of samples for use throughout this work. The results of this investigation are presented in the sections which follow.

3.2.1 Initial observations

In addition to the operational variables which were identified in Chapter 2 as having an influence on the quality of cement and S/S products, the following observations were made:

(i) Initial laboratory investigations showed that it was impossible to solidify the FeCr Dust without some form of **pre-treatment**. Untreated dusts to which cement was added failed to show any strength development whatsoever - the product was a putty-like solid, and no reduction in the leaching behaviour was achieved. In Chapter 2 it was identified that the

presence of both anions and cations in aggregates and mixing waters have the potential to retard or inhibit cement hydration. Furthermore, the surface character of an aggregate will determine the attachment of the cement hydration products to its surface and consequently affect the strength of the resulting product. In particular, the retardation of cement hydration by zinc has been demonstrated due to the formation of a low permeability coating on cement grains [Cocke et al (1992)]. This was discussed in section 2.4.3 (ii).

The dusts are seen in Table 3-1 to contain high concentrations of metal species. In Table 3-1 it can further be seen that some of these metals are mobile in water. When the dusts are mixed with water and cement, these mobile metals can enter the mixing water and affect hydration in accordance with the discussion of Chapter 2.

The 1 hour **water wash**, the results of which are reported in Table 3-1, removes a substantial amount of mobile Cr, Zn, Mg, Mn and Ca, as well as a number of anions (not shown in the Table) from the surface of the dusts. Removal of these species will be expected to change both the surface charge and surface texture of the dusts. A mixture of the washed dusts and cement set into a product which was self-supporting and in which metal mobility was reduced.

In all subsequent sample preparation the FeCr Dust was therefore subjected to a batch water wash, followed by pressure filtration, prior to cement addition. The residual moisture in the cake, expected to be of a similar composition to the filtrate as presented in Table 3-1, was available as some or all of the water for cement hydration. In Chapter 2 it was recognised that high concentrations of metals in mixing water (in this case the residual water in the filter cake) may affect the chemistry of the cement hydration reactions. This is explored further in Chapter 4.

This washing step was not found to be necessary to effectively solidify the ETP filter cake. A number of reasons are offered for this observation. Firstly, due to the origin of these products, the surface characteristics and chemical compositions of the ETP cakes and the FeCr Dust are different. Metal concentrations in this cake are observed to be lower than those in the FeCr Dust and are therefore suggested not to influence cement setting to the same degree. Finally the ETP products are prepared by precipitation of metals out of solution using $Ca(OH)_2$, implying an alkaline product. An alkaline environment is favourable for cement hydration [PCI (1986)].

(ii) Based on literature observations, three operational variables, **amount of cement added**, **water addition** and **curing time**, were chosen for study in this work for two reasons. Firstly, these variables are identified as having the most significant effect on the strength and permeability of cement and S/S products. Secondly, they are important practical variables for full scale operation in that they are readily measured and easily controlled. The investigation presented in this thesis focused on assessing the effect of changing these variables on the strength and leaching behaviour of the S/S products. Other significant variables identified in Chapter 2 were held constant through the course of this work.

(iii) Products dehydrated rapidly after mixing. All curing was done in sealed containers in which an open beaker of water was placed to ensure a constant ambient humidity during curing.

3.2.2 Sample preparation technique

Based on both initial laboratory trials and literature findings, the sample preparation technique presented in Appendix B was developed for both the FeCr Dust and ETP filter cake.

All of the research presented in this thesis was carried out on single batches of wastes, except where otherwise indicated. It is noted, however, that different batches of waste may vary in composition. In accordance with the literature review of Chapter 2, the chemistry of a waste has the potential to affect the hydration of cement and thus the solidification process. The effect of variability in waste compositions on the results presented is not discussed in this thesis.

3.2.3 Calculation of the Formulation of the S/S Products

The percentage of water in the filter cake after drying in an oven is calculated using:

$$PW = \frac{M_b - M_a}{M_b - M_c} x100$$

where PW = percentage of filter cake which is water

M_b = weight of wet dust + weight of crucible

M_c = weight of crucible

M_a = weight of dry dust + crucible

The required amount of cement for a fixed quantity of dust is then calculated as follows:

$$CM = CP * DW * (1 - \frac{PW}{100})$$

where CM = mass of cement to be used (g)
CP = required percentage of cement
DW = mass of wet filter cake used (g)

Finally, the amount of water required to bring the water to solids ratio up to the desired value is calculated by:

$$WM = WS * (CM + DD)$$

where WM = volume of water to be added (ml)
WS = desired water to solids ratio (ml/g)
DD = dry dust mass in filter cake(g)

As an example, for a mixture of 30% cement and a 1.18 water to solids ratio and using 200 g of wet filter cake with a water content of 32%:

$CM = 0.3 * 200 * (1 - 0.32) = 40.8g$ and $WM = 1.18 * (40.8 + 136) = 144.6ml$

3.2.4 Selection of Values for Operational Variables

(i) Open literature gave little assistance in selection of the **amount of cement** to be used in treatment processes. Percentages of cement to waste in literature reported studies range from 1%-2% for wastes with pozzolanic properties to up to 90% for liquid wastes. Based on initial exploration and consultation, it was decided to confine the range of cement additions used in the overall study to between 7% and 30% based on a dry mass of cement to dry solids in the filter cake. 7% was identified in initial laboratory investigations to be the minimum to give a product with an acceptable structural strength, while 30% would be the maximum which would be feasible in terms of costs and bulk increases when consigned to landfill. Where appropriate, selective tests were performed with higher cement additions.

(ii) Instead of controlling the water to cement ratio in the mix, the **water to solids ratio** was controlled. Due to the fineness of the particles in the filter cakes, far more water was required to

achieve a workable paste than is traditionally used in the manufacture of concretes. This observation is in line with texts such as PCI (1986). Water to solid ratios ranging between 0.86 and 1.5 were investigated in this work. It was found that higher water:solids ratios were required to obtain workable pastes in the case of the ETP products than in the FeCr Dust.

(iii) Although theoretically cement setting begins within a few minutes of contact between water and cement, it was found that a minimum **curing** time of two weeks was required before samples could be removed from their moulds intact, and a further two weeks required prior to being able to carry out the strength tests (see Chapter 5). No tests were therefore carried out before 28 days after mixing.

3.3 Conclusion

In the following sections of this thesis a variety of characterisations are carried out on the waste products described in this Chapter which have been solidified with cement. All samples were prepared using the techniques described here.

4.

Results of Fundamental Characterisations

Previous chapters have provided a background to S/S technology, the waste products of interest in this study and the procedure for preparation of the S/S products. This thesis considers characterisation of S/S products from two different aspects. In this chapter results of characterisations aimed at deducing the fundamental physical and chemical nature of the S/S product are presented. These include Scanning Electron Microscopy (SEM), Energy Dispersive X-Ray Spectroscopy (EDS), X-Ray Mapping, X-Ray Diffraction (XRD), Mercury Intrusion Porosimetry (MIP) and Permeability tests. The limitations of each tool are highlighted. Results are presented and discussed. At the end of the chapter a physico-chemical model of the product is proposed, drawing on both results of the fundamental characterisations and literature observations.

In Chapters 5 to 7 laboratory tests which establish strength and leaching characteristics of the S/S products are explored. Such tests are not only used to support the findings of the fundamental characterisations and the model presented in this chapter, but also provide information useful in predicting the behaviour of the S/S products in practice. This is discussed further in the relevant chapters.

4.1 Scanning Electron Microscopy (SEM), Energy Dispersive X-Ray Spectroscopy (EDS) Analyses and X-Ray Mapping

4.1.1 Background

SEM/EDS has been used widely in characterisation of the morphology of S/S products and distribution of the various elemental components therein [Ivey et al (1993), Mollah et al (1992), Ivey et al (1990)]. In SEM the surface of a material is scanned by an electron beam. The morphology at each point on the surface dictates the intensity of secondary electrons released at that point. These secondary electrons are collected and converted to light signals. A photomultiplier converts the light signals into electric currents which provide an image of the surface of the sample. This image can be viewed on a VDU or captured using image acquisition hardware such as camera film, video printers or computer files. The images thereby created are known as Scanning Electron Micrographs or SEM images.

In EDS analysis, the sample which is being examined is bombarded with X-rays. The high energy electrons from the X-Rays cause orbital electrons to be displaced from atoms in the solid, resulting in a vacancy within each individual atoms electron orbit. Electrons from a higher energy orbit immediately fill this vacancy and the difference between the two orbits is emitted as a X-ray Photon. The X-Ray Photon is characteristic of each element within the solid which is being bombarded. The X-Rays are measured using an energy dispersive solid state detector. The resulting spectrum of characteristic X-ray emissions allows for multi-element analysis.Matching routines are usually performed automatically by software which is built into the electron microscope.

Electron Microscopes can also be used for the purpose of X-Ray Mapping. The energies of X-Rays released by a scanned surface are interpreted to provide information as to the relative concentrations of various elements on that surface. X-Ray Mapping provides colour images representing a scanned surface. The intensity of colour at any point on the map indicates the concentration of the elements at that point.

4.1.2 Sample Preparation and Instrument settings

Prior to mounting specimens for SEM analysis are dried in an oven set at ≈70°C to constant mass. After drying, they are fractured using a sharp object and mounted onto stubs using a graphite-based glue, with the newly created fracture surfaces facing upwards. A small amount of 'silverdag' conductant is applied to ensure effective earthing of the material. Finally the stubs are sputtercoated with an Au/Pd coating and stored in a vacuum dessicator prior to analysis. For EDS and X-Ray mapping analyses, discussed in sections 4.1.3 and 4.1.4, the same preparation technique is used except that carbon coating is used instead of Au/Pd.

It is recognised that examination cryogenic fracture or freeze drying practices are preferable for the SEM examination of S/S products. No facilities were available for the former at UCT, while the latter was found to be excessively time-consuming, and, due to the number of sample which were examined for this work, was rejected as an option. For this reason, oven drying was used. It was noted in Chapter 2 that drying at below 105°C will not affect the CSH structure.

Ideally, it is preferable to scan an area which is flat, and polished samples are usually examined. The sample texture affects SEM only when the topology is so uneven that the sample's surface is not visible to the detector. It is noted that, when examining an unpolished sample, if high areas are brought into focus, the lower-lying areas may be out of focus. Furthermore, low areas may appear black if the number of electrons interacting with that area of the photo is low due to the positioning of the sample relative to the beam.

In this work an attempt was made to polish samples prior to SEM examination. Due to the putty-like nature of the samples, it was found that polishing smeared the surface of the sample and no useful scans were obtained from polished samples. For this reason, whilst recognising the limitations thereof as discussed, all SEM analyses presented are of unpolished samples.

In EDS analysis there is an approximately teardrop shaped interaction volume into the surface of the solid and for accurate quantitative analysis it is necessary to focus the electron beam onto the surface. Where voids exist within the sample, the signal may be weaker than expected and quantitative analysis may become difficult. This also applies to element mapping. Since unpolished samples were used in the analyses of samples presented in this work, only qualitative and semi-quantitative results could be obtained.

SEM/EDS and mapping analyses were performed on a Leica S440 Scanning Electron Microscope. Accelerating voltages of between 15 and 25 kV, and probe currents from 8 to 25 pA provided optimum resolution for SEM. For EDS analysis the probe current was adjusted to give count rates of ~ 2700 counts per second (cps). Counts were taken for 150s.

Samples for X-Ray Mapping were coated with Carbon. Analyses were carried out using a KEVEX ED detector attached to the SEM. Instrument settings found to be optimal for mapping include probe currents of between 800 and 1200 pA, EHT of 15 kV and a beam current of 300 pA.

It is noted that instrument settings are influenced by the type of filament fitted to the microscope at the time of analysis. During this work both tungsten and LaB_6 filaments were used.

4.1.3 SEM/EDS Results

The SEM/EDS analyses performed aimed at:

(i) Providing information on the effect of the composition of mixing water on the morphology and chemistry of the cement hydration products,
(ii) Characterizing the morphology and chemistry of the solidified FeCr Dust product and determining how this differs from pure cement and other S/S products presented in literature,
(iii) Determining the effect of the operational variables of interest (water to solids ratio, cement content and curing time) on the morphology and chemistry of the S/S product,
(iv) Identifying the effect of acid attack on the morphology and chemistry of the S/S product which will assist in predicting the long-term integrity of the S/S product.
Two sets of results are presented and discussed in the following sections. Section 4.1.3 satisfies aim (i) above. In section 4.1.3(b) selected images and scans, chosen as being representative of

the solidified FeCr Dust products under investigation here, are analyzed. This satisfies aims (ii) and (iii) above. Point (iv) is discussed in Chapter 7 and is not referred to further in this Chapter.

(a) Effect of Water Composition on Cement Hydration

To determine the effect of contaminated water on hydration, dry cement was mixed with the fluid of composition indicated in Table 4-1, referred to hereafter as "contaminated water". This water is representative of the filtrate recovered after washing the FeCr Dust for 1 hour in distilled water with a liquid to solid ratio of 10:1. The solution is high in zinc, magnesium, potassium and sodium. For comparison, control samples were made using distilled water. Both sets of samples were made with a 0.36 water to solid ratio, being the optimum for making hardened cement paste [PCI (1986)].

Table 4-1 - Composition of Water used for making "Contaminated" Cement Pastes (concentrations in ppm)

pH	Cr (tot)	Cr(VI)	Zn	Mg	Ca	Si	K	Na
6.6	15.7	14.1	581	313	33.7	10	849	1954

SEM micrographs of the contaminated and uncontaminated cement pastes cured for 24 hours and 28 days are presented in Figure 4-1 to Figure 4-4. Figure 4-2 and Figure 4-4 show the uncontaminated hcp structure to be identical to that identified by workers such as Double (1983) and Double and Hellawell (1977) .

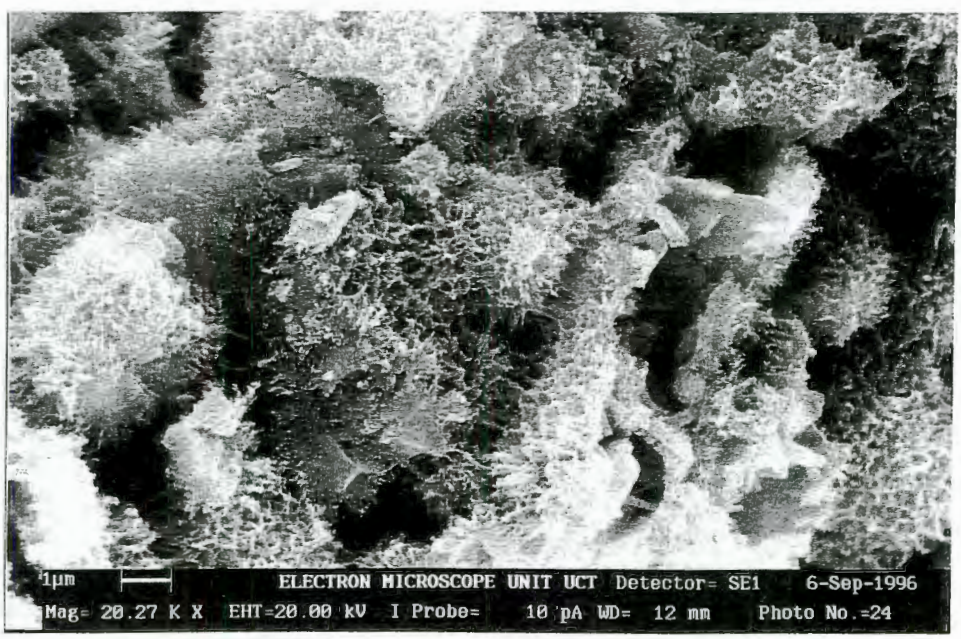

Figure 4-1 - "Contaminated" Sample after 24 Hours Curing

After 24 hours the development of fibrillar structures emanating from the surface of the cement particles is evident in Figure 4-2. At 28 days these have meshed to form an interwoven network of fibres, the interlocking of which is primarily responsible for the ultimate strength of the cement paste. This is seen in Figure 4-4. Cement made with contaminated water is similar in morphology to the control samples. For cements cured for 24 hours, little difference between the contaminated and control samples can be seen (see Figure 4-1 and Figure 4-2).

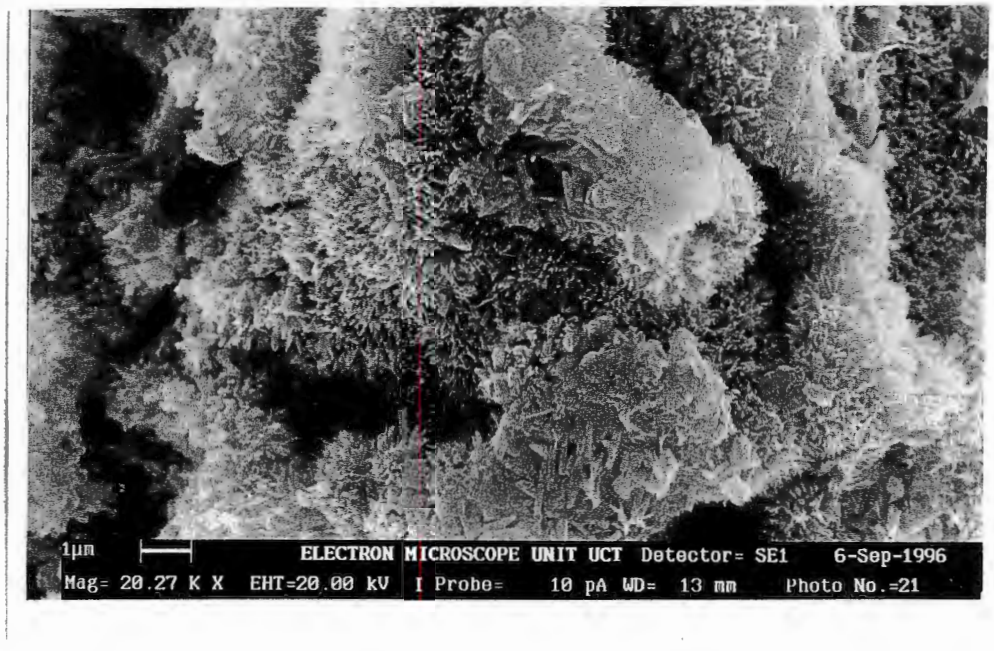

Figure 4-2 - Hardened Cement Paste after 24 Hours Curing

However for the cements photographed in Figure 4-3 and Figure 4-4 which have cured for 28 days it appears that the cement made with contaminated water has a lower density of cement hydration product (the 'fibrillar' structure identified previously) than uncontaminated cement. Furthermore the fibrils are shorter in length. This observation was constant for all further setting times investigated. Several researchers have made shown that metal species affect the morphology of cement. Literature observations presented in Chapter 2 showed the presence of a metal species in the mixing water to have the potential to accelerate, decelerate or completely inhibit cement hydration. The presence of zinc, chromium, magnesium, sodium and potassium in the mixing water of the samples presented here are all suggested to impact on cement hydration behaviour, ultimately resulting in a less developed cement structure. Isolating the individual effect of each of these elements on hydration is difficult due to the complex nature of the hydration reactions.

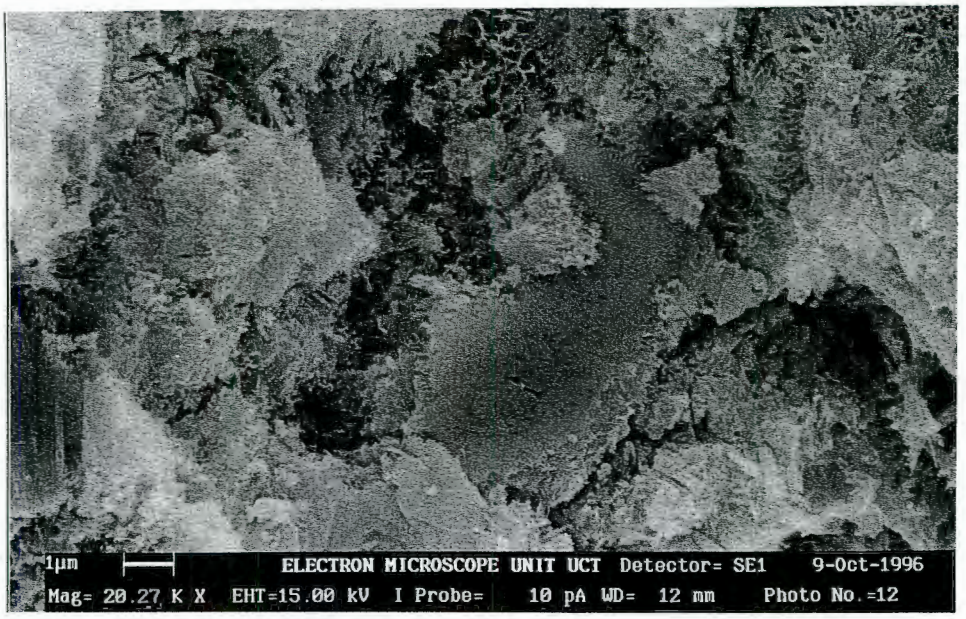

Figure 4-3 - "Contaminated" Sample after 28 Days Curing

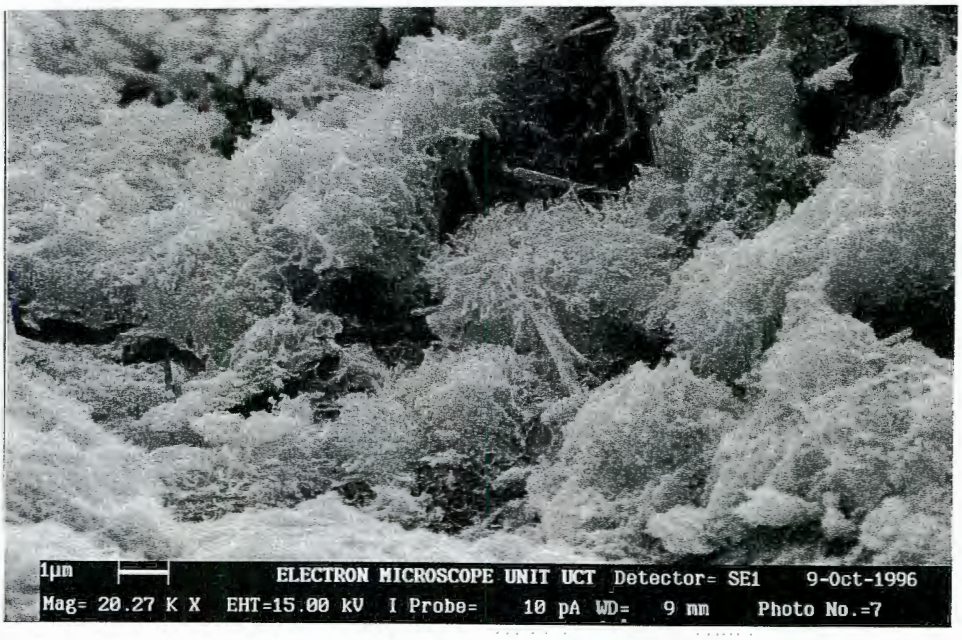

Figure 4-4 - Hardened Cement Paste after 28 Days Curing

In samples made with both contaminated and distilled water the presence of crystals which resemble Portlandite ($Ca(OH)_2$) identified by other workers was observed qualitatively. EDS analysis confirmed such crystals to contain calcium. The presence of metals in the filtrates therefore has no obvious effect on Portlandite formation.

EDS spectra of an area of approximately 1µm by 1µm of the solid surfaces were obtained. The scans are presented in Figure 4-5 and Figure 4-6 for cement pastes made with pure water

and cured for 12 days and 104 days respectively. For pastes cured for 12 days, Ca:Si ratios can be observed to range from 1.8 to 2.9 (all ratios presented here refer to molar ratios).

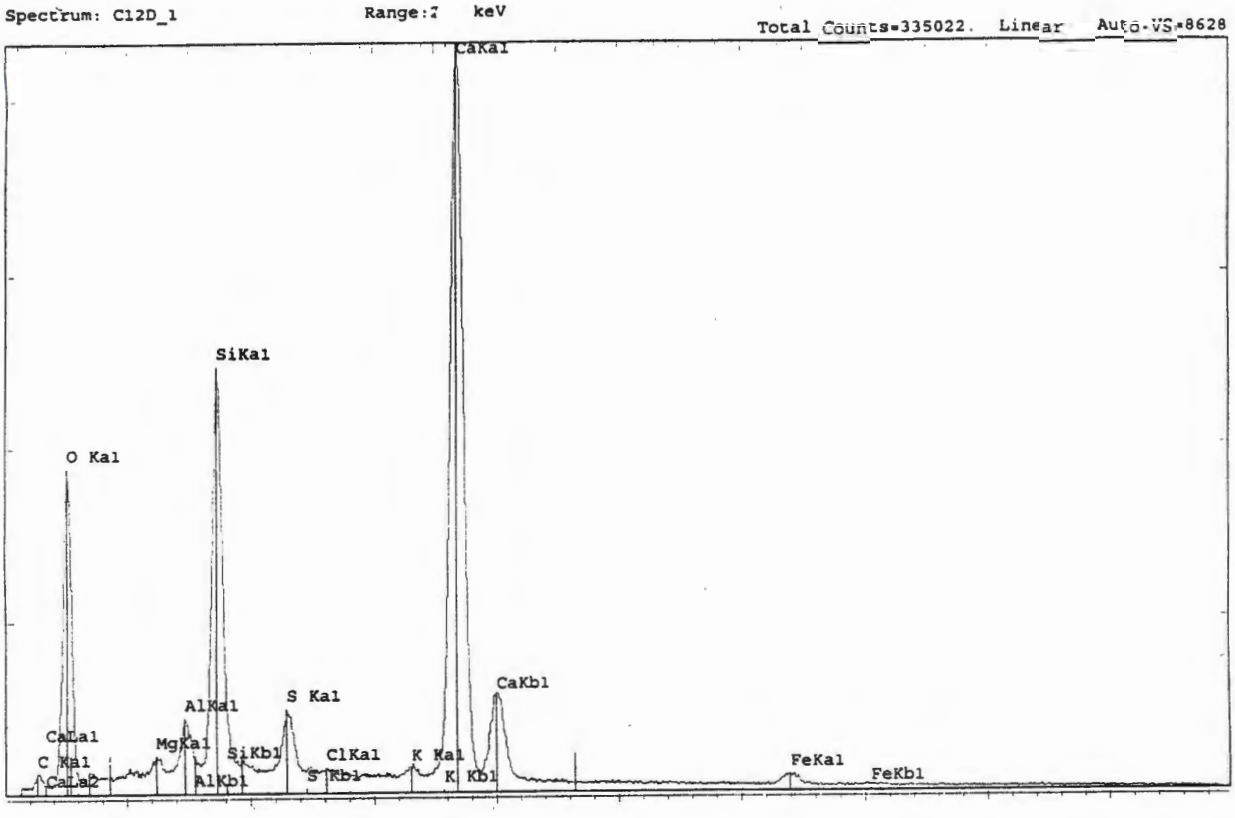

Figure 4-5 - EDS of Hardened Cement Paste after 12 Days Curing

In the case of pastes which had cured for 104 days, Ca:Si ratios were in the region of 1.7. Unhydrated cement is expected to have a Ca:Si ratio of ~ 2.5, while Calcium Silicate Hydrate (CSH), the primary cement hydration product, is expected to have a Ca:Si ratio of between 1.5 and 2.0 [Glasser (1993), Double (1983)]. This indicates that both CSH and unhydrated cement were present in the 12 day cured samples, while CSH gel is the dominant structure in the 104 days cured pastes. This is in line with expectations derived from literature reports.

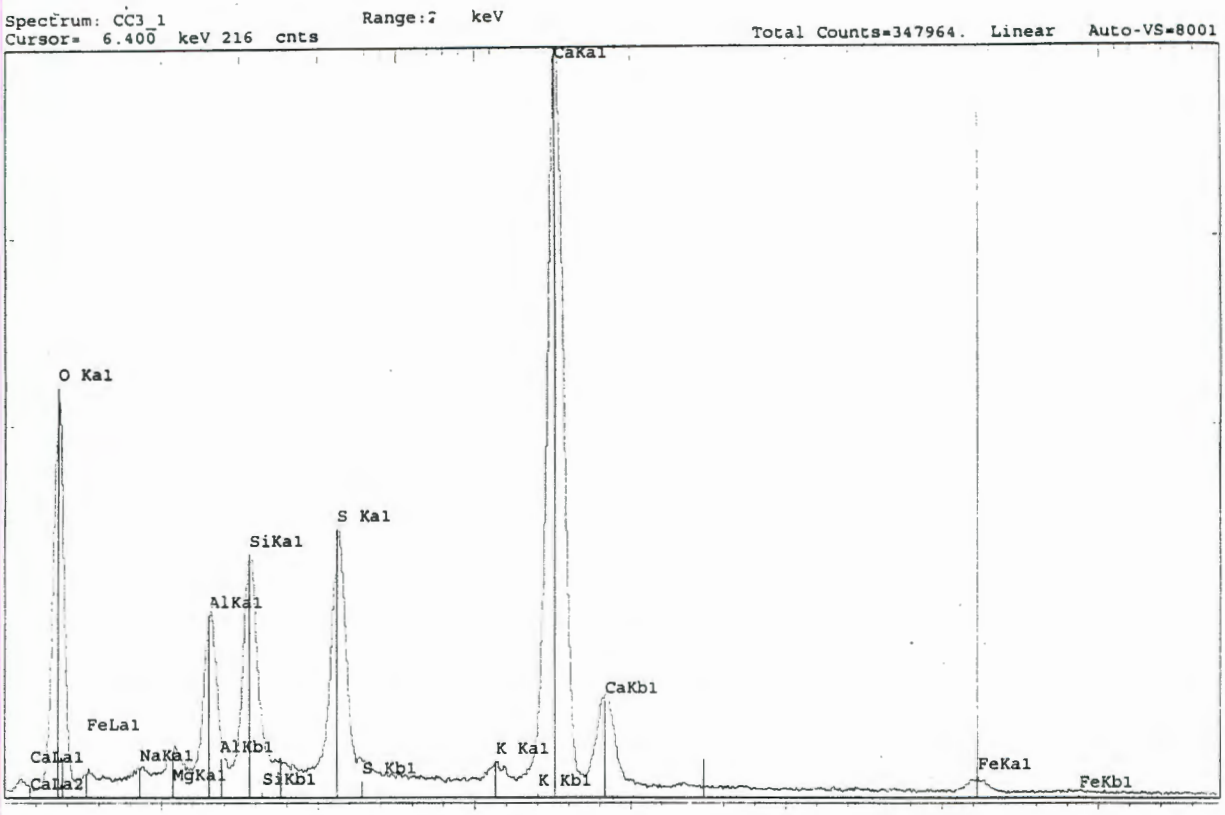

Figure 4-6 - EDS of Hardened Cement Paste after 104 Days Curing

An EDS scan of cement made with 'contaminated' water, presented in Figure 4-7, shows Ca:Si ratios ranging from 1.6 to 1.9 after 104 days curing. This is similar to the range observed for the distilled water control sample. Based on this observation it is suggested that the Ca:Si ratio of the CSH product is not significantly altered by the presence of metals in the mixing water. The Mg content of the scanned region in the contaminated sample is higher than in uncontaminated cement. This is attributed to Mg from the mixing water substituting for Si into the CSH structure as discussed in Chapter 2.

No Cr or Zn was detected by EDS in any of the scanned regions, even though they are present in the mixing water of the contaminated samples. It is suggested that either these elements are not chemically incorporated into the structures, and hence are not detected in the surface scan, or they are present in concentrations below the detection limit of the EDS.

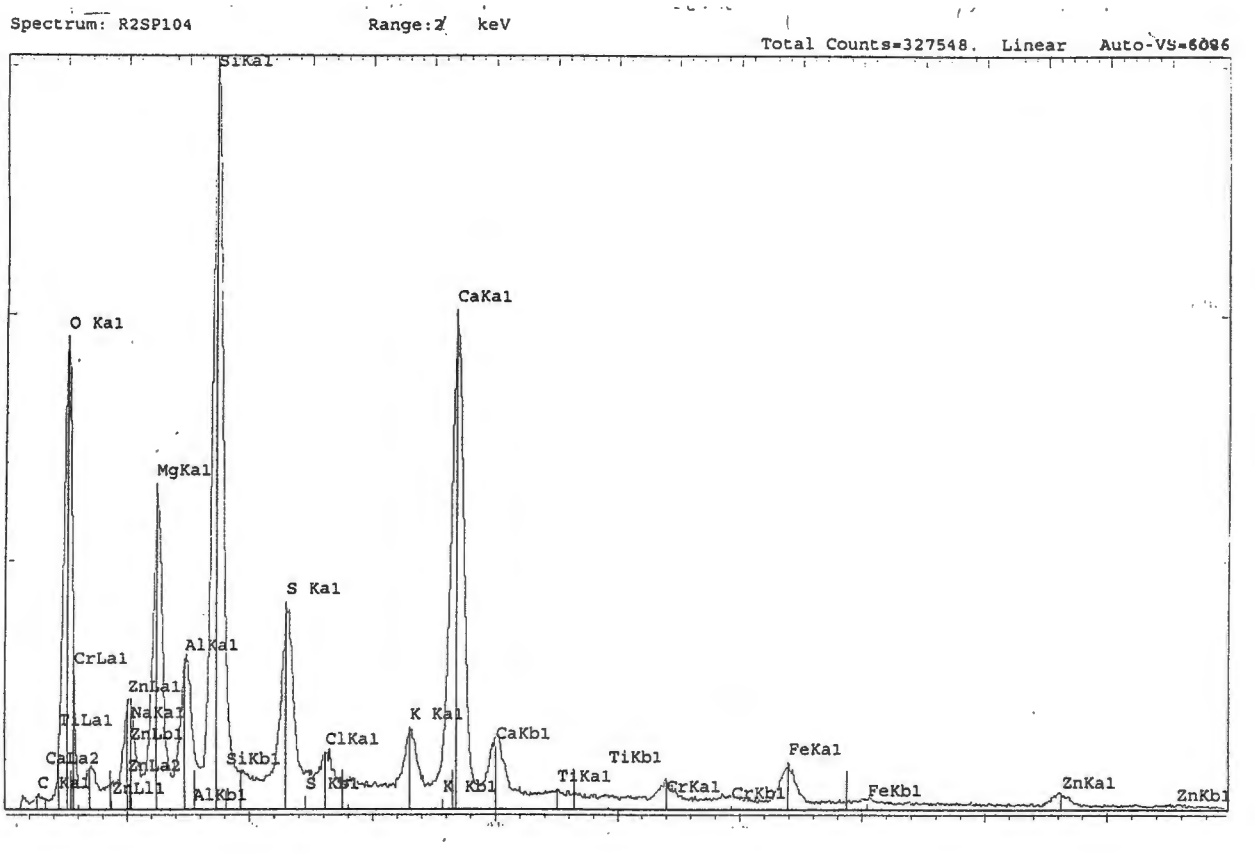

Figure 4-7 - EDS Scan of "Contaminated" Sample after 104 Days Curing

(b) SEM/EDS Results from the Solidified FeCr Dust Products

SEM Observations

Although the presence of metal species in the mixing water did not significantly affect the composition or structure of the cement product, the morphology of the solidified FeCr Dust is expected to be significantly different to that of the hardened cement paste. Firstly, a large proportion of the total solids will be the solid dust material. Secondly, the presence of the fine dust material is expected to affect the growth of the cement hydration products. Finally, a much higher water content is used in the mixing of the S/S products than cement as discussed in Chapter 3. This not only affects the porosity of the product but may also affect the microstructure of the cement hydration products [PCI (1986)].

Figure 4-8 to Figure 4-15 show micrographs of the solidified FeCr Dust. Comparison of the micrographs of the S/S product presented in Figure 4-9 and Figure 4-12 with that of hcp in Figure 4-4 shows the formation of the fibrillar matrix in the S/S product to be almost nonexistent relative to that found in hcp. Closer inspection of the S/S product in Figure 4-8 and Figure 4-10 shows that the fibrils do exist, although they are shorter than those seen in cement and do not form the same extensive interlinking network.

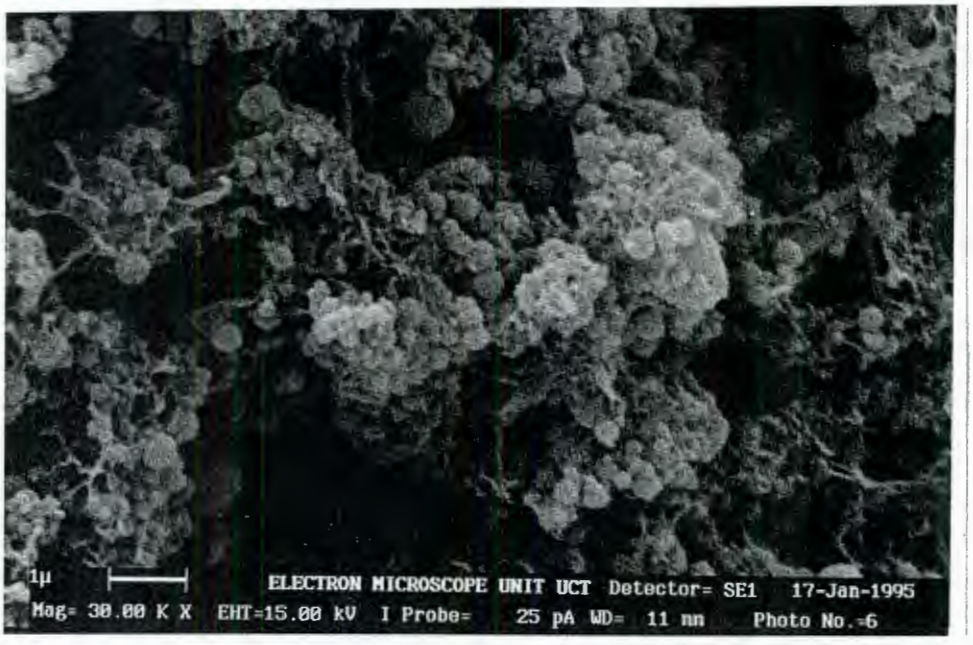

Figure 4-8 - SEM of S/S Product

26% Cement, 0.94 w/s, 150 Days Curing, Mag = 30000x

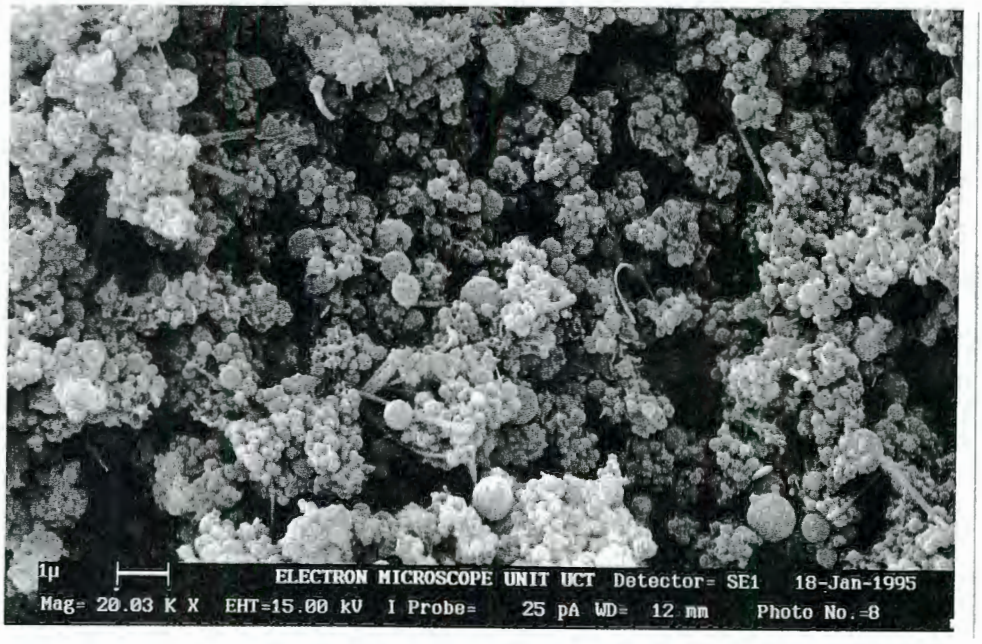

Figure 4-9 - SEM of S/S Product

26% Cement, 0.94 w/s, 58 Days Curing, Mag = 20000x

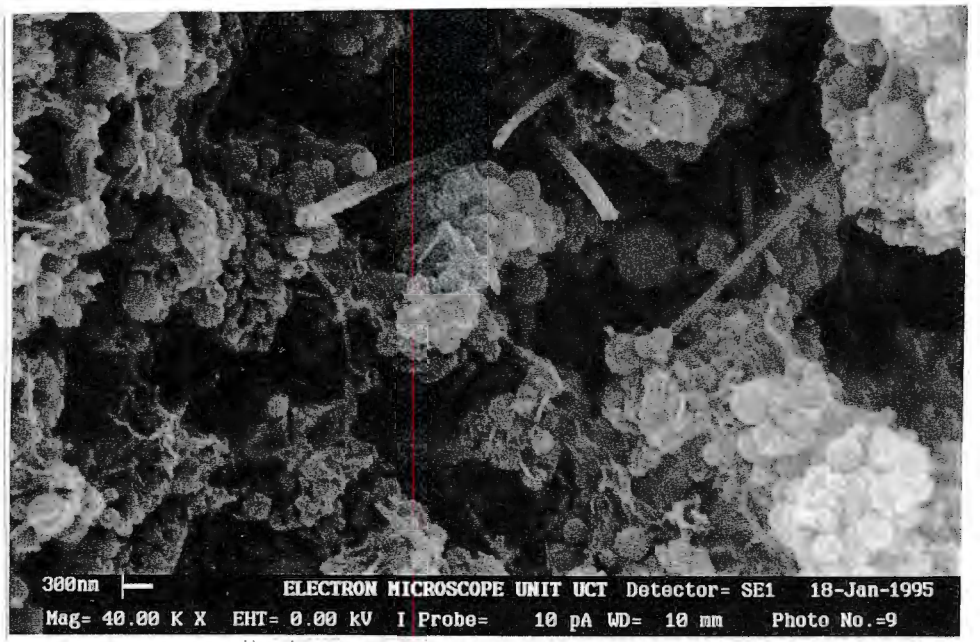

Figure 4-10 - SEM of S/S Product

20% Cement, 0.9 w/s, 104 Days Curing, Mag = 40000x

Portlandite crystals observed in pure and contaminated hardened cement pastes are absent from the S/S products. The spherical FeCr Dust particles, shown in Figure 3-2, form the dominant solid components of the S/S products. The S/S product is thus an agglomerate of dust particles, bound together by a small amount of cement hydration product. This cement hydration product is characterised further using EDS techniques described below.

While acknowledging the different magnifications in Figure 4-8 and Figure 4-9 a comparison of these micrographs indicates that as curing time increases, the integrity of the matrix appears to improve. Cement hydration proceeds slowly as a function of time, and as hydration proceeds, so the integral nature of the structure increases. The observation is consistent with those for cement pastes presented in section 4.1.3(a) and literature reports.

Water to solids ratio affects the size and volume of the pore spaces in an agglomerate. Comparing Figure 4-10 with Figure 4-11 shows that, as the water to solids ratio is increased, the product becomes more porous. This is in line with the discussion presented in Chapter 2 and observations presented in section 4.3.2 which follows.

Figure 4-11 - SEM of S/S Product

20% Cement, 1.48 w/s, 104 Days Curing, Mag = 7300x

The amount of cement present in the solidified dust products determines the ultimate volume of cement hydration product which can be formed. Figure 4-12 to Figure 4-15 show samples made with increasing amounts of cement. It is noted that, as the cement content increases, the water requirement for obtaining a workable paste during mixing decreases. The sample compositions examined in these micrographs were chosen to correspond with those characterised by the strength tests of Chapter 5 and the leaching tests of Chapter 6 and 7.

These micrographs can be compared to pure cement shown in Figure 4-2 and Figure 4-4. Associated with the increase in cement content is an increase in the connectivity of the fibrillar structures. Three reasons are offered for this observation. Firstly, as the cement content is increased, more cement hydration product will be formed. Secondly, in Chapter 2 it was indicated that a fine aggregate can have a significant negative effect on cement hydration and bonding - Malone et al (1983) recommend that not more than 3% of the total aggregate should be less than 75 µm when mixing concrete. In solids with less dust, and hence more cement, this effect is reduced. Finally, the lower water content associated with increased cement addition leads to the formation of a less porous solid as discussed above.

In summary, it is seen that the physical nature of the solidified FeCr Dust product is a porous structure in which the dust particles are held together by fibrillar cement hydration products, the degree of development of which depends on the cement content in the product and the time allowed for curing.

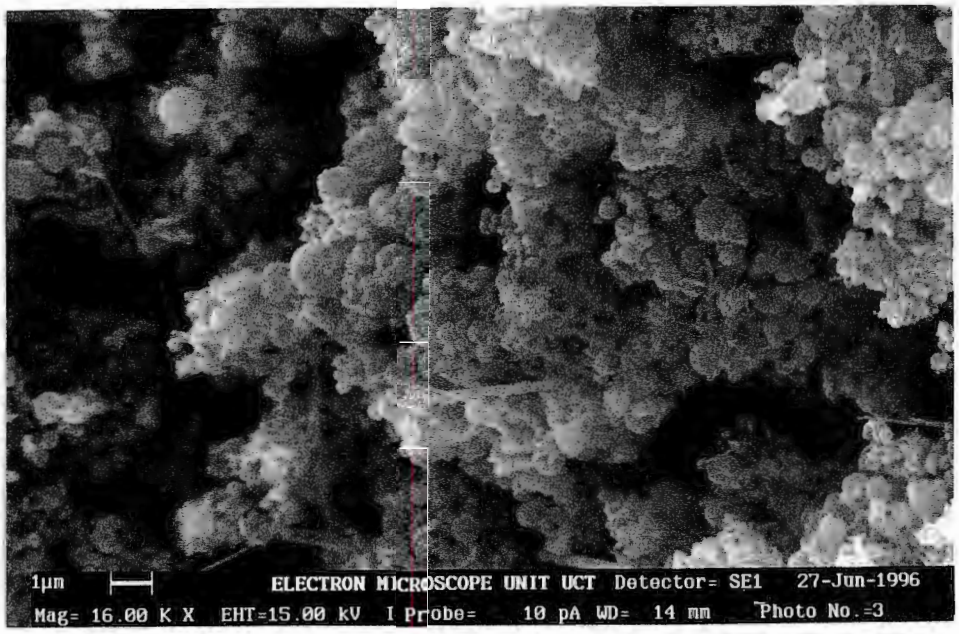

Figure 4-12 - SEM of S/S Product

20% Cement, 1.48 w/s, 104 Days Curing, Mag = 16000x

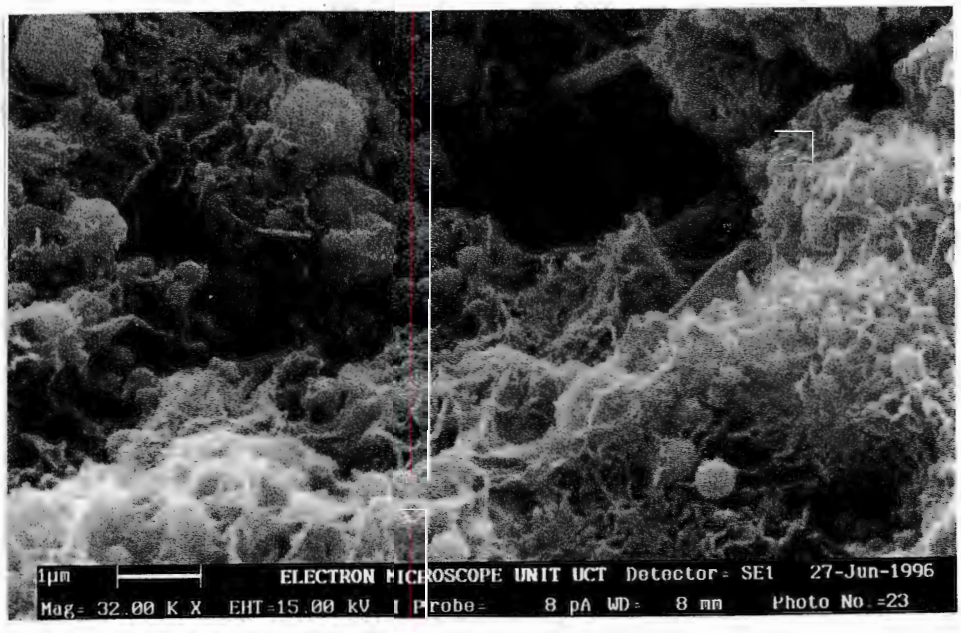

Figure 4-13 - SEM of S/S Product

30% Cement, 1.36 w/s, 104 Days Curing, Mag = 32000x

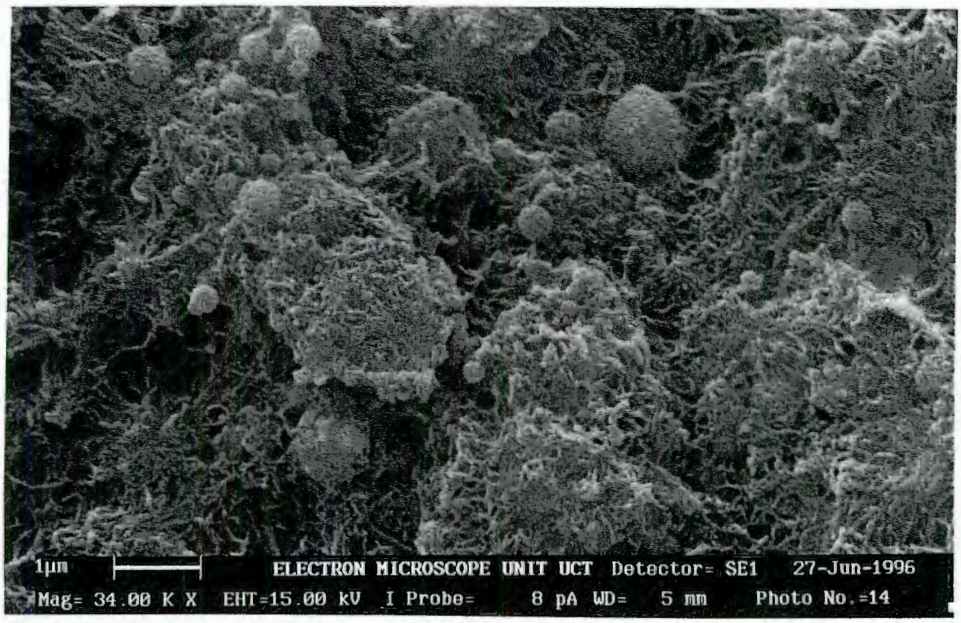

Figure 4-14 - SEM of S/S Product

50% Cement, 1.12 w/s, 104 Days Curing, Mag = 34000x

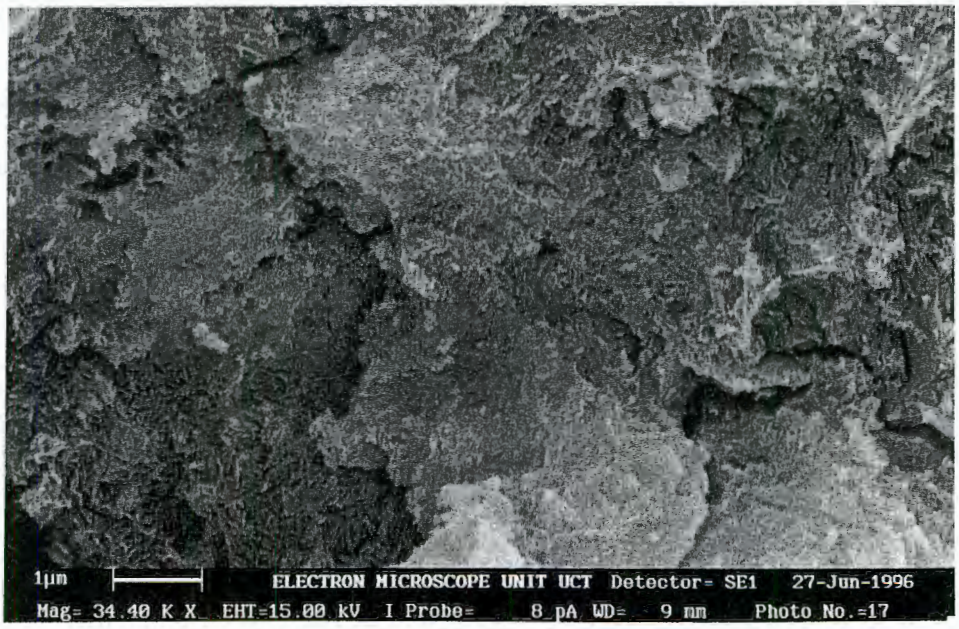

Figure 4-15 - SEM of S/S Product

75% Cement, 0.86 w/s, 104 Days Curing, Mag = 34400x

EDS analyses

An EDS spectrum representative of the S/S products observed in Figure 4-8 to Figure 4-13 is presented in Figure 4-16, again for an area of approximately 1μm by 1μm. A considerable difference between the composition of these structures and that of hardened cement pastes (hcp) (Figure 4-6) is observed. Ca:Si ratios are between 0.33 and 0.64 versus 1.7 for hcp. A summary of the results for hcp, the "contaminated" hcp and the S/S product appears in Table 4-2.

Table 4-2 - Ca and Silica in the cement hydration product for hardened cement paste, "contaminated" hcp and the S/S Products as determined by EDS

Material	Calcium Content	Ca:Si Ratio
hcp	63-68% CaO (w/w)	1.7
"Contaminated" hcp	approx. 68% CaO (w/w)	1.6 to 1.9
S/S product	10% Ca (w/w)	0.33 to 0.64

The differences between hcp and the S/S products are explained as follows. Firstly, cement contains 63-68% CaO [PCI (1986)] while the S/S products contain less than 10% Ca (on a mass basis). Since formation of the cement hydration product is as a result of precipitation of calcium and silica from solution, the lower total calcium contents in the solidified FeCr Dust versus the cement will result in lower Ca:Si ratios. Secondly, calcium may be consumed by the formation of complexes with other metals in the pores: it has been suggested previously that compounds such as calcium zincate may form [Cocke and Mollah (1993)].

The EDS spectrum identifies the presence of Cr and Zn in the cement hydration products in trace amounts. These elements may be incorporated within the solid, physisorbed on the surface of the solid, or merely deposited during drying of the samples prior to SEM examination.

Based on the EDS results, therefore, the CSH found in the S/S products is suggested to be lower in Ca than in hardened cement paste. No evidence of the incorporation of Cr or Zn into the hydration products is found from the EDS results. The results of Table 4-2 are used further in the interpretation of leaching data in Chapters 6 and 7.

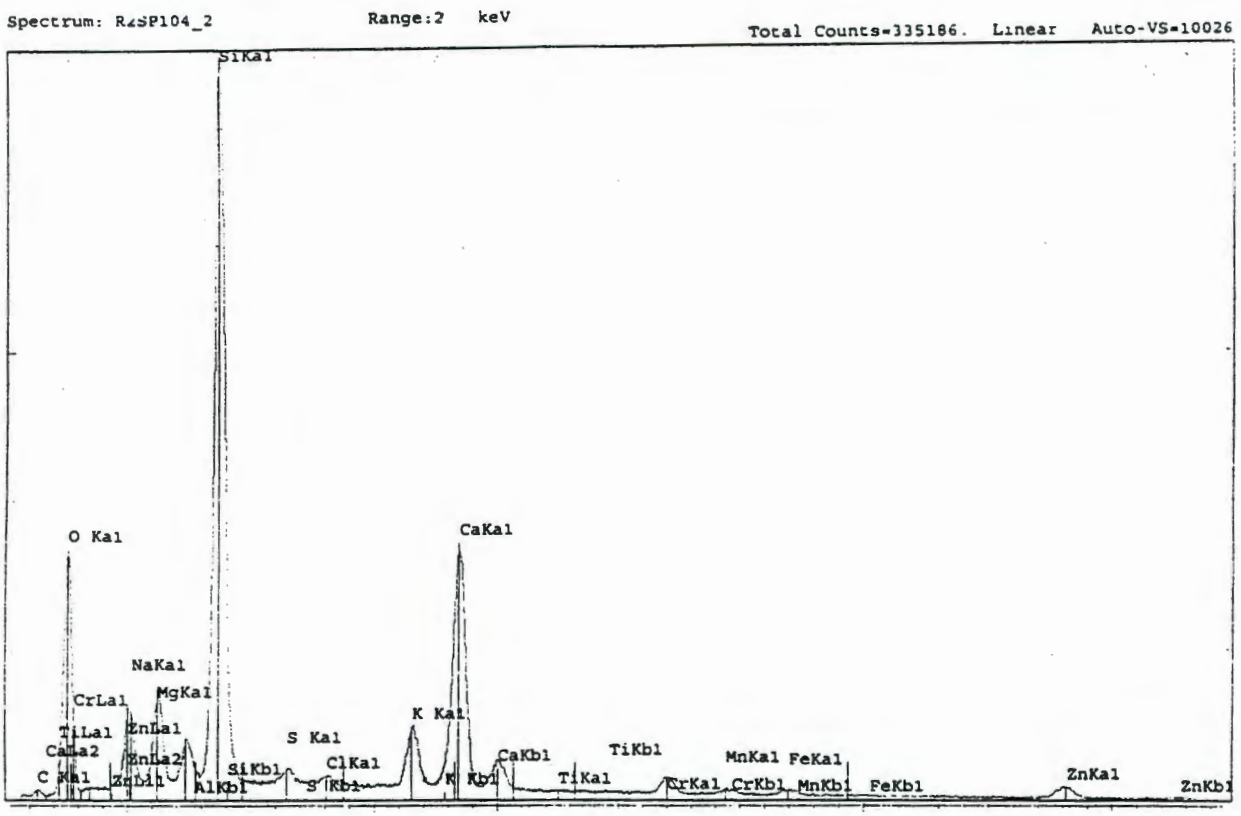

Figure 4-16 - EDS of S/S Product

30% Cement, 1.36 w/s, 104 Days Curing

4.1.4 X-Ray Maps of Solidified FeCr Dust

Figure 4-17 and Figure 4-18 present maps indicating typical distributions of elements for the images such as those presented Figure 4-8 to Figure 4-15. The intensity of colour indicates the concentration of a specific element at any particular point. Quantitative analysis was not possible for two reasons. Firstly, as in the case of EDS analysis, an interaction volume into the sample surface occurs, which makes acquiring a high degree of resolution, and hence accurate quantitative data, difficult. Since unpolished samples were analysed in this work, quantitative data could not be obtained. Secondly, no standards were available for this product which also contributed to the lack of quantitative analyses. The following qualitative observations are, however, highlighted:

(i) *Chromium* appears to be localized at various points through the scanned area, although small amounts are seen throughout the sample. Figure 4-17 and 4-18 show the high Cr concentrations to be associated with high concentrations of both *Fe* and *Zn*. This is most likely due to the presence of $(Fe,Zn)Cr_2O_4$ which forms in electric arc furnaces and hence is expected to be found in FeCr Dust. Furthermore, areas with high concentrations of Cr are sometimes associated with high iron concentrations in the absence of zinc. The ore in

ferrochrome smelters is chromite ($FeO.Cr_2O_3$) . The central core of the dust products is expected to be the residual from the original ores, hence the existence of the iron-chrome interaction [Gencor (1996)].

(ii) *Zinc* is evenly distributed over the entire scanned area. No localization of Zn is observed. Zinc is therefore suggested to be contained in the pores and during drying prior to SEM, deposited evenly over the solid surface. The potential for the formation of calcium zincate has been suggested. No common high calcium-zinc concentration areas are observed and hence no support for the formation of calcium zincate suggested in Chapter 2 is provided by the X-Ray maps.

(iii) *Silica* is the dominant component and is observed in high concentrations everywhere in the sample. Si is one of the primary component of both the dust material and cement. The high concentrations and even distributions are thus expected.

(iv) Areas with high *Potassium, Sodium* and *Magnesium* concentrations show low *Calcium* levels. Cement hydration is due to a precipitation reaction with silica in the pore solution. Furthermore, in Chapter 2, it was suggested that the hydrated cementitious product is variable in composition. At points of high K, Na and Mg concentrations, these cations may have substituted for Ca in the cement structure, and hence the low calcium concentrations at these points.

In summary therefore, the majority of the Cr is seen to be primarily contained at localized points in the structure, assumed to be in the form of $FeO.Cr_2O_3$. This complex is stable which has implications for the long-term stability of the product, discussed further in Chapter 6. Further Cr is distributed throughout the sample. Zn, however, appears to be deposited on the solid surfaces during drying. This would suggest that Zn is contained in the pores of the S/S products either as a soluble or insoluble species. Finally, it was observed that K, Mg, and Na can replace Ca in the cement hydration products.

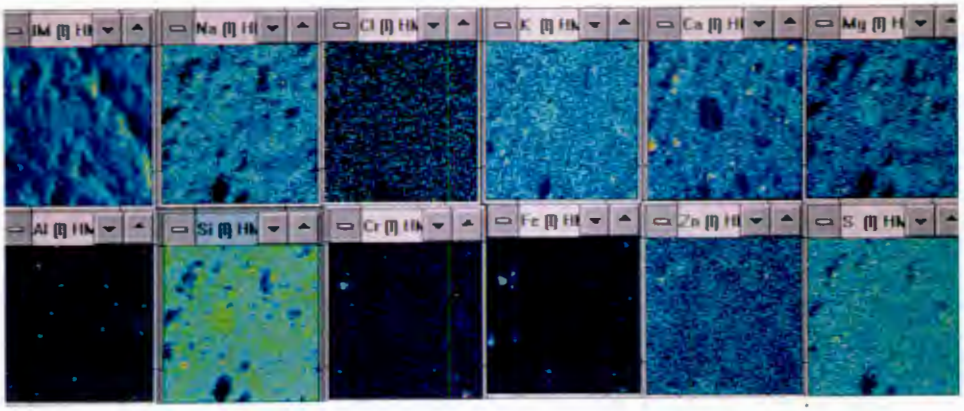

Figure 4-17 - X-Ray Map of S/S Product

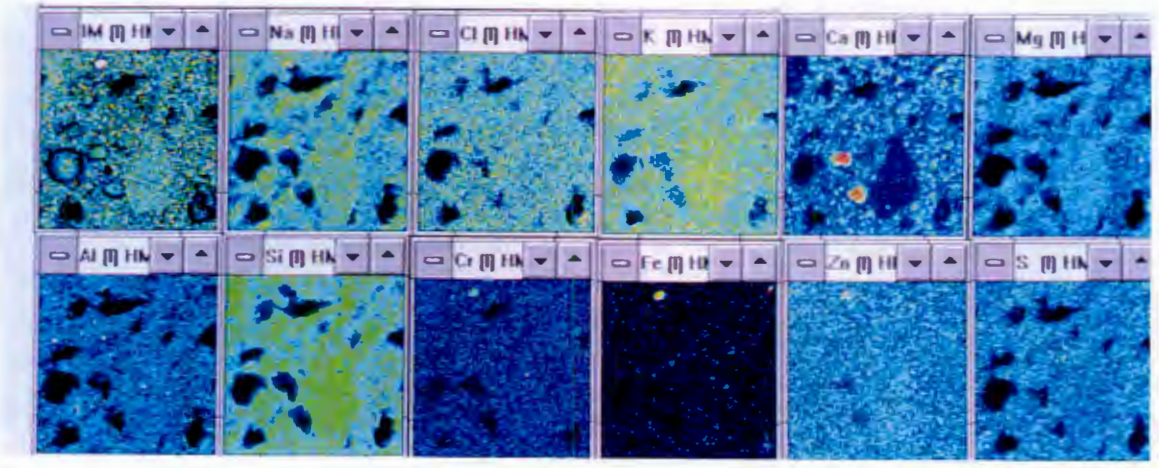

Figure 4-18 - X-Ray Map of S/S Product

4.1.5 Limitations of SEM/EDS and Mapping Techniques

Sample preparation, mounting and coating techniques can affect results and should be kept constant. Variables such as drying time and temperature prior to sample mounting, and the

manner in which samples are fractured and handled, all have an influence on the structure of the sample surface. Furthermore, optimization of the electron beam affects observations. Optimization is a sensitive procedure and it is often not possible to obtain an identical beam each time the microscope is used.

For quantitative EDS and X-Ray mapping it is necessary to have standards from which to work. Without such standards, the relative proportions of various elements in the solid can be identified. No further quantitative information can be obtained.

It is once again stated that SEM observations are, to some degree, subjective. When analysing highly heterogeneous samples such as S/S products, the possibility exists that photographed areas are not representative of the sample. Visually inspecting an entire sample prior to capturing a micrograph ensures that representative micrographs are obtained.

4.2 X-Ray Diffraction (XRD)

4.2.1 Background

X-Ray Diffraction (XRD) techniques are based on the work of William and Lawrence Bragg [Laidler and Meiser (1982)]. X-rays are electromagnetic radiation with wavelengths of about 100 pm and are produced by bombarding a metal with high energy electrons. The electrons decelerate as they plunge into the metal and generate radiation with a continuous range of wavelengths. When passed through a crystal structure these X-rays are diffracted, with the angle of diffraction determined by spacings between the atoms in the crystal structure. The d-spaces (distances in the crystal lattice) and intensity of the rays for over 33 000 compounds have been documented [Sarkar (1992)]. Matching of observed diffraction patterns from materials with known patterns, via knowledge of the chemical composition of the materials and computer based search techniques, enables characterisation of crystal phases.

Sample preparation for XRD involves grinding the specimen to uniform particle size if possible. This is important to get a good packing without orientation. The packing procedure is significant as it is easy to orientate the crystals during packing and thereby influence peak intensities. This is avoided by randomising the orientation by side or back loading the sample. All samples for XRD were ground to approximately one micron. In scanning, the source of radiation used for these samples was $Cu_{k\alpha}$. During scanning a step size of 0.1° 2θ and a scan rate of 0.1° 2θ /s was used.

4.2.2 Discussion of Results

Figure 4-19 presents the XRD trace of hardened cement paste made with distilled water with a w/s ratio of 0.36 and cured for 104 days. Once again, this is regarded as the optimum w/s and 104 days is a "fully cured" sample. Peaks for $Ca(OH)_2$ (Portlandite) and CSH (in the form of either $Ca_{1.5}\ SiO_{3.5} \bullet xH_2O$ or Kilchoanite $Ca_9Si_6O_{21} \bullet H_2O$) are identified. These crystalline CSH structures have Ca:Si ratios of 1.5 which is in accordance with those identified in the EDS results of section 4.1.3. No ettringite or other crystalline calcium sulphate structures were detected in the hardened cement pastes. This is explained in two ways. Firstly, ettringite is expected to form immediately upon contact of the cement with water. After a few days, this ettringite is expected to convert to crystalline calcium sulpho-aluminate [Alexander (1993)]. Secondly, considering the low Al contents found in OPC, it is suggested that formation of ettringite and crystalline calcium sulpho-aluminate is minimal.

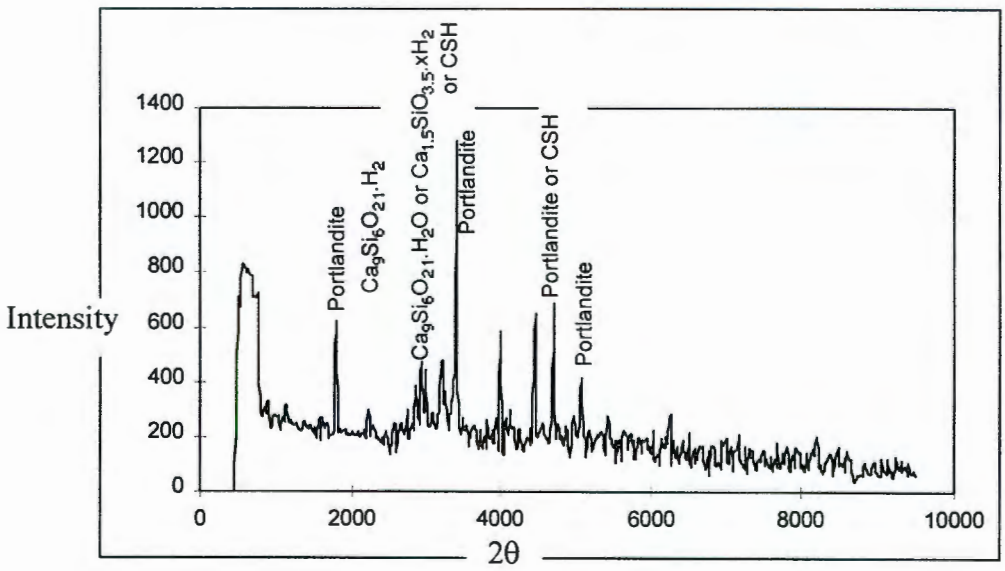

Figure 4-19 - XRD Trace of Hardened Cement Paste, 104 days Curing

A XRD plot of a sample of cement made with 'contaminated' water as described in section 4.1.3(b) appears in Figure 4-20. The same crystalline structures as those found in the uncontaminated cement can be observed, indicating once again that the presence of metal species in the mixing water at concentrations found in the filtrate from the FeCr Dust does not alter the nature of the crystalline CSH phase. This is in line once again with EDS observations of section 4.1.3.

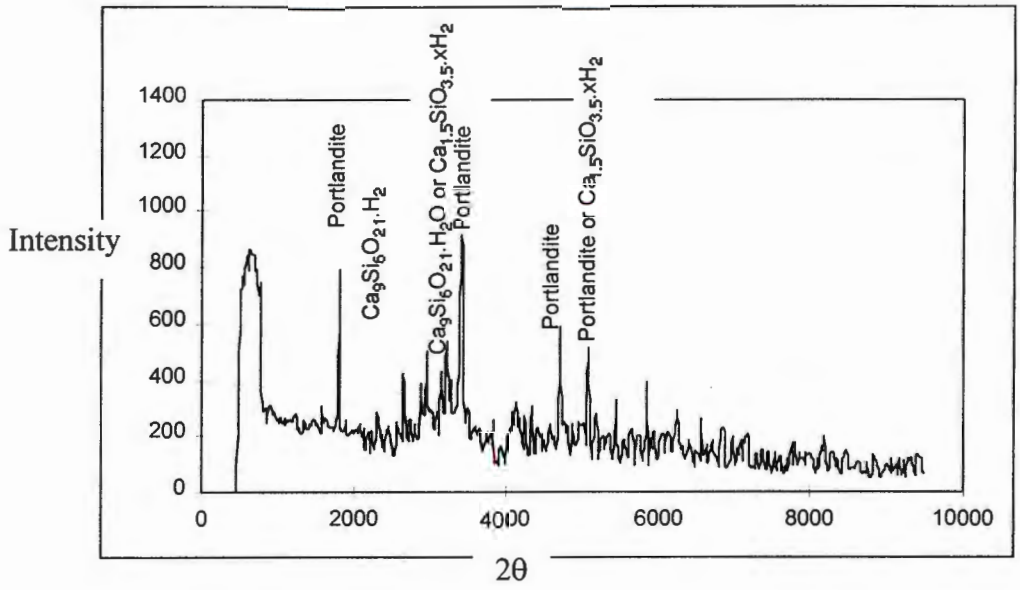

Figure 4-20 - XRD Trace of "Contaminated" Cement, 104 days Curing

It is noted here that XRD only detects *crystalline* structures. Since CSH is primarily amorphous (non-crystalline) only a small proportion of the CSH can be characterised by XRD [Double (1983)].

XRD scans are presented in Figure 4-21 and Figure 4-22 for the S/S product. These are typical of those observed for the S/S products. From the plots it appears that the products are primarily amorphous. Neither of the crystalline CSH products identified for the hardened cement pastes were identified in the S/S products. Two suggestions are made for this observation. Firstly, the CSH which does form may be amorphous and is therefore not detected on the XRD scans. Secondly there is far less cement in the solidified FeCr Dust product and hence the quantity of CSH formed is less than in hcp. The EDS analyses of section 4.1.3 suggested that the CSH product in the S/S product is different in chemical structure to the cement pastes.

Classification of the peaks on the scan of the S/S product was difficult as computer based scan- and match- databases were unable to identify the peaks on the plot. The S/S products show no evidence of formation of crystalline Portlandite ($Ca(OH)_2$). This is consistent with observations from SEM images presented in section 4.1.3(b). Two suggestions were made previously for this observation. Firstly, the cement contains 63-68% CaO [PCI (1986)] while the S/S products contain less than 10% Ca (on a mass basis). Secondly, any Ca which may be released into the

pores may combine with other metals in the pore solution to form complexes other than Portlandite. Other peaks may represent anhydrous cement compounds, but this could not be confirmed.

XRD has thus established that the S/S products are amorphous, and that crystalline Portlandite is not found in these products.

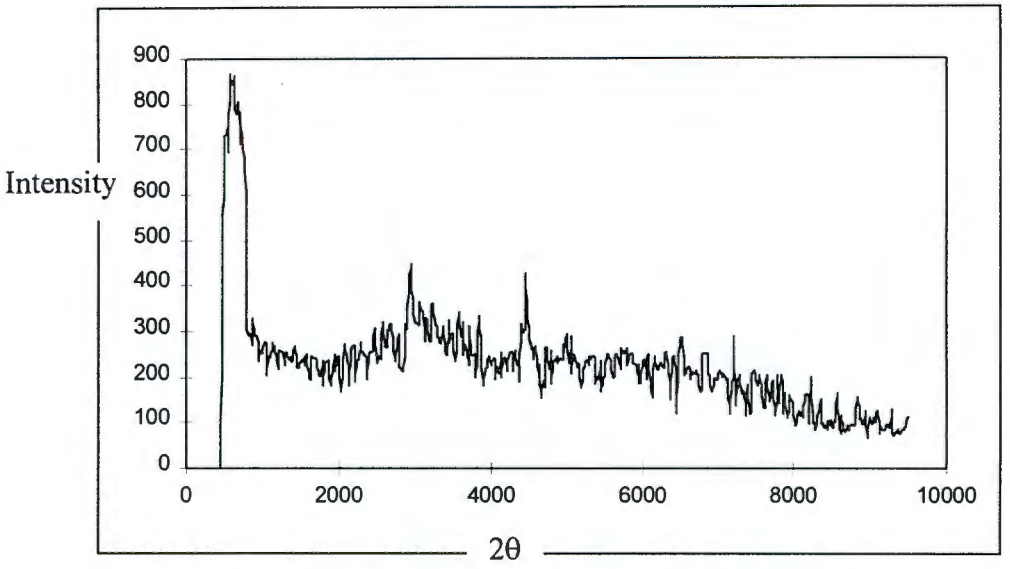

Figure 4-21 - XRD Trace of Solidified FeCr Dust

20% Cement, 0.9 w/s, 104 Days Curing

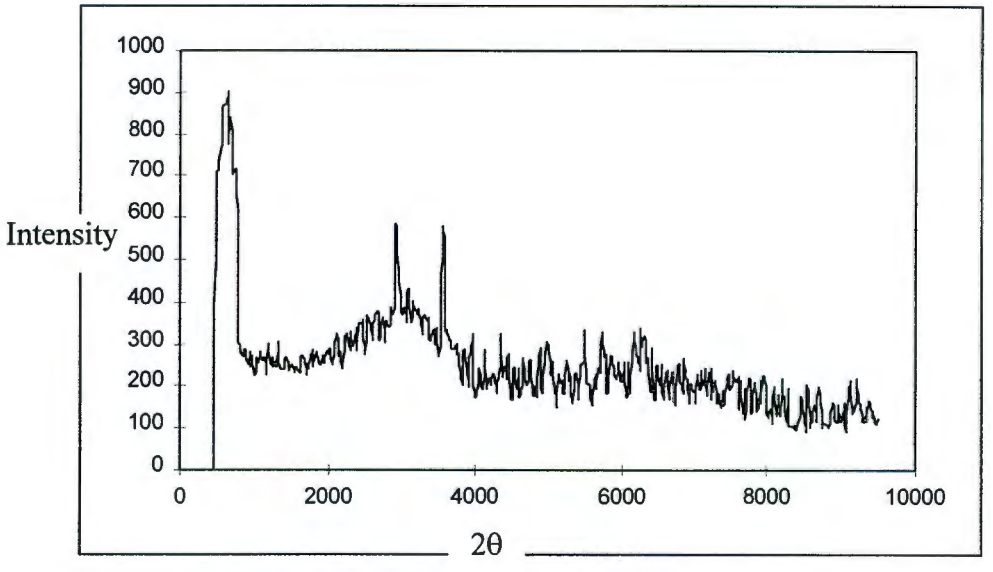

Figure 4-22 - XRD Trace of Solidified FeCr Dust

30% Cement, 1.36 w/s, 104 Days Curing

4.3 Mercury Intrusion Porosimetry

Mercury Intrusion Porosimetry (MIP) characterizes the pore size distribution and pore volume of solid materials. These two parameters are important in assessing the extent of setting of the cement and the degree of cross-linking of the cement hydration products in the S/S products. They are also related to the permeability of the cement product and are therefore suggested to be representative of the accessibility of leachants to sites at which contaminants are contained in a S/S product, resulting in leaching from the solid [Goto and Roy (1981)]. This is explored further in Chapters 6 and 7. MIP has shown good correlation between pore structure and permeability [Poon et al (1986)].

MIP has been used previously to determine the effect of addition of different chemical species to cement, and to determine the change in pore structure during leaching. Some support has been provided by MIP for theories on the mechanisms of containment and leaching of lead and mercury from a solidified product [Sollars and Perry (1989)].

In MIP analysis, isolated pores which have no access to the exterior cannot be detected.

4.3.1 Functioning of a Mercury Intrusion Porosimeter

A sample of predetermined mass is placed into a special holder known as a penetrometer. The penetrometer is placed in a low pressure chamber on the porosimeter and a vacuum is created. Mercury is transferred into the sample holder. The chamber is slowly pressurised and the volume of mercury intruded versus required pressure to effect intrusion is monitored on an incremental basis. The size of the pores is directly proportional to the pressure required for intrusion and hence a number of discrete data points are acquired.

For pores greater than 7mm in size it is necessary to monitor intrusions at pressures less than atmospheric pressure. Pressure generation takes place from 50mm Hg up to atmospheric pressure. The sample is then placed in a high pressure housing for pressurization up to 60 000 psig. This will allow for analysis of pores down to radii of 0.018mm.

In this work a Micromeritics Autopore II 9215 Mercury Intrusion Porosimeter was used. Computer software attached to this instrument performs data logging and analysis.

4.3.2 Results

Table 4-3 shows the effect of increasing cement content on percentage porosity. It is again noted that products with more cement require less water to ensure a workable paste. All samples for which results are presented in this table were cured for 104 days prior to testing and correspond to those characterised by SEM in section 4.1.3.

An increase in cement content leads to a reduction in total pore volume. This is due to a combination of two factors. Although there is expected to be an increase in the cement hydration product present as the cement content is increased, the reduction in water content as the cement content is increased also results in reduced porosity, as discussed in Chapter 2.

Table 4-3 - Effect of Cement Content and Water to Solids Ratio on total pore volume

% Cement to total dry solids in sample	Water to dry solids ratio	% Porosity	% Porosity Change per % Cement Increase
10	1.48	71	-
20	1.36	72	0.1
50	1.12	68	0.13
75	0.86	57	0.44
100	0.36	24	1.32

Increasing the cement content in the solidified FeCr Dust products results in a change of porosity of between 4% and 10%, or a change of between 0.1% and 0.4 % per percentage increase in cement addition. The difference in porosity between a product made with 75% cement and pure hardened cement paste is 33%, or a 1.3% increase in porosity per percentage increase in cement addition - over four times greater than between the various S/S products. The presence of waste thus increases porosity considerably. Furthermore, metal species in the pore

solution have been shown in previous sections to limit formation of cement hydration products. Finally, the physical presence of fine aggregates such as the dust products may limit cement hydration, the products of which fill the pore spaces [PCI (1986)]. This observation is in accordance with observations on SEM micrographs presented previously.

The total pore volume for the pure cement is within the ranges quoted by Glasser and Cocke and Mollah (1993) which indicates that other results should be accurate.

The cumulative percentage intrusion as a function of pore size for the samples in Table 4-3 is presented in Figure 4-23. It can be seen that for the S/S products, as the amount of cement is increased (and the water content is decreased) the pore sizes shift toward smaller sizes. More cement implies a greater extent of formation of hydration product which fills the pores.

For pure cement the average pore size lies between those for the S/S products. Based on literature reports, however, a smaller mean pore size is expected. Goto and Roy (1981) report the mean pore size for hcp to be between 0.0075 and 0.014 μm, depending on the w/s ratio and curing time. Smaller pore sizes than those reported here would thus be expected for hcp, which would fit with the trend expected from the S/S products. Problems with the operation of the porosimeter limited the number of results obtained and hence this trend could not be confirmed.

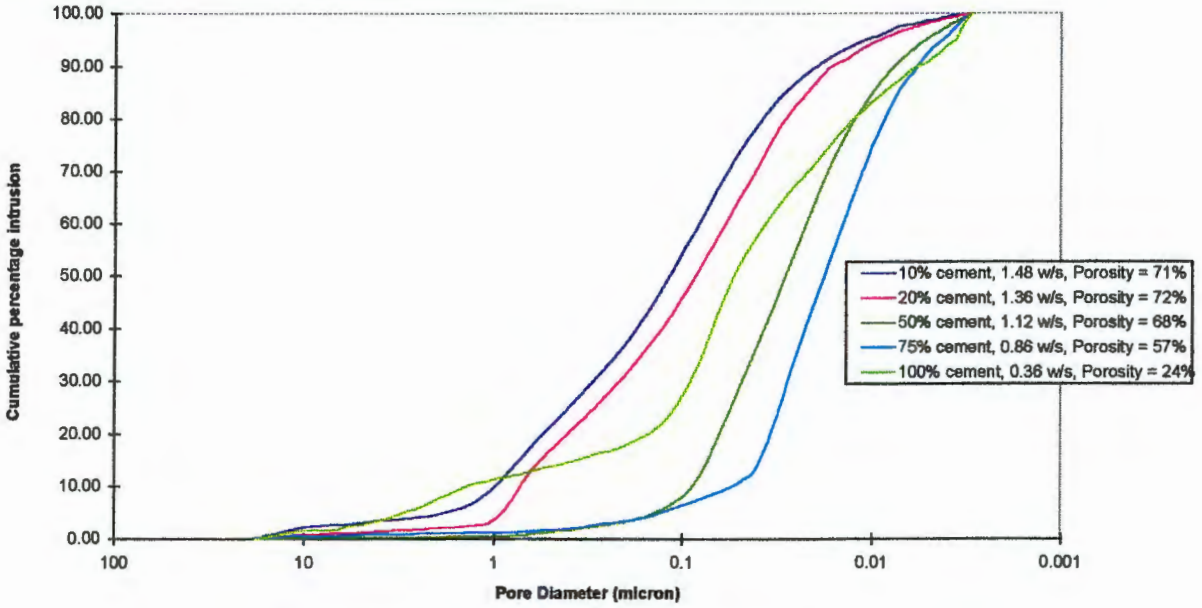

Figure 4-23 - Cumulative % Intrusion as a Function of Pore Size for the Samples in Table 4-3

All pore volumes of S/S products observed here are higher than those observed for S/S products in texts such as Cocke and Mollah (1993). The samples in the present work are made with higher water to solids ratios and lower cement contents than those used by other researchers. This explains the higher observed pore volumes.

4.4 Permeability

Permeability is a measure of the potential for a gas or liquid to flow through a solid body. Although permeability is not strictly a 'fundamental' characteristic of the product, results of permeability testing are presented here as the permeability is related to both pore volume and pore size distribution [Goto and Roy (1981)].

4.4.1 Theory of Permeability

The flow rate of a gas or liquid can generally be expressed as follows:

$$\text{Flow rate} = \frac{\text{Driving Force}}{\text{Resistance}}$$

For the flow of gases and liquids through porous media this is stated as Darcy's Law:

$$u = -B_l \frac{\partial P}{\partial x} = B_l \frac{\Delta P}{L}$$

where u = apparent linear flow rate (Pa/s)

B_1 = permeability coefficient (cm/s)

ΔP = pressure gradient across the sample (Pa)

L = path length (cm)

and u, the apparent linear flow rate, is assumed to be parallel to the x-axis. ΔP is the total pressure drop (driving force) across a sample of length L. The resistance of the medium can be

expressed as L/B_1, where B_1 is the permeability coefficient. The permeability coefficient was originally defined to correspond to a flow of 1 ml/s across a unit cube with a pressure difference of 1 dyne/cm^2 between the opposite faces. The above equation must be multiplied by an empirical constant of 100 cm/Pa in order to express the permeability coefficient in the conventional cm/s.

Darcy's law as expressed above relies on the following assumptions:

(a) the fluid is incompressible,

(b) flow is laminar,

(c) resistance to flow is entirely due to viscous drag

(d) the fluid is inert in the porous medium. That is to say it does not react with or adsorb onto the porous media and no electrical, electrochemical and capillary effects are present.

Although permeabilities of porous media are usually measured experimentally, models have been developed to relate the permeability of a substance to the geometry or "texture" of the pore space. It is very difficult to develop an exact relationship between permeability and pore texture. The relationships which have been developed rely on simple models. Examples of these models include the parallel pore and random pore models which are discussed by Smith (1981). However, the rough correlations between permeability and pore structure are often not relevant to hardened cement pastes. This is primarily due to the fact that a proportion of the pores in cement pastes are 'blind', or sealed off, and do not therefore contribute to permeability.

4.4.2 Permeability Testing

Various devices have been designed to determine the permeability of porous samples. Standard test methods for concrete include the use of triaxial cells or hydraulic head apparatus. The measurement of water permeabilities of S/S products is fraught with problems [Poon et al (1986)]. Long time periods (8 to 10 days) are required to reach a steady flow regime. During this period the microstructure and amount of unbounded water changes due to further hydration. The leaching of cement and wastes contained in the product is enhanced by the fluid passing through the solid in the test. This may modify flow regimes.

Gas permeability testing overcomes these difficulties. There is, however, no way of correlating gas and water permeabilities. This is a problem since the latter are clearly more relevant to S/S products. The advantages of gas permeabilities include shorter measurement times (hours as opposed to days), improved reproducibility of results and the fact that the microstructure does not change during testing [Poon et al (1986)].

For the purposes of testing S/S products, Cullinane et al (1986) suggests the use of a triaxial compression chamber with back pressure. The permeabilities of S/S end products which have been determined by such methods are to the order of 10^{-4} to 10^{-8} cm/s [Cullinane et al (1986)].

Ballim (1991) has developed an air permeameter for testing concrete in which permeability is measured by falling head tests. This equipment is used in the scope of this thesis and has the advantages of low cost, simplicity, flexibility for a wide number of samples and that tests require short testing periods. A schematic representation of the permeameter is presented in Figure 4-24.

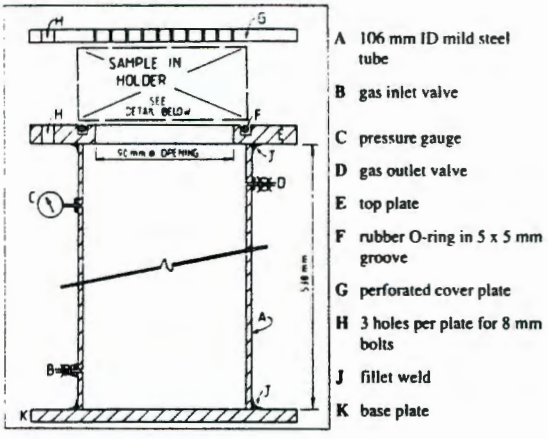

Figure 4-24 - Schematic of the Falling Head Permeameter

Permeability is calculated according to the equation:

$$k = \frac{\omega V_a g}{RA} \frac{d}{\theta_o t} \ln \frac{P_o}{P} \qquad (4\text{-}1)$$

where k = coefficient of permeability (m/s),

ω = molecular mass of permeating air (kg/mol),

V_a = volume of air under pressure (m^3),

A = superficial cross sectional area of sample (m^2)

θ_o = absolute temperature (K)

t = time for pressure to decrease from P_o to P

P_o = pressure at beginning of test (kPa)

P = pressure at end of test

4.4.3 Results

Table 4-4 presents the results of nitrogen permeability tests carried out on solidified ETP wastes. The reason for the FeCr Dust products not being tested is discussed below. Samples were made in accordance with the procedures detailed in Chapter 3. The water to solids ratios and cement contents presented in Table 4-4 were chosen to represent the outer limits of the operational variables which would give a suitably workable paste and a self supporting product as discussed in Chapter 3.

Table 4-4 - Permeability Results for Selected Solidified ETP Samples

Material	Cement Content (%)	Curing time (days)	w/s	Permeability (cm/s)
ETP 1	14	91	1.13	1.31E-6
ETP 1	20	92	1.1	1.25E-6
ETP 1	20	76	1.18	8.37E-7
ETP 1	20	92	1.18	9.55E-7
ETP 1	26	83	1.23	3.08E-6
ETP 1	30	48	1.18	7.55E-6
ETP 2	14	85	1.13	9.78E-7
ETP 2	20	58	1.1	2.17E-6
ETP 2	20	76	1.18	1.86E-6
ETP 2	26	85	1.13	1.04E-5

Each of these results is an average of three readings. In initial testing, 10 samples were tested for permeability. It was found, however, that coefficients of variation between samples were less than 1%. Due to the time consuming nature of permeability testing, and the low coefficient of variation, it was decided to take permeability of a sample as an average of three tests [Miller and Freund (1985)]. Results presented in Table 4-4 are thus an average of three readings. No trends were observed in these results. ETP 1 and ETP 2 gave similar permeabilities for similar cement and water contents. It is suggested that the permeability measurement is not sufficiently sensitive to detect the small differences in permeability which may occur between S/S products of different compositions.

From the results presented in Table 4-4 it was felt that permeability testing would provide minimal further information on the fundamental nature and chemical behaviour of the S/S products and its use as an analytical tool during this project was limited. For this reason no further tests were carried out on the solidified FeCr Dust products. For comparison, however, the FeCr Dust products required lower water contents to give rise to workable pastes than the ETP products. As has been suggested previously, higher w/s ratios will give rise to higher porosities. Furthermore, higher porosities suggest higher permeabilities. For this reason, the FeCr Dust products would be expected to be less permeable than the ETP products.

Due to the compressive nature of air, correlation between gas and liquid permeabilities is not possible. All results in Table 4-4 are observed to be within regulatory requirements set out in texts such as US EPA (1980).

4.5 Proposed Physico-Chemical Model of the S/S Products

Chapter 2 provided a discussion of cement hydration behaviour and summarized literature reports on the mechanism of containment of various metals in cement-based S/S products. Chapter 3 presented the results of a chemical and physical characterisation of the solid waste products of interest in this study, as well as a discussion of a preliminary qualitative assessment of the applicability of S/S to the FeCr Dust dusts. In this chapter a chemical and physical characterisation of the S/S products has been presented.

In summary of these observations, the following points are highlighted:

(i) Cement strength is attributed to the precipitation of fibrillar structures during hydration.

(ii) The chemistry of these products, rate of hydration, strength and permeability are influenced by a number of operational variables during mixing and curing, as well as

the presence of fine solids and anionic, cationic and organic species in the mixing water.

(iii) No ettringite is expected to be formed after a few weeks of curing. Furthermore, the presence of high concentrations of Cr(VI) in the pores restricts ettringite formation [Kindness et al (1994), Ivey et al (1993)].

(iv) Residual water in the pores of the cement product is expected to be alkaline due to calcium hydroxide released in the hydration reactions.

(v) Literature reports indicate the following. The fate of chromium in cement S/S products is uncertain; some speculation exists that Cr(III) may be incorporated chemically into the CSH hydration product [Mollah et al (1992), Ivey et al (1990)]. Cr (VI) is suggested to remain solubilized in the pore solution. Poelmann et al (1993) and Glasser (1993) have proposed that Cr(VI) may be incorporated into ettringite should it be formed. Zn is suggested to remain in the pore water or be physisorbed to the CSH surface and is not incorporated into the CSH. In the alkaline pore solution, Zn in the pores will exist as the insoluble hydroxide species.

(vi) No evidence of metal incorporation into the cement hydration structures has been found using the fundamental characterisation tools presented in this Chapter. The low cement contents (and hence low quantities of cement hydration product formed) and relevantly low concentrations of metals may restrict incorporation. It was suggested, however, that Mg, K and Na may substitute for Ca in the cement hydration product.

(vii) Up to two weeks was required before products could be removed from the moulds intact. The time required for development of a self-supporting structure was thus slower than expected from literature reports. As was discussed in Chapters 2 and 3, the presence of a wide variety of anions and cations in the pore solution have the potential to affect the cement hydration reactions. It is suggested that the observed slow formation of strength is due to retardation of the cement hydration reactions by species from the pore solution. Zn, present in high concentrations in the S/S products, is one element specifically known to retard cement hydration [Claudio and Pedro (1990)].

(viii) Large amounts of water were required to obtain a workable fresh paste for the S/S products at hand. High water contents in agglomerates lead to high porosities.

(ix) Most of the cement-based S/S product characterisation studies presented in literature have focused on treatment of metal-containing liquid wastes and slurries. Little work has been reported on the characterisation of S/S products made from solid wastes. It is based on this observation that the present study was undertaken.

Based on these and other previously mentioned observations, a physical and chemical picture of the S/S product is proposed below.

(i) The **physical model** addresses binding within the product, which will affect the ultimate strength and permeability characteristics of the solid.
(ii) The **chemical model** describes the chemistry of the solid and liquid phases in the product and assists in describing the containment within-, leaching from- and chemical breakdown behaviour of the product.

4.5.1 Physical Structure

The physical structure of the solidified FeCr Dust product will be similar to that observed for an extremely fine aggregate mixed with cement and allowed to set, with the resultant macro-granular composite being an agglomerate of unreacted cement particles and aggregate particles being bound together by cementitious products and liquid bridges. The physical interaction between aggregate and cement depends on particle size, shape, rigidity and surface texture of both materials [PCI (1986)].

Based on reports presented by Double (1983, 1977), Grudemo (1979), Winslow and Diamond (1970) on the structure of cement-aggregate products, as well as the results of SEM characterisations presented previously in this chapter, a graphical representation of the physical structure is presented in Figure 4-25 for the solidified FeCr Dust product. Shown here are the unreacted cement and solid particles bound together by a solid material similar in structure to that formed during cement hydration. Due to the high water addition, the product is highly porous. In the case of the ETP products, the only difference which is expected is the substitution of the solid dust particles by the fine-grained metal hydroxide solids.

CSH, suggested to be the primary hydration product, has been reported by Double (1983) to form as fibrillar, crumpled sheet and tubular structures, with the first mentioned being the most predominant. In the SEM micrographs of section 4.1.3, only fibrillar structures were observed. Although EDS analysis identified these fibrillar structures to be different in chemical composition to that observed by Double and other workers, these "CSH" - type fibrils are proposed to be the solids responsible for maintaining the physical structure of the S/S products. Fine material in an aggregate may coat larger particles and result in a weakening of bonds between the cement and the particles (see Chapter 2). The presence of fine aggregates may also change the morphology of the hydration products.

In pure cements and concretes the formation of calcium hydroxide crystals is observed. Such crystals were not observed in the SEM and XRD analyses presented in sections 4.1.3 and 4.2. It is proposed that the hydroxide ions found in the pore water of the S/S products may precipitate with metal species such as Zn, Cr(III), Mg and Mn. These and other precipitation products, expected to be primarily amorphous, may be loosely contained in the pore spaces and have the potential to contribute to the strength of the S/S product.

The strength of the S/S products is thus a combined function of the intermeshing of the cement hydration products, primarily CSH, any other solid material precipitated in the pores and liquid-liquid bridges formed by residual water in the pores. Different mechanisms of physical bonding are discussed in Chapter 5.

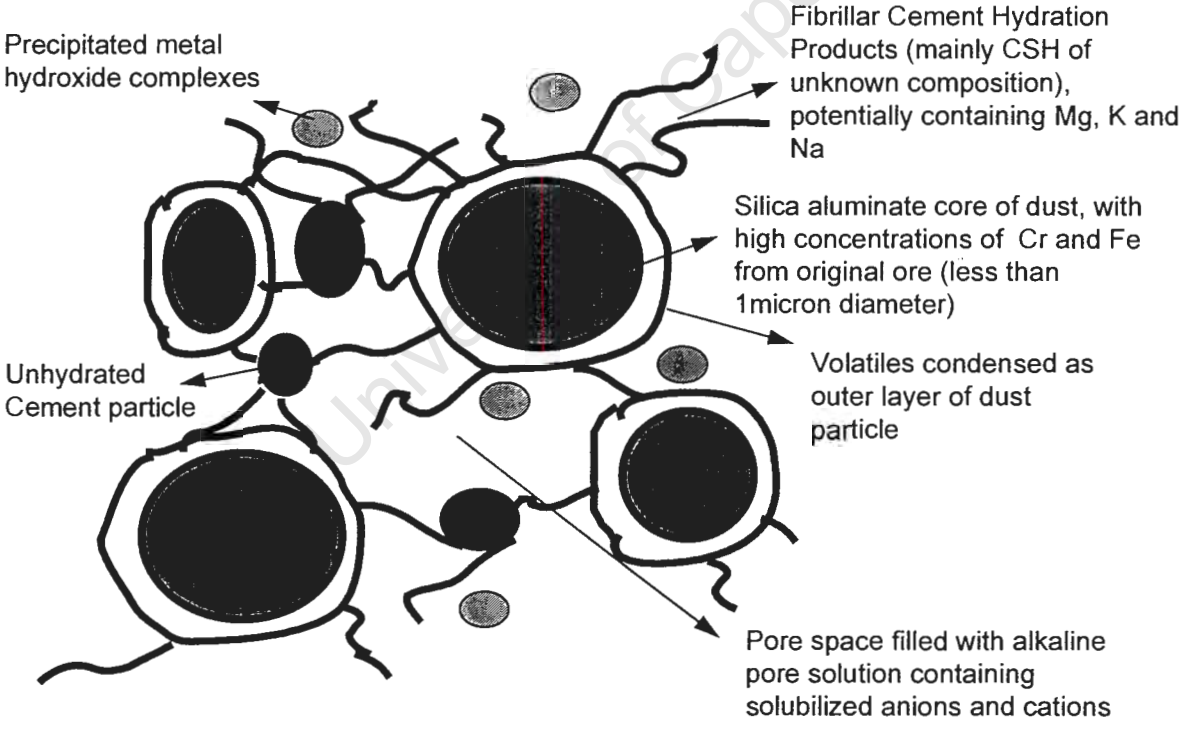

Figure 4-25 - Proposed Model of the Solidified FeCr Dust Product

Pore size and distribution have a strong influence on the strength of cement. In a "fresh" cement paste, the capillary pore network is continuous. Over time, continued hydration of the cement occurs, resulting in infilling of the pores to some degree and causing the pore network to become less continuous. Although insufficient data was obtained from SEM and MIP to provide unconditionally conclusive results for the S/S products, these tests do appear to support observations presented in literature.A small amount of the cement will remain unreacted over time scales extending from 6 weeks to 10 months [PCI (1986)]. For hardened cement pastes made with a water to cement ratio of less than 0.38, all the capillary pores have been shown to be filled eventually with CSH gel [Winslow and Diamond (1970)]. Struble et al (1989) suggest that voids of up to 5mm can occur as a result of air entrapment, while Popovics (1982) has identified the presence of air bubbles ranging from 10 to 1000 μm in size.

The porosities of the S/S products in this study have been seen to be higher than those of a typical hardened cement paste, due to the high water content required for the mixing. It is suggested that the pores will be a continuous network, with the degree of saturation of pores dependant on the ambient humidity; curing in 100% humidity should ensure a saturated pore network. Upon exposure to air, during testing for example, it would be expected that dehydration would occur to some degree [PCI (1986)].

For the solidified ETP products a similar physical model is expected. Due to the higher water contents, a more porous structure is expected, but the ultimate physical structure will be that of a porous solid in which the fine precipitate particles are held together by the cement hydration products. The pore spaces will be filled by liquid.

4.5.2 Chemical Structure

The development of a chemical model of a S/S product requires consideration of two aspects: (i) the chemistry of the pore environment and (ii) that of the solid material. The proposed chemistries are dealt with independently, even though they are intimately linked.

(a) Pore Environment

The chemistry of the pore solution will be determined by both the chemistry of the mixing water and the complex chemical equilibrium set up during hydration of cement. In turn, the

cement hydration reactions will be affected by the composition of the pore solution. Both CSH and $Ca(OH)_2$ are soluble in the pore solution, with a semi stable equilibrium eventually set up between the solid and liquid phases. The mixing water for the S/S products is a combination of the residual water in the solid and any extra make-up water. For the FeCr Dust dusts the composition of the filtrate in terms of cations, expected to be similar to the water contained in the filter cake, is presented in Table 3.1.

The pH of the pore solution of cement is a complex function of the equilibrium between the solid and liquid phases. Glasser (1993) reports that pH does not depend on the amounts of $Ca(OH)_2$ and CSH present but on the continued presence of both solids and the maintenance of a steady state, quasi-equilibrium between solid and aqueous phases. Other alkali species present in the cement also contribute to the alkaline pore environment. Glasser (1993) reports that in the presence of CSH the pH of the pore solution of hcp is expected to remain above 11, although the pH in the pores of hardened cement paste can be as high as 13.

In S/S products, hydroxyl ions released during cement hydration will interact with metal ions released by the waste products into the pore solution, resulting in the formation of hydroxyl complexes of the general formula:

$$M_x(OH)_y^{(Vx-y)+}$$

where M is the cation and V is the valence [Roy and Scheetz (1993)]. As has been discussed in Chapter 2 and illustrated in Fig 2.2, the solubility of many metal species is a strong function of pH, with the pH of minimum solubility depending on the metal. Those metals which exhibit low solubility at pH's typical of the pore environment will be more effectively retained than those which are more soluble.

From Figure 2-2 the pH of minimum solubility for the primary metals in the wastes being considered here can be obtained. At a pH of 11, found in Chapter 6 to be that of the pore solution, solubility of $Cr(OH)_3$ is to the order of $1x10^{-5}$mg/l, amorphous $Zn(OH)_2$ to the order of 5 mg/l and $Mg(OH)_2$ to the order of $1.8x10^{-5}$ mg/l. The FeCr Dust contains high levels of Cr, Zn and Mg, while the ETP contains only Cr and Mg. Based on solubility constraints, it is

suggested that a large proportion of the metals in the pore solution will be present primarily as the insoluble hydroxide. In the case of the FeCr Dust, zinc remaining solubilized in the pores may also be physisorbed to the negatively charged solid surfaces. Trying to determine the electrostatic potential of the solid surfaces is complex. Zeta potential measurement is a common tool used to quantify surface charge. Obtaining results from such zeta potential measurements requires a comprehensive understanding of the ionic nature of the pore solution. The characterisation of ionic balances within the pore solution has not been carried out in the scope of this work, and hence zeta potential and surface charge have not been determined here.

Cr(VI) exists as the ion, CrO_4^{2-}, at pH 11, and is soluble over the entire pH range. Work which has been conducted at UCT has shown that Cr in the (VI) oxidation state has the potential to adsorb onto the surfaces of the dust products [Petersen (1997)]. An equilibrium will exist between Cr(VI) solubilized in the pore water and that adsorbed onto the dust surface. This adsorption effect was, however, shown to decrease with increasing pH, and is expected to be minimal in the S/S product.

Other metals present in the FeCr Dust wash water (and in the ETP filter cake in the case of these solidified products), will remain as either soluble or insoluble constituents in the pore solution. From literature reports the cement hydration product's surface is expected to be negatively charged. Although this has not been confirmed here, should it be true positive species in solution may attach to the negatively charged surfaces by electronic interaction in a similar manner to that proposed for Zn.

The pore water of the S/S product (shown in Table 4-1) contains the elements from the water entrained in the washed FeCr Dust and ETP filter cake prior to solidification as discussed in sections 3.1.1 and 3.1.2. Furthermore, the pore solutions of hardened cement pastes contain Si, Al Ca, Cl, NO_2, PO_4, NO_3, K, Na, SO_4 and other ionic species which are released during cement hydration [Roy and Scheetz (1993)]. Table 4-5, taken from Roy and Scheetz (1993), presents the composition of a typical pore solution of a hardened cement paste. The pore solution of the solidified products is expected to contain these species and others, although not necessarily in the same concentrations.

Table 4-5 - Composition of Pore Water in Ordinary Portland Cement (ppm) [Roy and Scheetz (1993)]

Element	Conc	Element	Conc	Element	Conc
Al	10.9	K	11 100	Cl	14.2
Ba	0.5	Mg	0.3	NO_4	11.8
Ca	19.1	Mn	0.3	PO_4	45
Cr	0.7	Na	3 600	NO_3	48
Fe	0.4	Si	470	SO_4	1 460

The pH of the pore solution of hardened cement paste is approximately 13.5. At this pH, the alkali metals, except for K, and the alkaline earth metals are expected to exist as solvated cations. Magnesium exists as the stable hydroxyl-magnesium ion. Al will be present as the aluminate anion, while Fe will be present as a cation. Silica and carbonate will be present in the form of both anionic and neutral species. Due to the presence of cement in the solidified products, it is assumed that the pore solution of these solids is also alkaline, and a discussion similar to that presented here would hold. The chemical environment of the pore solutions of the S/S products is discussed further in Chapter 6.

The pore solution environment in the S/S product can thus be seen to be a complex equilibrium between all of the anionic and cationic species in the pores.

(b) Solid chemistry

Considering the low amount of cement used in making the S/S products, the solid will primarily consist of the solid FeCr Dust particles. The differences in the FeCr Dust and the ETP solids require that these two wastes be discussed separately. In Chapter 3 it was proposed that the dusts consist of a central core of mineral material around which is condensed volatile species from the pyrometallurgical process. Furthermore, X-Ray mapping indicated that the dust materials contained high levels of Cr and Fe, suggested to be from the original ore feed to process. Metals contained within the dust core, and those not mobilised during the washing process, are expected to be stable in their original mineral form. The potential does exist for long term solubilisation of such metals by slow acid breakdown, but should the flow of the acid leachant through the solid be low due to a relatively impermeable

product, mobilization rates will be slow. In reality it is this mechanism which is expected to limit mobility of heavy metals from the solidified FeCr Dust products studied here.

The ETP solids are a fine-grained crystalline metal hydroxide species including high levels of solid $Ca(OH)_2$ which was added during the neutralization/ crystallization process. Rapid resolubilization and mobilization of the metal species in low pH environments is feasible, and the 'stable dust core' effect observed for the FeCr Dust is not seen here.

As has been stated already, the primary cement hydration product is expected to be amorphous Calcium Silicate Hydrate (CSH). A number of researchers including Wiles and Lyn Apel (1985) and Double (1983) have highlighted that metals can, however, significantly alter the chemical reactions and structure of the cement hydration products. In Chapter 2 the potential for substitution of metal ions, most notably Cr(III), into the CSH product was highlighted. No evidence of this occurring has been observed in the fundamental analyses of this chapter.

The EDS results presented for the solidified FeCr Dust products indicated that Ca:Si ratios in the CSH of the S/S products are lower than for hardened cement pastes. This was suggested to be due to the overall lower calcium contents in the S/S products. In the case of the ETP products, higher calcium contents may give rise to CSH with higher Ca:Si ratios.

Minimal formation of calcium aluminate complexes is expected, although this has not been detected in the tests outlined in this Chapter. Formation of such complexes is either restricted by the presence of Cr(VI) in the pore solution [Kindness et al (1994), Ivey et al (1993)] or else is minimal due to the low cement contents used in making the products.

As has been mentioned previously, the potential exists for certain species from the pore solutions to precipitate as a wide variety of solids. Prediction of such solid formation is difficult. XRD did not identify the formation of any new crystalline products. Furthermore, no new products were characterised by SEM/EDS.

4.6 Summary

The work presented in this Chapter uses fundamental characterisation tools to characterise the physical and chemical nature of the cement S/S solid waste products. The following summary of results is presented:

The effect of the Wastes on Cement

The effect of the wastes on cement was analysed from two aspects. Firstly, the effect of metal ions in mixing water on hydration was determined. Thereafter, the effect of the presence of solid wastes on the morphology of the end product was observed. The following observations were made:

(i) Metals ions in water used for mixing cement affects the morphology of hardened cement paste. The chemistry of the hydration products is, however, not affected. The effect of morphology was suggested to be due to retardation of hydration reactions by metal ions.

(ii)The morphology of the solidified FeCr Dust is significantly different to that of hardened cement paste. The 'fibrils' formed during cement hydration form a less extensively developed and interlocking matrix. The majority of the S/S product is made up of the solid waste FeCr dust.

(iii) The Ca:Si ratio of the fibrils in the S/S products is lower than for the CSH found in hardened cement pastes. Furthermore, XRD identified two crystalline CSH structures in hcp which were not isolated in the S/S products. Cement hydration, discussed extensively in Chapter 2, is the precipitation of CSH from the pore solution. In the S/S products, the pore solution is different to that found in normal cement. This will result in precipitation of cementitious products of altered composition, explaining these observations.

The above three points thus indicate that, although the S/S products studied here consist of a fine aggregate held together by products of cement hydration, both the chemistry and morphology of the product are significantly different to what is traditionally found in cements or concretes. Two further points with regard to the chemistry of the S/S products were made:

(i) No crystalline $Ca(OH)_2$ was observed in the S/S products, despite the fact that Portlandite is usually found in hardened cement pastes. In cements to which pozzolans have been

added, the amount of Portlandite will be reduced due to reaction with Si and Al from the pozzolans to form CSH or calcium alumino hydrate structures. Its absence in the S/S products being studied here, however, is attributed to the lower Ca contents of the S/S products versus those of hardened cement pastes.

(ii) Ettringite, also usually found in cement, was not detected in the S/S products. This is as a result of both low Al contents of the S/S products and the fact that ettringite is expected to be converted to calcium sulpho-aluminate a few days after mixing.

Metal Containment in the S/S product

The primary aim of S/S is to retain metals within a solid monolith. Characterisations aimed at identifying the location of metals within the S/S products showed the following:

(i) No evidence of metal incorporation in cement hydration structures was found. The low cement contents (implying low amounts of cement hydration product formed in the product) will limit the degree of incorporation which may occur. Any incorporation which does occur is not detected due to limitations in the analytical equipment.

(ii) X-Ray maps indicated high Cr contents to be associated with high Fe contents. The original ores used in process are iron chromites ($FeO.Cr_2O_3$). The Fe-Cr interaction may be explained as residual chromites which are not converted during process and end up in the waste dust products.

Physical Properties of the S/S Products

In this chapter two physical properties of the S/S products were measured:

(i) Mercury Intrusion Porosimetry indicated a decrease in pore size and pore volume as cement addition increased. This is explained due to the increase in formation of cement hydration product as cement content is increased, and by the fact that lower water contents were required to obtain workable pastes in products with high cement contents. More water implies a more porous product. More samples would, however, be required to confirm the observed trends.

(ii) Permeabilities of the S/S products were observed to be within regulatory requirements. Permeability measurement was seen to be too insensitive to detect the effect of the operational variables on permeability.

Physico-Chemical Model

Finally, a physical and chemical model of the S/S product was proposed here, based on the above experimental observations, the results of previous chapters and on literature observations. This model is further explored in the following chapters. In Chapter 5 which follows, the physical model will be explored using strength characterisation tests, while in Chapters 6 and 7 the chemical model is expanded using observations made about the responses of the S/S products in a number of chemical leaching tests.

5.

Material Strength and Fracture Mechanisms

Previous chapters have presented information regarding the fundamental physical and chemical structure of the S/S products under investigation. It is now significant to continue the characterisation of these products in terms of physical responses under conditions which will be encountered when the processes are employed in full-scale service. Desirable characteristics of cement-based S/S products include good handling and strength properties. This requirement is significant for a number of reasons. Firstly, transportation and placement costs into the landfill are lower for solid materials than for liquids. Secondly, once the S/S mixture is placed into landfill and allowed to set, it is desired that it develop sufficient strength to bear the weight of additional product, overburden and moving machinery. It should also be able to sustain the stresses imposed on it by natural ground movement.

Since the cement hydration products (such as Calcium Silicate Hydrate (CSH)) identified in Chapters 2 and 4 are suggested to be responsible for the ultimate strength of a cementitious body, strength of the products provides an indication of the extent to which cement hydration has occurred. The extent of cement hydration influences the porosity of the body, which again can affect the extent of- and rate at which- leaching can occur. Strength should therefore provide some indication of the containment capabilities of the set S/S product. Leaching mechanisms and leach kinetics of S/S products are explored in Chapter 6 and 7. The hypothesis of a relationship between strength and leaching behaviour is investigated in Chapter 8.

In this current Chapter the fundamental characteristics of porous media and the nature of bonds which occur between particles in such media is discussed. This leads into a discussion of bonding in real materials and S/S products and definitions of strength and failure. Different experimental strength measurement procedures are explored. The application of such tests to S/S products is discussed. Experimental results and the interpretation thereof are presented.

5.1 Agglomerates - Definitions and Types of Bonds

5.1.1 Definitions

The term *agglomerate* is often used to describe porous media such as granules or lumps which consist of smaller particles. *Porous media* refers to materials in which the existence of a continuous or non-continuous pore structure can be identified. *Unconsolidated media* are made up of discrete particles while *consolidated media* have a continuous and permanent structure.

Unconsolidated media can be formed by allowing particles to settle into a bed under gravity or, with fine powders, by compressing rigid particles into a plug or wad. The porosity of randomly packed unconsolidated media depends on particle size, shape and closeness of packing.

In consolidated media, individual particles have lost their identity since they are not merely in contact but have been joined together by sintering, melting, deformation under pressure or by substances which have been deposited from a solution. Traditional examples of consolidated media include sandstone, sintered glass, unglazed ceramics and cements.

The S/S products here were shown previously to be porous solids composed of fine dust and cement products joined together by cement hydration products and water and are therefore said to be porous, consolidated agglomerates.

5.1.2 Types of Bonds

Many different bond types can contribute to the solid nature of an agglomerate. Such bonds are broadly divided into (i) forces of attraction between individual particles and (ii) bridges formed by a binder mixed with the solid particles which hold the constituent particles together.

(a) Molecular or Atomic Forces

Molecular or atomic forces between particles include van der Waals', ionic, metallic, covalent or chemical and electrostatic forces. These forces are discussed in detail and expressions presented for calculation of their magnitudes in texts including Tabor (1987) and Rumpf (1977).

Molecular or atomic forces act over short ranges and have almost vanished at particle separations of 1 μm or above. Bonds formed by liquid and solid bridges may be anywhere from a fraction of a micron to a number of millimetres long. Furthermore, molecular or atomic forces have been established experimentally to be weak compared to the type of bonds formed between particles by solids and liquids [Rumpf (1962)]. This same author suggests that the bonds formed by such forces may be disregarded as granule-forming bonds where other types of bonds exist, and, considering this thesis focuses on agglomerates which have been formed by the addition of liquid, and cement which results in the formation of solid bonds, molecular bonds are not discussed in any further detail here.

(b) Formation of Bridges Between Particles

Studies of particulate agglomerate bonding via the formation of bridges between particles are based primarily on the work of Rumpf (1977, 1962). This author developed expressions for agglomerate strength based on the mechanism of formation of bonds between constituent particles of an agglomerate. In the Rumpf analyses, isolation of the bonding mechanisms is necessary in order for the strength of the agglomerate to be calculated. Once the type of bonding within the agglomerate has been isolated its strength can be calculated, based on the assumption that all bonds within the agglomerate are of the same magnitude. Four distinct bonding mechanisms (via the formation of bridges) were identified in Rumpf's works:

1. *Liquid bridge bonding with movable liquid surfaces:* When a liquid is added to a powder during granulation, the forces holding the particles together result from the interfacial tension at the liquid surface and the pressure deficiency or suction created within the liquid by curvature at the liquid surface. There are four different states which can occur within the agglomerate, depending on the percentage of saturation. These are the pendular state, the funicular state, the capillary state and that of particles in a liquid droplet (see Figure 5-1). Rumpf (1962) provides equations developed for the calculation of the tensile strengths of such agglomerates as a function of the surface tension of the liquid, the size of the particles and the voidage of the agglomerate.

Figure 5-1 - Liquid Bridge Bonding with Moveable Liquid Surfaces

(a) The *pendular state* occurs by the adsorption of moisture onto particles from the atmosphere. It is characterised by torous-shaped bridges between the particles, as depicted in Figure 5-1. At the solid-liquid-gas contact line, the surface tension is directed along the liquid surface. Within the liquid bridge a negative capillary pressure exists if the solid is wetted. Both of these components contribute to attraction between the grains. Only the interfacial forces at the liquid-gas interface contribute to bonding between the grains. The tensile strength of this bridge is given by:

$$H = \gamma_s d \left(\frac{\pi}{1+\tan\frac{1}{2}\theta_l}\right) \qquad (5\text{-}1)$$

where

H = tensile strength of a single bond

γ_s = surface tension of the liquid

d = particle diameter

θ_l = semi- angle of the liquid ring

d and θ_l are shown schematically in Figure 5-2.

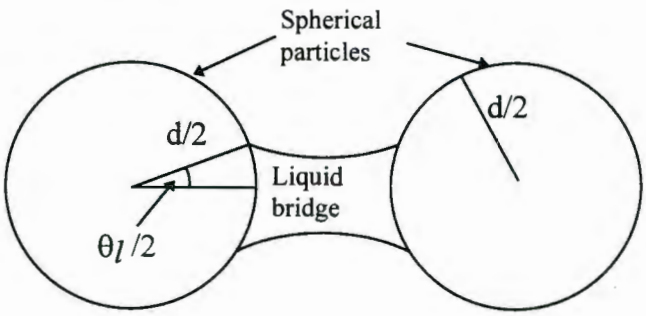

Figure 5-2 - Graphical Representation of d and θ_l

(b) The *funicular state* is characterised by a continuous network of liquid interspersed with air. The tensile strength of the agglomerate in the funicular state, σ_t, can be approximated by:

$$\sigma_t = S_l C_l \frac{1 - \varepsilon_f}{\varepsilon_f} \frac{\gamma_s}{d} \tag{5-2}$$

where S_l is the fractional saturation, defined as the proportion by volume of the liquid phase in the pore space, C_l is a dimensionless parameter related to the specific surface of the solid particles and accounts for the non-sphericity of the particles, ε_f is the void fraction of the assembly and d is the particle diameter.

(c) The *capillary state* occurs when the void space is completely filled with liquid. Here the interfacial forces exist only at the surface of the agglomerate particles and give rise to the bonding forces. For irregular particles in which the liquid completely wets the solid, the following equation holds:

$$\sigma_t = C_l \frac{1 - \varepsilon_f}{\varepsilon_f} \frac{\gamma_s}{d} \tag{5-3}$$

(d) At high liquid contents the liquid can completely envelop the particles. The particles are held together by the interfacial tension of the convex surface of the continuous liquid drop.

In agglomerates which are held together by movable liquid bridges, adhesion of the liquid to the solid and forces between particles within the liquid must be of sufficient magnitude to transmit the tensile stress and to sustain the capillary pressure. This condition is fulfilled because the molecules responsible for the tensile strength of the bridge are found only on the outer surface of the adhering bridge. The number of particles at the air-liquid interface is considerably less than are found within the bridge. Considering the force between particles, and hence the strength of the bridge, is a function of the distance between the particles (with stronger forces being found at shorter distances), an increase in the strength of the bridge can be effected by more particles moving to the air-liquid interface. When a stress is placed on the bridge rearrangement of the particles within the bridge occurs to account for this

stress. This can occur until a threshold stress is reached, at which point the liquid bridges will rupture, forming two adhering drops [Rumpf (1962)].

2. *Liquid bridge bonding with nonmovable liquid bridges:* These bonds can be understood in one of two ways:

   (a) As the viscosity of the binder is increased, the magnitude of forces between individual particles in the liquid becomes greater. The effect of the interfacial forces at the air-liquid interface become less signficant in determining the shape of the liquid surface and all particles in the cross-section of the bridge contribute to the strength of the bridge. The most favourable energy state of the bridge at the surface is one of constant liquid pressure at the air-liquid interface. The reduced mobility of the bridge as a whole, however, prevents the formation of a constant liquid pressure. The agglomerate is thus more likely retain any surface shape given to it because the energy required to deform the bridge is greater than the decrease in surface energy from rearrangement of the particles at the air-liquid interface.
   (b) Thin adsorption layers of a liquid binder which may form around particles are also not freely movable. Should such adsorption layers come into contact, they can form strong bridges as a result of molecular attraction.

3. *Solid bridges:* Solid bridges are formed in one or more of five ways: by sintering, melting, chemical reaction, hardening bonding agents and by crystallization of dissolved materials [Rumpf (1962)].

4. *Mechanical Interlocking:* By the interlocking of fibrous, flat-shaped and bulky particles.

For cases 2, 3 and 4, where bonding is localized at the points of contact between the particles, Rumpf (1962) provides an equation for the calculation of the tensile strength of the agglomerate as a function of void fraction of the assembly (ε_f), the diameter of the particles (d) (assuming monosized spheres), the tensile strength of a single bond (H) and the coordination number (k). In deriving the equation, a cross-section of the agglomerate is taken and the average number of bonds in a cross section is determined and integrated over the volume of interest. The equation thus rests on the assumption that all bonds are of equal strength and is expressed as follows:

$$\sigma_t = \frac{9}{8}\frac{1-\varepsilon_f}{\pi d^2} kH \cong 1.1\frac{(1-\varepsilon_f)}{\varepsilon_f}\frac{H}{d^2} \qquad (5\text{-}4)$$

The factor 9/8 is introduced to take account of the statistical distribution of tensile strength. The second part of this relationship comes about by relating the coordination number and porosity of packed spheres, given as $k\varepsilon \cong 3.1 \cong \pi$ [Rumpf (1962)].

The value of H cannot be determined from theory for all the bonding mechanisms: Van der Waals forces, electrostatic attraction and mobile liquid bridges can be computed for simple geometries but solid and immobile liquid bridging and high viscosity liquids are less amenable to theoretical calculation.

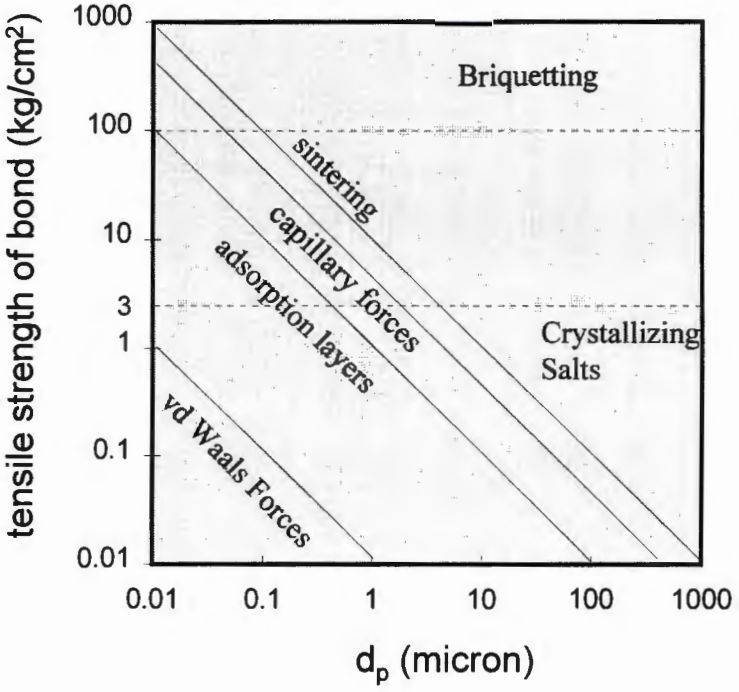

Figure 5-3 - Agglomerate Strength as a Function of Type of Bonding and Particle Size [based on Rumpf (1962)]

The question thus arises as to the relative magnitudes of the strengths of liquid and solid bridges. Figure 5-3, extracted from Rumpf (1962), shows the theoretical strengths of agglomerates as a function of the type of bonding and the particle sizes in the agglomerate. This indicates that as soon as capillary forces and solid bridges are formed, van der Waals forces can be discounted. It is also seen that the magnitude of the strength of liquid bonds can be of a

similar magnitude to solid bridges, depending on the particle sizes. The following section discusses bonding in real agglomerates, where more than one type of bond exists.

5.2 Bonding in Real Agglomerate Materials

Bonding in most composite materials is as a result of a combination of the types of bonds discussed in section 5.1. The bonds formed, and their contributions to the strength properties of the material as a whole, depends on the composition of the agglomerate. Consider a dry solid powder which has undergone no chemical reactions or compaction. The individual particles will likely form agglomerates held together by molecular or atomic forces.

Any liquid which is introduced into the solid assembly will form liquid bridges between the individual solid particles. The nature of such bridges will depend on the amount and viscosity, of the liquid added as discussed above. Electrostatic forces become less signficant (as discussed in section 5.1.2) and liquid bridges are now primarily responsible for bonding between the particles.

Should the solid contain chemical species which are soluble, these may be released into the liquid. Such species can alter the surface tension of the liquid (see section 5.4 below) and hence change the strength of the bonds. Quantification of the effect of metal species on the surface tension of a liquid and hence the bond strength is complicated to resolve [Hiemenz (1986)]. A more significant effect is that of such chemical species which may reprecipitate out of the liquid, forming crystals which result in the formation of solid bonds.

Solid bridges can be formed in a number of ways. Should the pore solution contain ionic species as discussed in the previous paragraph, these may precipitate or crystallize out of solution, reducing the volume of the pore space and, in accordance with the previous discussion, contribute to an increase in strength. Furthermore, the newly formed solids may attach to the surfaces of particles in the agglomerate forming interparticulate bonds. This is the mechanism of bonding identified in Chapter 2 to occur in cement. Solid bridges may also be formed by

heating either the solid or the solid-liquid combination which results in sintering or melting and an associated change in solid-solid bonding.

In all real solids one or more of the above effects are significant. The S/S products in this work were shown in Chapter 4 to be a mixture of different liquid and solid phases and therefore fall into the category of 'real solids'. Bonding in S/S products is discussed in the following section.

5.3 Bonding in cement-based S/S Products

Cement-based S/S products in general are made by mixing cement and other binder materials with a solid or liquid waste and make-up water where necessary. The types of bonds in the resulting product will depend on both the physical and chemical nature of the waste being treated, the amount of liquid present and, ultimately, the extent of cement hydration and other complexation reactions.

Particle-particle forces are expected between the dry, unhydrated cement particles. Once water, liquid waste products or slurries are mixed with these cement particles, liquid bridges will form as described above. The molecular or atomic forces become less significant. The nature and strength of the liquid bridges will be determined by the chemical compositions of the liquid, the liquid-solid interaction and the solid surface chemistry.

Pure water is the simplest case of liquid bonding. The surface tension of water can be determined and the interaction of a solid surface with water can be readily assessed. As the ionic strength of the liquid forming the binder bridges changes (with an increase in the concentration of solubilized components) so the wetting behaviour of the solid and surface tension of the liquid will change, thus changing the strength and possibly the shape of the bonds. Once again, the effect of ionic strength on surface tension is identified to be difficult to quantify [Hiemenz (1986)]. Very viscous liquid wastes (such as highly concentrated solutions and certain organic liquids) will form non-movable liquid bridges as described above.

Where ionic species are found solubilized in the liquid filling the pores between the particles, as would be expected in the case of a metal-containing waste such as the ones being studied here, metal complexes may precipitate or crystallize in the pores. The resulting solids have a two-fold

effect. Firstly, to reduce the void space or porosity of the system, which, according to the equations presented in section 5.1.2, increases the strength of bonds in the agglomerate. Secondly, these solids may intermesh or attach to other solid materials forming solid bridges which add to the strength of the product.

Hydration of cement was shown to be a specific case of the above, and hydration mechanisms and chemistry are detailed in Chapter 2. In summary, calcium and silicon are released into the pore solution and precipitate to form, amongst other phases, calcium silicate hydrate (CSH). CSH is the primary solid bridge forming material in cement, concrete and S/S products.

S/S products in general will thus be held together by a combination of liquid and solid bridges.

5.4 Bonding in S/S products formed from Ferro-alloy Wastes

In Chapter 4 a visual and qualitative chemical representation of the S/S product was developed using a number of tools including Scanning Electron Microscopy. Bonding is suggested to be as a result of the following contributing forces:

(i) Water added to the S/S mixture will result in formation of liquid bridges between particles. From the discussion above it would be expected that, since the water contents are high (up to 50% in some cases) either the capillary state or complete enveloping of the particles by the liquid will occur (Figure 5-1 (c) and (d)). The discussion presented in Chapter 3 showed the mixing water used for making these S/S products to contain a large concentration of dissolved species (see Table 3-1). Using the ASPEN simulation package, a preliminary analysis was carried out to determine the the effect of ions in solution on surface tension. This analysis indicated an insignificant difference in surface tension between pure water and a pore solution simulation. It is suggested, therefore, that the presence of dissolved species in the pore water is suggested have an minimal effect on the strength of liquid bonds which are formed in the solid, and this effect is thus not considered further.

(ii) Several solid bridge types are formed in the S/S product. The most significant are those formed by the calcium silicate hydrate (CSH) cement hydration products identified by EDS and XRD analysis presented in Chapter 4. These extend between the surfaces of the cement particles (see the discussion of cement hydration in Chapter 2), and possibly attach to the

No information can be isolated on the fracture behaviour or strength of the individual bonds from such a test. Later on in this chapter the tools afforded by Linear Elastic Fracture Mechanics (LEFM) are employed with the aim of identifying the factors which control the fracture process.

What are acceptable strengths for S/S products? The Nuclear Regulatory Commission guidelines of 1983 call for Unconfined Compressive Strengths to the order of 1.035 MPa [Cullinane et al (1986)]. British waste disposal authorities and the US EPA recommend a compressive strength of not less than 0.35 MPa for S/S end products which are to be placed in a landfill site [Arniella and Blythe (1990), Sollars and Perry (1989)]. For comparison, commonly achieved compressive strengths for concrete are to the order of 10 MPa [PCI (1986)].

5.7 Stresses and Strains, Young's modulus, Notching, Plastic and Elastic Energy Dissipation

Prior to launching into a full discussion of fracture mechanics, it is worthwhile to provide here a brief discussion of a number of terms which the reader may encounter in the course of the following sections.

> "All this brings us to the question of stresses and strains, words which the layman is apt to regard as alarming, distressing and confusing. This is perhaps partly because the words may conjure up the idea of a wilderness of mathematics but probably no more because the words have been borrowed or stolen by non-scientists to describe the mental condition of human beings. In this connotation the words have no very precise meaning and commonly stress and strain are used interchangeably as if they meant the same thing."
>
> Gordon (1988)

The terms 'stress' and 'strain' have distinct meanings within materials science. The tensile stress is a load per unit area given by $\sigma=F/A$ with units of kN/m^2. Tensile strain is the amount of stretch or deformation under load per unit length in response to the stress. Strain is given by $\Delta L/L$, where ΔL is the deformation and L is the original length of the object under strain.

When a stress is applied to an object, the deformation may or may not be visible. If the stress is released and the solid returns to its original form, the deformation which occurred is said to be *elastic*. While under stress, the bonds within the solid are under strain and the applied energy is said to be stored as strain energy and is recoverable. *Plastic* deformation, however, occurs when the applied energy has been dissipated by permanent modification of the bonds in the solid and the object can not return to its original state even once the load is removed.

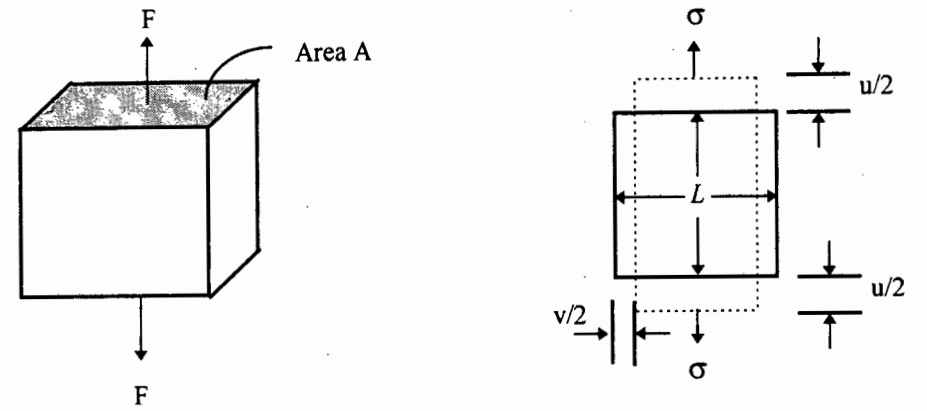

Tensile stress $\sigma=F/A$

Nominal tensile strain=u/L
Nominal lateral strain=v/L

Figure 5-5 - A Graphical Representation of Stress and Strain

Materials to be tested in laboratory conditions are often *notched* or *precracked* prior to testing. When a notched material is placed under stress there is a concentration of stresses near the tip of the notch. Analysis of these stresses and subsequent failure of the material provides information on the bonding within the solid and the strength of the material.

Mullier (1991) suggests an alternative definition for deformation in terms of deformation with or without flow, and with or without cracking. Flow is when the physical form of a material is permanently changed by changing the shape of the interparticular bonds, and rearrangement of the particles in the solid without breaking any of the bonds. If flow occurs prior to failure it is termed *ductile* whereas if flow does not occur the fracture is termed *brittle*. Failure by cracking with no flow is known as *elastic fracture* and if flow occurs it is *plastic failure*.

Originally, fracture analysis techniques were developed for testing of linear elastic materials [Adams et al (1989a)]. These are materials in which applied stress is directly proportional to the

resultant strain, where the proportionality constant is known as the Young's modulus, traditionally given the symbol E. The Young's modulus is a material constant and can be obtained from the linear section of a plot of stress vs strain for a material. Most solids are elastic to very small strains (up to about 0.001) [Ashby and Jones (1989)]. Beyond that some fracture and others deform plastically. Some solids (such as rubber) are elastic up to strains of 4 to 5, but cease to be linear elastic after a strain of about 0.1 [Ashby and Jones (1989)].

5.8 Modes of Failure

It is relevant here to distinguish between the three distinctly different modes by which failure of a material is observed to occur. These are depicted in Figure 5-6. Mode I or opening mode is the normal separation of the crack walls under the action of tensile stresses. Mode II, sliding mode, corresponds to mutual shearing of the crack walls in a direction normal to the crack front and mode III or tearing mode, corresponds to mutual shearing parallel to the crack front. Failure can occur by a combination of these modes [Lawn and Wilshaw (1975)]. In the sections which follow, discussion is focused on test configurations in which failure occurs due to tensile stresses being placed on a material. Further discussion in this document is thus directed primarily at the mathematical and experimental description of Mode I failure.

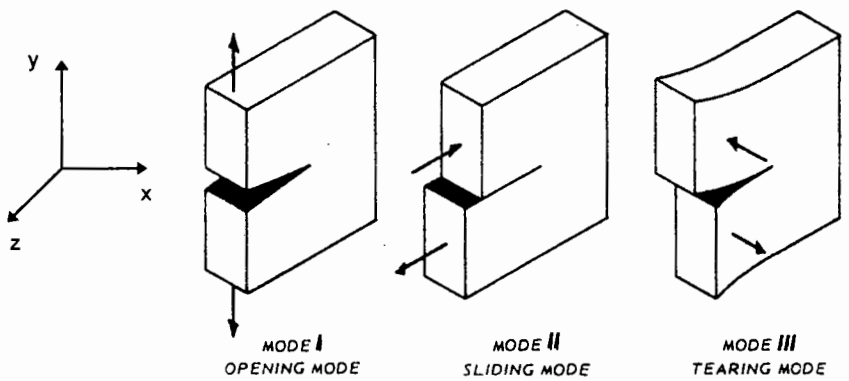

Figure 5-6 - Modes of Notch Opening [Ewalds and Wanhill (1984)]

5.9 Measuring Strength - The Linear Elastic Fracture Mechanics (LEFM) Approach

The UCS and indirect tensile tests (ITT), and the simple Rumpf models discussed above, isolate a macroscopic material strength parameter based on failure occurring instantaneously at all points in the failure plane. Although for ideal materials or those in which the strength is purely

a function of the individual bonds in the solid the strengths can be predicted by the Rumpf models, most real materials are observed to fail at strengths which are sometimes as much as one or two orders of magnitude lower than their theoretically predicted values [Irwin (1957), Griffith (1920)]. The reason for this observation is as follows: most materials which are put into use have small cracks which result from handling or which occur while the material is performing the function for which it is required. An ideal material will fracture when an applied stress exceeds the fracture stress of all of the individual bonds as discussed.

In a cracked material, however, a concentration of stresses occur at the tip of the crack. This implies that although the applied stress to a material may be lower than the fracture stress, the localized stress at the crack tip may exceed the fracture stress at the tip of the crack. This can cause the crack to propagate through the material at a stress lower than that predicted by theory. Initiation and subsequent propagation of cracks is discussed further in section 5.9.1 onwards. In order, therefore, to evaluate effectively the stress which a real material containing inherent cracks can be expected to bear in practice without failing, it is not possible to make use of the equations provided for ideal materials. The effect of cracks on the failure of materials must thus be included in the calculation of their ultimate bearing stresses.

The strength properties of a multiphase material such as hardened cement paste (hcp) or concrete are influenced directly by the relative proportions of phases of different strengths, and by the internal microstructure of the material. The arrangement of particles relative to each other, the size and shape of the particles, the structure and nature of the surface at the phase boundaries and the strength of inter-particle bonds will all directly influence the strength of the material.

Linear Elastic Fracture Mechanics (LEFM) is a name given to a science which is aimed at understanding the effect of flaws on the strength of materials. Using LEFM techniques information can be gained about the distribution and dissipation of strain energy in a stressed material. Initially the tools it afforded were used to describe purely linear elastic materials. In recent years the some work has been carried out which focusses on extending these analyses to describe a broader base of non-homogeneous materials such as granular agglomerates [Xu et al (1995), Mullier (1991), Adams et al (1989a)]. In the case of a multiphase material such as the

S/S products, the techniques and analyses can be further extended to provide information on which of the bonds as described above are limiting in determining strengths. A discussion of such analyses is presented in the following sections.

5.9.1 Griffith's Energy Balance

Griffith (1920) was the first person to describe fracture mathematically using an energy balance approach. Consider a rectangular sample of a linear elastic material subjected to a tensile stress σ. Plastic dissipation of energy is assumed to be negligible and the strain energy will be stored elastically throughout the specimen. The stress is proportional to the applied strain given by:

$$\sigma = E\,\varepsilon \tag{5-5}$$

where E is called the Young's modulus. The strain energy density $\hat{E}$ (or energy stored per unit volume) can be found by integration from $\varepsilon=0$ to $\varepsilon=\varepsilon$, giving:

$$\hat{E} = \int_0^{\varepsilon} \varepsilon \, d\varepsilon = E\frac{\varepsilon^2}{2} \tag{5-6}$$

Now, substituting in Equation (5-5) gives:

$$\hat{E} = \frac{\sigma^2}{2E} \tag{5-7}$$

If a through-thickness notch of length a is introduced into the stressed material the bonds which were strained along the length of the notch are broken. As a result of the breaking of these bonds there is a further release of strain energy in a region extending from above and below the crack (see Figure 5-7). This strain-free region may be approximated by a triangle of height which is dependent on a, represented as βa.

The value of β will depend on whether the material under tension is in plane stress or plane strain (see section 5.9.3 for a discussion on plane stress and plane strain). For plane stress $\beta=\pi$ and for plane strain $\beta=\pi(1-\nu^2)$ where ν is Poisson's ratio. Poisson's ratio is defined as the negative ratio of lateral strain to tensile strain [Ashby and Jones (1980)].

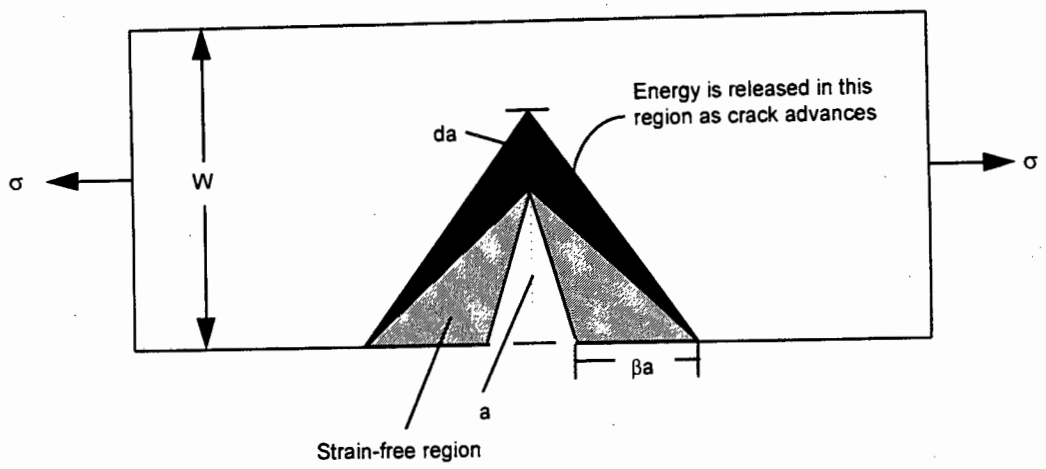

Figure 5-7 - Notched Elastic Material under Tension

If the thickness of the sample is B, the volume of the relaxed area shown in Figure 5-7 is $\beta a^2 B$. The energy, U, which is released as a result of the introduction of the notch as described above is given in plane stress as the strain energy density * volume [Knott(1973)]:

$$U = -\frac{\sigma^2}{2E}.\beta a^2 B \tag{5-8}$$

As the crack extends by a distance da, the extra strain energy released is given as:

$$\partial U = -\frac{\sigma^2}{E}\beta a B\, \partial a \tag{5-9}$$

According to Griffith's energy balance, as the crack advances into the solid, the strain energy released at the crack tip provides the energy required to continue creating new surfaces. Fracture occurs when the stored elastic energy released by crack propagation exceeds the energy required to break the bonds responsible for holding the solid together at the crack tip and thereby creates new surfaces. These bonds will be those formed by liquid and solid bridges as described previously, and thus the total energy required for creating new surfaces will be the sum of the energies required to break the individual bonds across the failure plane. The crack propagation process marks a move from a higher energy to a lower energy state, being a thermodynamically favourable transition [Mullier (1991), Knott (1973)].

Expressed mathematically, the Griffith criterion for crack propagation is given by:

$$-\frac{\partial U}{\partial a} \geq \gamma \frac{\partial A}{\partial a} \tag{5-10}$$

The left hand side of this equation is the strain energy released per unit crack length as the crack propagates and is given the symbol G. The right hand side of the equation represents the rate at which surface energy is absorbed in creating new surfaces. γ is the surface free energy of the material and A is the fracture surface area. In the case of poly-phasic materials such as the S/S products, the surface free energy is the energy required to break the bonds between the particles in the agglomerate which results in the formation of new surfaces. According to the Griffith criterion, therefore, crack propagation occurs when G reaches a critical value, G_c. If one assumes that all of the strain energy goes into the creation of new surfaces, then G_c is also equal to twice the surface free energy of the material, 2γ. The factor of two comes about as two new surfaces are formed as the crack propagates. The factor 2γ is sometimes called the crack resistance, R.

The disadvantage of the analysis afforded by Griffith's approach presented above is that the parameters are calculated assuming the energy dissipated in the system is consumed solely in the creation of new surfaces. It was thus developed for materials which behave purely elastically. In most real materials some energy is dissipated in plastic deformation or microcracking prior to macroscopic fracture. An alternative approach is thus appropriate to account for such energy dissipation processes.

5.9.2 Irwin's Approach to Describing Fracture

Irwin (1957) proposed an alternative to Griffith's energy balance, which investigates failure in terms of the elastic stress field around the crack tip. The components of the stress field σ_{ij} around the crack are shown schematically in Figure 5-8. From Irwin (1957) an analysis of the stress function around the crack tip in terms of complex numbers allow the stress components to be expressed as:

$$\sigma_{ij} = \frac{K}{\sqrt{2\pi r}} f_{ij}(\theta) + \text{non} - \text{singular terms} \tag{5-11}$$

In equation (5-11) K is known as the stress intensity factor and defines the magnitude of the stress field at a specific point. The complex number analysis gives rise to a harmonic equation, explaining the origin of the non-singular terms (which are a function of θ) in equation (5-11). An analysis of such theory is beyond the scope of this review but can be found in texts such as Knott (1973). The equations are complicated to solve mathematically and simplifications are often introduced to allow for easy solution of the model. Westergaard's solution [Westergaard (1939)] assumes that the crack tip is perfectly sharp. Then, close to the crack tip, the non-singular terms become negligible [Lawn and Wilshaw (1975), Knott (1973)]. Expressions for $f_{ij}(\theta)$ are presented in texts such as Knott (1973) as:

$$\begin{aligned} f_{xx} &= \cos\tfrac{1}{2}\theta(1-\sin\tfrac{1}{2}\theta\sin\tfrac{3}{2}\theta) \\ f_{yy} &= \cos\tfrac{1}{2}\theta(1+\sin\tfrac{1}{2}\theta\sin\tfrac{3}{2}\theta) \\ f_{xy} &= \cos\tfrac{1}{2}\theta\sin\tfrac{1}{2}\theta\sin\tfrac{3}{2}\theta \end{aligned} \qquad (5\text{-}12)$$

In practice, $f_{ij}(\theta)$ is defined as an empirical function of a/W, the crack length and the specimen height, and is given the symbol Y. f(a/W) for different geometries is documented in texts such as Rooke and Cartwright (1976) and British Standard 7448 (1991).

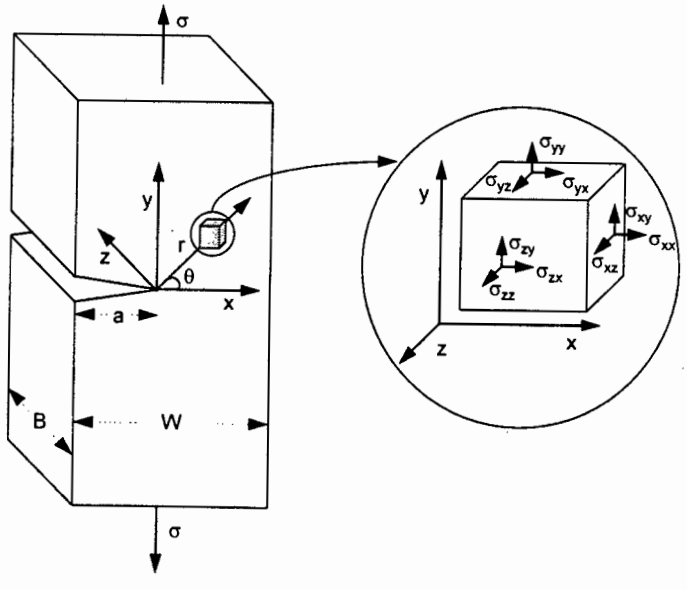

Figure 5-8 - Stress Field near the Crack Tip

Most LEFM analyses are carried out using experimental configurations in which Mode I deformation occurs (see section 5.8) [Knott (1973)]. In mode I deformation, which is the focus of this current work, the stress intensity factor is expressed as K_I, and only the plane of opening

(the xy plane in Figure 5-8) is considered. Changing from spherical to cartesian coordinates, r becomes equivalent to a, the length of the crack. Using cartesian coordinates, replacing $f_{ij}(\theta)$ by Y and discounting the non-singular terms, Equation (5-11) becomes:

$$K_I = \sigma\sqrt{\pi a}\ f(a / W) = \sigma Y\sqrt{\pi a} \tag{5-13}$$

Crack propagation, which signifies failure of the solid, occurs when the applied stress reaches some critical value σ_f. The stress intensity factor calculated at this failure load is known as the critical stress intensity factor (or the fracture toughness) and is given the symbol K_{IC} (having units of Force/Distance$^{3/2}$). K_{IC} is an inherent material property and signifies the resistance of a material to crack propagation. Since the strength of a material depends on the combined strength of the individual bonds within that material as described above, K_{IC} is also a function of the strength of those bonds. Changes in the nature and composition of liquids and solids connecting particles in an agglomerate will thus change K_{IC} in a fashion similar to the effects on strength discussed in sections 5.2 to 5.4.

5.9.3 Plane Stress and Plane Strain

Figure 5-9 shows a representation of the shape of the area surrounding the crack tip in a through-thickness notched plate under tension, as presented in texts such as Ewalds and Wanhill (1984) and Brown and Srawley (1966). *Plane strain* conditions are said to occur when one of the principal strain components is zero, while *plane stress* occurs when one of the principal stresses is zero.

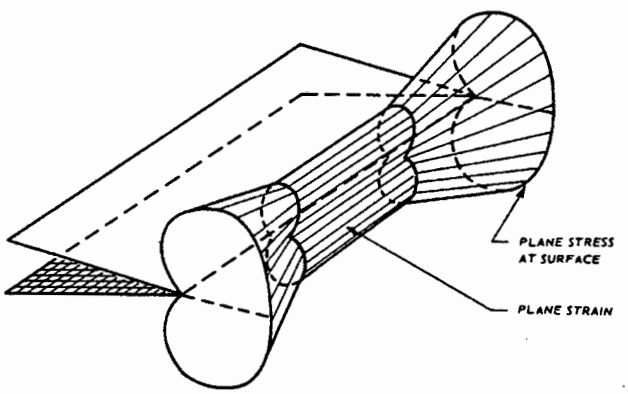

Figure 5-9 - Through-thickness Plastic Zone in a Plate of Intermediate Thickness [Ewalds and Wanhill (1984)]

Consider Figure 5-9. Near the surface of the plate there are no stresses in the thickness (z) direction of the plate, so there exists a biaxial condition of stress along the x and y axes - known as plane stress. Furthermore, the plastic zone is able to flow freely in this region. As one moves inwards toward the centre of the plate, plastic flow of the material is restricted by surrounding elastic material, and the effect of the free edge as a stress release diminishes. In this region the material tends towards a state of plane strain.

The plastic zone therefore extends much further ahead of the crack near the faces than it does near the middle of the notch, and this influence of the free surface is proposed to extend into the thickness of the specimen for a distance which is proportional to $(K_I/\sigma_{YS})^2$ [Ewalds and Wanhill (1984)].

When the thickness is less than a critical value proportional to $(K_I/\sigma_{YS})^2$, the plane stress influence of the free faces will extend through the entire thickness, and the sample will fail by plastic deformation before the stress intensity reaches K_{IC}. The effect of any opening-mode (Mode I) crack extension which occurs is masked by the effect of the plastic deformation.

Consider Figure 5-8. When plane stress exists, as in a thin sheet, there are no through-thickness stresses so that $\sigma_{ZZ} = 0$. Yielding occurs along the planes of maximum shear stress which are set up at 45° to the x and z axes. When the specimen is in plane strain, the minimum principal stress becomes σ_{XX}. Yielding, discussed in section 5.9.7, occurs when the principal stress reaches some critical value, given by:

Plane stress	$\sigma_{YY} = \sigma_Y$	(5-14)
Plane strain	$\sigma_{YY} = \sigma_Y + \sigma_{XX}$	

In other words higher stresses are required to produce failure in plane strain than in plane stress. K_{IC}, the parameter of interest in this study, is a measure of the *plane strain* fracture toughness for a material. Considering Figure 5-9, it is essential that specimen dimensions are chosen such that plane strain fracture does, in fact, occur. Should this not be the case, the K_{IC} of the material will be underestimated.

5.9.4 Relationship Between K_{IC} and G_C

Since K_{IC} and G_C both relate to the strength of the material, a relationship exists between them. A full derivation of this relationship is presented by Knott (1973) and gives:

$$G_C = \frac{K_{IC}^2}{E'} \tag{5-15}$$

where E' is given by E, the Young's modulus, for plane stress and $E/(1-\nu^2)$ for plane strain. For mortars and concretes, values of the Poisson's ratio, ν, have been found to lie between 0.1 and 0.22, with the value of ν decreasing as the fraction of aggregate within a given volume is increased [PCI (1986)]. For most metals ν lies between 0.28 and 0.33 [Knott (1973)]. If one takes 0.1 as the minimum and 0.33 as the maximum possible values of ν which would be found in S/S products, the term $(1-\nu^2)$ will lie between 0.89 and 0.99. It is suggested that this term is insignificant in the above calculation and disregarding it makes E' equivalent for plane stress and plane strain, given the symbol E. E can be determined experimentally from the linear region of a plot of applied stress vs the resultant strain for a given material.

Table 5-1 presents values of G_c and K_{IC} for a number of different materials

Table 5-1 - G_c and K_{IC} for a number of different materials [Ashby and Jones (1980)]

Material	G_c/kJ m^{-2}	K_c/MN m$^{-3/2}$
Pure ductile metals (e.g. Cu, Ni, Ag, Al)	100–1000	100–350
Rotor steels (A533; Discalloy)	220–240	204–214
Pressure-vessel steels (HY130)	150	170
High-strength steels (HSS)	15–118	50–154
Mild steel	100	140
Titanium alloys (Ti 6Al 4V)	26–114	55–115
GFRPs	10–100	20–60
Fibreglass (glassfibre epoxy)	40–100	42–60
Aluminium alloys (high strength–low strength)	8–30	23–45
CFRPs	5–30	32–45
Common woods, crack ⊥ to grain	8–20	11–13
Boron-fibre expoxy	17	46
Medium-carbon steel	13	51
Polypropylene	8	3
Polyethylene (low density)	6–7	1
Polyethylene (high density)	6–7	2
ABS polystyrene	5	4
Nylon	2–4	3
Steel-reinforced cement	0.2–4	10–15
Cast iron	0.2–3	6–20
Polystyrene	2	2
Common woods, crack ∥ to grain	0.5–2	0.5–1
Polycarbonate	0.4–1	1.0–2.6
Cobalt/tungsten carbide cermets	0.3–0.5	14–16
PMMA	0.3–0.4	0.9–1.4
Epoxy	0.1–0.3	0.3–0.5
Granite (Westerly Granite)	0.1	3
Polyester	0.1	0.5
Silicon nitride, Si_3N_4	0.1	4–5
Beryllium	0.08	4
Silicon carbide SiC	0.05	3
Magnesia, MgO	0.04	3
Cement/concrete, unreinforced	0.03	0.2
Calcite (marble, limestone)	0.02	0.9
Alumina, Al_2O_3	0.02	3–5
Shale (oilshale)	0.02	0.6
Soda glass	0.01	0.7–0.8
Electrical porcelain	0.01	1
Ice	0.003	0.2*

* Values at room temperature unless starred.

5.9.5 Crack Initiation and Propagation Energies

In order for a crack to grow through a material, a critical energy is required to initiate growth. Once initiation has occurred, three types of further propagation are defined - unstable, semi-stable and stable. The force-deflection curves for each of these mechanisms of crack propagation is presented in Figure 5-10 a-c. In the case of an unstable crack, sufficient strain energy is stored in the specimen to allow for propagation of the crack across the width of the specimen. A stable crack will require further energy to continue propagation. A semi-stable crack is one which starts off unstable before crack arrest occurs. In semi-stable crack propagation crack arrest occurs when sufficient strain energy has been used in crack propagation to reduce the stored strain energy to be less than the energy required for further propagation, prior to complete fracture of the solid.

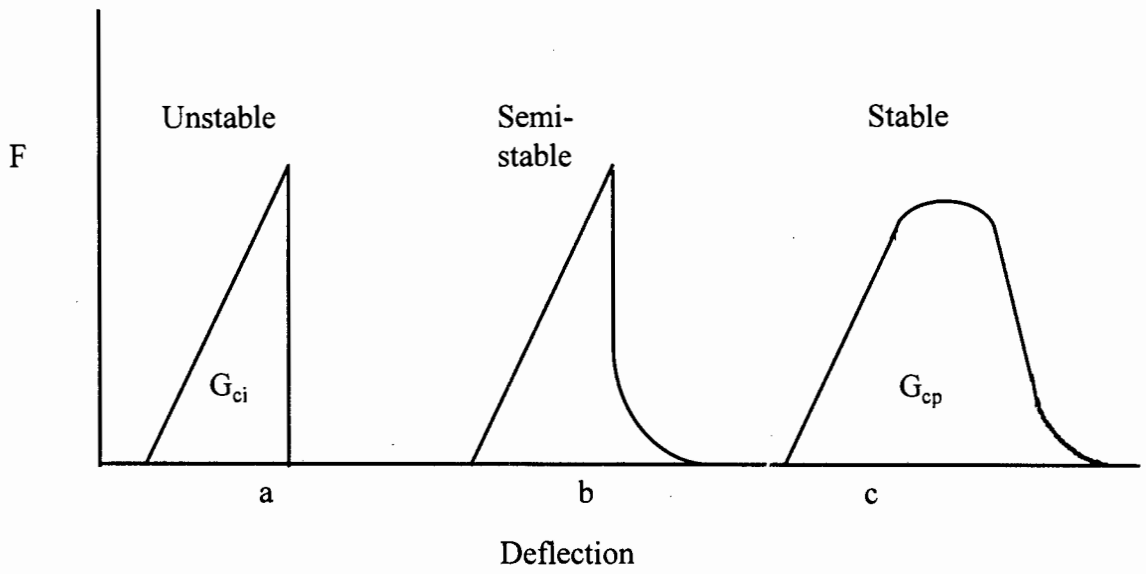

Figure 5-10 - Crack Propagation Modes

According to equation (5-10), initiation of propagation occurs when the strain energy release rate, G, is greater than the crack resistance, R. R was defined previously as the energy required to create new surfaces and is given as twice the surface free energy of the material. For the crack to continue propagating without further work, it is required that:

$$\frac{dG}{da} > \frac{dR}{da} \qquad (5\text{-}16)$$

At this point it is appropriate to introduce a parameter known as the *compliance* of a system. For a specimen which is assumed to deform in a totally elastic manner C, the compliance, or inverse of stiffness, is purely a function of the crack length (a) and the geometry of the test setup. C is defined as the ratio of the deflection of the system (x) to the applied force causing that deflection (F) (Plati and Williams (1975)):

$$C(a) = \frac{x}{F} \tag{5-17}$$

Since the system is entirely elastic, all of the energy supplied by the applied load goes into causing the deformation. Furthermore, the relationship between applied load and deformation will be linear. The energy absorbed will thus be given by the area under the triangle in the load-deflection diagram:

$$U = \frac{1}{2}Fx = \frac{1}{2}F^2C \tag{5-18}$$

Now, from equation (5-10), the strain energy release rate for uniform thickness B, G is given by:

$$G = \frac{1}{B}\frac{dU}{da} \tag{5-19}$$

Initiation of crack growth has been discussed previously to occur when G reaches a critical value G_C, which, substituting equation (5-18) into (5-19) gives:

$$G_C = \frac{F^2}{2B}\frac{dC}{da} \equiv \frac{WF^2}{2B}\frac{dC}{d(a/W)} \tag{5-20}$$

at the critical force F which initiates crack growth. The second part of this equation is used further.

A factor ϕ is now introduced to make the analysis applicable to other geometries. Before proceeding further in the development of this analysis, therefore, it is necessary to introduce

the geometry of the tests to be used in this work. The three point bend test is presented in Figure 5-11 and is discussed in section 5.11.1, and the analysis presented here will relate specifically to this test system. In this case ϕ is defined as [Plati and Williams (1975)]:

$$\phi = \frac{C}{dC / d(a / W)} \tag{5-21}$$

and is thus a calibration factor which is a function of a/W and s/W. It is presented as an empirical function of a/W for various values of s/W in texts such as Plati and Williams (1975). These functions were determined experimentally by measuring the change in compliance for different values of a/W.

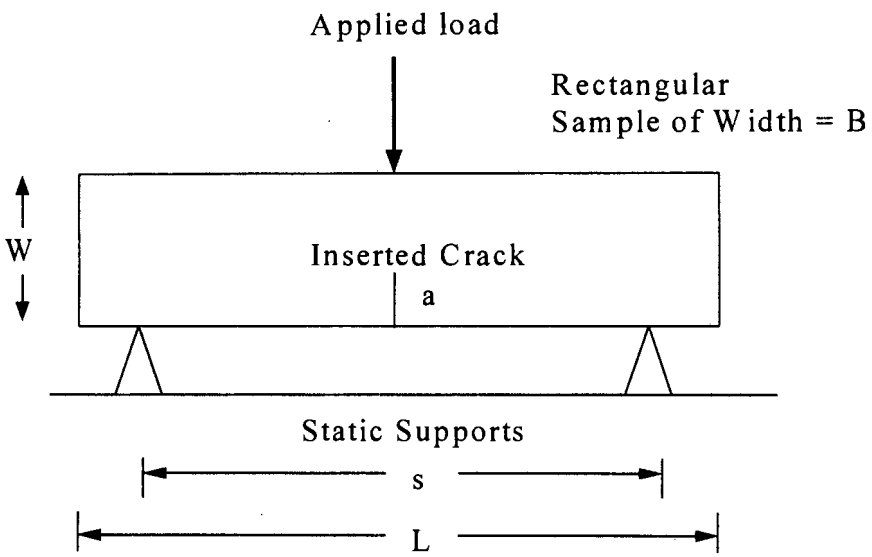

Figure 5-11 - Configuration for the Three Point Bend Test

Substituting equation (5-21) and equation (5-20) into equation (5-18) and rearranging gives the value of the strain energy release rate for crack initiation for both stable and unstable fracture G_{CI} as:

$$G_{ci} = \frac{U}{BW\phi} \tag{5-22}$$

In this equation ϕ is a function of the geometry of the test system. If the crack is semi-stable or stable, the total energy required for fracture (initiation and propagation), U_p, is given by the total area under the load versus displacement curve. The strain energy release rate required for further crack propagation, G_{CP}, can thus also be calculated. This is given by:

$$G_{CP} = \frac{U_P}{B(W-a)} \tag{5-23}$$

5.9.6 Prediction of Crack Stability

Using the development presented in the former sections, it is possible to determine whether crack propagation will be stable or unstable. An unstable crack will propagate after initiation without the addition of any more work. If the crack resistance, $R=G_C$, is constant, for unstable crack propagation, equation (5-16) gives:

$$\frac{dG}{da} > 0 \tag{5-24}$$

In the case of a linear elastic material, the stress is directly proportional to the strain. The energy required for crack initiation/propagation for such a material in unstable fracture is given by the triangular area under the load-displacement curve, thus $U=\frac{1}{2}Fx$. Now, according to the discussion in the previous section, $F=x/C$. For a constant x, equation (5-20) can be rearranged [Ewalds and Wanhill (1984)] to give:

$$G = \frac{1}{2B}\left(\frac{x}{C}\right)^2 \frac{dC}{da} \tag{5-25}$$

For a constant $R=G_c$ (that is, $dR/dA=0$), and assuming the kinetic energy changes with crack length may be ignored, equation (5-25) is substituted into equation (5-24) and solved to express equation (5-24) in terms of compliance (see Appendix C1 for the derivation of this equation) [Mullier (1991), Williams (1984)]:

$$C\frac{d^2C}{da^2} > 2\left(\frac{dC}{da}\right)^2 \tag{5-26}$$

Using ϕ from Equation (5-21), this may be manipulated to give [Williams (1984)]:

$$-\frac{d\phi}{d(a/W)} > 1 \tag{5-27}$$

for initiation of crack extension. The derivation of this equation is presented in Appendix C2.

Now, in order to determine whether a crack will propagate over the entire sample, return to equations (5-22) and (5-23). The former is written in terms of the energy required for the crack to initiate propagation, and the latter in terms of the energy taken up by propagation. For a crack to continue propagation, therefore, the released stored strain energy in the sample, represented by the initiation energy of the crack, must be greater than the energy required for propagation. Using equations (5-20) and (5-21):

$$G_C BW\phi > G_C BW\left(1-\frac{a}{W}\right) \qquad \text{or} \qquad \phi + \frac{a}{W} > 1 \tag{5-28}$$

for unstable crack propagation through the entire sample [Williams (1984), Mullier (1991)]. The inequalities provided in equations (5-22) and (5-23), along with the empirical functions of ϕ, provide a means to predict whether notch propagation will be stable or unstable for any given system of which the geometry is known. It is once again noted that this is for linear elastic materials. The interpretation of this analysis for materials in which either plastic or other energy dissipation mechanisms occur prior to fracture is continued in section 5.9.8.

5.9.7 The Yield Stress - Definition and Experimental Determination

In an ideal linear elastic material, strain energy is stored elastically until brittle failure occurs. When a real material is loaded, however, energy dissipation and failure may occur due to ductile yielding. Here the material in the failure zone flows until failure. The von Mises criterion for yielding was developed to predict the point at which plastic flow in a stressed material will begin to occur. A full derivation of the von Mises criterion (presented in German in von Mises

(1913) and summarized in English in Williams (1983)) is not relevant in the scope of this work. The criterion is based on an analysis of the principle stresses in the solid and says that yielding will occur when the sum of the stresses along the various axes reaches a critical value, σ_Y.

If one takes the three principle stresses σ_{XX}, σ_{YY} and σ_{ZZ} as shown in Figure 5-8 and denotes them as σ_1, σ_2 and σ_3 with $\sigma_1>\sigma_2>\sigma_3$, then the von Mises criterion predicts that the material will flow plastically when:

$$(\sigma_1-\sigma_2)^2 + (\sigma_2 - \sigma_3)^2 + (\sigma_3 - \sigma_1)^2 = 2\sigma_Y^2 \tag{5-29}$$

where σ_Y is the yield stress of the material.

This solution provides an accurate prediction of the yield stress [Mullier (1991), Williams (1973), Tabor (1948)]. The solution of this equation when axial symmetry is involved is difficult to resolve and an approximation of the von Mises criterion is often used to describe yielding. The Tresca criterion (see, for example, Knott (1973)) was developed based on the fact that yielding is a shear process, and states that yielding takes place on planes at 45° to the principle axes when the maximum shear stress reaches some critical value, that is to say when

$$\frac{\sigma_Y}{2} = \frac{\sigma_1 - \sigma_2}{2}, \frac{\sigma_2 - \sigma_3}{2}, \frac{\sigma_3 - \sigma_1}{2} \tag{5-30}$$

whichever of these terms is the greatest. It is noted that although this approach is simpler to solve mathematically it is generally inferior to the von Mises criterion [Williams (1973)]. Experimentally, the yield stress, σ_Y, can be determined using the configuration suggested by the Brinell hardness test which is performed using a spherical indenter. This configuration is shown in Figure 5-12 and discussed in section 5.14.1. The following discussion, based on Mullier (1991) and Tabor (1948), provides an understanding of the energy dissipation occurring in this test configuration which allows for calculation of the yield stress σ_Y.

A typical force-deflection plot from the spherical indentation for the material used in this work is presented in Figure 5-13 (the slope-deflection curve, calculated as dF/dδ, shown on this plot is discussed further below).

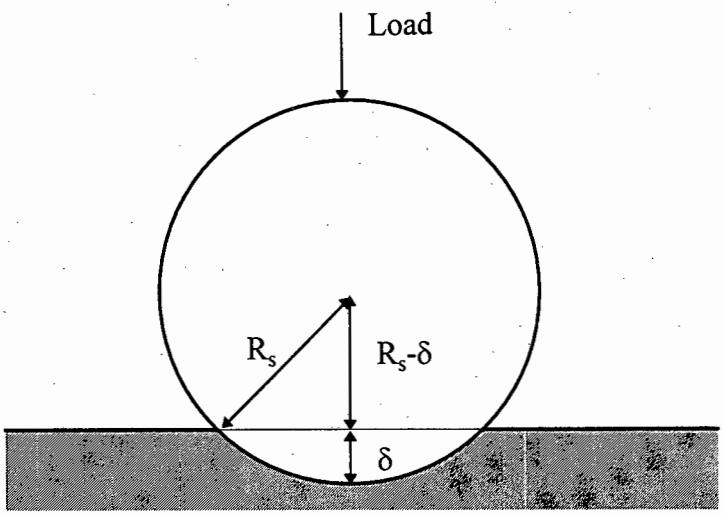

Figure 5-12 - Configuration for Spherical Indentation Testing

When an ideally plastic material is subjected to a load, initially it will deform elastically, even if only to a small degree. Eventually a force is reached where plastic deformation begins to occur. The von Mises criterion mentioned previously states that the material will begin to deform plastically in a region below the surface when the mean surface pressure on the material reaches a value of approximately 1.1 σ_Y. At this stage the plastic zone, and the resulting permanent deformation, is small. As the force is increased, the size of the plastic region grows until it extends over the whole region of the deformation caused by the indenter. At this stage, the pressure - yield stress relationship is given by:

$$P_m \approx c\sigma_Y = H \tag{5-31}$$

where H is the Brinell hardness, and c is a proportionality constant which lies between 2.6 and 3, depending on the depth of the indentation and the type of the material. The value of c can be determined experimentally [Mullier (1991)]. Materials such as foams have low values of c since there is very little deformation prior to collapse, while denser materials will have a higher value of c. For agglomerate bars made with a particles bound by a polyvinylpyrrolidone (PVP) binder

Mullier (1991) uses a value of c=2.7. In preliminary work for this thesis it was seen that a 4% increase in the calculated value of yield stress was observed by changing c to 2.6 and a decrease of 10% by using c=3.0. A value of c=2.7 is used further in the interpretation of data in this thesis, while recognising that samples may be denser than those found in the work of Mullier (1991) due to the smaller particle sizes which result in closer packing. If the latter is true, the yield strength may be slightly overestimated in the current work.

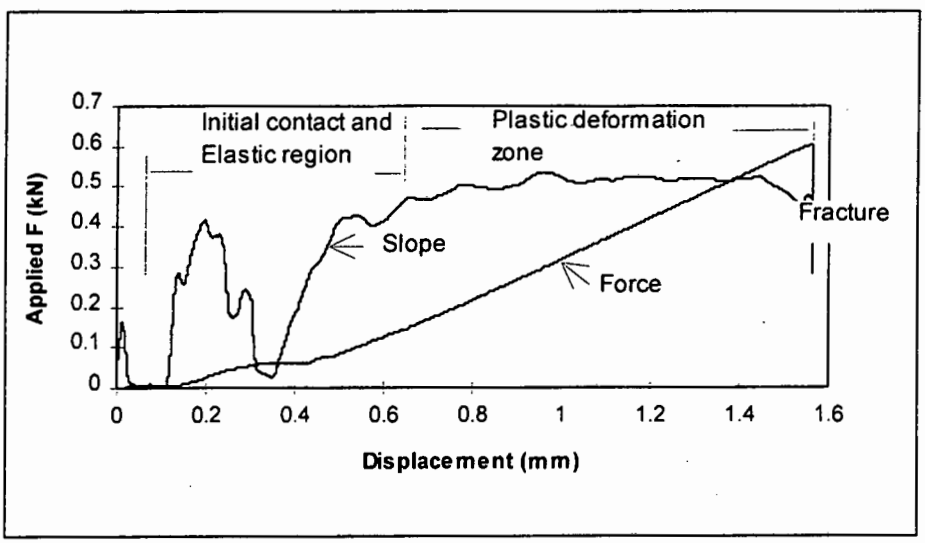

Figure 5-13 - Typical F-Displacement and Slope-Displacement Curves for the Sperical Indentation Test

Relating pressure to the applied load (F) gives $P_m=F/A=F/\pi a^2$. Considering the geometry of the system as shown in Figure 5-12, the contact radius of the indenter (a) can be expressed in terms of the depth of indentation (δ) and radius of the indenter (R) as follows:

$$a^2 = R^2-(R-\delta)^2 = 2R\delta - \delta^2 \qquad (5\text{-}32)$$

When the radius of the indenter is chosen such that $R>>\delta$ then the force - penetration depth relationship is given by:

$$F = c.2\pi R\delta\sigma_Y \qquad (5\text{-}33)$$

According to this relationship the slope of the linear section of a plot such as that shown in Figure 5-13 will give σ_Y, the yield stress. The region in which the relationship is linear is

determined by calculating the slope of the F-δ graph (dF/dδ) and plotting slope as a function of penetration distance. Such a graph is also shown in Figure 5-13.

Using a value of R of 12.5 mm (as used in this work - see section 5.14.1) and an average penetration depth of 1 mm, the simplification of ignoring the δ^2 term results in an error of 5% in predicting the value of σ_Y.

The assumptions in this development are of an 'ideally' plastic solid in which all permanent energy loss prior to failure goes into plastic deformation - that is to say there is no energy loss via microcracking or other dissipation mechanisms. The indenter is also required to be frictionless.

The assumption of an 'ideally' plastic solid needs to be questioned in the case of agglomerates such as S/S products. Energy dissipation via processes such as microcracking has already been discussed. Such microcracking processes can be detected as distinct, but small, peaks in a load-displacement curve. In this work it is suggested that such microcracking processes are insignificant relative to the plastic deformation and that the assumption of the 'ideal' plastic solid holds.

5.9.8 Interpretation of Data for Plastically Deforming Materials and Agglomerates

The Irwin analysis for ideal linear elastic materials in which crack propagation occurs solely due to the elastic dissipation of strain energy has been discussed in the preceding text. In such a material the stress-strain relationship is linear until fracture. In a material such as the S/S products being considered, other mechanisms of energy dissipation will occur.

In most materials some plastic deformation will be expected to occur prior to gross fracture. Equation (5-11) predicts infinite stresses at the crack tip where r=0. In practice this indicates that the yield stress of the material, σ_Y, is exceeded and plastic deformation occurs around the crack tip in a "plastic zone". The size of this zone can be estimated from evaluating σ_{YY} at θ=0. From equation (5-11):

$$\sigma_{YY} = \frac{K_C}{\sqrt{2\pi r}} \qquad \text{or} \qquad r = \frac{1}{2\pi}\left(\frac{K_c}{\sigma_{YY}}\right)^2 \tag{5-34}$$

The limiting or yield stress is reached when $\sigma_{YY} = \sigma_Y$. The material then deforms which will mean a reduction in the load-carrying capacity of the material in the region of the crack tip. In response to this yielding the elastic field in the region of the crack extends, so that the size of the plastic zone doubles, giving:

$$r_p = \frac{1}{\pi}\left(\frac{K_c}{\sigma_Y}\right)^2 \tag{5-35}$$

It is this equation which is used to calculate the radius of this plastic zone using K_{IC} as determined in the three point bend test and σ_Y as determined in the spherical indentation tests.

Further to exhibiting energy dissipation via plastic deformation, other strain energy dissipation mechanisms are expected in agglomerate materials such as hardened cement pastes, particle-binder mixtures and S/S products. A uniform energy distribution will not be expected. Hardened cement paste (hcp) and concrete are both two phase materials, with strong particles dispersed in a weaker matrix. In the case of hardened cement paste the strong particles of unreacted cement are dispersed in CSH, while in concrete the aggregates are dispersed in the weaker hardened cement paste [Mindess (1983)]. Strain energy will be distributed to different extents in these two phases which may allow for failure of one phase prior to the other. As in the case of cement pastes, microcracking due to flaws around the crack tip and at phase junctions will be expected [Grudemo, (1979)].

For materials which exhibit energy dissipation via other mechanisms than elastic fracture such as microcracking described above, the graph of fracture stress vs inverse of notch length is expected to be of the form shown in Figure 5-14. To account for non-recoverable energy dissipation prior to gross fracture, a number of researchers have suggested and used the concept of an *effective* crack length or *process zone* in the energy balance equation for the interpretation of fracture behaviour [Xu et al (1995), Mullier (1991), Adams et al (1989a), Mullier et al (1987)]. By this approach an increment to the notch length, Δa, is added to the actual notch

length, a. This represents the sum of any *natural flaw size* due to particle packing effects, a *microcracking zone* which takes into account energy dissipation processes such as microcracking and microscale repacking effects (this not very sensitive to composition or voidal variations), and the *plastic deformation zone*, r_p [Adams et al (1989a)]. Such an analysis technique is advantageous in that it provides an easy to use tool to make allowance for total energy dissipation prior to failure, regardless of the mechanism, for a wide variety of systems. The 'black-box' approach, in which all energy dissipation prior to fracture is accounted for by one parameter, has the disadvantage that the different individual mechanisms of energy dissipation cannot be isolated.

The effective crack length ($\bar{a}$), which is the sum of the introduced crack (a) and the notch length increment, Δa, is then used in the energy balance equation. The measured values of E, K_c and G_c are noted by Adams et al (1989a) to be sensitive to porosity. No further record is given of how to quantify these effects, but agglomerates prepared for testing account for these effects by ensuring consistent compaction of material during sample preparation.

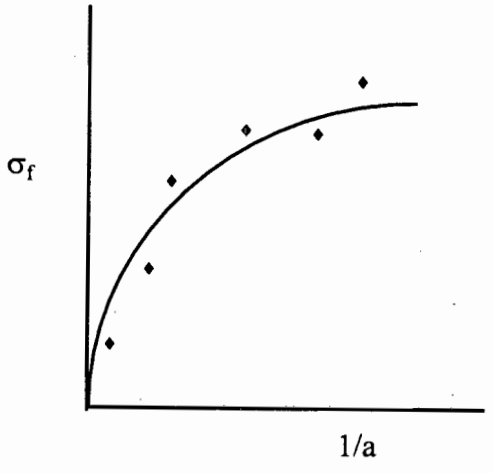

Figure 5-14 - Expected Stress-Strain Plot for Material Showing Plastic Deformation or Microcracking

K_{IC} is now a function of $(a+\Delta a)$ as follows:

$$K_c = Y \sigma_f \sqrt{\pi(a+\Delta a)} \qquad (5\text{-}36)$$

and G_C is now given by $2\gamma + \gamma_p$, where γ_p is a term introduced to account for the energy dissipation described.

Adams et al (1989a) present an iterative graphical procedure for calculating the value of Δa and K_{IC}. A number of sample specimens with different notch lengths are tested using the triple point bending test as described previously. According to equation (5-13), $(\sigma_f Y)^2$ vs 1/a is plotted, using the inserted notch length a in the calculation of Y and 1/a. For samples with a significant process zone, this graph shows a marked curvature. The initial slope is used to calculate a first estimate of K_{IC}, $K_{IC}^{(o)}$ by:

$$K_{IC}^{(o)}=(\pi \text{ slope})^{1/2} \qquad (5\text{-}37)$$

This is substituted into equation (5-36) above, using an estimate value of $Y = 1.12\pi^{1/2}$ being that of a surface crack in a semi-infinite plate, and the value of σ_f for an unnotched bar to give a first estimate of Δa, $\Delta a^{(o)}$. The next step is to plot $(\sigma_f Y)^2$ vs $1/\bar{a}^{(1)}$ where $\bar{a}^{(1)} = a + \Delta a^{(o)}$ and $Y = Y(\bar{a}^{(1)})$. $K_{IC}^{(1)}$ is calculated from the slope of this graph. This value of $K_{IC}^{(1)}$ and $Y = Y(\Delta a^{(1)})$ and the fracture stress of the unnotched bar is used to calculate a new value for Δa, $\Delta a^{(1)}$. $\Delta a^{(1)}$ is used to calculate $\bar{a}^{(2)}$ and $Y(\bar{a}^{(2)})$. $(\sigma_f Y(\bar{a}^{(2)}))^2$ vs $1/\bar{a}^{(2)}$ is plotted and $K_{IC}^{(2)}$ determined from the slope. The process is repeated until $K_{IC}^{(n+1)}= K_{IC}^{(n)}$, or until the slope of the plot shown in Figure 5-14 gives the best linear fit. Adams et al (1989a) suggest that five to eight iterations are usually required. The final value of $\bar{a}$ is used in the calculation of G_c. A discussion of the statistical analysis of the results follows below.

Mullier (1991) found, however, that the use of the unnotched bar in the calculation above gave high values of $1/\Delta a$, or small inherent process zones for the unnotched bars. This significantly biased the fit of her data in such a way as to lower the calculated value of K_{IC}. Mullier presents no explanation for this observation, but excludes the unnotched bars from further calculations. Only fracture stresses of samples with notches of between 0.8 and 5.1 mm, which equated to samples of a/W between approximately 0.04 and 0.255, were used in her calculations. For each successive iteration, a set value of 0.1mm was added to Δa until the best fit of the data was obtained. The next step in her analysis was to iterate this value by smaller increments down to 0.01mm until once again the best fit was obtained. The final value was taken as Δa. In the work

of Mullier it was found that some samples showed no improvement in linear fit when Δa was introduced. This observation was attributed to experimental error.

5.9.9 A Review of Published Studies on LEFM techniques Applied to Agglomerates

A summary from the literature of experimental work using LEFM to determine the strength of agglomerate-type materials is presented in Table 5-2.

Table 5-2 - Literature Reports of LEFM results Applied to Agglomerates

Researcher	Description of solids	Constituent Particle Sizes (μm)	Plastic Zone Size (μm)	Process Zone Size (μm)
Adams (1985)	Sand and PVP binder	180-250	not reported	900[†]
Adams (1989a)	Sand and PVP binder	60	not reported	1201[†]
Mullier (1991)	Sand and	45-180	3 to 1307[‡]	750 to 2150[†]
	PVP binder	180-250	9 to 644[‡]	550 to 2230[†]
Xu et al (1995)	Moist coal powder compacts	10.4	not reported	93 to 659[*]

[‡]Determined via Spherical Indentation test

[†]Determined via Three Point Bending Test

*Found using a cantilever test rig

From these results it can be seen that the reported plastic zone sizes range from 0.03 to 11.6 times the average particle size, while the process zone size (which includes the plastic zone) ranges from 2.6 to 63 times the average particle sizes. Furthermore, as the average particle size in the agglomerate increases, both the plastic zone and process zone sizes appear to increase.

Mullier (1991) observed that the plastic zone size increases with both binder concentration and binder molecular weight. For low binder concentrations or binders with low molecular weights, the plastic zone size was of the order of the size of the binder bridges which were observed by Scanning Electron Microscopy (SEM). As the binder concentrations and molecular weights increase, the size of the plastic zone extended over several particle diameters, which was taken

to imply that the plastic zone is not restricted to a single binder bridge. This is in line with suggestions by workers such as Davies (1949) who stated that the distribution of stresses into the solid is not limited to the point of contact between an indenter and the solid and extends through the solid for a finite distance.

In the case of the S/S products here, this would suggest that an increase in the concentration of binders in the solid, shown previously to be mixing water and cement hydration product, would increase the size of the plastic zone. Furthermore, assuming the ratio of plastic zone and process zone sizes to particle size in the S/S products will be similar to those in the work of Mullier (1991), the size of the plastic zone for the S/S products will lie roughly between 0.01 and 30 μm and that of the process zone between 4 and 48 μm. It is recognised that the assumption that the ratios of plastic zone and process zone sizes are similar to those of other workers has no real basis, but its use does provide an indication of the order of magnitude of process zone sizes expected in the S/S products.

In the study by Xu et al (1995) powder compacts with low water content showed no plastic dissipation of energy. As the water content was increased from 0.1% to 0.3% (by wt of liquid to solid) some degree of plastic deformation was observed. This is attributed to the formation of liquid bridges in the capillary gaps at high water contents. The presence of these large bridges allow for greater deformation prior to rupture. The authors suggest that, although these bridges exist at low moisture contents, they are likely to allow only limited particle-particle separation before fracture occurs. The increase in water content also led to an increase in fracture toughness. The observations of Xu et al are thus in line with those of Mullier presented above: an increase in binder content increases the degree of plastic deformation and the fracture toughness of the agglomerate.

5.10 Results of the Indirect Tensile Test (ITT)

The ITT was carried out on S/S products made from both the FeCr Dust and ETP filter cake. The aim of these tests was to

(i) characterise the strength of the materials in terms of a macroscopic strength parameter

(ii) provide an indication of the effect of the operational variables cement content, water to solids ratio and curing time on strength.
(iii) to identify a relationship between strength measured via the ITT and that measured via three point bending. Such a relationship has the potential to allow the use of an easy-to-obtain strength tool to predict a fundamental strength parameter (K_{IC}).
(iv) Strength has been seen previously to depend on both physical nature of the aggregate (particle size, surface texture) and the chemical composition of the mixing waters and aggregates/ wastes. The ETP was observed to be finer than the FeCr Dust, finer particles resulting in lower strengths of cements (see Chapter 2). Chemically, the ETP products are higher in Fe and Ca (primarily as $Ca(SO_4)$) and contain no Zn. The differences in both chemical and physical nature of the two waste products would thus suggest different strength behaviour. It was aimed to thus determine how physical size and chemical composition affect strength for these S/S products.

5.10.1 Experimental Determination of Tensile Strength

Material for unconfined strength tests was formulated and mixed in the manner described in Chapter 3. The cylindrical moulds used for the material were 32 mm in diameter and approximately 90 mm in length. The moulds were filled with the fresh mixture to between 60 and 75 mm height in order to give cylinders with length to diameter ratios of approximately 2 as required by the standard testing procedures. These cylinders are recognised to be smaller than the USA standard cylinder of 305 mm height by 152 mm diameter. A shortage of waste product required using smaller amounts of material in all tests and hence the smaller cylinders used [PCI (1986)].

After curing for various periods of time the samples were subjected to the indirect tension or splitting test on an Instron 5567 materials testing rig fitted with a 5 kN load cell (see Figure 5-15). The nominal rate of displacement of the moving crosshead was set at 0.5 mm/s. This is much lower than that required by traditional concrete testing standards such as the SABS 863 Standard method for testing of Compressive Strength of Concrete which requires a rate of loading of 0.25 MPa/s. The low strengths of the materials at hand, however, required that a lower rate of loading be used.

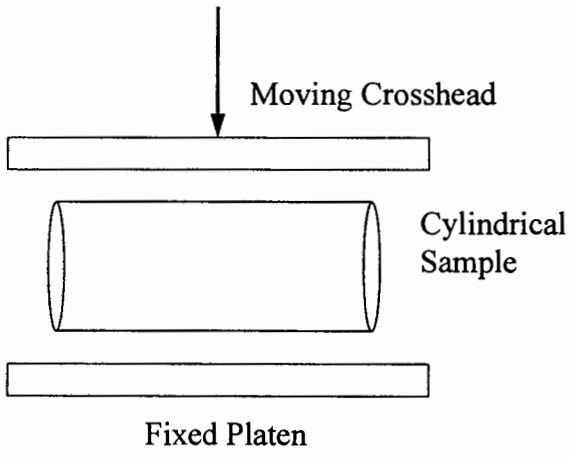

Figure 5-15 - Configuration for the ITS

The effect of rate of loading on measured strength of concrete is shown in Figure 5-16 [PCI (1986)]. Standard control tests are usually considered as static tests. As the rate of loading becomes large compared to the velocity of stress waves through the concrete, dynamic effects due to inertia become important and increase the observed strength. Should the same apply for S/S products, the strengths determined in the tests presented previously may be underestimated.

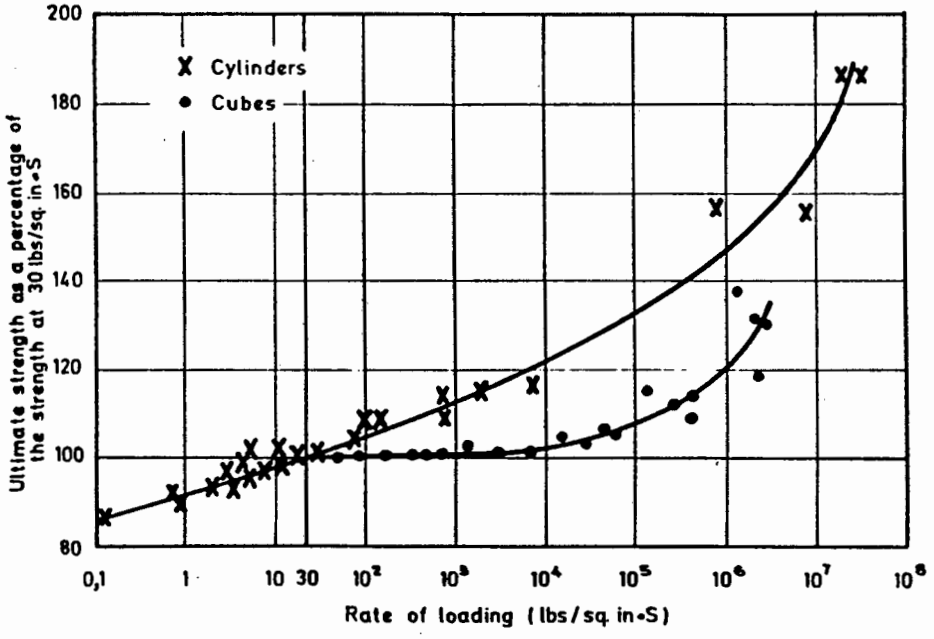

Figure 5-16 - Effect of Rate of Loading on Measured Strength of Concretes [PCI (1986)]

The load at which a sample fails (the "critical load") is seen as a sharp drop in load on a plot of the applied load vs crosshead displacement. The tensile strength, σ_t is calculated by:

$$\sigma_t = \frac{2P}{\pi DL} \qquad (5\text{-}38)$$

where P = Failure Load (kN)
D = diameter of sample (m)
L = length of sample (m)

5.10.2 Trends Highlighted by the Indirect Tensile Test

The ITS of the solidified waste products was observed to be dependant on a combination of the water to solids ratio, cement content and curing time. The interaction between the variables is explored further by means of a factorial design in Chapter 8. The following comments are presented here.

Table 5-3 provides ITS results for selected samples of solidified Ferrochrome Smelter Dust (FeCr Dust) and the metal hydroxide-containing precipitate from a wastewater stream (ETP). These samples represent a number of different operational variable values (cement, w/s and curing) within the range of interest in this thesis as defined in Chapter 3.

Table 5-3 presents ITS results for selected samples of solidified FeCr Dust and the metal hydroxide-containing precipitates from a wastewater stream (ETP 1 and ETP 2). The effect of type of waste on strength is discussed in (a) below. In Table 5-3 ITS results are presented for a number of different values of the operational variables. The effect of the operational variables on strength is discussed in (b) which follows.

The following is highlighted from Table 5-3:

(a) Overall Strength of the Materials

In order to compare the strengths of hardened cement pastes against literature reported values, the work of Wright (1955) was used. He found the compressive strength of cubes to be approximately 14 times strengths of cylinders of concrete measured via the ITT. Using this conversion factor for hardened cement paste (104 days curing) this would give a compressive strength to the order of 56 MPa. Although reported compressive strengths for hcp vary widely, the value of 56 MPa is in line with those reported in texts such as PCI (1986).

Table 5-3 - ITS Results for solidified FeCr Dust and ETP Products

Material Type	W/S Ratio	Cement Content (%)	Curing Time	Mean ITS (MPa)
FeCr Dust	0.9	20	104	0.465
FeCr Dust	0.94	26	35	0.353
FeCr Dust	0.94	26	58	0.361
FeCr Dust	0.94	26	149	0.386
FeCr Dust	0.99	20	28	0.178
FeCr Dust	0.99	30	35	0.453
ETP 1	1.18	20	28	0.139
ETP 1	1.18	20	49	0.198
ETP 1	1.18	20	70	0.197
ETP 2	1.1	20	49	0.312
ETP 2	1.18	20	49	0.280
ETP 2	1.26	20	49	0.219
hcp[✣]	0.36	100	8	3[*]
hcp[✣]	0.36	100	104	4[*]

[✣] hardened cement paste

[*] These results are approximates. Available equipment could measure maximum break loads of 5 kN or 100 kN. These samples failed under loads in between these values and these were therefore obtained from the 100kN equipment which offers less sensitive results.

For comparison of the strengths of S/S products to regulatory requirements the relationship between UCS and ITT as approximated by Wright was once again employed. Using this conversion, all strengths reported in Table 5-3 are found to equate to compressive strengths of greater than 2 MPa. The EPA and British Waste disposal authorities recommend minimum strengths of about 50 psi, or 0.35 MPa [Arniella and Blythe (1990), Sollars and Perry (1990)]. This is based on the load at the bottom of a landfill 30.5m deep containing waste with a mean bulk density of 1121 kg/m^3. The S/S products in this work have a mean bulk density of 1340kg/m^3. Although this is slightly higher than 1121 kg/m^3, it is suggested that the strengths of the S/S products are well above the required minimums.

Products made from the FeCr Dust appear, on the whole, to show higher strengths than those from the ETP cakes. The following reasons are offered for this observation:

(i) The different chemical species in differing concentrations, may affect the chemistry, extent of formation and strength of the cement hydration products. Of particular note is the much higher amount of Ca in the ETP compared to the FeCr Dust (see Table 3-1 and 3-2): Ca was used in the neutralization process responsible for the production of these dusts. Since Ca is a product of the hydration reactions, an excess of Ca in the pore solution would reduce the equilibrium conversion within the pores to CSH (see the reactions presented in Chapter 2) and hence may be responsible for the reduction of strength.

(ii) Although a quantitative evaluation of the size distributions of the ETP products was not carried out due to limitations in the capacity of available equipment at the time of this specific experimental work being carried out, the ETP cake appeared qualitatively to be finer than the FeCr Dust. The presence of fine materials was identified in the literature review of Chapter 2 to have a deleterious effect on the strength of cements and is expected to have an influence here.

(iii) The ETP cake products were made with higher water to solid ratios than the FeCr Dust products. An increase in the water to solids ratio results in a decrease in strength of the product [PCI (1986)].

Although all three of the above points are suggested to be of significance, it is suggested that the greatest difference between the different wastes is in chemical composition, with the other two points above (size distribution and w/s) being less signficant. Chemical composition is thus suggested to be the overriding factor which determines the changes in strength from one solidified waste to another.

(b) Effect of Operational Variables on Strength

While it is recognised that the operational variables have an interactive effect on strength (ie the combination of variables relative to each other is important), all three operational variables under investigation are observed to affect the ITS:

(i) **Curing Time** - Increased curing times result in increased strengths. Cement curing has been identified to continue for periods of up to a year [PCI (1986)]. Product strength is a function of the extent of cement hydration. As hydration progresses, therefore, so the product strength will increase.

(ii) **Water to Solids ratio** - A higher water to solids ratio will give a product which is more porous and thus weaker. This trend is observed in Table 5-3.

(iii) **Cement Content** - The more cement which is present in a given sample, the more hydration products which will be formed. Since these hydration products are the strength - giving materials, a higher cement content will give a higher strength product, a suggestion which is confirmed by the results in Table 5-3.

The observations are explored further using Linear Elastics Fracture Mechanics (LEFM) techniques in the following sections. The interactive effect of the variables on ITS is explored via a factorial design approach in Chapter 8.

5.10.3 Variability in ITS Results

Table 5-4 presents the variabilities of ITS results for three different sets of data expressed as the coefficient of variation (standard deviation/mean)

The solidified ETP products (ie lime-based neutralization products identified in Chapter 3) gave lower variabilities than the FeCr Dust products. The initial mixture is a combination of unhydrated cement, water and solid waste material. The bonding in the initial mixture will be dependent primarily on the liquid bridges between the particles, although some degree of cement hydration will occur shortly after contact with water. Assuming the funicular or capillary degrees of saturation due to the high water contents in this initial mixture, the strength was shown previously to depend on the void fraction of the mixture. Although an attempt was made to keep packing consistent by vibration of the mixture into moulds directly after mixing, some variability in packing directly after mixing would still be expected.

Table 5-4 - Variability in ITS Results

Set No	Material Type	No of Specimens	W/S Ratio	Cement Content (%)	Curing Time	Mean ITS (MPa)	Standard Deviation	**Coeff. of Variation**
1	FeCr Dust	4	0.99	20	28	0.178	0.0505	**28.1%**
2	FeCr Dust	23	0.94	26	35	0.353	0.0772	**21.9%**
3	FeCr Dust	8	0.99	30	35	0.453	0.1029	**22.7%**
4	ETP 1	6	1.18	20	49	0.198	0.0304	**15.3%**
5	ETP 2	6	1.18	20	49	0.280	0.0242	**8.6%**

As the cement hydrates, however, the void spaces between solid material (initially filled by water) will be filled by hydration products which then become significant in bonding the solid together. The void fraction of the assembly becomes less and therefore variabilities due to packing effects will become less significant. It is suggested that increased curing times (of the ETP vs the FeCr Dust) allows for greater infilling and hence lower variabilities.

Coefficients of variation presented in Table 5-4 are, on the whole, higher than those reported in Wright (1955) for concrete prepared with river sand and gravel. In the work of Wright, coefficients of variation ranged from 4% to 8%. This observation is attributed to the differences in sample sizes used by Wright and those used in obtaining the results presented in Table 5-4. Larger sample sizes, as used in the work of Wright, lead to lower observed coefficients of variation [PCI (1986)].

The ITT provides a quick and economical test which allows for meaningful characterisation of the effect of operational variables on strength, albeit that inherent variabilities in measured results are high. Should a test with lower coefficients of variation be required to characterise strength properties, however, it is suggested that another test method be used. Both sample sizes and the type of test used affect the observed variabilities [PCI (1986)].

5.10.4 Summary of Observations from the ITT

In summary, therefore, the ITT provides a tool whereby the macroscopic strength of S/S products, and the effect of changing operational variables on this strength, may be characterised. Strengths for all S/S products are suggested to be acceptable in terms of US EPA regulations.

The ITT gives little information as to the exact mechanisms of fracture. To this end, Linear Elastic Fracture Mechanics (LEFM) techniques are employed.

5.11 Linear Elastic Fracture Mechanics Approach to Strength Determination

The literature review section of this chapter provided the history and theory behind LEFM testing. Here experimental techniques and results are presented.

5.11.1 Experimental Determination of K_{IC} and G_C - The Three Point Bend Test

A number of tests are commonly used for measuring K_{IC} and G_C. British Standard 7448 (1991) provides details of the three point bend test and compact tension testing. Brown and Srawley (1966) show configurations of specimens with centre cracks, double edge cracks and samples in four point bending. For non self-supporting solids, cantilever tests have been employed [Xu et al (1995), Abdel Ghani et al (1990)].

For the purposes of this work the three point bend test as shown in Figure 5-11 was chosen. This test configuration is often favoured, especially for multiphase materials, since it is well understood and samples are easily prepared [Xu et al (1995), Mullier (1991), Higgins and Bailey (1976)].

For this work samples were formed in 120mm x 45mm x 20mm rectangular moulds using the procedure described in Appendix B. A number of notched and unnotched samples were tested for each formulation. Individual sample dimensions are presented in Appendix D1. On

the day prior to testing, samples were notched using a bandsaw. The effect of this notching method will be discussed later.

The distance between the supports, s, was set at 2.2 times the sample height, W, and the load was applied at a constant rate of displacement of the crosshead of 0.08 mm/min. This is lower than what was used in the ITT and works out to be lower than what is required by the British Standard BS 7448 (1991). It was decided to use a low rate of loading to ensure that the failure load detected was static failure and that dynamic effects did not come into effect.

The load vs displacement data were logged and the load at failure was obtained. After failure, the length of the notch was measured to two significant figures on a millimetre scale using an optical microscope.

In the three point bend tests, the stress responsible for fracture is taken to be an indirect stress as applied at the ends of the sample across the entire height as indicated by σ in Figure 5-17. A representation of the envisaged stress lines in such a sample is also shown in Figure 5-17. According to this representation, the fracture stress, σ_f, as given in equation (5-13) for a three point bend test is calculated using simple beam theory [Lawn and Wilshaw (1975)]. This analysis gives a value of:

$$\sigma_f = \frac{3Ps}{2W^2} \tag{5-39}$$

where P is the load at fracture divided by the width of the bar, B (kN/m)
s is the distance between the supports (m).

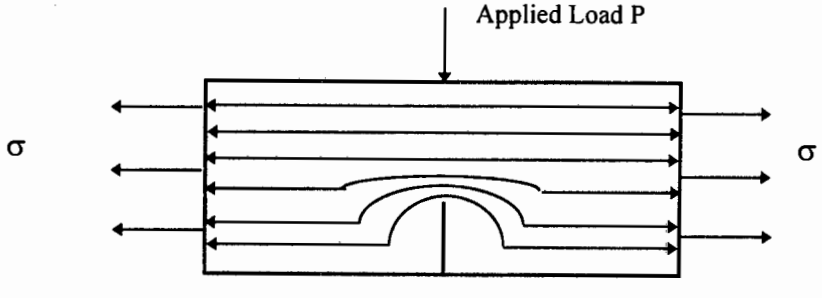

Figure 5-17 - Stress Lines in a Notched Specimen under Indirect Tension

5.11.2 Acceptable Test Configurations to ensure Plane Strain Failure

In accordance with the discussion in section 5.9.3, specimen dimensions in the triple point bending test must ensure that the sample fractures in plane strain. The following table provides suggestions by various texts as to valid specimen dimensions to ensure that plane strain occurs:

Table 5-5 - Valid Specimen Dimensions for Plane Strain Fracture

Text	Valid Specimen Dimensions
British Standard 7448 (1991)	a, (W-a), B $\geq$ 2.5 $(K_{IC}/\sigma_{YS})^2$
Adams et al (1989a)	B, W/2 $\geq$ 2.5 $(K_{IC}/\sigma_{YS})^2$
Mullier (1991)	a, B, W/2 $\geq$ 2.5 $(K_{IC}/\sigma_{YS})^2$
Brown and Srawley (1966)	a, B $\geq$ 2.5 $(K_{IC}/\sigma_{YS})^2$

Furthermore, British Standard BS 7448 (1991) requires that the value of a/W lie between 0.45 and 0.55. No information is available as to how these numbers were chosen. Brown and Srawley (1966), however state that " there is no reason why smaller values could not be used in special circumstances provided there is adequate crack length", ie that the notch is long enough that plane strain fracture is ensured.

The above relationships are based on experimental data [Brown and Srawley (1966)]. If one takes the requirements for crack sizes in the British Standard into account, it is seen that the requirements of this work and those of Mullier (1991) and Adams et al (1989) reduce to approximately the same with respect to W and B. In this current work with S/S materials the requirement of a, B, W/2 $\geq$ 2.5 $(K_{IC}/\sigma_{YS})^2$ will be satisfied. Although this provides a minimum test configuration, British Standard 7448 (1991) recommends that, where possible, larger test pieces should be used . This is to take into account uncertainties such as the underestimation of K_{IC} and the possibility of the test not meeting some of the other safety criteria.

Brown and Srawley (1966) recommend that a/W be less than about 0.5, since the geometrical correction factor Y=f(a/W) increases rapidly after this point. This implies that a small error in the measurement of a has a large effect on the calculated K_{IC} value.

Furthermore Brown and Srawley (1966) recommend that s/W is not less than 4. This is to avoid errors resulting from specimen indentation and friction at the supports. In the case of the work presented here, this requirement has not been satisfied and may be cause for error. This is discussed later.

5.11.3 Y, the Geometrical Correction Factor

A number of different workers have presented empirical equations for the value of Y, the geometrical correction factor depending on the configuration of the test. In this work a three point bend test was chosen. The reason for the choice of this test include the ease of implementation of the test and preparation of samples. Furthermore, the traditional linear elastic approach to analysis of results from this test has been extended successfully to describing the fracture of agglomerate materials [Mullier (1991), Mullier et al (1987), Adams (1985)]. The equations suggested by Rooke and Cartwright (1976) and Brown and Srawley (1966) and used by Mullier (1991) and Higgins and Bailey (1976) for this configuration are:

$$\begin{aligned} Y &= 1.09 - 1.735(a/W) + 8.2(a/W)^2 - 14.18(a/W)^3 + 14.57(a/W)^4 \text{ for } s/W = 4 \text{ and} \\ Y &= 1.107 - 1.552(a/W) + 7.71(a/W)^2 - 13.55(a/W)^3 + 14.25(a/W)^4 \text{ for } s/W = 8. \end{aligned} \quad (5\text{-}40)$$

where a is the notch length, W is the height of the sample and s is the distance between the supports (see section 5.11.1 and Figure 5-11).

It was found in preliminary investigations that samples used in this work were not self-supporting for values of s/W suggested by other workers. For this reason, a value of s/W of 2.2 was used - chosen as being the maximum for which the samples were self-supporting. The equation for Y was obtained by extrapolation and was found to be given by:

$$K_I = \left(1.08 - 1.82(a/W) + 8.45(a/W)^2 - 14.55(a/W)^3 + 14.8(a/W)^4\right) \quad (5\text{-}41)$$

where K_I is given as in equation (5-11).

Equations (5-40) and (5-41) are presented graphically in Figure 5-18. Based on Figure 5-18, where it can be seen that the plots for the three values of s/W are of similar shape and lie close

together, it is suggested here that the extrapolation which results in equation (5-41) provides an accurate equation for the value of a/W for s/W=2.2.

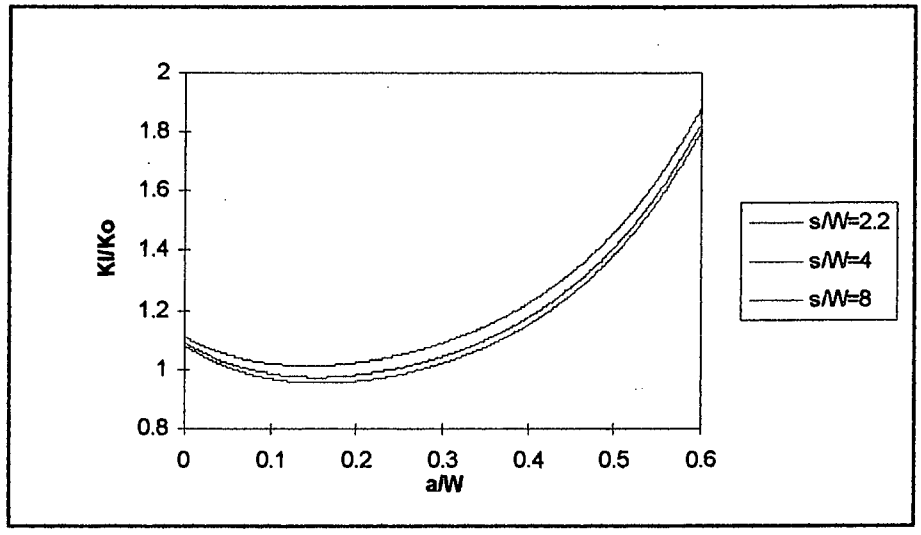

Figure 5-18 - Plot of Y values for Different Values of s/W

5.11.4 Prediction of Notch Stability

Criteria for determining the conditions under which notch propagation would occur were presented in section 5.9.5. Equation (5-27) showed that for notch propagation to occur:

$$\frac{-d\phi}{d(a/W)} > 1 \qquad (5\text{-}27)$$

Furthermore, unstable propagation occurs when:

$$\phi + \frac{a}{W} > 1 \qquad (5\text{-}28)$$

Plati and Williams (1975) provide values of ϕ vs a/W for values of s/W=4, 6, 8, 10 and 12. These values are presented graphically for s/W = 4, 6 and 8 in Figure 5-19. In the experimental work reported in this thesis, s/W was set at a value of 2.2, as this was the value at which samples were found to be self-supporting. Using the values presented in Plati and Williams, ϕ was determined for this s/W via linear interpolation.

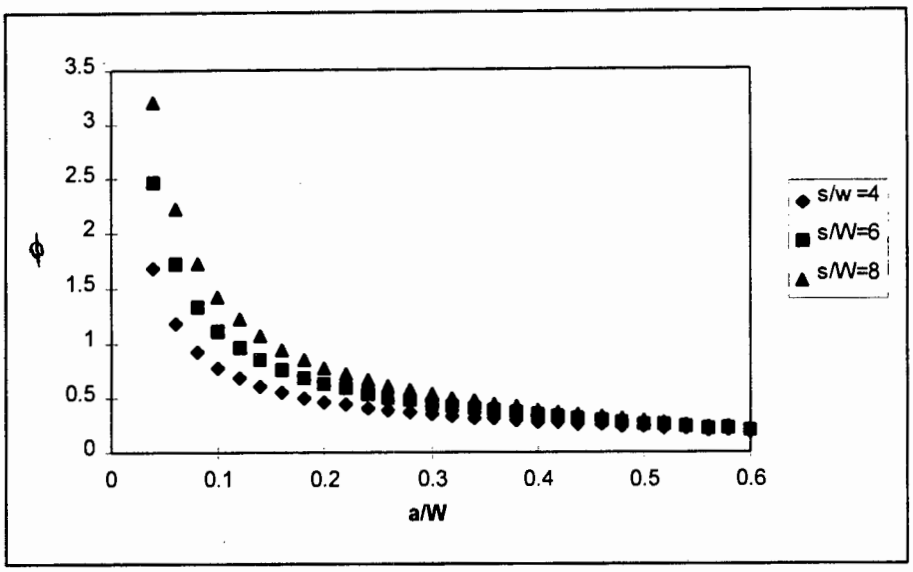

Figure 5-19 - Values of ϕ for s/W=4, s/W=6 and s/W=8

The curve for -d ϕ/d(a/W) was determined using the central difference method. Figure 5-20 presents a plot of ϕ, ϕ+a/W and -dϕ/d(a/W) for s/W = 2.2.

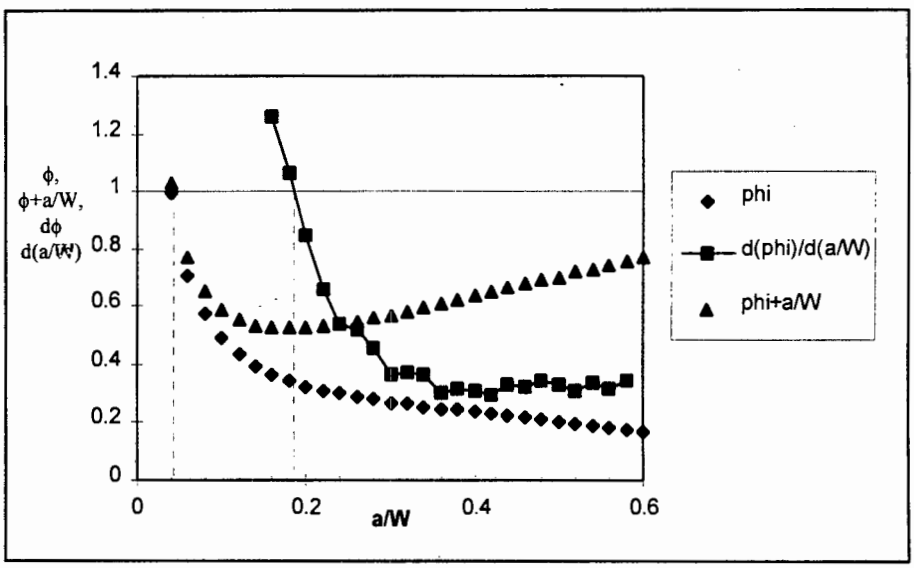

Figure 5-20 - Plot of ϕ, ϕ+a/W and dϕ/d(a/W) for s/W = 2.2

A horizontal line is drawn on Figure 5-20 where ϕ and - dϕ/d(a/W) = 1. According to equation (5-27), stable fracture occurs for all values of a/W which lie to the right of where this line intersects the plot of -dϕ/d(a/W) (ie where -dϕ/d(a/W) < 1). For these values additional energy is required to be added to the system for further notch propagation to occur.

Similarly, according to equation (5-28), unstable fracture occurs where $\phi+a/W$ is greater than 1, ie to the left of where the horizontal line intersects the curve of $\phi+a/W$.

In the zone lying between these two values, notch propagation will initially be unstable, but crack arrest will occur when notch reaches a length such that $-d\phi/d(a/W) = 1$. Such failure is known as semi-stable fracture.

Using the above analysis, unstable fracture occurs for cases where $a/W<0.038$, semi-stable fracture for $0.038 < a/W < 0.184$ and stable fracture for $a/W > 0.184$. For bars of height 43 mm (the average of those used in this work) this equates to $a<1.6$mm, $1.6\text{mm}<a<7.9$mm and $a>7.9$mm respectively.

A number of bars with different notch lengths were tested to see whether the predictions of the stability of fracture were valid. The force-deflection plots, presented in Figure 5-21 were examined and compared to Figure 5-10.

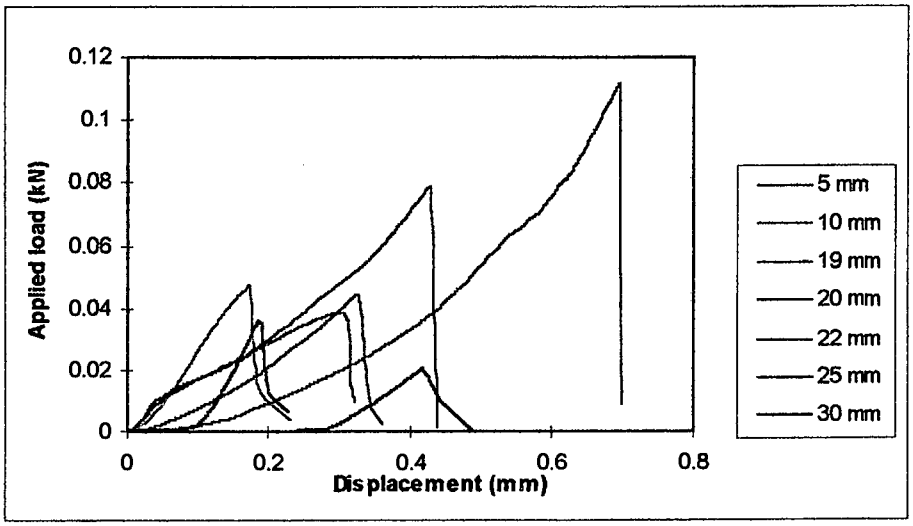

Figure 5-21 - Applied Load vs Displacement for a Number of Different Notch Lengths

Table 5-6 presents the predicted and observed modes of failure for a number of samples.

Table 5-6 - Predicted and Observed Failure Modes

a	a/W	Predicted failure mode	Observed Failure Mode
0 mm	0	Unstable	Unstable
1 mm	0.02	Unstable	Unstable
5.1 mm	0.12	Semi-Stable	Unstable
10.1 mm	0.23	Stable	Unstable
19.1 mm	0.44	Stable	Semi-stable
30.1 mm	0.7	Stable	Stable

It can be seen that as notch length increases the failure mode tends to greater stability as would be expected from theoretical prediction. Predicted and observed modes of failure do not always correspond. The stability of fracture can be affected by other factors including the composition of the sample. In Mullier's work (1991) as binder concentration was increased failure tended towards becoming increasingly unstable. It was thus deduced that other factors have an effect on notch stability and the predictions provided in equations (5-27) and (5-28) require experimental confirmation.

5.11.5 Critical Stress Intensity Factor, K_{IC}

The calculation procedure for calculating K_{IC} was outlined in section 5.9.2 and 5.11.1. In summary, the fracture load is identified as a peak on a plot of load vs displacement. The fracture stress is calculated using equation (5-39) and Y, the geometrical correction factor from equation (5-41). In accordance with equation (5-13), the fracture stress vs inverse of notch length is plotted. A plot typical of those found in this work is presented in Figure 5-22.

5.11.6 Statistical Analysis of Results

To determine a "best fit" straight line to data, a least squares approach as detailed in texts such as Miller and Freund (1985) and Topping (1965) is used, where a linear equation of the form $y=mx + c$ is fitted to the data. If the ith residual, d_i is given by:

$$d_i = mx_i + c - y_i \tag{5-42}$$

then the sum of d_i^2 is minimised to give the best fit of the straight line equation by changing m and c.

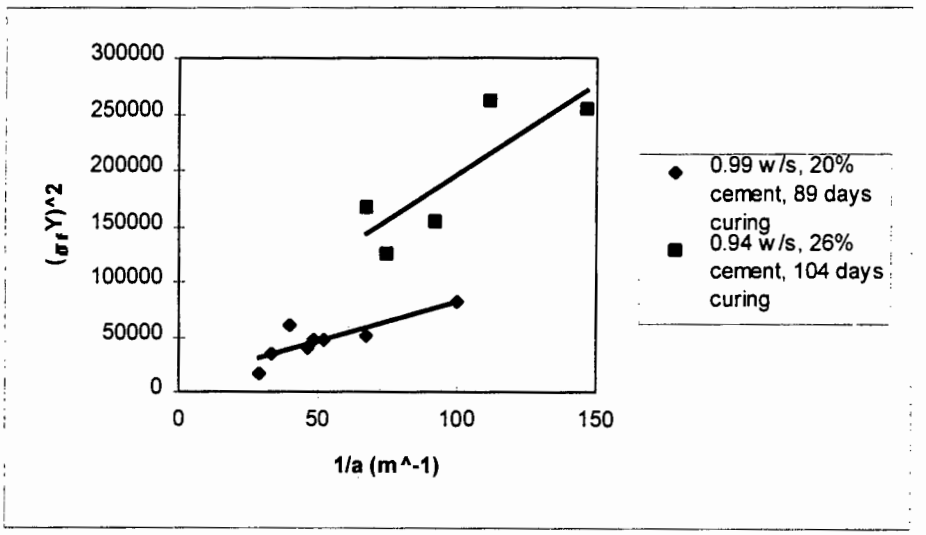

Figure 5-22 - Typical Plot of $(\sigma_f Y)^2$ vs 1/a

The coefficient of correlation, r^2, of the least squares fit provides an indication of the accuracy of the fit and is given by:

$$r^2 = \left(\frac{s_{xy}}{s_x s_y} \right)^2 \tag{5-43}$$

r^2 lies between 0 and 1, with r^2=1 representing a perfectly linear fit. The best fit is taken to be that which gives the highest r^2 value. In the above equation, s_x and s_y are the sample variances in x and y and are given by:

$$s_x^2 = \frac{\sum (x - \bar{x})^2}{n} \quad \text{and} \quad s_y^2 = \frac{\sum (y - \bar{y})^2}{n} \tag{5-44}$$

and s_{xy} the covariance:

$$s_{xy} = \frac{\sum(x-\bar{x})(y-\bar{y})}{n} \tag{5-45}$$

where n is the number of data points. These calculations can all be performed using the built in functions in MS EXCEL spreadsheeting package.

According to equation (5-13), K_{IC} is calculated from the slope of a plot of the fracture stress vs notch length:

$$K_{IC} = (m\pi)^{1/2} \tag{5-46}$$

where m is the slope of the graph.

The error in the calculated gradient is used to calculate the error in the calculated value of K_{IC} as follows:

The standard error in the fit of n points is given by:

$$\alpha = \sqrt{\frac{\sum_{i=1}^{n} d_i^2}{(n-2)}} \tag{5-47}$$

The "loss" of the two degrees of freedom is explained by the fact that the two coefficients m and c in the linear equation are replaced by their least-squares estimates. The standard error in the gradient, α_a, which is based on the standard deviation of a normal distribution of the errors, is related to α by:

$$\frac{\alpha_a^2}{n} = \frac{\alpha^2}{\Delta} \tag{5-48}$$

where $\Delta = n\Sigma x^2 - (\Sigma x)^2$. A simple error analysis (see Topping (1948)) predicts that the fractional error in K_{IC} is given by $\alpha_a / 2K_{IC}^2$.

5.12 K_{IC} Results

Due to the time consuming nature of LEFM testing, it was decided to focus on the FeCr Dust products for the LEFM analysis. Part of the aim of this work is to develop a relationship between K_{IC}, the stress intensity factor, and the ITS. This is discussed in section 5.15. Should such a relationship hold, it can be used to predict the K_{IC} results for the ETP products from ITS results. This is discussed further in Chapter 8. The discussion which follows, therefore, refers only to the solidified FeCr Dust products.

5.12.1 Observations on the Plot of $(\sigma_f Y)^2$ vs 1/a

A typical plot of $(\sigma_f Y)^2$ vs 1/a for the solidified FeCr Dust products is presented in Figure 5-22. The straight line through this plot is a linear regression for the data. For notch lengths of greater than 5 mm (equating to a value of a/W of approximately 0.11), a linear relationship between fracture stress and the inverse of notch length was observed. The linear relationship is discussed further below. Details of the results on notch length, sample sizes, fracture load, fracture stress and K_{IC} for all samples are presented in Appendix D1.

An attempt was made to further linearize these plots for all experimental data in accordance with the discussion presented in section 5.9.8. In Table 5-7 the effect on r^2 of introducing various values of Δa in to the calculation is shown. It can be seen that as Δa is increased, little effect on r^2 is initially seen. As r^2 becomes larger, the goodness of fit is reduced. The iteration process described for resolving the size of the process zone thus shows no application in improving the fit of data for the work presented in this thesis.

Table 5-7 - Effect of da on linear fit of $(\sigma_f Y)^2$ vs 1/a showing r^2 as a function of Δa

Sample Details			Δa				
Cement (%)	**w/s**	**Curing**	**0**	**0.01**	**0.05**	**0.1**	**0.5**
20	0.9	104	0.990	0.990	0.990	0.990	0.989
20	0.99	89	0.946	0.946	0.945	0.943	0.932
75	0.86	104	0.994	0.994	0.994	0.993	0.992

According to the discussion of the work by Xu et al (1995), Mullier (1991), Adams et al (1989a) and Adams (1985) presented in section 5.9.8, the linearization technique is used to account for the process zone during calculation of K_{IC}. This zone is the sum of a plastic energy dissipation zone and a zone in which processes such as microcracking accounts for energy dissipation prior to fracture.

In the work of the abovementioned researchers, process zones (the sum of the plastic zone and a zone which allows for energy dissipation due to microcracking) were identified which lay between 2.6 and 63 times the average particle size. Considering that the FeCr Dust and cement particles in the S/S products are all extremely fine (mostly < 2μm), a rough calculation based on previous workers calculations would predict the process zone size to lie between 5 μm and 126 μm.

Notch measurement after fracture was to two decimal places on a millimeter scale. This would not be sensitive enough to characterize a process zone in samples prepared from primary particles. Discussion of the process and plastic zone sizes is continued in section 5.14.

Furthermore, the effect of the method by which samples were notched will affect the observed results. Initially an attempt was made to insert a blade into the fresh mixture prior to hardening. In this way a 'sharp' notch would be ensured, and there would be no problems associated with fatigue during post-setting notching. It was found, however, that most samples broke on removal of the blade. For this reason it was necessary to notch after samples had hardened. Notching was done using a hardened steel bandsaw. It is recognised here that this does not result in a perfectly sharp notch and has the potential to cause microcracking ahead of the notch tip during notching. This microcracking may have been observed as permanent deformation prior to gross fracture during loading in the three point bend test. Hence permanent energy dissipation which should have been observed during testing occurs during sample notching.

Finally, cement which has been well mixed and vibrated will still contain air bubbles [Popovics (1982)]. Air bubbles were observed at the fracture surface of the S/S products.

These air bubbles may result in stress concentration and dissipation at sites away from the notch tip, thus causing a 'masking' of any process zone.

Contrary to what is predicted by equation (5-13), the regression lines such as that shown in Figure 5-22 do not pass through the origin. Inherent variability in the fracture loads of the samples used in the three point bend test was found to lie between 5% and 30%. This inherent variability in the fracture loads of the materials is suggested to be responsible for the regression lines not passing through the origin. This behaviour was observed by Mullier (1991). Force fitting the lines through the origin increases the calculated values of K_{IC} of the various samples by between 2% and 11%.

5.12.2 Experimental Results

Table 5-8, Table 5-9 and Table 5-10 show the effect of cement content, water to solids ratio and curing time on K_{IC}. It should be noted that in the case of increased cement contents, the water to solids ratio was decreased as the cement content increased in order to obtain a workable paste. Trends in K_{IC} observed in Table 5-8 will be as a result of a combination of changes in cement content and w/s.

Presented alongside the K_{IC} results are the r^2 values for the linear fit of the $(\sigma_f Y)^2$ vs 1/a data and the error in the calculation of K_{IC} from the slope as detailed in section 5.11.6. Details of sample sizes, fracture loads and calculation data appear in Appendix D1.

Table 5-8 - Effect of cement content on K_{IC}

Cement (%)	w/s	Curing time (days)	K_{IC} (kN/m$^{3/2}$)	$100r^2$	$\frac{100\alpha_a}{2K_{IC}^2}$
20%	0.99	104	59.5	77.8	4.9
50%	1.12	104	71.0	78.1	6.0
75%	0.86	104	123.7	99.4	1.0
100%	0.36	104	418.2	89.3	3.9

Table 5-9 - Effect of w/s on K_{IC}

Cement	w/s	Curing time	K_{IC}	$100r^2$	$\frac{100\alpha_a}{2K_{IC}^2}$
20%	0.9	104	62.8	99.0	1.1
20%	0.99	104	59.5	77.8	4.9
20%	1.08	104	39.2	95.9	2.3

Table 5-10 - Effect of curing time on K_{IC}

Cement	w/s	Curing time	K_{IC}	$100r^2$	$\frac{100\alpha_a}{2K_{IC}^2}$
20%	0.99	28	32.5	99.5	0.8
20%	0.99	89	50.2	94.7	1.4
20%	0.99	104	59.5	77.8	4.9
20%	0.99	180	79.6	99.2	1.0

The effect of the operational variables on K_{IC} is discussed in sections 5.12.3 to 5.12.5, while the $100r^2$ and $100\alpha_a/2K_{IC}^2$ results are discussed in section 5.12.6.

5.12.3 Effect of Cement Content on K_{IC}

As expected, K_{IC} increases as the amount of cement in a given sample increases. Strength formation within the S/S products is as a result of a combination of the bridges formed by water and those formed by cement hydration product. Rumpf (1962) suggests that solid bridges are generally higher in strength than liquid bridges and hence will be more significant contributors to overall strength. The more cement which is present, therefore, the more hydration product formed and hence theoretically the stronger the structure. MIP results, presented in Chapter 4, showed that, as the amount of cement is increased, so the total porosity and average pore size decreases. SEM microscopy results, presented in Chapter 4 also showed a structure which appeared to be of greater integrity with higher cement contents.

Samples with less cement required a greater water to solids ratio to form a workable paste. Although increasing the amount of water added to cement has been shown to lead to a more

porous product [PCI (1986)], MIP results presented in Chapter 4 showed that the total porosities of the S/S products ranged from 57% to 71%. Although these porosities are high, it is suggested that the range in porosity between samples with different formulations is not sufficient to result in the trend in strengths with cement content. The effect of differences in porosity is therefore expected to be second order.

The following should also be considered: the water available for cement hydration in all dust-containing products consists of both the residual water in the filter cake from dust washing, containing high levels of metals, and added make-up water. The more cement which is present, therefore, the lower the total concentration of dissolved salts and metals in the mixing water. The 100% cement product was made with pure distilled water. High levels of salts and metals in the mixing water have been shown to inhibit the setting of cement and may reduce the strength of the cement product (see Chapter 2). An attempt was made to determine the effect on strength of 'doping' the mixing water for hardened cement paste. Available strength testing equipment was fairly inaccurate at the strengths of these hardened pastes and no conclusive statements can be made about the effect of the composition of mixing water on strength. SEM/EDX analysis showed, however, that although the 'doped' mixing water did not chemically alter the cement hydration products, the density of the solid structure was reduced due to the doping.

Lydon (1979) presents a summary of K_{IC} values determined by a number of different researchers for pure hardened cement pastes determined by three point bending. These values range from 130 to 320 $kN/m^{3/2}$. Grudemo (1979) suggests values of 150 to 450 $kN/m^{3/2}$. The result in Table 5-8 for hardened cement paste falls within the values suggested by these reports.

5.12.4 Effect of w/s on K_{IC}

An increase in the water to solids ratio results in a decrease in the strength of the material. A higher water content results in both a more porous mixture and hydrated product. A higher porosity implies more spaces unfilled by cement hydration product and filled with water.

Bonds formed by liquids have been suggested by workers such as Rumpf (1962) to be weaker than solid bonds. Based on this suggestion, the final product is expected to be weaker.

The effect of water content on the integrity of the cement product is reflected in the ITS results shown in Table 5-3, MIP results presented in section 4.3 and SEM micrographs which were presented in Chapter 4, all of which indicate a higher water content leading to a weaker and more porous product.

5.12.5 Effect of Curing Time on K_{IC}

An increase in K_{IC} with curing time is observed. The explanation for this is in agreement with that presented in the case of w/s ratio and cement content. Cement has been observed to continue hydrating for periods of up to one year [PCI (1986)]. As curing proceeds cement hydration products continue to form, providing the higher bonding strengths associated with the products and at the same time reducing the pore spaces filled by water.

In Chapter 3 it was noted that samples for K_{IC} analysis could not be removed effectively from their moulds in curing times of less than 14 days. To determine the development of strength as a function of curing time during the early stages of setting, other tests for measuring K_{IC} should be used which will measure samples with much lower strengths. Such tests are proposed in texts such as Xu et al (1995) and Abdel Ghani et al (1990).

5.12.6 Values of $100r^2$ and $(100\ \alpha_a/2K_c^2)$

The coefficient of correlation, $100r^2$, as presented in Table 5-8 to Table 5-10 provides a measure of the accuracy of fit of a straight line to the $(\sigma_f Y)^2$ vs 1/a data. A value of between 78 and 99 was obtained for all data. The accuracy of the linear fit is determined using simple statistical tools such as those presented in texts such as Miller and Freund (1985). For the linear fit to be meaningful:

$$-1.96 < \sqrt{n-3}.Z \text{ OR } \sqrt{n-3}.Z > 1.96 \qquad (5\text{-}49)$$

where n is the number of data points and Z is determined from r^2 from statistical tables, such as that presented in Appendix E. The minimum number of data points and corresponding values of r^2 to ensure a meaningful correlation was calculated and is presented in Table 5-11.

Table 5-11 - Number of Data Points and Values of r^2 to ensure meaningful linear correlation

Number of Data Points	Minimum r^2 Value
4	0.924
5	0.780
6	0.660

A comparison of the $100r^2$ values presented in Table 5-8 to Table 5-10, the results presented in Appendix D1 and the values shown in Table 5-11 indicate that only one correlation is questionable. For the sample made with 50% cement and 1.12 w/s cured for 50 days, 4 data points were used in the calculation of K_{IC}. A value of r^2 of 0.924 is required to ensure an accurate correlation, which is higher than the actual value of 0.781. All of the other results indicate acceptable prediction of K_{IC} from the slope of the linear plot.

It is seen that more data points ensure a higher a degree of confidence in the prediction. As has already been discussed, an attempt to further improve the linear fit of the data using the procedure outlined in section 5.9.8 did not increase the value of $100r^2$.

The value of $(100\ \alpha_a/2K_c^2)$ indicates the error in K_{IC}, calculated according to the procedure detailed in section 5.11.6. The values range from 0.8% to 6%. The variability results from a number of different factors (i) the inherent variability in the fracture loads of the material due to packing defects and inherent differences in extent of hydration between specimens in a sample; (ii) errors in measurement of the notch lengths (notches were measured to two decimal places (on a mm scale) on an optical microscope) and (iii) the calculation procedure whereby K_{IC} was determined from the linear fit of the data presented in section 5.11.6.

These errors are lower than was observed for the ITS results, presented in section 5.10.3. The differences in the test configurations are responsible for this observation. For the K_{IC} results,

the sample is prenotched, resulting in a predetermined concentration of stresses which result in fracture. In the ITS, however, non-uniform stress distributions due to inherent flaws (such as air bubbles) result in higher variabilities.

The lower errors show that K_{IC} provides a more accurate measure of the strength of the S/S products than ITS, as was proposed at the beginning of this Chapter . It was observed furthermore that the error decreased as the number of data points available for calculation increased.

5.13 Results for E and G_c

Since most samples failed by unstable propagation (see Table 5-6), only initiation values of G_c could be determined. This was done both experimentally using the area under the force deflection curve (see section 5.9.1) and by calculation using equation (5-15). Both sets of results, as well as values of the Young's modulus, E, calculated from the slope of the linear region of the stress-strain curve are presented in Table 5-12, Table 5-13 and Table 5-14.

Table 5-12 - Effect of cement content on G_c and E

Cement (%)	w/s	Curing time (days)	G_c exptl J/m^2	E MPa	G_c calculated J/m^2
20%	0.99	104	58 ± 32	200 ± 27	19 ± 3
50%	1.12	104	56 ± 15	220 ± 42	24 ± 4
75%	0.86	104	64 ± 25	831 ± 410	23 ± 15
100%	0.36	104	382 ± 72	765 ± 412	304 ± 194

Table 5-13 - Effect of w/s on G_c

Cement (%)	w/s	Curing time (days)	G_c exptl J/m^2	E MPa	G_c calculated J/m^2
20%	0.9	104	99 ± 28	356 ± 66	13 ± 2
20%	0.99	104	58 ± 32	200 ± 27	19 ± 3
20%	1.08	104	69 ± 19	269 ± 48	9 ± 2

Table 5-14 - Effect of curing time on G_c and E

Cement (%)	w/s	Curing time (days)	G_c exptl J/m^2	E MPa	G_c calculated J/m^2
20%	0.99	28	57 ± 29	217 ± 49	10 ± 3
20%	0.99	89	42 ± 16	307 ± 81	9 ± 2
20%	0.99	104	58 ± 32	200 ± 27	19 ± 3
20%	0.99	177	32 ± 9	229 ± 78	13 ± 4

5.13.1 Effect of Operational Variables on E

Cement content showed the greatest influence on E. As the cement content increased from 50% to 75%, E increases considerably. As has been discussed previously, as cement content increases (and water content decreases) a stronger, more integral and less porous product is formed. The pores are expected to be filled primarily with water. Since the bonds formed by liquids are weaker than those formed by solids [Rumpf (1966)], the extent of deformation of an agglomerate in which bonding is predominantly as a result of liquid bonds will be greater than for an agglomerate in which solid bonding plays a more significant role for a given load. The large difference between the value of E for 50% and 75% is explained, therefore, by the greater extent of development of cement hydration products.

The other operational variables were also expected to affect the value of E. Bonding, and hence the response of a material to strain, indicated by E, is expected to be a function of w/s and curing time as reflected in the K_{IC} results. Contrary to expectation, however, no trends could be observed. E is determined from the stress-strain curve, and hence the result will be sensitive to sample surface irregularities, the precision of the INSTRON and inherent material defects. Ashby and Jones (1989) confirm that the above method of measuring E can lead to errors and large variabilities in the calculated values. They suggest the use of other methods including the frequency of vibration of the material.

5.13.2 Effect of Operational Variables on G_c

No trends are observed in the G_c values in Table 5-12 to Table 5-14 as a function of the operational variables for the S/S products. Since G_c is a function of both E and K_{IC}, which are

strong functions of the operational variables, it would be expected that G_c would change as the operational variables are changed. The high variability in G_c results seen in the tables will, however, mask any such trends which do exist.

Pure hardened cement paste (hcp) shows a significantly higher G_c than do the S/S products. SEM images, presented in Chapter 4, showed hcp to be a far denser and completely different solid structure to S/S products (see Figures 4-1 to 4-4 and 4-9 to 4-16) , the former which was confirmed by MIP. Furthermore XRD showed the crystal structure of these solids to be different, with Ca:Si ratios being 1.7 in the hcp and between 0.33 and 0.64 in the S/S product. It is not known which of these two solid phases will be stronger. An agglomerate in which there is a greater degree of solid bonding, however, will require greater energy to rupture the bonds per unit area to create new surfaces than one which has a lower density of bonds. Since G_c is equal to twice the energy required for the creation of new surfaces, the increase in G_c is as expected.

5.13.3 Variabilities in E and G_c Results

Both the E and G_c results show a high degree of variability. As in the case of K_{IC}, results are subject to variations due to packing effects during moulding of the samples (human error) and inherent differences in curing. Furthermore, the calculated value of G_c is determined using equation (5-15), in which the values of K_{IC} from Table 5-8 to Table 5-10 are substituted. Variabilities in K_{IC} values are therefore carried forward into the calculation of G_c. Variabilities are in line with those observed by Mullier (1991).

In calculating the value of G_c use was made of E, whereas strictly speaking for plane strain loading the Poisson's ratio, ν, should be used in the calculation. For porous systems ν is expected to lie between 0.2 and 0.3. It was found that introduction of such values bring about an across the board change of between 4% and 9% in the calculated values of G_c. This change is not responsible for the observed variabilities and is insignificant relative to the observed variabilities in results. Should more accurate results be required the value of ν needs to be determined for these products and substituted into the calculation.

5.14 Yield Stress and Plastic Zone Size

5.14.1 Experimental Technique

In the scope of this work, yield stress was determined using the configuration shown in Figure 5-12. The solidified FeCr Dust material remaining from the three point bend tests was used for yield stress determinations. The results presented below show that the dimensions of these halves were many orders of magnitude greater than the size of the plastic zone and the broken specimens from three point bending were therefore suggested to be large enough to ensure that the specimen sizes were not limiting in terms of edge effects. The radius of the indenter used was 12.5 mm, chosen as being much greater than the average particle size in order to ensure that the load was spread over many particles. The rate of crosshead movement was set at a nominal value of 0.05mm/min. The slope of the linear region of the applied force - penetration distance plot was determined and the yield stress calculated using equation (5-33).

5.14.2 Results

Table 5-15 and Table 5-16 show the effect of cement content and water content on the yield stress of the material. In Table 5-16 the plastic zone size is calculated in accordance with the discussion presented in section 5.9.8 using the values presented in section 5.12. An average of 5 readings was used in calculation of the yield stress. Yield stress testing was carried out near the end of the experimental programme. Due to a limitation in the amount of waste material available, tests to determine the effect of curing time on σ_{YS} and r_p could not be performed.

Table 5-15 - Effect of w/s on σ_{YS}

Cement	w/s	Curing time	σ_{YS} (MN/m^2)
20%	0.9	340	33.03 ± 3.10
20%	0.99	340	25.51 ± 1.18
20%	1.08	340	20.37 ± 3.30
20%	1.18	340	14.25 ± 1.95

Table 5-16- Effect of cement content on σ_{YS} and r_P

Cement	w/s	Curing time	σ_{YS} (MN/m^2)	r_P (m)
20%	0.99	104	15.57 ± 2.26	nm
50%	1.12	104	49.11 ± 4.97	(6.81 ± 1.41) E-07
75%	0.86	104	69.66 ± 8.3	(1.05 ± 0.31) E-06
100%	0.36	104	175.90 ± 35.05	(1.99 ± 0.91) E-06

Both Table 5-15 and Table 5-16 are presented graphically in Figure 5-23 and Figure 5-24.

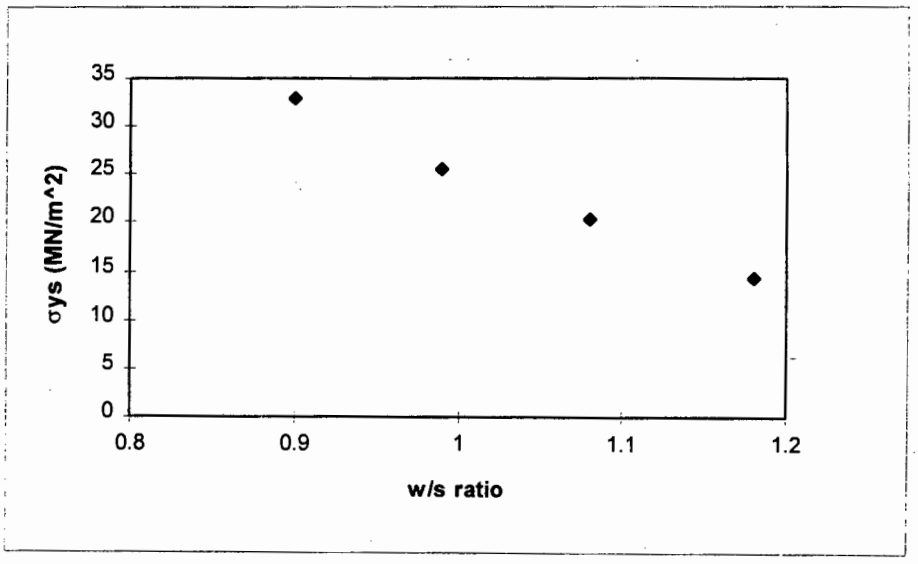

Figure 5-23 - Plot of Yield Stress and Plastic Zone Size as a Function of Cement Content

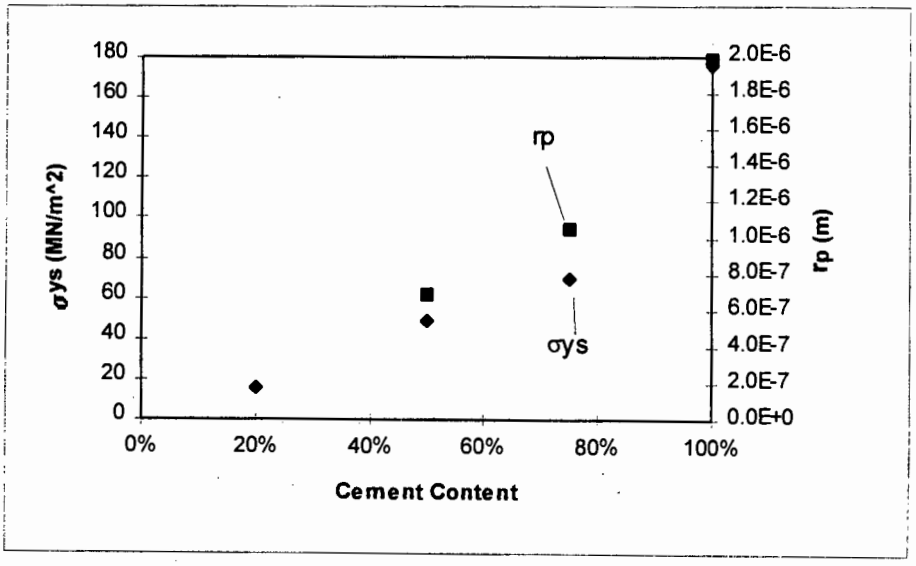

Figure 5-24 - Plot of Yield Stress as a Function of Water to Solids Ratio

5.14.3 Discussion of Yield Stress and Plastic Zone Size Results

In section 5.12.1 it was shown that the three point bend test as applied in this work was not sensitive enough to identify the existence of a *process zone*. The size of the *plastic zone* can be determined via spherical indentation testing. The above results indicate that the plastic deformation zone (which forms a part of the process zone) lies in the 10^{-5} mm to 10^{-4} mm size range. In the work of other researchers identified in section 5.9.9, process zones were identified which were up to two orders of magnitude greater than the plastic zone size using techniques such as the three point bend test.

Notch measurements made after fracture in the three point bend tests were only made to two decimal places on a mm scale. A process zone to the order of 10^{-2}mm (or indeed a plastic zone of 10^{-4} mm) would therefore not be detected from a graph of $\sigma_f Y$ vs 1/a by the procedure of section 5.12.1. This observation substantiates, therefore, the observation that the three point bend test as used in this study is not sufficiently sensitive to resolve the size of the process zone of the S/S products. Furthermore, it is suggested that the effect of such inherent process zones on energy dissipation during loading is insignificant.

The coefficients of variation for the calculated yield strengths and plastic zone sizes were observed to be high - up to 30% for some samples. In the calculation of r_p, an average value of K_{IC} from section 5.12 was used. Variability in K_{IC} will therefore affect the calculated value of r_p. Furthermore, since the indentation occurs over a relatively small area of the sample surface, mixing and hydration variabilities across the sample surface will contribute to the high variabilities in r_p and σ_{YS}.

A number of observations can be made from the data presented in Table 5-16 and Table 5-15.

(a) Effect of Water Content on σ_y

The yield stress, σ_y, is observed to decrease with increasing water content. As the water content increases, the porosity of the material increases, with the pore spaces being filled with water. In samples with lower water contents, solids density will thus be higher than in solids

with higher water contents. Water in the pores of the solid is likely to be permanently displaced under lower loads than will the solid structures themselves. The solids will thus absorb energy elastically to higher loads than will more porous solids in which water fills the pores and the latter solids thus show permanent energy dissipation or plastic deformation at lower yield strengths.

(b) Effect of Cement Content on σ_y and r_p

As the cement content increases (and the water content decreases) the yield stress increases. The calculated plastic zone size is also suggested to increase. The effect observed here is a dual one. In (a) above, an increase in water content was shown to give a decrease in yield strength. The higher cement contents have also been shown to reduce the porous nature of the solid. The denser the "fibrillar" structure as a result of higher cement contents, the greater the energy which can be stored elastically prior to permanent deformation. This explains the observed increase in yield stress.

The plastic zone is a zone over which permanent energy dissipation occurs prior to fracture. As the structure becomes more integral, energy can be distributed over a larger area. The greater the area over which energy dissipation is occurring, the larger the size of the resultant plastic zone.

5.15 Correlation between ITS and K_{IC}

It has been shown here that both ITS and K_{IC} are a measure of the strength of the solids. While K_{IC} provides a means of deducing accurate information on the mechanism of fracture, and was found to give lower variabilities, the ITS is a quicker, easier and more economical test to perform. It is therefore appropriate to explore the relationship between the ITS and K_{IC} and in this way use the ITS for predicting more fundamental strength parameter, K_{IC}.

In the ITS, a sample is loaded such that the stress is distributed across a failure plane, the length of which is the diameter of the sample. This implies that energy dissipation may occur by elastic or plastic deformation or microcracking across the entire plane, prior to fracture.

Gross failure in the ITS occurs when the bonds across the failure plane are stressed to beyond their failure limit. Since bonds formed by solids are expected to be stronger than liquid bonds, it is suggested that as the concentration of solid bonds increase across the failure plane (with more cement, lower w/s and longer curing time), the higher will be the measured strength.

In the three point bend test, however, stresses are concentrated in a region close to the tip of a notch in the sample. Similar pre-fracture energy dissipation mechanisms to those suggested in the ITS may come into play. These will be confined to a region close to the notch tip. According to the Griffith (1920) criterion for failure, the strain energy released at the notch tip as the notch propagates provides the energy required for the creation of new surfaces. Once again the energy required for the creation of these new surfaces will depend on the type and extent of formation of bonds ahead of the notch tip.

Since both strengths are dependant on the concentration of bond-forming material, in the ITS across the entire failure plane and for K_{IC} ahead of the notch tip, it would be expected that an increase in ITS would imply a proportional increase in K_{IC}. A linear relationship between the two parameters is proposed.

Figure 5-25 presents a plot of K_{IC} vs ITS for the solidified FeCr Dust products. Error bars fitted to the data are an average of the errors in results determined in section 5.10.3 and 5.12. The plot excludes the samples made with 75% and pure hcp. It was decided to initially exclude these two samples due to the fact that low cement containing samples are of interest in this work and the ITS of the higher cement samples were far higher than the rest of the results. Their inclusion therefore diminished trends in the area of interest. Furthermore, the high strength measurements were carried out on less sensitive strength testing equipment than the rest.

Shown in Figure 5-25 is a linear fit to the data. The equation for the line is:

$$K_{IC} = 39.1\ ITS + 54 \qquad (5\text{-}50)$$

where K_{IC} is in $kN/m^{3/2}$ and ITS is in MPa. The coefficient of correlation of this linear fit is 22%. Although the fit is poor, the error bars indicate that the variability in results is responsible for the scatter in results and hence the poor fit of the line. The linear fit does not pass through the origin, as it would be expected to. If the linear fit is forced through the origin, a negative coefficient of correlation is observed. The slope of the line through the origin is 188.4.

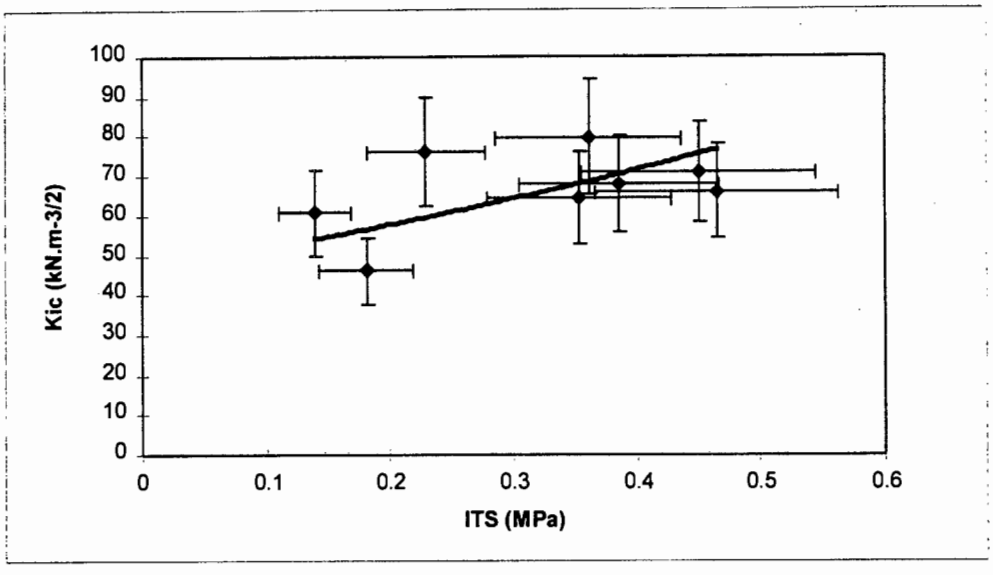

Figure 5-25 - Correlation between ITS and K_{IC} (low strength S/S products)

An attempt was made to fit other types of curves to the data. The best-fit exponential, given by the equation

$$K_{IC} = 53 \exp (0.67 \text{ ITS}) \qquad (5\text{-}51)$$

gave a r^2 value of 23.9%, a slight improvement. It was, however, decided to continue to use the linear fit since such a relationship is what would be expected.

A line with a slope of 188.4 was plotted through all the results, including those for the high strength materials (75% and 100% cement). This plot is shown in Figure 5-26. The line correlates closely with the best linear fit through all of the data, the latter having a slope of 196.3. While taking into account both the variabilities in ITS and K_{IC} results, and the inaccuracies in the measurement of the high strength results, it is suggested that the difference

between the slope given by the low strength results (188.4) and that given by all the results (196.3) is relatively insignificant.

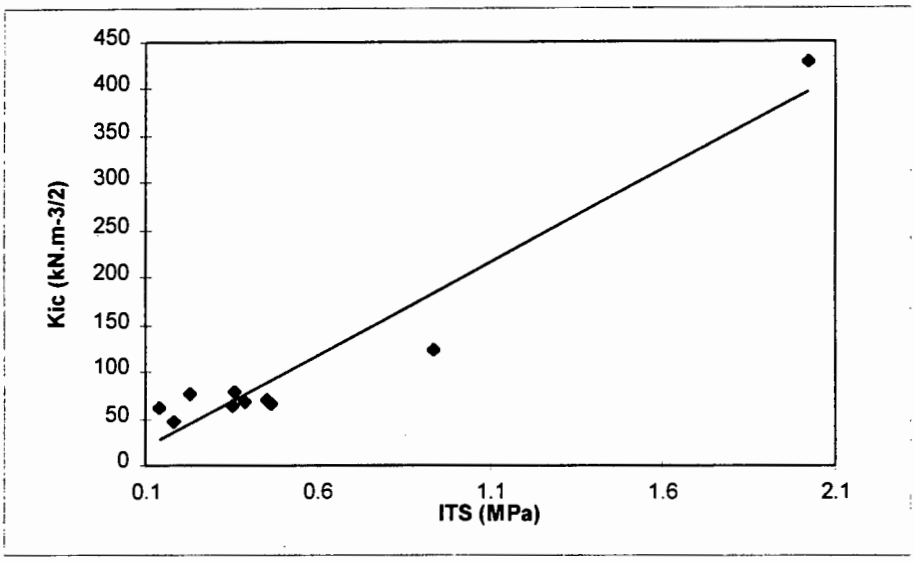

Figure 5-26 - Correlation between ITS and K_{IC} (all results)

It is thus suggested that the ITS - K_{IC} correlation is good and may be used to predict K_{IC}, a more time consuming parameter to establish, from the relatively easier to determine ITS. The relationship is suggested to be given by:

$$K_{IC} = x \text{ ITS}, \text{ where } 188.4 < x < 196.3 \qquad (5\text{-}52)$$

Here K_{IC} is in $kN/m^{3/2}$ and ITS is in MPa. A number more repeat tests will provide an accurate value of x in this correlation.

5.16 Conclusions

5.16.1 Summary of Results

The strength characteristics of S/S products were reported and discussed in this chapter. It was found that the ITS of the S/S products was significantly higher than those required by statutory requirements. ITS results were suggested to be a function of all of the operational variables investigated in this work.

K_{IC} was observed to be a strong function of cement content and water to solids ratio. It was observed that K_{IC} will be related to both the extent of hydration of the cement and the porosity of the end product which will in turn be influenced by these operational variables.

G_c did not vary considerably between the various S/S products, and the high variability in results was suggested to mask any trends which may have been expected.

The yield strength and plastic zone size once again were a function of the operational variables which influence cement hydration and porosity. σ_{YS} decreased with water to solids ratio and increased with increasing cement content. r_p increased with increasing cement content.

A correlation was identified between the ITS and K_{IC} of the S/S products and it was suggested that this correlation could be used to predict K_{IC} provided sufficient repeat tests were carried out.

5.16.2 Comments with Regards to the Fundamental Model

The model proposed in Chapter 4 suggested that the S/S product was an agglomerate of particles held together by liquid in the pores and cement hydration product. From the results of this current Chapter it was seen that all three variables of interes in this work (cement content, w/s ratio and curing time) affect the strength of these agglomerates in that they determine the porosity of the product and the extent of cross-linking of the cement hydration products between the waste particles. Results presented here thus provide support for the proposed model.

In Chapters 6 and 7 the chemistry of the agglomerates is studied using a variety of leaching tests. Discussions and interpretations of results presented in Chapters 6 and 7 draw on the results of the physical characterisations, and are used to further develop both the physical and chemical model.

6.

Leaching I:
Batch Extraction Tests

The work presented thus far has focused on fundamental chemical (in Chapter 4) and physical (in Chapter 5) characterisations of the S/S products. In this current chapter and Chapter 7, responses of the products to a number of different leach tests are presented. Four distinct aims of leach testing are identified in the context of this work:

(i) To assess the effectiveness of the S/S operation in reducing the mobility of metal species from the waste products.
(ii) To provide information as to the containment mechanisms of metals in S/S matrices, and in this way extend the chemical description of the S/S products developed in Chapter 4.
(iii) To predict the long-term leaching behaviour of, and the mechanisms controlling leaching from, S/S products. This is included under the general term 'leach modelling'. Results from this section of work are further applied in the development of the chemical model.
(iv) To compare different combinations of operational variables to find an optimal treatment strategy.

These aims are not unrelated but the complexity of the S/S products makes it impossible to define a single laboratory-scale test procedure which can achieve all of the above aims simultaneously [Wastewater Technology Centre (1990)].

This chapter starts with a summary of the proposed mechanisms of removal of metals from S/S products which was explored in detail in Chapter 2. Literature reports of the use of batch extraction tests are discussed and the results from such tests as used in this work are presented and interpreted. These results satisfy aims (i) and (ii) above. In Chapter 7 leaching kinetics (aim (iii)) is explored. In Chapter 8, optimisation of operational variables (aim (iv)) is investigated using a factorial design approach.

In the choice of leach tests and the planning of an experimental procedure for leach testing for both this Chapter and the following, a wide variety of tests was performed on a number of different samples. At the outset of experimental planning it was recognised that less tests procedures could have been used if a number of assumptions regarding the behaviour of the

S/S products were made. Furthermore, the number of tests used in this work could have been reduced using a factorial design technique. It was, however, decided to carry out the variety and repetitions of tests presented in this Chapter to reduce any bias which would have arisen by making such initial assumptions. The use of factorial design to reduce the number of tests is explored further in Chapter 8.

Leach testing presented in the following three chapters explores the leaching of specific cations from the S/S matrix. A study of the behaviour of anions is recognised to be equally important in the development of a full picture of the behaviour of the cementitious products in leach tests, due to the fact that anions play a role in determining ionic strength, conductivity and the overall salt balance. The effect of anions, and their leaching behaviour is not addressed in this thesis.

6.1.1 The Steps Associated with Leaching from S/S Products

The removal of metals or other species from S/S products is via liquid phase transport through- and out of- the solid. The following steps in this removal process are identified:

(i) Removal of metals from the solid phase into the liquid phase. Metals sorbed to the solid surface desorb into solution. In the case of metals precipitated as insoluble hydroxides, a drop in pH or a change of the chemical equilibrium in the pores is required to resolubilize these precipitates. This process is suggested to be rapid [Côté (1986)] and will be discussed further in this chapter. Other metal complexes found in the pores can be resolubilized in the liquid phase. For metals incorporated chemically in the cement hydration products, their mobilization into the liquid phase requires chemical breakdown of these products.

(ii) Transport of the dissolved metal species, as well as those metals originally solubilized in the pore solution, to the surface of the solid (intra-particle diffusion).

(iii) Transport from the surface of the solid into the bulk liquid phase (external mass transfer).

(iv) Movement away from the solid in the bulk liquid solution, either via diffusion in the case of a stationary fluid or via advective (bulk liquid) transport in the case of a moving fluid.

6.1.2 Summary of Metal Containment Mechanisms

In Chapter 2 the proposed mechanisms of retention of Cr and Zn ions in cement-based S/S products were discussed. In summary, the following points were highlighted:

(i) Metals such as Cr(III) and Zn(II) were shown to be insoluble at intermediate pHs, with solubility increasing with both an increase and decrease in pH. This is known as amphoteric behaviour.

(ii) Cr(III) is expected to be found in the $Cr(OH)_3$ form. Cr(VI) is soluble over the entire pH range and is therefore expected to remain solubilized in the pore solution of the S/S products.

(iii) Zinc was identified to be retained in one of two ways. The first suggestion is that it is contained in the pore solution, either solubilized or as the insoluble hydroxide species. Secondly, zinc ions may be adsorbed to the negatively charged surface of the cement hydration products [Mollah et al (1993)]. As mentioned in Chapter 4, the existence of negatively charged surfaces could not be confirmed for the specific products of this investigation. No agreement has been reached as to whether this adsorption is reversible over time. In Chapter 5 it was identified that the contribution of electrostatic forces to the overall strength of the S/S products is insignificant relevant to liquid and solid bridges. Although electrostatic interaction between Zn (or indeed other metal ions) and the solid surface may have significance in metal retention, the contribution of electrostatic effects to the ultimate strength of the product is minimal (see Chapter 5) and hence the statements of Chapter 5 still hold.

(iv) Although several researchers have shown the release of metals from S/S products to be affected by pH [Stegemann (1996), Heimann et al (1992), Roy et al (1992), Bishop (1986)], pH will not be the only controlling parameter. Effects such as diffusion and complexation also play a role. Chemical or physical retention effects will affect release.

Due to differing waste compositions and their effect on cement hydration, prediction of the interactions within the S/S products, and consequently release mechanisms of contaminants from the solidified products based on literature reports, is thus complex. Laboratory leach testing is required to characterize release mechanisms for the individual products. In the following sections it is shown how results from such leaching tests can be extrapolated to provide an understanding of mechanisms of containment of metals in the products.

6.2 Batch Extraction Tests

'Batch Extraction' in the context of this work refers to once-off chemical extractions in which the amount of a contaminant released in a specific test configuration is measured. Such tests provide no information about temporal effects. Batch extractions used in this work include

Pore Solution Extrusions, the US EPA's Toxicity Characteristics Leaching Procedure (TCLP), the Equilibrium Extraction (EE) and the Sequential Chemical Extraction (SCE). Each of these is discussed in detail below.

6.2.1 Pore Solution Extrusions

As has been demonstrated in previous chapters, the S/S products are porous composites, the pores spaces being filled with a liquid phase. To gain insight into retention and leaching mechanisms associated with the S/S products, it is significant to characterise the fluid filling the pore spaces. In the scope of this work, pore fluid extrusions were performed using a high pressure device similar to that used for cements and concretes. Details of the design of this device are presented in texts such as Barneyback and Diamond (1981).

A sample is placed into a confined chamber and pressure is exerted until liquid is extruded from the solid through a collection device. The device is illustrated and discussed further in section 6.3.2 on page 179. The extruded liquid is collected, diluted where necessary, and sent for analysis via Atomic Adsorption Spectroscopy.

6.2.2 Agitated Tests

In agitated tests, a sample of material is placed in a leachant solution and stirred, shaken or mixed to promote contact between the waste and leachant. Agitation minimizes external mass transfer resistances. The size of the material used in the tests is often reduced via crushing or milling to increase the surface area for mass transfer and to reduce the path length over which internal mass transfer occurs.

The **Toxicity Characteristic Leaching Procedure (TCLP)** [Code of Federal Regulations (1988)] is the most widely used leaching test to determine whether waste products, including S/S end products, require disposal in landfills characterised as "hazardous". This test is an agitated batch test which has largely replaced the Extraction Procedure (EP) [Code of Federal Regulations (1980)] used previously. Unlike the EP, the leachant used in the TCLP is buffered, and therefore no adjustment of pH during the test is required. The TCLP can also monitor

release of organics from the wastes using a special extraction vessel, called a Zero Headspace Extractor.

A description of the TCLP as used in this work appears in Appendix A2. In summary, a crushed sample of S/S product (<9.5 mm) is agitated in a leachant solution for 18 hours. The composition of the leachant used depends on the pH and buffering capacity of the sample. For alkaline products the leachant is a 1.0 N acetic acid solution. For acidic products NaOH is added to the leaching solution as a buffer.

Although this test is widely used as a 'pass-fail' criterion for wastes and solidified products requiring disposal to hazardous landfill, it has come under wide criticism for several reasons. Firstly, the test makes use of a crushed material in which the surface area available for leaching is increased and the path for diffusion of the species is decreased over the monolithic structure expected in landfill. Secondly, the choice of leaching medium is debatable. Initially the choice of acetic acid as a leachant was based on the fluid which would be expected in a landfill should the waste be co-disposed with domestic waste products. In practice, co-disposal of hazardous with domestic wastes is uncommon. It would be more likely that liquid passing through the landfill would be closer to a weak inorganic acid, resembling the composition of acid rain.

In the scope of this work, therefore, the TCLP is used as a comparative tool. Its use does not support its application as a waste classification standard.

The second batch agitated test used in this work is the **Equilibrium Extraction (EE)** [Wastewater Technology Centre (1990)]. In this test a low liquid to solid ratio is employed, and distilled water is used as leaching fluid. In this way the pH of the leachant is determined by the free alkalinity present in the solid. The aim of such tests is to characterise the equilibrium amounts of species releasable from the solid, assuming that the pH of the sample does not change. Theoretically this provides an indication of what is mobile from the pores of the sample, including what is sorbed onto the surfaces of the hydration products. Any components of the solid which are immobile due either to the pH of the pore solutions, or to their incorporation into the solid structure, will not be solubilized as would be expected in the TCLP

where acid breakdown of the structure is possible. The differences between the EE and the TCLP are tabulated in Table 6-1.

In the EE a dried sample of the material is crushed to -149 μm and agitated with four times the weight of the sample in distilled water for 7 days ± 1 hour. At the end of the test the filtrate is filtered through a 0.45 μm filter paper and the liquid tested for metal contents. A separate procedure used for organics is not presented here.

Table 6-1 - Comparison between the TCLP and the EE

Test Condition	TCLP	EE
Leachant	1.0 N Acetic Acid	Distilled water
Liquid to solid ratio	10:1	4:1
Test duration	18 hours	7 days
Particle sizes	-9.5 mm	-149 μm
Use	Waste Classification Tool, 'Worst-case' Scenario where acid attack on products occurs with an associated drop in pH	Identify Soluble components

6.2.3 Sequential extraction tests

These tests are carried out in one of two ways. Different samples of the waste can be subjected to leachants of differing strengths. Here it is assumed that each stronger leachant will also extract the total sum of the components from the weaker leachants. The other type of sequential extraction test is performed by subjecting the same sample to differing strengths or types of leachant. It is assumed that the contaminant extracted in each step is associated with a different form or mineral phase within the waste matrix.

In this current work, the **Sequential Chemical Extraction (SCE)** test is used. This is a procedure developed by Wastewater Technology Centre (1990) based on that of Tessier et al (1979). A sample of the S/S product is subjected to five consecutive extraction steps each with a different leachant solution. Table 6-2 presents the solutions used in each step, along with the associated species which the step aims to extract. A full description of the procedure is presented in Appendix A3.

Table 6-2 - Leachants used in the SCE and the associated extracted species

Step No	Solutions used	Release subject to changes in	Species Extracted
1	0.25 M $CsCl_2$ and 0.75 M Li Cl in 60% CH_3OH	Ionic Composition	Ion Exchangeable Fraction
2	1 M CH_3COONa adjusted to pH 5 with CH_3COOH	pH	Surface oxides, hydroxides and carbonate bound metal ions
3	1M $NH_2OH{\cdot}HCl$ in 25% CH_3COOH	Eh	Metal ions bound to Fe and Mn oxides
4	0.02 M HNO_3 in 30% H_2O_2; 1.2 M CH_3COONH_4 in 20% HNO_3	Eh	Metal ions bound to organic matter and sulfides
5	Fusion digest as used in Chapter 3	Stable species	Residual metal ions

There is some question as to the appropriateness of the reagents chosen for these tests. Originally the procedure was developed for characterising sediments from natural water systems. Since cements and such sediments are fundamentally different in chemical nature, the solutions are not necessarily appropriate for S/S products. Furthermore, reproducibility of this test has been found to be poor [Stegemann, (1996)]. Stegemann (1996) suggests that Step 2 is sufficient to tell whether there is any stabilization other than precipitation of metals as hydroxides.

The SCE is thus not expected to provide accurate quantitative information, but is suggested to provide a rough estimate of the relative proportions of metals found in the various phases. It is used as such in the context of this work.

6.2.4 Other Types of Leach Tests

A number of other tests with a variety of different aims have been suggested in literature. These include Concentration buildup tests, the Multiple Toxicity Characteristic Leaching Procedure (MTCLP) [Lee et al (1994)], flow around tests and soxhlet tests [Wastewater Technology Centre (1990)]. Upon analysis of the procedures in the context of this work, none of these tests was found to provide any more information than those chosen for use here.

6.2.5 Variables Affecting Leaching

The conditions under which a specific test is conducted will directly affect the results of the test. A few of the most important parameters affecting leaching are discussed below.

(i) Sample Preparation

Particle size reduction is carried out to reduce the time required to reach steady state by increasing the surface area of contact between the solid and the leaching liquid. Size reduction can be effected by grinding in a mortar and pestle or by milling. Samples are sometimes washed to remove soluble salts and fine particles adhering to the surface [Wastewater Technology Centre (1990)]. An increased surface area reflects a 'worst case' scenario in which gross decrepitation of the solid material occurs.

(ii) Leachant Composition

The release during a test is strongly dependant on *leachant composition*, especially in tests with high liquid to solid ratios. In low liquid to solid ratios the solid may determine the chemical environment. Commonly used leachants are water, simulations of landfill leachates and various laboratory solutions, including acid rain simulations and those used in the SCE described above [Wastewater Technology Centre (1990)]. There is no way of developing a single leaching fluid which closely simulates the fluid expected in landfill situation with respect to pH, Eh and concentrations of chelating and complexing agents [USEPA (1980)]. Traditionally an aggressive leachant with low pH and Eh is used to represent a worst case scenario.

(iii) Amount of Leachant

The *liquid to solid ratio* is defined as the ratio of the volume of leachant in contact with the waste to the amount of waste being leached. The choice of liquid to solid ratio depends on the objective of the leaching test, the solubility of the species of interest and the analytical constraints involved [USEPA (1990)]. The liquid to solid ratio must be low enough to prevent analytical problems (ie contaminants below detection limits) but high enough to prevent the solubility of the components from limiting leaching.

(iv) Temperature

Both the van't Hoff relationship (which describes thermodynamic equilibrium constants and solubility products) and the Arrhenius relationship (which describes kinetic processes such as desorption and diffusion) are strong functions of *temperature*. Since reaction and diffusion processes are significant in the leaching process, leaching will be dependant on temperature. For practical reasons, most leaching tests are done at 25°C [USEPA (1990)].

(v) Other Variables

The *time* over which a test is run will directly influence the amount of a constituent leached. For long-term effects such as structural breakdown to be observed, tests need to be run over a long period of time. The method by which the leachant and waste are *separated* is significant. If the waste was crushed prior to leaching, a 0.45 μm membrane filter is commonly used for separation [USEPA (1990)]. This is the convention to define a soluble species.

6.2.6 Summary

Batch extractions are used to provide chemical characterisation of the S/S products under specific laboratory conditions. Although they often do not represent conditions expected in a landfill situation, a suitable choice of leachant and test conditions can provide useful information as to the mechanisms of containment and release from such products.

6.3 Results of Batch Extraction Tests

The above review presented different batch tests available for the testing of S/S products. In the course of this work four of these tests were used in characterizing the solidified ferro-alloy wastes: Pore Solution Extractions, the Toxicity Characteristic Leaching Procedure (TCLP), the Equilibrium Extraction (EE) and the Sequential Chemical Extraction (SCE).

This chapter discusses the results of the characterisations as applied to the solidified FeCr Dust. In Chapter 8 the TCLP is further applied to the ETP products where the use of an experimental design technique in predicting the results of the TCLP is investigated.

6.3.1 Percentage of Water in the S/S products

Prior to understanding containment of the various metal species within the S/S product, it is necessary to quantify the residual water in the pores of the solid product. This was determined by drying a sample of the solid in an oven at 60°C until constant mass was obtained. Between 38% and 52% of the solid was found to be free water. The water contents were less than the amount of water used in the initial mixtures (see Table 6-3). This is explained as follows:

The samples were cured under saturated conditions. Minimal evaporation from the solid into the surroundings is therefore expected. The S/S products were observed to be hydrophobic (dehydrated readily upon exposure to air) and would therefore not be expected to absorb more water from the surroundings. The water loss needs to be considered, therefore, in terms of that consumed during cement hydration.

Consider, for example, 100g of a mixture of cement, FeCr Dust and water, containing 30% cement and a water to solids ratio of 1.36. This gives a mass percent of water in the original sample of 57.6%. Of the 100 g, 12.7 g will be cement. In Table 6-3, a summary is given of the approximate amount of water required for hydration of this cement. Since the composition and hydration reactions of cement have been highlighted to be variable and not well understood, the values in the table are estimates.

Table 6-3 - Water required for the hydration of cement

Constituent	Molar ratio in which it reacts with water	Mass Percent in Typical Cement	Mass of constituent in 12.7 g	Mass of water required for hydration
C_3S	1:3	35-55%	4.4 to 7 g	4.4 to 7 g
C_2S	1:2	20-40%	2.5 to 5 g	0.8 to 1 g

Of the original 57.6 g of water, therefore, between 5.2 and 8 g is consumed in hydration of the major cement constituents. The 100 g sample used in this specific example was found to have 51.8 g water after curing for approximately 6 months. The difference between the initial water content of the mixture and that of the cured product is therefore approximately equivalent to that consumed in cement hydration.

6.3.2 Results of Pore Water Extrusions

The composition of the liquid contained in the S/S product was determined by extruding the pore water from the S/S products. A sample of material was placed in the equipment illustrated in Figure 6-1. A load of 220 kN was applied using an Amsler compressive testing rig. This load was found by experiment to be that required to initiate extrusion of liquid from the sample. Higher loads forced solid material through the liquid collection tube. After extraction and filtration, the liquid was diluted and analysed via AA spectroscopy (for metals content) and UV spectroscopy (for Cr(VI)).

Performing pore water extrusions was difficult. For any given sample approximately 1ml of liquid was extruded. This solution required filtration and dilution prior to analysis, both steps having the potential for loss of liquid and the introduction of error. Only a small number of extrusions was performed. Hence the results can be considered to provide only estimates of the pore water composition.

Results from the extrusion tests appear in Table 6-4. No repeatability tests were carried out. Furthermore, since not all the liquid was expressed from the solid during the test, it was not

possible to complete the mass balance on the remaining solid material. The results are presented as volume concentrations and as percentage element in the pores of the total amount of the individual element in the solid. Owing to the small amount of liquid extruded, only selected analyses were carried out. The following results were obtained:

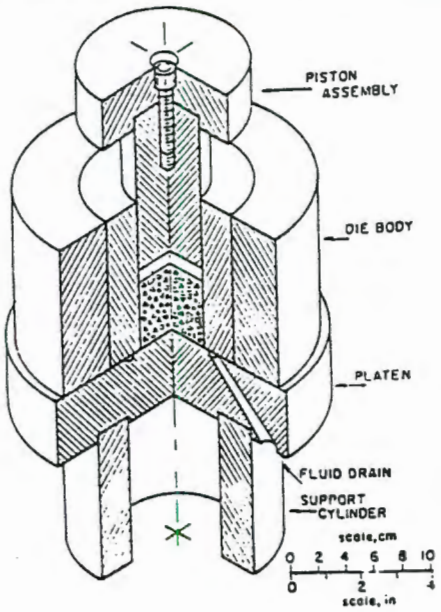

Figure 6-1 - Schematic of Pore Water Extrusion Device

(i) pH

The pH of the pore solution lies between 10.5 and 12.6. This is lower than is expected for hardened cement pastes (≈ 13.6) [Roy and Scheetz (1993)]. For some of the extrusions, insufficient liquid was extruded for pH to be measured. In both hardened cement pastes (hcp) and the S/S products, the high pH is attributed to the solubilization of hydroxides in the pores, including those of Ca and K.

The pores solutions contained considerably less K and more Ca than do the pores solutions of hcp. Both potassium and calcium hydroxides are expected to dissociate according to:

$$M(OH)_x \leftrightarrow M^{x+} + xOH^-$$

The more OH^- ions present in the solution, the greater its pH. Hence the more K and Ca which have dissociated, the higher the expected pH. This is discussed further in the analysis of K and Ca concentrations in the pore solution.

Table 6-4 - Composition of Pore Water Solutions of selected S/S Products

Cement (%)	w/s	Curing (days)	Cr in pore solution mg/l	Cr in pore solution as % of Total Cr† in Solid	Cr(VI)‡ in Pores as a % of Total Cr in pore solution	Ca (ppm)	K (ppm)
Normal Portland Cement*			0.7			19.1	11100
14	1.04	434	491	0.95	77	121	nm
20	0.9	89	311	0.78	72	112	38
20	0.9	111	244	0.97	nm	127	nm
20	0.9	295	256	1	nm	218	30
20	0.9	300	307	0.72	nm	100	23
20	0.99	20	41	0.22	nm	249	nm
20	0.99	419	254	1.2	nm	125	25
20	0.99	451	357	0.86	87	100	nm
26	0.94	116	306	0.59	74	70	29
30	0.99	230	380	0.79	74	69	nm
50	1.12	212	339	0.76	nm	60	28
75	0.86	212	277	0.8	nm	36	35

Notes:

* Roy and Scheetz (1993)

†Determined by fusion as detailed in Chapter 3

‡Determined by UV spectroscopy

nm = not measured due to insufficient solution

The above table represents elements *contained solubilized in the pore solution.* Since the liquid is filtered prior to analysis through a 0.45 μm filter paper, no precipitates will be included. It is suggested furthermore that should any surface adsorbed species be present in the S/S product, they will not desorb during the pore solution extraction and are hence not included in the above concentrations.

(ii) Chromium

A small proportion (≈1%) of the total Cr is found to be solubilized in the pores. The rest of the Cr is expected to be present as insoluble chrome oxides such as the chromite species in the dust core mentioned previously or precipitated as one of the Cr(III) compounds described in Chapter 2, with $Cr(OH)_3$ being the most likely at pH≈11 [Pourbaix (1966)]. Cr has also been suggested in literature reports [Poelmann et al (1993), Glasser (1993), Mollah et al

(1992), Ivey et al (1990)] to be chemically incorporated in the cement hydration products. No evidence thereof was found in the results of Chapter 4.

The amount of Cr contained in the pore solution is approximately ten times that which was contained solubilized in the filtrate from the FeCr Dust washing step, and hence in entrained water in the filter cake, prior to solidification (see Chapter 3). The higher Cr contents in the pore solution over the "mixing" water (entrained in the filter cake) can be explained in one of three ways. Firstly, water is consumed in hydration of the cement and, to some degree, by evaporation. The reduction in water content will result in concentration of the Cr in the pores.

The second explanation is the following. The FeCr Dust was proposed in Chapter 3, and demonstrated in Chapter 4, to consist of a "rim" layer of volatile elements condensed on the surface of a silicate dust core [Gencor (1996)]. Upon contact with water constituents of this layer can enter solution. The one hour pre-solidification water wash of the dusts results in some solubilization, as is shown in Table 3-1. As curing proceeds, a kinetically-controlled solubilization of the outer layer of the dust particle may occur, allowing for release of its constituents, including Cr, into solution. This may explain the higher amount of Cr in the pore solution over that entrained in the filter cake.

The final possible explanation for this increase is oxidation of Cr(III) (which is primarily insoluble at the pH of the pore solution) to the more soluble Cr(VI). This reaction is feasible at all pH values above 2. Furthermore, the reaction is catalysed by the presence of $Ca(OH)_2$, which will be found in the S/S products. The reaction has, however, been observed to proceed slowly and is expected to have a limited effect on Cr leaching [Petersen (1997)].

No conclusive statements can be made from Table 6-4 with regard to the effect of the operational variables on the percentage of Cr which is contained in the pore solutions. It is suggested once again that the small amount of pore solution extracted from the solid limits the accuracy of these results and hence, should the operational variables have an affect on the amount of Cr solubilized in the pores, this is not observed here.

The location of the other approximately 99% of the total Cr in the S/S product not contained in the pore solution is explored further via the Toxicity Characteristic Leaching Procedure (TCLP) in section 6.3.3, the Equilibrium Extraction (EE) in section 6.3.4 and the Sequential Chemical Extraction (SCE) tests in section 6.3.5.

While recognising that the small amount of liquid obtained from the extrusions limits the accuracy of the results, it is interesting to note that between 72% and 87% of the total chromium in the pore solutions is present as Cr(VI). The rest is assumed to be the Cr(III) form. From the discussion of Chapter 2, it would be expected that, at the pH of the pore solution found here, the solubility of Cr(III) would be to the order of $1x10^{-5}$ mg/l [Pourbaix (1966)]. The rest would be expected to be precipitated out of solution as the $Cr(OH)_3$ species. Since the solution is filtered prior to analysis, the detected Cr(III) is soluble Cr, and is not merely suspended precipitate. This provides evidence that the complex pore chemistry and highly concentrated pore solution causes a deviation in solubility behaviour from what is observed for a pure Cr-water system.

(iii) Zinc

As seen in Chapter 3, high levels of Zn are found in the S/S products. No Zn was, however, detected in any of the pore water samples. As in the case of Cr, some of the Zn is expected to remain in stable complexes in the original dust particles. In solution, Zn(II) can form a number of oxides and hydroxides, with amorphous $Zn(OH)_2$ being the most soluble (1.2 mg/l) at the pH of the pore solution, and ε-$Zn(OH)_2$, a white orthorhombic solid, being the least soluble (0.08 mg/l) and also the most stable [Pourbaix (1966)]. No evidence of crystalline $Zn(OH)_2$ formation was found in the XRD results of Chapter 4, and based on these XRD results, it is suggested that, although the formation of the crystalline zinc hydroxide species (in the form of the α, β, γ and ε complexes) is feasible, it would be limited to a value below the detection limit of the XRD.

According to solubility-pH relationships, should amorphous $Zn(OH)_2$ be present in the pore spaces, it would be soluble at levels of up to 1.2 mg/l. As in the case of Cr, solubility-pH relationships for Zn presented in Chapter 2 were developed for pure systems and, thus, should

amorphous $Zn(OH)_2$ be present, its solubility is potentially reduced by the presence of other ions in solution. This is explored further in the TCLP results of section 6.3.3.

(iv) Calcium

Calcium concentrations in the pore water of the S/S products are higher than those of hardened cement paste (hcp). The pore solution of both the cement pastes and the S/S products are expected to be saturated with $Ca(OH)_2$ [Diamond (1975)]. The differences as shown in Table 6-4 may be understood in terms of changing calcium solubility as a function of pH and ionic strength. Figure 6-2, reproduced from Moragues et al (1988), provides a graphical representation of the predicted concentration of Ca^{2+} in solution for the Ca-water system as a function of pH. Above a pH of approximately 12.4 the concentration of free Ca ions in solution shows a rapid drop-off. This is the pH of water saturated with $Ca(OH)_2$, at which $Ca(OH)_2$ solubility is 933 mg/l, or 505 mg Ca^{2+}/l. From solubility curves for the $Ca(OH)_2$ - water system, the solubility of Ca^{2+} in solution drops to approximately 7.4 mg/l at a pH of 13.5 (the pH of the pore solution of cement) and increases to 740 g/l at a pH of 11 (that of the S/S products) [Pourbaix (1966)].

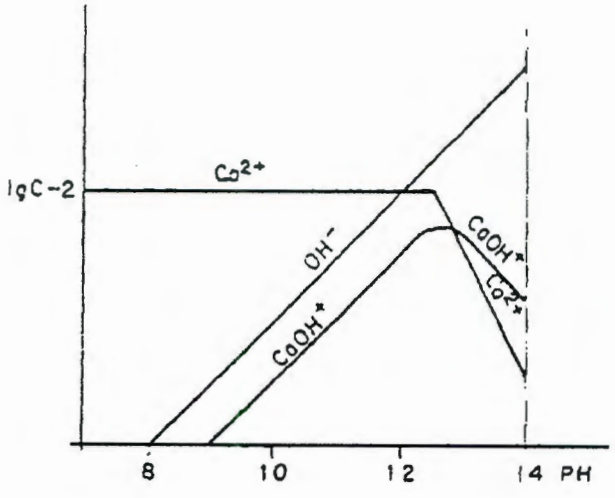

Figure 6-2 - log $[Ca^{2+}]$, log $[OH^-]$ and log $[CaOH^+]$ versus pH [Moragues et al (1988)]

These results are for a pure $Ca(OH)_2$-water system. In Moragues et al (1987) the effect on soluble Ca^{2+} concentrations of adding K(OH) and Na(OH) to a saturated calcium hydroxide solution is presented. Selected results from their work appear in Table 6-5.

Table 6-5 - Effect of OH^- species on Ca^{2+} in Solution in a Saturated $Ca(OH)_2$ solution (extracted from Moragues et al (1987))

Species	Concentration (mol/l)	Ca^{2+} in solution (mg/l)	pH of Solution
$Ca(OH)_2$	saturated solution	505	12.0
KOH	0.1	258	13.0
KOH	0.35	72	13.5
KOH	0.7	49	13.7
NaOH	0.01	722	12.6
NaOH	0.5	50	13.5

From Table 6-5 it is seen that both Ca^{2+} solubility and the pH of a saturated $Ca(OH)_2$ solution are strongly affected by other species in solution. Although solubility decreases with pH as in the case of the pure system, concentrations are reduced by the presence of other ions in solution.

In summary, therefore, the higher calcium concentrations of the S/S product pore solutions over hcp is attributed to both lower pH and different ionic strength. The ionic strengths of the pore solutions could not be measured due to the small amounts of solution extracted.

(v) Potassium

Potassium in the solidified FeCr Dust product is observed to originate from two sources. Firstly, it is found in the FeCr Dust, either as soluble species such as KOH which solubilizes readily upon contact with water, and secondly in the condensed layer around the outside of the dust particles as a potassium oxide species. From Chapter 3, the unwashed, unsolidified dust consists of 4% K (w/w). One quarter of this is removed during the washing step - assumed to be the soluble KOH species. In a TCLP of the washed material, little further potassium is released (approximately 60 mg of a possible 1740 mg). The remainder is thus suggested to be retained in the form of insoluble complexes as in the case of Cr and Zn discussed previously.

K is also contained in the raw cement, in a mass percent of less than 1% K_2O [PCI (1986)]. This hydrates readily upon contact with water to form KOH which dissociates, resulting in the high K concentrations in the hcp pore solutions. KOH is highly soluble over the whole pH range [Pourbaix (1966)].

The above discussion suggests that K contained in the pore solution originates from that contained in the cement while that in the volatile layer of the dust particles is immobile. Based on this assumption, it would be expected that, as cement contents in the S/S products increase, more K should be found in the pore solutions. A combination of three effects explain why this is not observed. Firstly, the ionic strength of the pore solution of the S/S product is different to that of hcp. The pore environment contains a number of metal ions in high concentrations which are not ordinarily found in cement, including soluble Cr and insoluble Zn. Ionic strength has already been suggested to have a strong influence on solubility and dissociation behaviour of hydroxide species within the pore solutions. These effects are discussed further in this Chapter.

The second effect is the following. When comparing a S/S product made with 75% cement with hardened cement paste, it is noted that different w/s ratios were used for making these samples, with the S/S products requiring higher water contents due to the presence of the fine dust materials as was discussed in Chapter 3. The level of cement addition reported here in Table 6-4 is on a dry cement to dry dust basis and thus, in a sample reported to contain 75% cement on a dry cement to dry dust basis, the amount of cement added based on total mass in the sample is 23% (w/w). This is a little over one third of the cement which is contained in a hcp made with 0.36 w/s, for which the results are presented in Table 6-4. Lower cement contents, and consequently a large amount of dust, are once again taken to imply a lower mobile K fraction.

Thirdly, in the X-Ray mapping results of Chapter 4, it was suggested that K may have substituted for some of the Ca in the cement hydration products in the solidified FeCr Dust. K contained in the cement hydration products will not readily enter the pore solution.

It is noted here that the differences in K concentrations of the pore waters between the various S/S products in Table 6-4 is suggested to be due to experimental scatter and not due to actual data trends.

In Table 6-5 the effect of K(OH) in solution on the solubility of Ca^{2+} can be seen [Moragues et al (1987)]. This is explained by the common ion effect as follows. Consider the dissociation of any metal hydroxide species presented previously:

$$Me(OH)_x \leftrightarrow Me^{x+} + x(OH)^-$$

K(OH) is highly soluble. The common ion effect implies that, as K(OH) dissociates, the overall equilibrium for hydroxide species shifts to the left, and other positive ions, including Ca, precipitate out as insoluble metal hydroxides. The presence of other anions and cations in the pore solution of both hcp and the S/S product implies that this equilibrium is a simplification of reality. It does, however, explain the results of Table 6-5 in terms of reduced calcium solubility and pH in the presence of K.

In hcp, the amount of solubilized K is high, assumed to be from the hydroxide species. The high proportion of OH^- ions in the pore solution of hcp will drive the above equilibrium to the left as described above, thereby reducing the amount of soluble Ca in solution. In the S/S products, less K in solution implies lower concentrations of OH^- ions from K(OH) and, consequently, increased dissociation of $Ca(OH)_2$ and more soluble Ca.

(vii) Summary of Observations from Pore Water Analyses

(i) pH of the pore solutions of S/S products is lower than for hardened cement pastes. The difference between pH of hcp and S/S products is suggested to be primarily the result of differences between potassium hydroxide contents of the pore solutions of cement and the solidified FeCr Dust respectively.

(ii) Only a small percentage of the total Cr is present in the pore solution. Of the Cr in solution, between 72% and 86% is Cr(VI), the rest being Cr(III). This indicates that Cr(III) solubility is a function of the ionic strength of the pore solution and not solely the

pH of the liquid. Cr not in the pore solution is suggested to exist as insoluble hydroxide or as the chromite in the original dust core. This is explored further below .

(iii) Zinc in the pore solutions is negligible and is expected to be insoluble at the pH of the pore solution. This implies that Zn is contained either as one of the insoluble hydroxide species at the pH of the pore solution or in the layer deposited around the dust core, possibly as a Fe-Cr-Zn oxide [Gencor (1996).

(iv) The pore solution is suggested to be saturated with calcium, the solubility of which is affected by other ions in solution.

(v) K originating from the cement is suggested to be readily soluble, while the dust is expected to contain K in both the mobile (KOH) and immobile (as K_2O from the original dust particles) species.

In Chapter 4 it was proposed that the S/S product is a porous solid, the pores being filled by a fluid. The results of the above tests have both identified and partially quantified the metal species contained in this fluid. In the results of the leaching tests which follow the species which are releasable in a variety of extraction tests on the S/S product are characterised. These results are used to expand our understanding of the speciation of the remaining metals in the solid.

6.3.3 Toxicity Characteristics Leaching Procedure (TCLP) Results

In the scope of this study the TCLP results were used in three ways. Firstly, to identify S/S products which, according to the EPA regulations, could be consigned to non-hazardous landfill, where monitoring requirements are less onerous for operators. Secondly, the TCLP was used to identify the effects of the operational variables on leaching. Finally the results were used in conjunction with other batch and kinetic leach tests to further the development of the chemical model proposed in Chapter 4.

Although the TCLP is probably the most widely used test for characterising a waste as "hazardous" or "non-hazardous", it is recognised to have little predictive value for long-term behaviour. The use of the TCLP here does not support its application as a waste classification tool. This was discussed previously .

The TCLP test procedure as used in this work is presented in Appendix A2. The standard defines a maximum allowable concentration of a number of contaminants in the leachate from a test in parts per million (ppm) or mg/l. If the concentration of any contaminant is higher than this value, the waste or S/S product requires further treatment or consignment to hazardous landfill. These guideline concentrations are presented with the test procedure in Appendix A2.

To identify how effectively metals are contained in the product, and ascertain the effect of changing operational variables on the leaching process itself, it is necessary to take into account the dilution effect which occurs when mixing the samples. As the amount of cement or water in the formulation increases, the mass of FeCr Dust cake (and consequently the concentration of a given contaminant) in a given mass of S/S product decreases. To take such dilution effects into account, TCLP results in this study are presented as the mass of contaminant leached (in mg) per mass of wet material with which the S/S product was made (in g), along with the traditional ppm representation.

(i) Choice of TCLP Leachant

A number of samples were subjected to the specified preliminary assessment carried out in accordance with the procedure presented in Appendix A2. This aims to identify the leachant which should be used in the TCLP. It was found that the solidified materials required the leachant solution specified for alkaline materials - a 1.0 N acetic acid solution prepared using distilled water and glacial acetic acid.

(ii) Qualitative Comments

The TCLP standard requires that material be crushed to less than 9.5mm prior to leaching. No minimum size is specified. After the 18 hour leaching period it was observed that, for all tests, the residual material was less than 1mm. Based on this observation it was suggested that the leach test results in the breakdown of the solid both due to attack by the acetic acid and, to a lesser degree, to attrition. This breakdown increases the exposed surface area and furthermore reduces the intra-particle diffusion path. The physical breakdown will thus

reduce the effect of physical encapsulation on the retention of soluble or solubilizable constituents in the pores.

To determine the significance of acid attack on solid breakdown, a repeat test was carried out using distilled water. Significantly less disintegration occurred - approximately 96% of the material was still in the initial size range used in the test. Acid attack is, therefore, the primary cause of breakdown during the TCLP tests, with attrition playing a secondary role.

The pH of TCLP leachates lie between 5.3 and 7.3. The buffering capacity of the S/S products is insufficient to raise the pH of the leachant to the pH of the pore solutions, shown in section 6.3.2 to lie between 10.5 and 12.6. Acid attack, associated with break-down of the solid and solubilization of hydroxide species, continues through the whole leaching period. The TCLP thus provides a 'worst case scenario' for leaching - that of consistent acid attack on a material which has limited physical integrity and buffering capacity.

(iii) Leachate Analyses

Table 6-6 provides TCLP leachate analyses for selected S/S products made from the FeCr Dust. Sample compositions for which results are presented in this table were selected to represent high, medium and low values of the operational variables as discussed in Chapter 3. A complete set of TCLP results, showing all samples tested in this work, appears in Appendix D2. Variability in results is discussed in section (iv) below.

Samples in Table 6-6 and Appendix D2 are identified by the cement added on a dry cement to dry solids ratio, the water to total solids ratio in the initial mixture, and the time for which the samples cured prior to testing. Results are presented in both ppm and as mg element released/g wet filter cake material used in making the S/S product. Also presented in the table are TCLP results from the washed FeCr Dust prior to S/S, as presented in Chapter 3.

pH of the Leachates

Table 6-6 shows a narrow spread in the pH values of the TCLP leachants. Changing the operational variables does not appear to have a significant effect on leachate pHs. A slight

increase in pH with an increase in the amount of cement in the mixture is observed, however. This is as expected since cement contains higher levels of free potassium than the FeCr Dust. The effect of K on pH is discussed further below. As was mentioned previously, the buffering capacity of the products is insufficient to raise the pH of the leachants to the natural pH of the S/S products.

Increased pH has been discussed previously to be advantageous in reducing solubility of metal ions. In the range of cement additions under investigation here, however, the effect of cement content on pH is not significant enough to make conclusive comments on the advantages of increasing the amount of cement in the mixture.

Chromium Leaching

None of the S/S products were found to meet the TCLP regulatory standard of 5 ppm for Cr for consignment to non-hazardous landfill. Comparison of the TCLP data for the washed FeCr Dust prior to solidification and the solidified FeCr Dust products shows that solidification does not significantly reduce Cr leaching from the wastes. In some cases, no reduction is effected. It is seen that there is a decrease in leaching with increased cement addition. This is discussed further below.

Only a small proportion of the total Cr in the samples (0.79% to 1.61%) is removed during the TCLP test. This was suggested above to include the Cr(VI) identified in Table 6-4 to be contained in the pore solution, as well as some of the previously insoluble Cr(III) which has resolubilized in the acidic leaching medium. The remaining Cr in the S/S product must, therefore, exist as insoluble Cr(III) hydroxides (see the discussion below), incorporated into the cement matrix (although no proof of this was found in XRD analyses) or as the stable chromite species. Based on the X-Ray maps presented in Chapter 4, the last-mentioned is thought the most likely.

Table 6-6 - TCLP results from selected FeCr Dust products, presented as ppm in TCLP leachates and mg element released per g wet filter cake in the S/S product

Cement Content	w/s ratio	Curing time (days)	pH	Cr		Cr(VI)	Zn		Mg		Ca		Si		K	
				ppm	mg/g cake	ppm	ppm	mg/g cake	ppm	mg/g cake	ppm	mg/g cake	ppm	mg/g cake	ppm	mg/g cake
Washed FeCr Dust[†]			4.5	27.6	0.38	9.0	595	8.09	238	3.24	27.3	0.37	-*	-	60.8	0.83
14%	1.04	59	6.2	11.4	0.41	6.7	421	14.98	257	9.14	1279	45.50	292	10.39	89	3.18
14%	1.04	149	5.8	10.4	0.37	6.9	360	12.82	159	5.66	1286	45.75	303	10.78	142	5.03
14%	1.04	288	6.0	9.5	0.34	-*	328	11.67	186	6.64	1125	40.02	305.4	10.87	201	7.15
10%	0.99	104	5.3	15.2	0.45	10.6	350	10.35	181	5.34	832	24.61	286	8.46	95	2.8
20%	0.99	104	6.7	9.3	0.30	7.0	302	9.81	173	5.62	1462	47.51	197	6.40	86	2.8
30%	0.99	104	6.9	8.6	0.30	5.8	111	3.90	162	5.68	1392	48.96	273	9.60	127	4.46
20%	0.9	104	6.3	8.4	0.26	5.6	212	6.57	178	5.50	1534	47.56	57.3	1.78	139	4.32
20%	1.08	104	6.1	12.4	0.42	8.9	297	10.07	174	5.88	1436	48.70	77.2	2.62	140	4.75
20%	1.18	104	6.7	9.4	0.35	-*	242	9.02	143	5.33	841	31.37	145	5.40	142	5.29

[†] Results for the FeCr Dust cake (unsolidified) are presented as ppm released from the washed and dried filter cake in the TCLP. These results are then scaled to give mg of element released per g of wet filter cake, based on an average water content of the filter cake of 32% after filtration.

* These results were observed to be completely inaccurate and hence were excluded from this table.

Cr (VI) analyses showed that between 59% and 75% of the total Cr in the TCLP leachates is Cr(VI), the rest being assumed to be Cr(III). Furthermore, a rough calculation from the results of the pore extrusions presented in section 6.3.2 shows the Cr(VI) in the TCLP leachant solutions to be the equivalent of that which solubilized in the pore solutions found in section 6.3.2, within experimental error. This indicates retention of soluble Cr(VI) in the pore water is solely by physical retention. The Cr(VI) from the pores is readily released into the leachant when breakdown of the solid structure occurs by acid attack. The reason why the calculation is approximate is due to the previously mentioned errors in the pore water analyses.

Cr(III) concentrations in the TCLP leachate are higher than would be expected at the observed pH values. These were calculated as the difference between total Cr in solution determined by AA analysis and Cr(VI) determined by UV analysis and were found to be between 2 and 7 ppm. According to Figure 2-2, the solubility of Cr(III) at a pH of 6.5, the average pH of the TCLP leachates, should be approximately 2.6×10^{-3} ppm. The observation that Cr(III) concentrations are over 1000 times what would be expected is similar to what was observed in the pore water extrusions presented in section 6.3.2. Here the strong influence of other ions on solubility behaviour was demonstrated and the shortcomings of solubility diagrams such as that presented in Figure 2-2 in predicting the solubility behaviour of complex systems are once again highlighted.

Figure 6-3 shows the relationship between total Cr in the TCLP leachate and pH. As the pH of the TCLP leachate increases, the total Cr released decreases slightly. Also shown in Figure 6-3 is Cr(VI) release as a function of pH. Cr(VI) release is observed to show little variation with pH, as expected: Cr(VI) is soluble over the entire pH range. The drop in total Cr is explained, therefore, by a drop in Cr(III) solubility as pH increases.

The effect of the operational variables on Cr release is as follows:

(i) As curing time increases the amount of Cr in the TCLP leachate decreases. An increase in curing time was shown via SEM in Chapter 4 to result in a more developed product matrix in which interlinking of the fibrillar hydration products was more extensive. The more integral matrix results in a greater degree of isolation of Cr from the leachant solution.

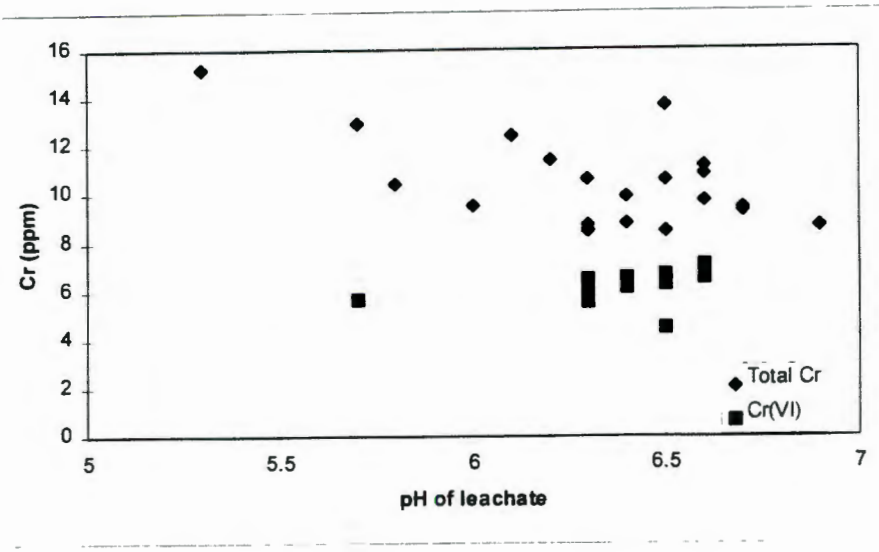

Figure 6-3 - Cr release as a Function of pH

(i) Increasing cement content had a similar effect to that of increased curing time, due to a greater degree of physical encapsulation which results from increased presence of cement hydration products. From these results it appears as if the effect of increased cement content is reduced as the amount of cement is increased, and it may seem as if above a certain level, increasing cement content may cease to have advantage in reducing Cr leaching. This is explored further in Chapter 8.

(ii) From the results presented here water to solids ratio shows the highest Cr leaching at the intermediate value.

It is reiterated that the effects of the operational variables cannot be considered in isolation as their effect on leaching is an interactive one. This interaction, and the effect of operational variables on leaching, is explored further in Chapter 8 using an experimental design tool.

Zinc Leaching

Zn concentrations in the leachates are high. Although no maximum concentration is set for Zn in the TCLP standard, the recommended maximum limit in South African drinking waters for Zn is 1 ppm [Pulles (1993)]. Since Zn levels in the TCLP leachates are mostly over 200 ppm it is felt the products should 'fail' the TCLP in terms of Zn release - that is to say, they should not be consigned to non-hazardous landfill.

Zinc leaching results are presented in Figure 6-4 as a function of pH. As in the case of Cr, a decrease in Zn in the TCLP leachate as pH increases is shown after a certain minimum pH. This is as expected given the solubility considerations presented in Chapter 2. Zn solubility at a pH of 6.5 predicted by the solubility diagrams is approximately 6500 mg Zn^{2+}/l for amorphous $Zn(OH)_2$ and approximately 1000 mg Zn^{2+}/l for ε-$Zn(OH)_2$. The Zn found solubilized in the TCLP leachate solutions is thus less than half that which would be expected from the solubility curves of Figure 2-2. Once again the solubility diagrams are for pure systems, and will not adequately describe complex systems. The other suggestion for this observation is the following. It has been suggested in Chapter 4 and section 6.3.2 that some of the Zn in the solidified product is contained in the volatile layer surrounding the dust. It is possible, therefore, that the TCLP mobilizes all of the $Zn(OH)_2$ previously precipitated in the pore solution, while the remainder is retained as part of the stable dust material and is not mobilized by acid attack over the 18 hour leaching period.

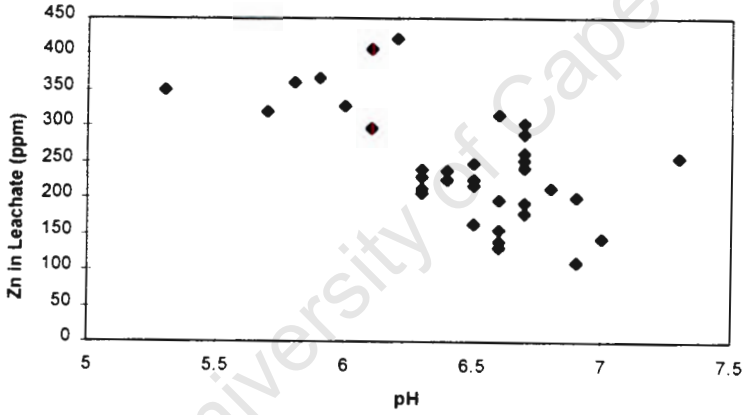

Figure 6-4 - Zn Leaching as a Function of pH

Although Figure 6-4 indicates a downward trend in Zn mobility as a function of pH, a wide scatter in results in observed in this plot. Owing to the fact that samples of different formulations are being compared in this figure, other effects such as cement addition, curing and the dilution effect discussed previously will also play a role.

In almost all of the cases, the solidified product leaches more than does the unsolidified washed cake on a mg Zn leached per g wet filter cake. This is not as expected based purely on pH considerations. Two explanations are offered for this observation. Firstly, the unsolidified

FeCr Dust was dried prior to performing the TCLP on the washed dusts, while the solidified dust products were not. The drying process could have resulted in the formation of insoluble Zn compounds by precipitation or crystallization which are not resolubilized during the TCLP. Secondly, as was suggested in the pore water results of section 6.3.2, long-term mobilization of the volatile outer layer from the dusts is possible. This will allow for mobilization of previously immobile Zn species.

Calcium

Calcium concentrations in the leachates are observed to be high - mostly above 1100 ppm. No regulatory limit is set for Ca in TCLP leachates. For comparison, however, recommended maximum drinking water limits in South Africa are 150 ppm [Pulles (1993)].

Calcium leached in the TCLP of the solidified FeCr Dust is significantly higher than that leached from the unsolidified FeCr Dust. The addition of cement to the dust increases the total amount of Ca present. This explains the higher levels of Ca leached from the solidified products over the unsolidified dusts. In acidic solutions $Ca(OH)_2$ will enter solution until the pH has been raised to above 11. In neither the TCLP on the S/S products (pH = 5.3 to 6.9) nor on the washed dust (pH=4.5) is solubility limiting in leaching.

The amount of Ca leached in the TCLP is greater than that contained in the pore solution of section 6.3.2. Solubility considerations can account for this observation. While the buffering capacity of the leachant is not consumed (as indicated by the low pH of the solution), Ca will continue to solubilize until the pH is above 11. In the alkaline pore solution, solubility constraints were observed to limit Ca present in the pore water. In the case of the TCLP results, the leachate pHs are low, and all of the $Ca(OH)_2$ from solution has the potential for mobilization. Furthermore, acid attack on the cement hydration products, which results in breakdown of the solid structure which contains Ca, may result in mobilization of Ca which was previously inaccessible for leaching.

The Ca leached in the TCLP represents between 20% and 40% of the total Ca in the sample used in the test. The rest is assumed to be removed with the solids during filtration either as

the insoluble complexes from the pores, or else as Ca remaining bound to Si in the CSH cement hydration product. This suggests that acetic acid does not completely destroy the CSH structure over the time periods studied here. Further long-term testing is required to determine whether a silicate framework remains after acid attack, or whether the entire CSH structure will ultimately be destroyed.

Potassium

Potassium released in the TCLP of the solidified FeCr Dust is greater than was found in the TCLP of the unsolidified dust. As has been discussed in the pore water results of section 6.3.2, the cement has a higher amount of free K than does the FeCr Dust (even though the total K content is lower), and hence the increased K leached is suggested to originate from the cement. Furthermore, using the pore extraction results of section 6.3.2, the amount of K in the pore solution can be calculated to range from 0.2 to 0.8 (mg /50 g wet S/S product). From the TCLP results, between 86 and 142 mg of K are released per 50 g of wet S/S product. This is two to three orders of magnitude more than what is contained in the pores. Two explanations are offered for this. Firstly, in the low pH environments of the TCLP leachates, dissolution of hydroxides is expected as was discussed in the case of Ca described above. Secondly, K was suggested to be potentially incorporated into the cement hydration products as observed in the X-Ray maps of Chapter 4. Acid attack causes breakdown of these cement hydration products as was indicated by the fineness of the particles after the test. This will result in release of K into solution.

(iv) Variability in TCLP Results

The coefficient of variation was used to provide an indication of the variability in results and to determine the significance of observed trends. The coefficient of variation is the standard deviation as a fraction of the mean of a sample set. The lower the coefficient of variation, the better the repeatability of results.

The coefficients of variation are presented for a number of elements leached in the TCLP in Table 6-7 below. The repeatability of results is high, with coefficients of variation all being

less than 7%. This suggests that the observations presented above are not merely due to experimental variability.

Table 6-7 - Coefficients of Variation in TCLP Results

Element	Coefficient of Variation in results
Cr	6%
Zn	3%
Mg	1%
Ca	2.5%
K	6.4%

(v) Summary of the TCLP Observations

(i) pH is not a strong function of the operational variables.

(ii) The buffering capacity of the S/S products is not sufficient to significantly raise the pH of the TCLP leachants to the natural pH of the products.

(iii) Cr(VI) is not effectively retained by the S/S products. This indicates that Cr(VI) is soluble in the pore solution and is readily released as the solid structure breaks down.

(iv) Cr (III) and Zn release is a function of pH, indicating their presence as hydroxide species, the solubility of which is a function of leachate pH.

(v) Between 0.79% and 1.61% of the total Cr in the product is released in the TCLP, the rest being either insoluble Cr(III) or the stable chromite species in the dusts. The latter is in line with observations from X-Ray mapping presented in Chapter 4.

(vi) The complex ionic chemistry in the pores results in more Cr(III) being soluble than would be predicted from literature reported solubility of Cr(III) in pure solutions.

(vii) Since the solubility of $Zn(OH)_2$ does not limit Zn release, it is suggested that Zn which is not released during the TCLP is contained as the stable species as part of the original dust samples. Gencor (1996) suggests that this may be in the form of a Fe-Cr-Zn oxide species.

(viii) Ca mobilization from the products is significant in the acidic environment.

(ix) More K is released than would be expected from the pore solution results. This indicates K mobilization is a result of both the acidic environments and breakdown of the solid structure.

6.3.4 Equilibrium Extraction Tests

The TCLP results presented in the previous section give an indication of the 'worst case' leaching situation: one in which there is constant contact with a low pH liquid phase. The low pH environment of the TCLP results in both mobilization of metal species which were insoluble at higher pH values, and acid attack and breakdown of the cement hydration product.

The equilibrium extraction (EE) is carried out in distilled water and indicates the amounts of various constituents removable from the solid at its natural pH conditions where chemical attack on the solid does not occur. Differences between the TCLP and the EE were outlined in Table 6-1. EE results are presented in Table 6-8. Each result is an average of two repeat tests.

Table 6-8 - Results of the Equilibrium Extraction Tests

Sample Description	pH	Cr	Cr(VI)	Zn	Si	K	Mg	Mn	Ca
20% cement, 0.9 w/s, 270 day	11.7	48.0	nm	nd	nm	461.5	1.2	nd	51.4
20% cement, 0.9 w/s, 335 day	11.7	49.3	46.2	nd	nm	149.8	0.5	nd	44.4
20% cement, 1.0 w/s, 230 day	11.5	55.8	53.8	nd	nm	552.7	0.9	nd	58.4
20% cement, 1.5 w/s, 104 day	11.1	58.6	55.1	nd	39.4	229.6	1.0	nd	171.4
30% cement, 1.4 w/s, 104 day	11.2	62.4	57.8	nd	49.7	523	0.8	nd	111.4
50% cement, 1.1 w/s. 104 day	12.1	57.5	53.7	nd	74.5	630.5	0.5	nd	43.2
75% cement, 0.9 w/s, 104 day	12.5	45.7	42.9	nd	51.4	1194.5	0.5	nd	37.7

nd = not detected

nm = not measured

(i) pH

In the EE, distilled water (pH ≈ 7) is used as the leachant solution. At the end of the leaching period leachant pH's were between 11.1 and 12.5. These pH values are similar to those of the pore solutions of the S/S products (section 6.3.2). The free alkaline capacity of the S/S products is thus sufficient to raise the pH of the distilled water to that of the pore solution.

The pH at the end of the leaching period was observed to be a function of the amount of cement used in making the samples: an increase in cement content in the S/S products from 20% to 75% resulted in an increase in pH of one unit. Associated with this is an increase in the amount of K in solution. As was highlighted in Table 6-5 and TCLP results, the pH of the solution appears to be a direct function of the amount of K(OH) which has dissociated into solution.

(ii) Chromium Release in the EE

Chromium released in the EE was primarily Cr(VI). As in the discussion of the pore water results, at the alkaline EE leachant pH the Cr(III) solubility is below detection limits of the AA spectrometer.

Chromium released in the EE was calculated to be to the order of 1% of the total Cr in the solid (determined via fusion digests). This is approximately equivalent to the amount of Cr contained in the pore solutions as Cr(VI), as found in section 6.3.2, and that Cr(VI) released in the TCLP (section 6.3.3). It is thus suggested that the Cr released in the EE extracts is the Cr(VI) present in the pore solution at the start of the leaching test. The remaining Cr is once again expected to be Cr(III), insoluble at the EE leachate solution pH, and that contained as the chromite species in the stable dust core.

There was insignificant change in the percentage of Cr released as the cement content was changed. The TCLP results suggested that increased cement content resulted in improved Cr retention. In the EE the S/S product is ground to less than 149μm prior to leaching, and the physical isolation effects due to the more integral S/S product expected with higher cement contents is reduced. Soluble Cr(VI) which may previously have been contained in isolated pores becomes available for leaching.

(iii) Zinc, Magnesium and Manganese Release

No Zn and minor amounts of Mg and Mn were detected in the EE leachates. As in the case of Cr(III) the solubility of these three species is expected to be at a minimum at the leachant pHs

(see Chapter 2). These metals will exist as insoluble hydroxide precipitates or stable metals in the dust core, both being removed with the solid material remaining at the end of the test.

(iv) Potassium and Calcium Leaching

The K in the S/S products originates primarily from the FeCr Dust. Cement contains small amounts of K: the total sodium + potassium oxides in unhydrated cement lies between 0.2 and 0.8 % (w/w) [PCI (1986)]. Consequently, as the amount of cement in the formulation increases, so the amount of K in the S/S product decreases. This is confirmed by characterisation via fusion.

Contrary to this, more K is released in the EE as cement content increases. This confirms the pore solution results of section 6.3.2. While the K from cement is in a soluble form, both in the pores and subsequently in the leachants of the TCLP, only small amounts of K from the dusts are available for solubilization. The rest is suggested to be retained on the layer deposited on the surface of the dusts or within the stable dust core.

A drop in the Ca concentration with increased K concentrations and pH is also identified. As more potassium hydroxide dissociates, so more $(OH)^-$ ions are present in solution. Due to the increase in $(OH)^-$ ions the solubility equilibrium of $Ca(OH)_2$

$$Ca(OH)_2 \leftrightarrow Ca^{2+} + 2(OH)^-$$

will shift to the left, thus reducing the Ca present in solution. This is the reverse of what was observed in the TCLP. In the TCLP an acidic medium is used as the leachant and the low pH solution caused the solubility equilibrium above to shift to the right.

(iv) Summary of Results from the EE

(i) The solid material raises the pH of the distilled water leachant solution to the pH of the pore solution.

(ii) Cr which is released in the EE is the Cr(VI) contained in the pore solution. This is in line with TCLP observations.

(iii) Cr(III) is removed as insoluble hydroxide species or in the stable dust core with the solid material.

(iv) Zn, Mg and Mn mobilization is negligible at the pH of the leachates.

(v) The equilibrium solubilities of the various alkali species are interrelated and affects pH.

6.3.5 Sequential Chemical Extraction Test

The TCLP and the EE tests identify those constituents of the wastes which are leachable using specific leachants. These tests have suggested that small amounts of both Cr and Zn are easily mobilized from the S/S products. The release of the rest of the Cr was expected to be insoluble in the leachant solutions, or contained in the stable dust cores. All of the Zn not mobilized in the TCLP was suggested to be contained as an immobile species in the dust particle.

In the Sequential Chemical Extraction (SCE) test a sample of the waste is subjected to five consecutive extractions. Each extraction uses a more aggressive leachant, the leachants being chosen to remove constituents of the product associated with specific phases. The aim of this test is thus to determine the *relative proportions* of each of the elements which exist in each phase as proposed in the pore solution extractions, the TCLP and the EE. A full description of the test and its shortcomings are described in section 6.2.3 and Appendix A2.

In Table 6-9 a summary of the five steps in the SCE and the retention mechanisms of metals extracted in each step is presented.

Table 6-9 - Summary of the Steps in the SCE

Step No	Release subject to changes in	Species Extracted
1	Ionic Composition	Ion Exchangeable Fraction
2	pH	Surface oxides, hydroxides and carbonate bound metal ions
3	Eh	Metal ions bound to Fe and Mn oxides
4	Eh	Metal ions bound to organic matter and sulfides
5	Stable species	Residual metal ions

The results from the SCE are presented graphically for one of the samples tested in Figure 6-5 as the percentage of the total amount of metal which is released in each step. The trends seen in this plot are similar to those observed for the other samples tested. A full set of results is presented in Appendix D3. The results presented are averages of two repeat tests.

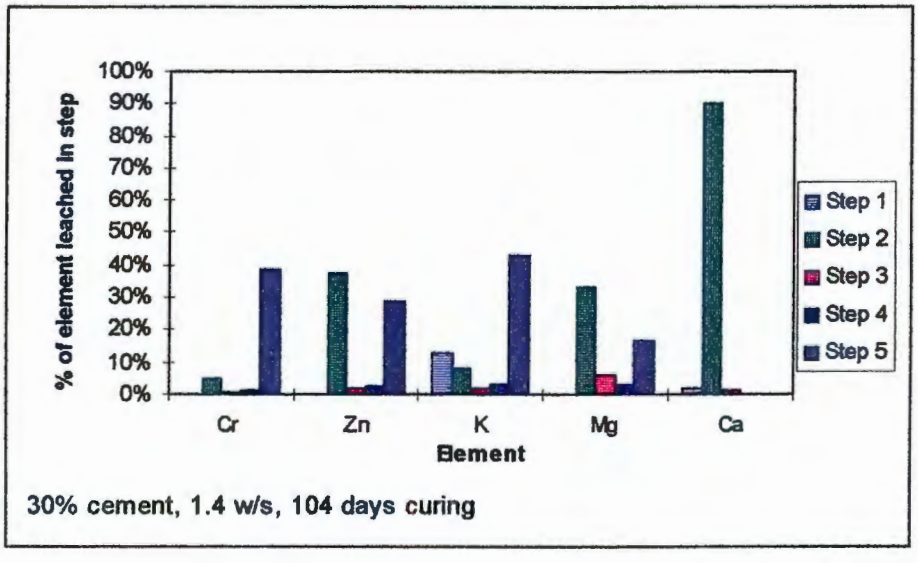

Figure 6-5 - Results of the SCE expressed as the Percentage of the Total Amount of Metal in the Solid Released in Each Step of the Test

Appendix D3 shows that the total mass of the various elements in the original sample determined via fusion was not equal to the total extracted in the five steps of the SCE for any of the samples tested. Two suggestions are offered for this observation. Firstly, due to the

heterogeneous nature of the solid and the small sample (0.5g) tested as specified in the test procedure, chemical differences between the samples used in the SCE and those used in the fusion to determine total concentration in the solid will contribute to the inconsistencies seen in the mass balance. Secondly, it is possible that loss of constituents occurs in the washing steps between extractions.

While taking into account the fact that the mass balance did not close, and that the test was not originally developed for testing S/S products as such, the results can be still be used to provide the following information:

(i) Chromium

Small amounts of Cr are released in the first step of the test (soluble and physisorbed species). This is equivalent (within experimental error) to the amount of for Cr(VI) previously identified to be contained in the pore solution and releasable in the EE. Of the total chromium, 4% to 5% is released in the second step of the test. This was said to be the step in which release is associated with pH and would account for $Cr(OH)_3$ solubilized at pH 5. The pH-controlled release of Cr is consistent with observations of TCLP (low pH) and EE (high pH) tests. In the TCLP, 0.79% to 1.61% of the total Cr is extracted, lower than is found for the SCE. In the case of the TCLP, however, solubility constraints limited dissolution of potentially soluble Cr species which were removed in the SCE extracts.

The majority of the Cr accounted for in the SCE is found in the final step of the test - that which theoretically characterises the stable residual. This is in line with suggestions made in the characterisations of Chapter 4 and the TCLP and EE results. The existence of 'stable' Cr, ie that not released in any of the other steps, can be discussed in a number of ways. The first, and most likely, which was presented previously, is that Cr is contained in the dust particles in the original stable chromite ($FeO.Cr_2O_3$) complex found in the original ore. The likelihood of this occurring is confirmed by Cox et al (1985). Furthermore, X-Ray mapping results presented in Chapter 4 showed that high concentrations of Cr were associated with high iron concentrations, lending further support to this theory.

Secondly, literature reports suggest that Cr(III) can be chemically incorporated into the cement hydration products. The fundamental analyses of Chapter 4, however, found no evidence thereof.

In summary, therefore, it is concluded from the SCE that approximately 1% of the Cr is contained as soluble Cr(VI) in the pores. Approximately 4% is present as the potentially soluble $Cr(OH)_3$ species, while the remainder is proposed to be stable in the dust core.

(ii) Zinc

Approximately equal proportions of the zinc are recovered in step 2 and 5; these being pH controlled release and that retained in the stable residue respectively. That released in step 2 was identified as soluble zinc hydroxide, releasable in the low pH conditions found in the TCLP. The zinc retained in step 5 is similar to what was proposed for Cr: remaining as part of volatile layer surrounding the stable dust particles, in which form it is resistant to leaching in any of the test conditions presented here. This is in line with results from the other batch tests.

(iii) Calcium

From Figure 6-5 the majority of Ca is observed to be released in step 2 of the test. According to Table 6-9, step 2 is associated with pH-controlled release of surface oxides, hydroxides and carbonate bound metal ions. The solution in this step is buffered to pH 5 using acetic acid. While the Ca from the S/S product which is solubilized does not exceed the buffering capacity of the solution, Ca will continue to be solubilized in the liquid. Although the leachate in this step was suggested to only mobilize insoluble species, the acetic acid solution used in the TCLP was found to result in gross disintegration of the cement hydration product, with subsequent release of Ca. Thus, although no conclusive statements can be made about the proportion of Ca contained in different phases in the product, the procedure indicates that Ca is readily removed from the S/S product by acid attack.

(iv) Potassium

Significant proportions of K are released in each step of the SCE. 18% to 20% of the K accounted for is released in the first step - that which removes the ion exchangeable, soluble

and sorbed species. Potassium hydroxide is highly soluble as was suggested in the analysis of the composition of the pore solution of hardened cement paste. This accounts for K released in the first and, to some degree, subsequent three steps.

Approximately 60% of the K accounted for is retained in the residual, implying that this K is contained as a 'stable species' in the product. This is in line with suggestions from the pore extrusion results, TCLP and EE: a large amount of the K is contained in the residual dust product core which was discussed previously. This K is immobile and does not enter the pore solution or the leaching solutions of the TCLP or EE.

6.4 Summary of the Batch Test Results

An attempt was made to correlate the results from the various tests to identify where results from the tests are consistent and to highlight inconsistencies to be resolved.

Table 6-10 (b) provides a summary of the Cr, Zn, Ca and K results from the EE, the TCLP and the SCE for 6 different samples. The values of the operational variables used in making these samples appears in Table 6-10 (a). All results have been scaled to represent 100 g of wet S/S product. Note furthermore that SCE results were scaled up to make the total recovery 100%. While recognising that the SCE did not account for all the element within the S/S product, the scaling was done in order to compare the SCE to the results of other tests.

Table 6-10 (a) - Composition of Samples Presented in Table 6-10 (b)

Sample No.	Cement (%)	w/s	Curing (days)
1*	14	1.04	434
2*	20	0.90	104
3	20	1.48	104
4	30	1.36	104
5	50	1.12	104
6	75	0.86	104

* Note that samples 1 and 2 were not tested in the SCE

From Table 6-10 (b) the following is highlighted:

(i) A small amount of the total Cr is contained solubilized in the pore solution, primarily as Cr(VI). This Cr is readily released in both the TCLP and the EE. Further Cr is released in the TCLP which is not found in the EE leachates or the pore solutions. This is suggested to be $Cr(OH)_3$, which is soluble in the acid TCLP leachates but insoluble in the alkaline pore solution and EE leachates. Finally, the SCE suggests a large proportion of the Cr to be contained as a stable species, presumably in the residual dust. In the model of Chapter 4, Cr was suggested to be contained solubilized in the pore solution, as the insoluble hydroxide species or in the stable dust core. Observations presented here for Cr thus confirm the model of Chapter 4, although in initial development of the model it was not identified that the *majority* of the Cr would be retained in the stable dust core, as is indicated by SCE results.

(ii) Zinc is released in the TCLP, and is not found in the pore solution or EE leachate. This indicates the effect of pH-solubility relationships on its release. Furthermore, the SCE indicates that roughly equal proportions of zinc are contained as (a) a species whose release is controlled by pH (suggested to be in the $Zn(OH)_2$ form) and (b) that contained as a stable, immobile species.

(iii)In the model of Chapter 4, it was suggested that Zn is evenly distributed through the pores of the S/S product. This may be true in the case of that contained as the insoluble hydroxide species, but that contained as the stable species in the dust is localized in the dust particles.

(iv) Large amounts of Ca are released in the TCLP. In the pore solutions and EE extracts only small amounts of Ca are detected. Furthermore, the SCE and TCLP indicate that a large proportion of the Ca is removed from the S/S product in low pH environments. Since Ca is expected to be contained in the cement hydration product, these results highlight that fact that these hydration products, identified in Chapter 4, are susceptible to breakdown via acid attack. This is in line with literature observations presented in Chapter 2.

Table 6-10 (b) - Summary of Results of the Batch Tests (all values reported are scaled up to represent mg released in that test per mg found in 100g of S/S product)

Chromium

Sample	Total (mg/100g)	Pore Solution Cr(Tot)	Pore Solution Cr(VI)	TC LP Cr(Tot)	TC LP Cr(VI)	EE Cr(Tot)	EE Cr(VI)	SCE Step 1	SCE Step 2	SCE Step 3	SCE Step 4	SCE Step 5	Total from SCE
1	1610	15.3	11.7	26	11.3	nm	nm	-	-	-	-	-	-
2	2290	12.6	9.1	19.6	12.2	nm	nm	-	-	-	-	-	-
3	2230	13.1	9.8	19.8	13.1	12.9	12.1	11.2	241	20.8	55	1950	2278
4	2190	nm	nm	17.2	nm	15.9	14.7	11.5	237	22.1	49.0	1861	2180
5	1810	15.3	11.3	20.6	15.1	13.6	12.7	7.7	258	17.9	37.7	1481	1802
6	1570	10	7.5	15.3	9.7	11.1	10.9	4.2	250	17.7	33.7	1258	1563

Zinc

Sample	Total (mg/100g)	Pore Solution	TCLP	EE	SCE Step 1	SCE Step 2	SCE Step 3	SCE Step 4	SCE Step 5	Total from SCE
1	3140	nd	640	nm	-	-	-	-	-	-
2	2130	nd	424	nm	-	-	-	-	-	-
3	6290	nd	850	nd	0.9	3098	161	243	2755	6257
4	5530	nd	720	nd	0.8	2896	163	200	2241	5501
5	5100	nd	690	nd	0.0	3023	121	112	1821	5077
6	4400	nd	685	nd	0.0	3168	102	119	996	4384

Table 6-10 (b) (cont)

Calcium

Sample	Total (mg/100g)	Pore Solution	TCLP	EE	SCE Step 1	SCE Step 2	SCE Step 3	SCE Step 4	SCE Step 5	Total from SCE
1	3030	3.7	2155	nm	-	-	-	-	-	-
2	2750	5.5	2430	12.9	-	-	-	-	-	-
3	6870	4.1	3050	37.7	72.5	3188.2	36.9	3.8	10.0	3311
4	7340	nm	3600	28.4	78.4	3407.0	42.5	3.5	6.5	3538
5	11050	2.7	4120	10.2	78.8	5856.1	73.2	36.2	0.0	6044
6	12060	1.3	4860	8.7	61.7	7516.6	88.5	5.6	9.7	7682

Potassium

Sample	Total (mg/100g)	Pore Solution	TCLP	EE	SCE Step 1	SCE Step 2	SCE Step 3	SCE Step 4	SCE Step 5	Total from SCE
1	nm	nm	179	nm	-	-	-	-	-	-
2	2640	0.95	279	91	-	-	-	-	-	-
3	2100	1.03	261	51	198	92	32.4	42.0	651	1014
4	2060	nm	321	133	188	115	30.8	43.8	615	993
5	1690	1.28	381	149	329	119	13.3	27.8	435	924
6	1560	1.26	435	277	449	191	14.6	32.7	307	994

(v) Potassium, the solubility of which is less dependant on pH than in the case of other metal species, is found in both the TCLP and the EE leachants. The pH of the pore solution and leachants is suggested to be determined by dissolution of K(OH) species. Furthermore, K is released in all of the steps of the SCE, with the soluble species, pH controlled release and that contained in the stable core being the most significant.

(vi) When comparing the initial amount of a constituent in the S/S products (determined via fusion) with the amount of the constituent extracted in the various tests and an analysis of the residual from the test, it is observed that the mass balance does not close. A number of factors have been highlighted previously which could contribute to the observed inconsistencies. These include the small sizes used in certain tests, effects of drying on chemical speciation (EE and SCE), dilution effects and errors in readings from analytical equipment.

6.5 Significance of these Leach Tests for the Proposed Chemical Model

Based on information from the SCE, which is supported by the results of the pore extractions, the TCLP and the EE, certain statements can be made about the chemical model presented in Chapter 4. Chapter 7 which follows presents further development of the chemical model.

Chromium: Approximately 1% of the total Cr is contained as soluble Cr(VI) in the pore solutions, a further 4% to 5% of the total Cr is in the form of hydroxide species (primarily Cr(III)) and the remainder is stable in the dust core.

Zinc: Roughly equal proportions of Zn are contained as solubilizable species in the pore solution and the rest is condensed as a relatively immobile species on the surface of the dust particles.

Potassium: Approximately 60% of the potassium is stable, contained as part of the dust or within the cement hydration products, while the rest is solubilizable and contributes to determining solution pH.

Calcium: A large proportion of Ca is readily releasable under acidic conditions and therefore exists in the pore spaces, or else is released as CSH is broken down by the acid.

7.

Leaching II:
Modelling the Mechanisms and Kinetics of Leaching

7.1 Introduction

In practical implementation of S/S, wastes are mixed with cement and cast into monolithic cells within a landfill (see Chapter 8 for more details of large-scale implementation of the technology). Leaching will be as a result of liquid moving around- and percolating through- the material in the cells. In order to understand kinetics of leaching from the monolith once placed in landfill, three types of tests are employed in this current chapter. The first looks at leaching on a particulate level, using agitated tests equivalent of those in Chapter 6. The second takes a more macroscopic view of the leaching process, with solid blocks of S/S products suspended in a bath of leachant solution. Finally the leaching behaviour and hydrodynamics expected in landfill are studied by percolating a leachant through a bed of the S/S product packed into a glass column.

Leaching is considered in the context of the testing of S/S products to be the transport of constituents from the solid, into the liquid filled pore spaces, and subsequently into a surrounding bulk liquid phase. Chapter 6 discussed results of leach tests aimed at determining the amount of various constituents removable from a S/S product in 'once-off' leaching tests. These test results were used to make assumptions about the chemical speciation of metals within the S/S product.

When considering the general definition of 'leaching' from a solid as described above, a number of discrete steps are identified in the removal of a component from the solid. These were presented in Chapter 6 and are given, in summary, as:

(i) *Mobilization* of components from the solid phase, typically through desorption, dissolution or reaction.

(ii) Movement via diffusion from the site at which the component is contained in the solid through the tortuous liquid filled pore network of the solid to the surface of the solid particle or monolith. This is known as *intra-particle diffusion.*

(iii) Transfer from the surface of the monolith into the bulk leaching solution. This will include mobilization reactions at the solid surface interface and movement of mobile constituents from the solid surface through a boundary layer into the bulk liquid phase.

Where the leachant is an acid medium, the above steps will be preceded by ingress of acid into the solid structure, potentially causing breakdown of the solid. The tests presented in Chapter 6 do not give any information as to which of the above processes controls the *rate* of leaching from the S/S products. The broad aim of tests presented in this current chapter is to identify which mechanisms are rate limiting in the leaching process, and to establish the values of parameters which describe mathematically this leaching process.

The chapter proceeds as follows. Mathematical expressions which describe each of the discrete steps in the leaching process described above are presented. Three different tests are described in which contaminant release rate is quantified. Such tests are broadly classified as "kinetic leaching tests". Test procedures are described and the results from the tests are presented and interpreted in a way which sheds light on the mechanisms which control leaching.

7.2 Development of Expressions for the Various Steps in Leaching

The interpretation of results from leaching tests requires an understanding of the mathematics which describe the various steps in the leaching process. To this end, the general equations of mass transfer are developed. This analysis is followed by consideration of the expressions for each of the individual steps in leaching presented above.

7.2.1 Differential Equations of Mass Transfer

Consider a control volume of material containing a component A around and through which a fluid (leachant) is flowing which has the potential to mobilize A. A general mass balance in the specific control volume is:

(Net rate of material leaving the a control volume) + (net rate of accumulation within the control volume) - (rate of chemical production of A within a control volume) = 0

(7-1)

The continuity equations describe mathematically the above mass balance for a species A [Bird et al (1960)]:

$$\underset{\sim}{\nabla}\cdot\underset{\sim A}{N} + \frac{\partial c_A}{\partial t} - R_A = 0 \tag{7-2}$$

where $\underset{\sim A}{N}$ is the molar flux of the component out of the solid, c_A is the concentration of component A in the control volume and R_A is the rate of molar production of A per unit volume. $\underset{\sim}{\nabla}$ (read 'del') is the directional derivative along the path of maximum gradient. In cartesian co-ordinates del is given by:

$$\underset{\sim}{\nabla} = \frac{\partial}{\partial x}\underset{\sim x}{e} + \frac{\partial}{\partial y}\underset{\sim y}{e} + \frac{\partial}{\partial z}\underset{\sim z}{e} \tag{7.3}$$

where $\underset{\sim i}{e}$ is the unit vector in the i direction.

The overall flux of A out of the solid, $\underset{\sim A}{N}$, will be due to a combination of two factors - diffusion within the fluid phase and a bulk fluid flow contribution:

$$\underset{\sim A}{N} = -cD_{AB}\underset{\sim}{\nabla}x_A + c_A\underset{\sim}{V} \tag{7-4}$$

Here c is the molar density of the mixture, D_{AB} is the diffusivity of component A in liquid B, x_A is the mole fraction of species A in the liquid and $\underset{\sim}{V}$ is the molar average velocity of the liquid phase.

If there is no bulk fluid flow through the control volume the second term of equation (7-4) becomes zero. Now, substituting equation (7-4) into (7-2) and dividing by the molecular weight of A gives:

$$\frac{\partial c_A}{\partial t} = D_{AB} \underset{\sim}{\nabla}^2 c_A + R_A \tag{7.5}$$

Equation (7-5) provides the unsteady state mass balance equation for component A over a defined control volume where there is no bulk fluid flow into or out of the control volume.

In the current work the control volume is the solid S/S product. Within this control volume, diffusion will not be along a linear path: the tortuous pore structure increases the length of the diffusion path. In such cases, the diffusivity D_{AB} should be replaced by the effective diffusivity, D_e, of the component, which takes into account the porosity and tortuosity of the solid. D_e and D_{AB} are related by:

$$D_e = \frac{\varepsilon D_{AB}}{\tau} \tag{7.6}$$

where ε is the porosity and τ is the tortuosity factor [Welty et al (1984)].

Expressions which describe leaching in each of the four individual steps in the leaching process described in section 7.1 are now handled individually. All of these equations are developed for situations where no bulk fluid flow occurs into or out of the solid.

7.2.2 Diffusion through the Solid

In cases where the rate of leaching is controlled by diffusion through the solid (referred to hereafter as 'intra-particle diffusion'), the resistance to leaching is described by the effective diffusion coefficient of section 7.2.1, which is a function of both molecular diffusivity and the tortuosity and porosity of the solid. For simplification in such cases the reaction term of equation (7-5) is often dropped, which suggests either that constituents are already mobile or that the reaction by which a previously immobile species A is mobilized is rapid compared to diffusion.

With the reaction term of zero, equation (7-5) is simplified by making a number assumptions about the initial and boundary conditions of the system. These are:

(i) *The sample*[1] *being tested is infinite or* $c_A=c_{A0}$ *as* $x\rightarrow\infty$[2] ***for all t***, where c_A is the concentration of contaminant A at position x measured inwards from the surface of the solid and c_{A0} is the initial concentration of A in the sample. Another way of stating this is that the concentration at the centre of the solid is constant throughout the test period. The application of this assumption to finite samples is discussed at the end of this section

(ii) *Concentration at the surface of the slab is constant and equal to the concentration in the bulk, or* $c_A=c_{A,S}=c_b$ ***at x=0***[3] ***for all t***. In accordance with the discussion in the previous section, transport from the solid surface to the bulk liquid (external mass transfer) is assumed to be rapid compared to transport through the solid to its surface for any materials in which diffusion through a tortuous solid occurs [Levenspiel (1979)]. This is suggested here to hold in the case of the S/S products, where constituents need to move through the tortuous solid to enter the bulk solution [Andres et al (1995), Côté et al (1987), US EPA (1980)]. A combination of sample size and shape, ratio of volume of leachant to surface area and leachant renewal frequency should be chosen such that the concentrations of components of interest in the leachates in each leaching interval do not reach levels where solubility constraints are limiting further solubilization.

(iii) *The contaminant is distributed homogeneously in the solid at the start of the leaching period or* $c_A=c_{A0}$ ***at t=0 for all x***[4] . This can be achieved by effectively mixing the waste-cement combination during sample making.

Based on these initial and boundary conditions, the following equation can be developed from equation (7-5) which describes the rate of release of a constituent from a solid where intraparticular diffusion is the controlling leaching resistance. The details of the derivation are presented in Appendix C3.

---

[1] It will be seen later that rectangular samples, left over from the three point bend test of Chapter 5, are tested in the kinetic tests. In the case of spherical particles the initial and boundary conditions become:

[2] $c_A=c_{A0}$ as $r\rightarrow 0$

[3] $c_A=c_{A,s}=c_b$ at $r=R_S$ for a sphere of radius R_S

[4] $c_A=c_{A0}$ at $t=0$ for all r

$$\frac{M_t}{M_0} = \frac{S}{V}\left(\frac{4D_e}{\pi}\right)^{0.5} t^{0.5} \qquad (7\text{-}7)$$

Here M_t/M_0 is the fraction of contaminant leached at time t, V/S is the ratio of sample volume to surface area and D_e is the effective diffusion coefficient.

Provided none of the ambient conditions (eg temperature, pressure) change, the molecular diffusivity is constant. Furthermore, if tortuosity and porosity remain constant during leaching, D_e will be constant. In such cases the term $S/V(4D_e/\pi)^{0.5}$ will be constant. Cases where tortuosity and porosity remain constant during leaching for S/S products are where no gross breakdown of the solid structure occurs. From the results of Chapter 6 it was seen that distilled water leaching results in limited breakdown of the solid, while acetic acid changes the solid structure considerably, implying a change in both tortuosity and porosity.

A number of researchers have found intra-particle diffusion to be the controlling resistance in determining the rate of leaching of different metals from monolithic S/S products [Andres et al (1995), Côté et al (1987), US EPA (1980)]. Results from literature reports are presented in section 7.6.1.

In laboratory scale testing of S/S products, samples of finite geometry are leached. To ensure that a sample of finite geometry approximates the "infinite geometry" as required in the above solution, the following condition is suggested. Say, for example, the infinite sample solution holds for a finite geometry provided the change in concentration at the centre of the solid is less than 0.5% throughout the leaching period. From the derivation presented in Appendix C3, the value of $X/(4D_et)^{0.5}$ can be calculated which corresponds to a value of $(c_A-c_{A0})/(c_{A,S}-c_{AO}) = 0.5\%$ at the centre as being approximately 2. Here X is the distance from any one face to the centre of the slab. Since erf (α) increases with α, the condition of a semi-infinite solid holds provided $X/(4D_et)^{0.5} > 2$ in a finite slab. Since samples used in tests presented here are rectangular, the finite slab condition is appropriate. In the case of cylinders and spheres, geometrical corrections to this equation are required.

7.2.3 Mobilization of Solid-Phase Constituents

Côté (1986) suggests two different situations which describe the mobilization of solid-phase constituents from the S/S products (leaching step (i) presented above). The first is rapid mobilization, which includes adsorption and desorption reactions and the solubilization of hydroxide species. The second describes slow chemical processes such as the breakdown of the cementitious products.

(i) Rapid or Instantaneous Chemical Reaction

The equilibrium between the solid phase and liquid phase concentrations of species which solubilize rapidly, such as those adsorbed to the solid surface, has been suggested by other authors in the case of S/S products to be represented by a linear equilibrium adsorption isotherm [Batchelor (1990), Côté et al (1987), Côté (1986)]. This allows for a simple analytical solution to the mass balance equation. The equilibrium is of the form:

$$K_d = \frac{C_{im}}{C_{mo}} \tag{7-8}$$

where C_{im} is the immobile or species attached to the solid surface, C_{mo} is the species in solution and K_d is an equilibrium constant. Using the above equation as the reaction term in Equation (7-5), (7-5) becomes:

$$\frac{\partial C_{mo}}{\partial t} = D_e \underset{\sim}{\nabla^2} C_{mo} - \frac{\partial C_{im}}{\partial t}$$

$$= D_e \underset{\sim}{\nabla^2} C_{mo} - K_d \frac{\partial C_{mo}}{\partial t} \tag{7-9}$$

$$= \frac{D_e}{1 + K_d} \underset{\sim}{\nabla^2} C_{mo}$$

where the reaction term has been replaced by the negative rate of change of immobile species or the rate of change of concentration of the mobile species.

This is equivalent to a release process which is controlled by diffusion as described in section 7.2.2, where the effect of mobilization of immobile species is to slow down the diffusion process by a factor of $(1+K_d)$, when a fraction equal to $1/(1+K_d)$ of the initial concentration C_T is mobile [Côté (1986)]. Providing the initial and boundary conditions of section 7.2.2 still hold, equation (7-7) becomes:

$$\frac{M_t}{M_0} = \frac{S}{V}\left(\frac{4D_e}{(1+K_d)\pi}\right)^{0.5} t^{0.5} \qquad (7\text{-}10)$$

In the case of the S/S products in this thesis, surface bound species will be those either physically adsorbed or electrostatically bound to the surfaces of the solid.

(ii) Kinetically Controlled Chemical Reaction

For the purposes of analytical solution of the mass balance equation for the S/S products, a number of researchers have suggested that kinetically controlled chemical reactions can be represented as first order rate processes, where the concentration entering solution is a function of the saturation concentration of the species in solution [Côté (1986), Godbee and Joy (1974)]. If the saturation concentration of a species A is $c_{A,sat}$ then the mobile species is produced at a rate of $k[c_{A,sat}-c_{A,mo}(t,z)]$ and equation (7-5) becomes:

$$\frac{\partial c_A}{\partial t} = D_{AB}\,\underset{\sim}{\nabla^2}\, c_A + k[c_{A,sat} - c_{mo}(t,z)] \qquad (7\text{-}11)$$

Godbee and Joy (1974) present a solution for the above equation for a semi-infinite medium of uniform initial concentration and zero surface concentration (see the discussion in section 7.2.2 above for conditions under which these initial and boundary conditions hold) as:

$$\frac{M_t}{M_0} = \frac{S}{V}(D_e k)^{1/2}\left[\left(t+\frac{1}{2k}\right)\mathrm{erf}(kt)^{1/2} + \left(\frac{t}{\pi k}\right)^{1/2} e^{-kt}\right] \qquad (7\text{-}12)$$

here erf is the error function and $D_e^{'}$ is defined as:

$$D_e^{'} = \frac{D_e}{(1+K_{d,0})^2} \tag{7-13}$$

where $K_{d,0}$ is given by equation (7-8) at t=0.

At small values of kt (small values of k or short time periods) this equation reduces to be of a form similar to the simple diffusion model presented in Equation (7-10). For large values of kt, erf(kt) approaches unity and this equation becomes:

$$\frac{M_t}{M_0} = \frac{S}{V}\left(\frac{D_e k}{(1+K_{d,0})^2}\right)^{1/2}\left(t+\frac{1}{2k}\right) \tag{7-14}$$

According to this model, therefore, if a chemical species is initially present in an immobile form which is slowly converted to a mobile form, a linear relationship between fraction leached and time is observed. The factor of 1/2k is a constant which implies a lag in observed leaching due to the slow mobilization. Based on experimental results, a linear relationship between mobilization and time has been suggested by workers such as Côté et al (1987) and Richardson (1981).

7.2.4 Surface or External Mass Transfer Processes

Two distinct processes potentially occur at the monolith-bulk liquid interface which may be rate limiting in leaching. These are a chemical exchange between the solid and the liquid phase and a transfer of mobile constituents at the solid surface into the bulk solution.

(i) Chemical Exchange between Solid and Liquid Phase at the Solid Surface

The exchange between a surface bound species j(s) and solubilized species j(*l*) is given by:

$$j(s) \underset{k_d}{\overset{k_l}{\rightleftharpoons}} j(l) \tag{7-15}$$

where k_l and k_d are rate constants describing the kinetics of the processes involved in releasing or attaching species j from or onto the surface. Pescatore et al, cited by Côté (1986), suggests that surface processes dominate leaching rather than bulk diffusion at short time periods. Côté (1986) presents the following expression for the fraction of the total of a component leached from a solid where fast surface processes control leaching:

$$\frac{M_t}{M_0} = k(1 - e^{-(k_l + \beta k_d)t}) \tag{7-16}$$

Here the constant β is the ratio of solid surface area to the aqueous solution volume. It can be seen that when the kinetics of the surface chemical exchanges are fast compared to other resistances which may become rate limiting, the exponential term of the above equation can be dropped, leaving a constant term which describes surface washoff.

(ii) Consideration of Film Mass Transfer Resistance

The rate of surface to bulk mass transfer of components which do not undergo a solubilization reaction can be expressed in terms of a mass transfer coefficient K_f:

$$\frac{d\left(M_t / M_0\right)}{dt} = K_f A\left(C^l_{sat} - C^l(t)\right) \tag{7-17}$$

where $C_{sat}^{(l)}$ is the saturation concentration in the liquid at the solid-liquid interface and $C^{(l)}(t)$ is the concentration in the liquid phase at the surface of the monolith at time t. Here A is the exposed surface area of the solid. The rate of release will be a maximum R_0 when the concentration in solution tends towards zero, giving:

$$R_0 = K_f A C^l_{sat} \tag{7-18}$$

Combining the previous equations gives the rate of leaching as:

$$\frac{d\left(M_t/M_0\right)}{dt} = R_0\left(1 - \frac{C^{(l)}(t)}{C_{sat}{}^{(l)}}\right) \tag{7-19}$$

In cases where the liquid volume is infinite, $C_{sat}{}^{(l)} >> C^{(l)}(t)$. Substituting this into the above equation and integrating gives:

$$\frac{M_t}{M_0} = R_0 t \tag{7-20}$$

A linear relationship between the fraction of the component removed and time is thus observed for film mass transfer of components which do not undergo a solubilization reaction.

7.2.5 Semi-Empirical Model which Isolates the Different Processes in Leaching

Côté (1986) and Richardson (1981) suggest that the cumulative amount or fraction of a component leached from a solid may be described mathematically by adding the equations developed thus far in section 7.2. The resulting semi-empirical model, presented in Equation (7-21) below, may be used to determine the most significant resistances to leaching.

$$M_t = k_1(1 - e^{-k_2 t}) + k_3 t^{0.5} + k_4 t \tag{7-21}$$

where M_t is once again the cumulative amount of a contaminant leached at time t. The equation consists of three terms with 4 constants. The first term on the right hand side of the equation represents the case where adsorption/ desorption of metals between the solid surface and the pore solution is rate controlling (Equation 7-16). When the kinetics of the adsorption/desorption surface phenomena are fast compared to the time span of the data being analysed (ie k_2 is large), the first term of the equation can be simplified by dropping the exponential. The remaining term, k_1, is a constant, which represents surface wash-off.

The second term represents diffusion within a porous matrix where k_3 represents the constant term in Equation (7-7). The final term in this equation represents leaching which comes about either as a result of slow mobilizing chemical reactions (Equation (7-14)) or due to

surface mass transfer (Equation (7-20)). After extended time periods, reaction controlled release may become rate limiting [Cote et al (1987)].

In using this equation, cumulative leaching data as a function of time is measured and the model is fitted to this data to obtain the values of k_1 to k_4. The magnitude of the constants obtained indicate the relative significance of the contribution of the resistances provided by the various mechanisms in determining the rate of leaching.

This equation was developed with the following assumptions. Firstly, that leaching takes place in a time-invariant chemical environment. This can be ensured by choosing a leachant renewal schedule such that excessive concentration buildups do not occur. The models describe a single species and do not consider the effect which other species may have on the chemical environment. Secondly, the derivation was once again based on the conditions of semi-infinite solid and zero surface concentration as described in section 7.2.2 above.

7.3 Discussion and Results from Kinetic Tests

Many kinetic tests have been used by other workers to model leaching from S/S products. The following sections of this current thesis investigate the rate controlling steps and kinetics of leaching from the solidified FeCr Dust in a static leachant solution. This information is used to comment on long-term stability and leaching behaviour of the S/S products.

A discussion of three kinetic tests used in this work is presented in this chapter. The tests are:

(i) *Kinetic Agitated Tests* in which a sample of a solid is contacted with a leachant which is agitated throughout the test period. These aim to provide an understanding of the kinetics of- and effect of particle size on- leaching in the TCLP and the EE of Chapter 6.

(ii) *Nonagitated or Static Tests*, in which a solid is contacted with a static solution. These aim to identify the rate controlling mechanisms and the kinetics of leaching.

(iii) *Flow-through* or *Lysimeter Tests* in which a moving liquid is contacted with a static solid. These are used to compare the results of the other static and dynamic leach tests to those

from larger-scale tests and provide more information on the expected long-term release behaviour from the S/S products.

Prior to discussing the kinetic tests and their results thereof, it is of value to provide here a summary of the results from Chapter 6 which will be of value in interpreting those from kinetic tests.

7.4 Summary of Results from Chapter 6

In Chapter 6 it was identified that a certain proportion of each component from the sold is soluble in an distilled water, a further proportion was soluble in acetic acid (that for which release is dependant on pH) and a further proportion was not mobile in any of the test employed in the scope of this work. The proportion of each component which is mobile is the different solutions is detailed in Table 7-1 below.

Table 7-1 - Summary of Results from Chapter 6

Element	% of total in solid which is soluble in distilled water	% of total in solid which is potentially mobile in acid	% of element which is immobile
Cr (III)	-	~4% to 5%	~90% to 95%
Cr(VI)	~1%	1%	-
Zn	-	~50%	~50%
K	~40%	~40%	~60%
Ca	-	~95%	~5%

It is reiterated here that these results are approximates - the mass balance did not close in the SCE and hence no accurate statements can be made. These results are, however, used further in interpretation of the kinetic leach tests of this current chapter, results of which are presented below.

7.5 Kinetic Agitated Tests

In section 7.1 the distinct mechanisms in the leaching process were identified, namely mobilization, intra-particle diffusion, mass transport from the surface into the bulk and movement through the bulk liquid solution. The purpose of agitation is to reduce the resistance to leaching provided by external mass transfer. It is proposed and explored further

here that if the agitation rate is chosen to be sufficiently high, external mass transfer resistances are negligible and can be discounted.

In the TCLP and EE tests of Chapter 6, a solidified material was contacted with a leachate solution for a set period of time and the amount of constituent present in the leachant determined at the end of the leaching period. The aim of the kinetic agitated tests is thus to provide an understanding of the mechanisms and kinetics associated with leaching in the agitated tests of Chapter 6.

Lee et al (1994), Batchelor (1992) and Bishop (1986) use a test in which a crushed sample of a S/S product is agitated in a leachant solution in a fashion similar to that of the TCLP of Chapter 6. Samples of the liquid are taken at various intervals and, based on the composition of the leachates, the kinetics of leaching are described.

For purposes of comparison of these tests with results of Chapter 6, distilled water and 1N acetic acid were once again used as leachates in the current work. Distilled water provides a medium in which no chemical attack on the S/S product occurs, while acetic acid was shown in Chapter 6 to result in breakdown of the solid product by such chemical attack.

The S/S product is crushed using a hammer and is mechanically sieved to obtain material in the size fraction of interest (discussed below). 50g of the material is placed into a 2*l* borosilicate glass bottle with the appropriate leachant with a liquid to solid ratio of 20:1. The bottles are agitated using the device used for the TCLP and samples of the leachate withdrawn at appropriate intervals (see Appendix A4 for details).

Results and the models developed from these tests are once again acknowledged to provide little comparison to conditions expected to be encountered in landfill situations. Such tests are necessary, however, to isolate individual processes in leaching. From this analysis a complete understanding of the leaching process can be developed.

7.5.1 Results of Kinetic Agitated Tests

The analysis of the leaching kinetics is divided into two sections. Firstly, the effect of **agitation rate** on leaching rate is investigated in section 7.5.2 below. A number of distinct mechanisms in the leaching process have been identified, namely mobilization, intra-particle diffusion, transport from the surface to the bulk and movement through the bulk liquid solution. By selecting a sufficiently large agitation rate, the contribution of the resistance provided by transport from the surface into the bulk can also be minimized. Based on this observation it is suggested that some agitation rate should exist above which the first two steps, namely reaction and intra-particle diffusion, are rate controlling. It is the aim here to identify this agitation rate.

Once this agitation rate has been established, the effect of **particle size** on leaching is investigated. The TCLP uses particles of less than 9.5mm with no minimum size. Four different particle size ranges, namely -11.2 + 8mm, -5.7 + 4.6mm, +2.8 -2mm and fines of less than 0.5 mm were tested in this kinetic work. These are standard sieve sizes which were chosen to represent the particles expected to be found in the TCLP, with -11.2 + 8mm as the maximum in the TCLP and fines of less than 0.5 mm to be the minimum. By reducing the particle size, the effect of intra-particle diffusion on leaching is reduced. It was initially suggested that sufficient reduction of particle size results in the resistance provided by intra-particle mass transfer to leaching becoming insignificant, thereby allowing reaction kinetics to be studied. This is explored further below.

Kinetic agitated tests were carried out using two leachants; distilled water to allow the solidified product to determine the pH of the leachate environment and to provide an environment in which chemical attack on the solid was limited (section 7.5.3). The second solution, 1N acetic acid, was used to assess the effect of acid attack on leaching kinetics (section 7.5.4). The latter tests could be compared to the TCLP results of Chapter 6. Results are discussed for pH and Cr and Zn, being the two metals of interest in this study, and Ca to provide an indication of breakdown of the solid cementitious phase.

Agitated tests were carried out on solidified FeCr Dust samples made with 20% cement and 0.9 w/s ratio cured for 250 days. From Chapter 6, this formulation can be regarded as a "fully cured" sample with the cement content being intermediate in the range of practically viable cement additions (see Chapter 3). It is noted that the amount of cement added and w/s ratio will affect both the rate of leaching, and the mechanisms which controlled leaching. This is explored further in the NKLT of section 7.6.

Solidified material was crushed, sieved to the required size range and agitated in a 10:1 liquid volume to solids mass ratio using the TCLP tumbling device. Samples of the leachant were extracted at set time intervals. These samples were filtered through 0.45μm filter paper and analysed for metals content using the AA spectrophotometer. For a full description of the test procedure, see Appendix A4.

7.5.2 Effect of Agitation Rate

The effect of agitation rate on leaching was established for particles of -2.8 +2 mm, being one of the two intermediate size ranges of those size ranges being considered. For these tests, the solidified FeCr Dust was leached in distilled water for five hours in the tumbling device used in the TCLP and EE. Acetic acid was not used in these tests since, as in the case of the TCLP of Chapter 6, rapid particle breakdown was observed in the acidic medium. The isolation of the effect of agitation rate on leaching from that of particle breakdown was thus impossible. In the distilled water leaches, 85% of the particles were still in the initial size fraction. No particle size distribution of the remainder was carried out at the time of testing.

Since these tests were performed in distilled water, the pH of the leachants was once again raised to the pH of the pore solution (≈ 11) by free alkalinity from the solid as discussed in Chapter 6. Due to the high pH, no Zn was found in the leachates. For this reason, only the release of Cr was considered in this analysis. Figure 7-1 presents chromium leaching as a function of time for three different agitation rates. No Cr(III) is expected to be detected in the leachate solutions due to the high pH and all Cr in solution was found by UV spectroscopy to be in the Cr(VI) oxidation state.

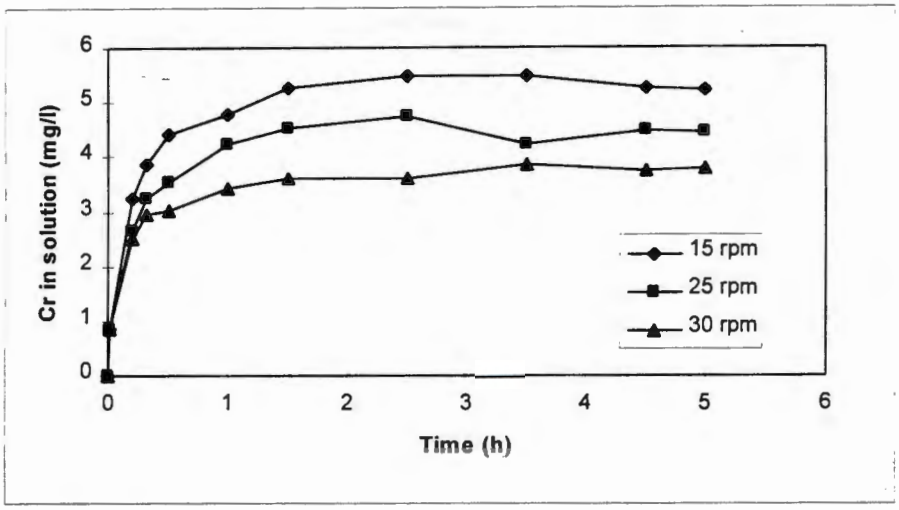

Figure 7-1 - Release of Cr as a Function of Time for Three Different Agitation Rates

(i) Initial Leaching Rate

In Figure 7-1 it is observed that the rate of leaching for approximately the first twenty minutes is independent of the rate of agitation. Cr(VI) has been suggested in Chapter 4 to be contained in the pore solution and bound on the outer, soluble surface of the dust particle. The exposed surfaces of the particles leached in these agitated tests contains a certain amount of surface bound Cr(VI). The dissolution of this Cr upon contact with water is expected to be rapid. Since the size distribution for the three agitation rates is the same, a similar amount of mobile Cr would be contained at the surface of the particles and the Cr would be released into the pores at the same initial rate.

(ii) Further leaching

As the tests progress, the rate of Cr(VI) leaching is observed to decrease as agitation rate increases. This is contrary to expectation - increased agitation was suggested previously to lead to reduced external mass transfer resistances and hence potentially higher rates of leaching.

Parallel work in the Department of Chemical Engineering (1995) focused on the kinetics of liquid-phase reduction of Cr(VI) to Cr(III) using $Fe(SO)_4$. During this work $Fe(SO)_4$ was

added to solution in a stoichiometric ratio to the soluble Cr(VI), and reduction was achieved. As time progressed, however, more Cr(VI) was found in solution. This observation was explained by adsorption of soluble Cr(VI) onto the highly active surfaces of the newly formed hydroxide precipitates, with desorption occurring as Cr(VI) in solution was depleted.

This potential for Cr(VI) to adsorb onto solid surfaces explains observations in the kinetic agitated tests. Although no particle size distribution was carried out on the residual from these tests (85% was in the original size fraction), it is suggested that higher agitation would arise in a greater degree of attrition and hence greater surface area for adsorption of Cr(VI). This would explain the reduced release as agitation rate is increased. Further clarification of details of such a reaction, including reaction kinetics, requires further research.

The results from this study, therefore, did not allow for conclusive statements to be made concerning the effect of surface processes on the rate of leaching and the effect of agitation rate on such resistances. The TCLP and EE procedures of Chapter 6 were performed using an agitation rate of 32 rpm. To allow for a consistency with the agitated tests of Chapter 6, it was decided to continue to use an agitation rate of 32 rpm in the agitated kinetic tests. The work of Drews and Mahote (1994) in the TCLP for similar solids above an agitation rate of 30 rpm suggested that external mass transfer resistances are insignificant. Results presented for agitated tests from this point onwards thus use an agitation rate of 32 rpm.

7.5.3 Leach Profiles - Distilled Water Leachants

In distilled water leaches, dissolution of components from the solid determines the pH of the leaching environment. Furthermore, the sample is not subjected to chemical breakdown which would be expected in the case of an acidic leach.

(i) Particle Disintegration

Particle disintegration was observed to be limited in distilled water leaches - after 15 hours of agitation approximately 85% of the residual solid lay within the original size fractions. The breakdown which was observed is attributed to attrition during tumbling. The particle size

distributions of the remaining material were not determined at the time of testing and hence no further comments are made about this attrition process.

(ii) pH profiles

pH profiles for the distilled water leaches appear along with those for the acid leaches in Figure 7-2. The pH of the leachant solutions were found to reach between 10.5 and 11 after half an hour and be maintained at this level. These pH values are similar to those of the pore solutions (see Chapter 6). Hydroxide species such $Ca(OH)_2$ and KOH from the pores raise the distilled water leachant pH from 7 to a pH equivalent to that of the pore solution of the S/S product (~10.5).

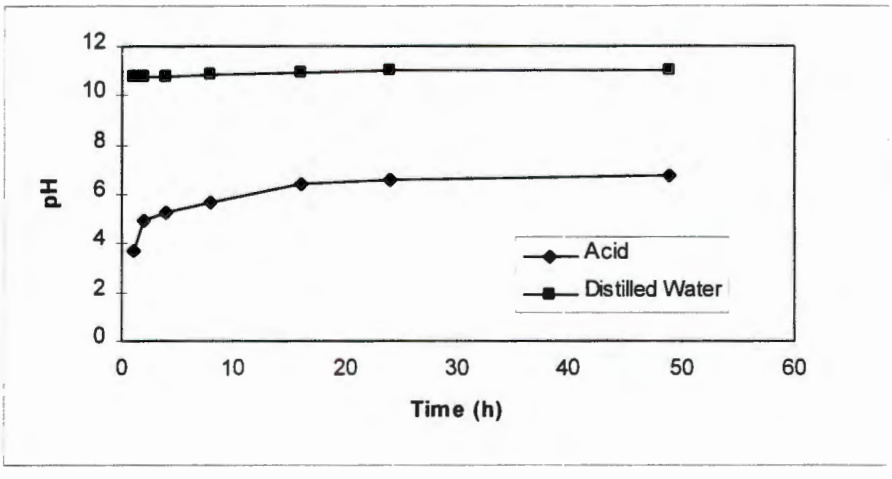

Figure 7-2 - pH profiles for the Distilled Water and Acid Leaches

(iii) Chromium Leaching

Figure 7-3 presents the cumulative fraction of total Cr in the solid leached as a function of time for three different size fractions. As the initial size fraction increases, for small time periods the rate of chromium release decreases. At short time periods, the Cr which is expected to be released is that contained at the surface of the particles. For larger particle size distributions the initially exposed surface area for leaching per unit mass of sample is less

than for smaller particle size distributions and hence the amount of surface bound Cr for leaching during short time periods is also smaller.

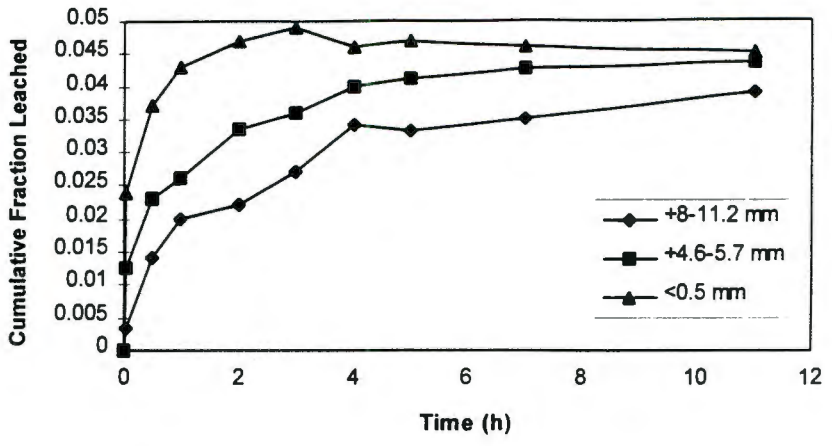

Figure 7-3 - Cumulative Fraction of Cr leached for three different Particle Sizes

Although the tests were carried out only over a period of 11 hours, it can be seen that the amount of Cr leached tends towards an equilibrium value. Furthermore, this equilibrium value appears to be independent of the initial size fraction. In Chapter 6 it was identified that only a certain proportion of the Cr in the solid is mobile in the case of a high pH leach. This Cr is the Cr(VI) contained in the pore solution. As leaching progresses, this mobile Cr is ultimately removed from the solid. This amount will thus be independent of initial particle size fraction.

(iv) Zinc Leaching

No Zn was detected in any of the leachate solutions. At the pH of the leachates, Zn is at minimum solubility (see Chapter 2) and potentially soluble Zn (ie that not contained as a stable complex in the dust particles) will be in the insoluble hydroxide form. This will be removed with the other solids during filtration prior to analysis of solution.

7.5.4 Leach Profiles - Acetic Acid Leachants

In the distilled water leachants, chemical attack on the solids in not observed. The TCLP tests of Chapter 6 showed two effects of an acidic medium on the S/S product. Firstly, the

solubility of a number of metals changes as pH changes. Secondly, acid was shown in Chapter 6 to cause breakdown of the cementitious structure.

(i) Particle Disintegration

Acetic acid was observed to cause rapid breakdown of the solid, and, after five hours, all of the solid particles had broken down to less than 0.1μm. This correlates with observations presented in Chapter 6 and the review presented in Chapter 2 which highlights that acid attacks the cement hydration products causing disintegration of the solid structure. This disintegration was observed to occur rapidly, and leaching profiles for the various constituents were identical for the different particle size distributions. It was decided, therefore, to continue the acid leaches with only an intermediate size fraction. The results which follow are for leaches performed only on the +2.8 -2 mm size fraction.

(ii) pH of the Leachants

Figure 7-2 presents a pH profile of the leachant solution. The original pH of the 1N acetic acid solution is 2.9. The pH shows a rapid initial rise and then continues to increase slowly up to a period of 16 hours, after which the pH reaches an equilibrium value of 6.6. As agglomerate breakdown occurs during the first 5 hours, the release of alkalis both from the pores and the cementitious products results in the rise in pH. Once this gross breakdown has occurred, further breakdown and acid attack on the fine agglomerates and individual dust particles will cause release of alkalis into solution. This explains the continued rise in pH even after gross breakdown has occurred. Eventually, however, the buffering capacity of the S/S product is consumed and the equilibrium pH is reached.

(iii) Chromium Leaching

Figure 7-4 presents a plot of the cumulative concentrations of total chromium and Cr (VI) leached as a function of time over a period of 50 hours. Figure 7-5 expands the time scale of Figure 7-4 to show the first 8 hours of leaching. It can be seen that both total Cr and Cr(VI)

concentrations reach a maximum after a very short time. The total Cr then drops off slightly until it reaches an equilibrium value. Cr(VI) remains at a constant value after 4 hours.

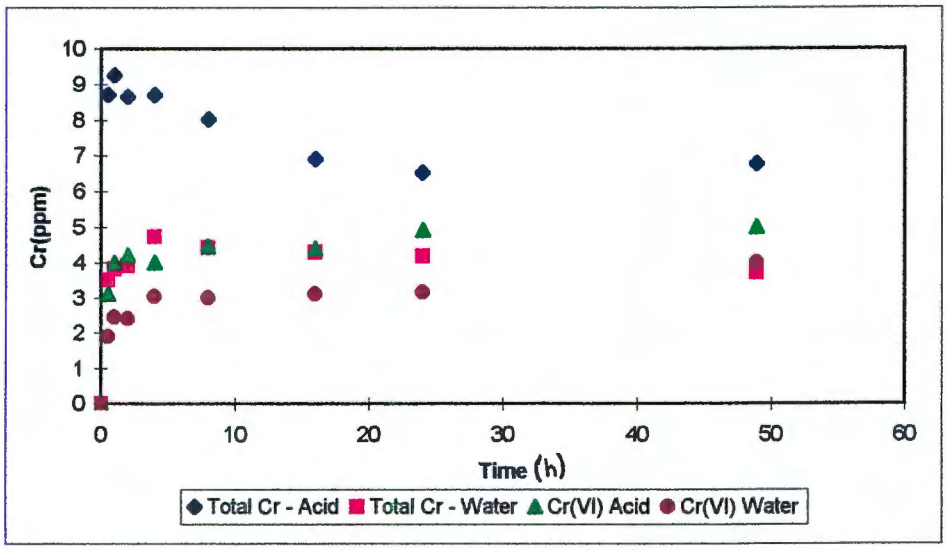

Figure 7-4 -Cumulative concentrations of Total Chromium and Cr (VI) Leached as a Function of time

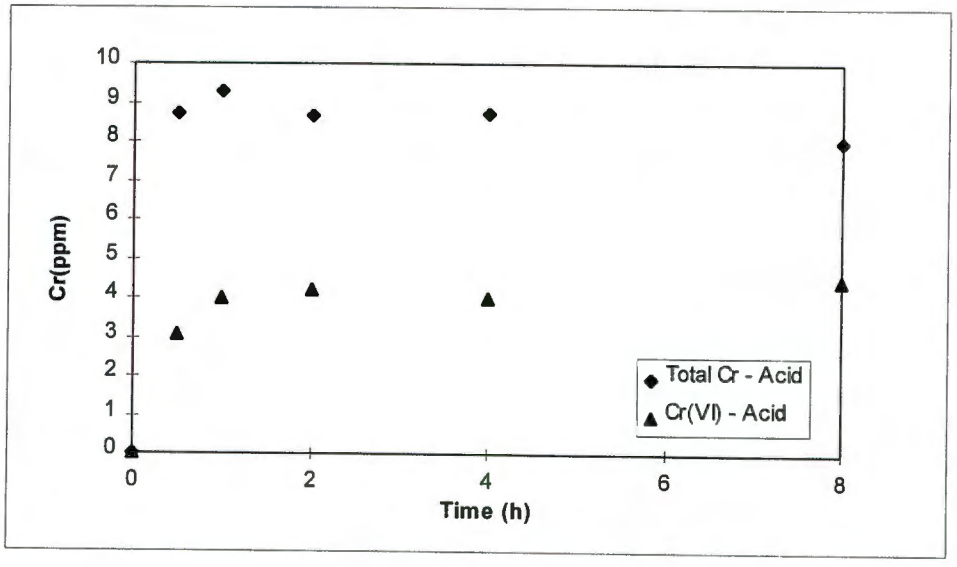

Figure 7-5 -Cumulative concentrations of Total Chromium and Cr (VI) Leached as a Function of time Showing First 8 Hours of Leaching

The initial rapid release is explained as follows. Chromium has been shown previously to be contained as Cr(VI) solubilized in the pore solution (see Chapter 6), as Cr(III) precipitated as a hydroxide in the high pH pore environments or as Cr bound as stable chromite species in the dust core.

Upon contact with the leachant, and as the S/S product breaks down, soluble Cr from the pores will rapidly be released into the leachant solution. Furthermore, at the initial pH of the acid leachants (between 4 and 5.5), insoluble $Cr(OH)_3$ will rapidly solubilize. The release of both of Cr(VI) and Cr(III) is therefore expected to be rapid and explains the initial rapid leaching of Cr.

The drop in total Cr in solution as a function of time is once again understood by the solubility behaviour of Cr(III) as a function of pH - Cr(III) solubility decreases as pH increases. As time progresses pH is observed to increase (see Figure 7-2) and hence Cr(III) concentrations in solution will decrease. Cr(VI) solubility is, however, not a function of pH and hence similar behaviour is not observed for Cr(VI).

(iv) Zinc Leaching

Zinc leaching is presented graphically as a function of time in Figure 7-6. The Zn concentration reaches a maximum almost instantaneously. The results of Chapter 6 suggest that no Zn was found to be solubilized in the pore solution. The Zn in the leachates is suggested to originate from zinc hydroxides (shown in Chapter 6 to be insoluble in the pores of the S/S products) which are now solubilized in the low pH leachate solutions.

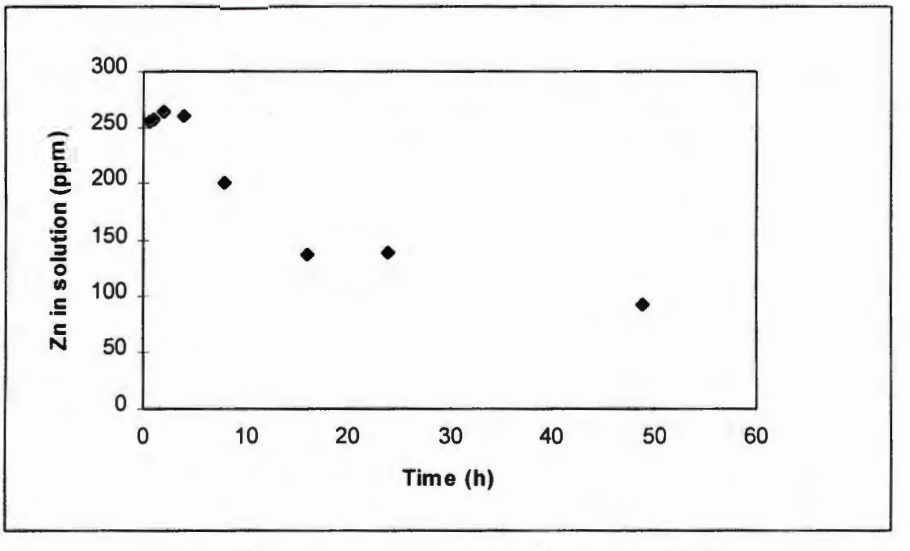

Figure 7-6 - Zn Leaching as a Function of Time

The observation that release is rapid supports the observation by other workers that solubilization of hydroxide species is rapid compared to other kinetic processes in leaching

[Côté (1986)]. As time progresses, the concentration of Zn in solution once again drops. This explanation is similar to that presented for Cr(III) in the previous section.

7.5.5 Summary of Observations from the Agitated Kinetic Tests

(i) An increase in agitation rate results in a decrease in the rate of leaching for Cr in a distilled water leach. This was attributed to a greater surface area for adsorption which is found with increased agitation rate.

(ii) pH of the acetic acid leachant rises rapidly initially and then evens off to an equilibrium value. This is suggested to occur when the buffering capacity of the solid has been consumed.

(iii) The pH of the distilled water solution reaches a value similar to that of the pore solution. Release of alkalinity from the pores is suggested to be responsible for this rise in pH.

(iv) In the acid leach, total Cr in solution rapidly reaches a maximum and then decreases. The drop-off is attributed to pH effects which results in a reduction of solubility of Cr(III).

(v) In the distilled water leaches, Cr leaching is initially more rapid for smaller particle sizes. This was suggested to be due to higher surface area initially exposed to the leachant. The total amount of Cr leached, however, appears ultimately to be independent of initial particle size.

(vi) The mobilization of Zn in the acid leachants is a function of $Zn(OH)_2$ solubility.

(vii) No Zn or Cr(III) is detected in leachants from distilled water leaches due to the high pH.

7.6 Nonagitated or Static Tests

In the tests described in section 7.5 the leachant is agitated to minimize the effect of external mass transfer resistances on leaching rates. In non-agitated tests a crushed or monolithic sample of solidified waste is contacted with a non-agitated leachant solution. The leachant is changed regularly and the concentrations of the contaminants of interest in the leachate solution are determined. The leach profiles can be used to make certain deductions concerning the resistances which determine the leaching process. Long contact periods with any one batch of leachant are preferably used in such tests to obtain representative information since it more closely reveals the situation in practice [Côté (1986)].

The most popular non-agitated test presented in literature is where a cylindrical or cubic monolith of the solid material is suspended in a leachant solution and the leachant is renewed at various intervals [Andres et al (1995), Cheng and Bishop (1990), Côté and Isabel (1984)].

A procedure based on the US EPA's Uniform Leach Procedure (ULP) [US EPA (1980)] and the American Nuclear Society's Dynamic Leach Test (DLT) [Andres et al (1995), Côté et al (1987)] was chosen for study of the kinetics in this current work. The tests differ from each other with respect to the choice of leachant and leachant renewal periods. From results presented previously in this current work, the choice of leachant solution clearly influences the results obtained. The ULP uses demineralized water equilibrated with air. The resultant solution is saturated with respect to oxygen and carbon dioxide and has a pH of between 4 and 5.5. US EPA (1980) states explicitly that this leachant does not attempt to simulate conditions under which wastes are disposed. The ULP's main aim is to provide information for comparative or quality assurance purposes.

The Dynamic Leach Test procedure uses distilled water as the leachant. Again this leachant solution provides no real measure of real-life leaching. It was initially used to provide an indicator of the leachability of radioactive wastes.

In the scope of this current work a ULP/Dynamic Leach-type test, known from this point onwards as the Non-agitated Kinetic Leach Test (NKLT), with two different leachants was used:

(i) *Distilled water*. Based on the results of Chapter 6, it is assumed that with the excess of alkalis associated with the S/S products, distilled water will quickly reach the natural pH of the products. Hence only readily mobile ions will be removed from the pores. Distilled water also causes minimal chemical attack on the solid structure. It is noted that deionized water could have been used in this test, although it was found qualitatively that upon exposure to air the rapid diffusion of a variety of ions from the air into the water occurs, with the resultant water being of similar ionic composition and strength to distilled water. The advantages of using deionized water over distilled water in these tests were thus suggested to be minimal.

(ii) A 1N *acetic acid* solution. The effect of the acidic leachant is two-fold. Firstly, not only will the acid leach soluble elements as in the case of the distilled water leaches, but insoluble metal hydroxides contained in the pore solution can be solubilized at the lower pH values and leach into the bulk solution (see the discussion of pH-solubility relationships in Chapter 2). Secondly, acetic acid was found in Chapter 6 to cause breakdown of the cement hydration products, resulting in both a more permeable product and the potential for release of constituents initially chemically bound within the solid. The specific choice of 1N acetic acid over other acidic solutions as the leaching medium was to bring these results in line with those obtained in the Toxicity Characteristics Leaching Procedure (TCLP) of Chapter 6.

The volume of leachant to surface area of sample commonly used in NKLT-type tests is 10. This was selected as a compromise between having sufficient volume to minimize leachate composition changes and to ensure that solubility limits are not met during the leaching period, while having a small enough volume to produce measurable changes in concentrations of the leached species analysed over this period.

The first step in the ULP/Dynamic Leach Tests quantifies *surface washoff*. This is the removal of soluble salts loosely bound to the external surface of a monolith. Surface washoff is suggested to occur rapidly and the results are generally not included when interpreting the *kinetics* of leaching. The sample is immersed in the leachant to be used for the test for 30 seconds prior to the first leaching interval. The concentrations of the species of interest are determined in this solution. Thereafter the sample is subjected to 10 successive leaching intervals. A full description of the test procedure used in this work, including the leachant renewal intervals, can be found in Appendix A5.

The agitated kinetic test results described leaching from the S/S products based on behaviour of individual particles. Non-agitated tests were undertaken to model leaching kinetics from monolithic S/S products, where no agitation occurs. These tests were carried out according to the procedure presented in Appendix A5 using both distilled water and 1N acetic acid as leachants. A total of 10 leachant renewals is required by the test procedure, the first after 2 hours of leaching and the last after a total of 336 hours leaching.

Three samples of solidified FeCr Dust were chosen for testing. Their compositions are shown in Table 7-2. In Chapter 4 it was found that both cement content and water to solids ratio affect the pore volume and pore size distribution of the S/S product. Comparison of samples made with 20% cement (2 and 3) with those made with 50% cement (1) indicates the effect of cement addition on leaching kinetics. Comparison of samples 2 and 3 show the effect of raising the water to solids ratios on leaching kinetics in the NKLT.

Table 7-2 - Samples used in NKLT-type tests

Sample No.	Cement Content	Water to solids	Curing time
1	50%	1.12	260 days
2	20%	0.99	260 days
3	20%	0.9	260 days

Hereafter these are denoted samples 1, 2 and 3 respectively. All NKLT results presented are an average of two tests.

7.6.1 Literature Reports of Leaching Kinetics

Several researchers [Andres et al (1995), Côté et al (1987), US EPA (1980)] have found diffusion through the solid phase to be the resistance controlling leaching from various S/S products in tests such as the NKLT. Diffusion controlled leaching has been found to be preceded by surface washoff in which soluble constituents near the surface are removed. Such constituents are removed in the 30 second wash-off step described in section 7.6 and in the first one or two leaching intervals in the leaching test [Andres et al (1995)]. Once surface washoff has been accounted for, a linear relationship between the cumulative amount of contaminant leached and the square root of time has been shown for a number of metals contained in solidified matrices. A selection of the results obtained by other workers, as well as values of D_e calculated from the slope of the plots described using equation (7-9) are presented in Table 7-3.

Table 7-3 - Literature Reports of Metals for which Diffusion Controls Leaching Rate and calculated values of D_e for these metals

Metal Species	Type of S/S Binder	Leachant	$D_e(cm^2/s)^{\ddagger}$
Pb[†]	Cement	Distilled Water	$4.7x10^{-13}$
Pb[†]	Cement + Anhydrite	Distilled Water	$6.0x10^{-13}$
Zn[†]	Cement	Distilled Water	$3.7x10^{-15}$
Zn[†]	Cement + Anhydrite	Distilled Water	$5.4x10^{-15}$
Cr[*]	Fly Ash + Cement	Distilled Water	$1x10^{-14}$
Cr[*]	Clay + Cement	Distilled Water	$1x10^{-14}$
Cr*	Soluble silicate + Cement	Distilled Water	$1x10^{-14}$

[‡]The results of Côté (1986) suggest that the variability of calculated values of D_e is as high as one order of magnitude

[†] Andres et al (1995)

[*] Côté et al (1987)

The following comments are offered with reference to the above results. It is seen that, from the results of Andres et al (1995), the addition of anhydrite to cement slightly increases the resistance to leaching (D_e) for both Pb and Zn. With different binders, different pore structures are expected to evolve. D_e is based both on tortuosity and porosity of the product and when these values change, so will D_e. The addition of anhydrite thus results in a more tortuous and/or less porous product. It is noted from the results of Côté et al (1987) that changing the binder does not always have a large effect on D_e - the values of the diffusion coefficient for Cr from three different binders are not significantly different to each other. It is difficult, therefore, to predict from theory the effect of binder on leaching kinetics.

All experiments for which results are presented in Table 7-3 were conducted in distilled water. Based on the results of Chapter 6, which indicated that an acid leachant causes breakdown of the solid structure, it is proposed here that acid leachants would cause a change in the pore structure of the S/S products and result in higher values of D_e. This is explored further in this current chapter for the solidified FeCr Dust products.

Côté et al (1987) apply the equation presented in section 7.2.5 to interpreting leach data from various solidified waste products, in which cement on its own (or in conjunction with other binders) is used as the solidification agent. For all metal species, an initial wash-off term was found at small time periods. This accounts for metal species loosely bound at the exterior surface of the monolith which are released rapidly by desorption or dissolution. Côté et al (1987) further indicate that for Cd, Cr and Pb diffusion is the mechanism controlling leaching. Their tests were, however, carried out for over two years of leaching. Such long-term tests are clearly not practical to carry out on a regular basis and in shorter tests different results may be observed.

Andres et al (1995) found similar results to Côté for the leaching of Pb and Zn which were solidified in Portland cement and Portland cement + anhydrite. For lead and zinc in the first matrix and zinc in the second matrix initial surface washoff followed by diffusion controlled leaching was observed. For lead in Portland cement + anhydrite a delay in leaching followed by diffusion controlled leaching was observed.

7.6.2 Interpretation of Results

The interpretation of results from the NKLT proceeds as follows. Firstly, qualitative observations are presented. Thereafter, the results of the 30 second surface washoff step are discussed. The pH profiles and cumulative amounts of contaminants leached as a function of time for the 10 leaching intervals are presented for Cr, Zn, K and Ca: the first two being the metals of interest in this study, the last two having been found to be significant in determining leachate pH, with Ca indicating the extent of solid breakdown. The parameters of the model presented in section 7.2.5 are determined and the mechanisms of leaching thereby inferred. Finally, rate constants which describe leaching kinetics are calculated.

7.6.3 Qualitative Observations - The Formation of a Leach Front

In material which was leached in distilled water for 336 hours, no distinct 'leach front' was observed. In the case of acid leaching a definite 'leach front' was observed, dividing a leached layer on the outside of the sample from an unleached core. In the leached layer

material had become paste-like and had lost its integral solid structure. Scraping this layer off revealed the solid core, similar in form to the solid which remained after the distilled water leach. It was difficult to measure the distance of penetration of the leach front of the wet material due to its paste-like nature.

Upon drying the monolith in an oven at 60°C to constant mass, the leached layer became brittle and cracked, while the material in the unleached core retained its solid structure. Photograph 7-1 shows the slabs of dried, unleached material and the same material after acid leaching and drying. The cracked outer layer, the leach front and unleached core can be clearly observed. The cracked outer layer was easily brushed off and the distance of penetration of the acid measured. It was found that after 2 weeks of leaching in acetic acid the penetration depth of the leach front into the solid slab was 3.2 ± 0.3 mm. This was after drying and therefore includes shrinkage which occurs during drying.

Photograph 7-1 - Unleached and Leached Solidified FeCr Dust (Both after Drying)

SEM images were taken of the leached layer and unleached core. These are presented in Figure 7-7 and Figure 7-8. The structure of the unleached core (Figure 7-8) is comparable to what was observed for the solidified products prior to leaching, as presented in Chapter 4. Whilst acknowledging the different magnifications in Figure 7-7 and Figure 7-8, the leached section is seen to be more porous than the unleached layer. It is suggested that the cementitious products responsible for the structural strength of the agglomerate are removed from the S/S product by the acid, leaving behind the spherical dust particles. The chemical

removal of the cementitious products observed here is suggested to explain the physical breakdown of the solid which was observed in the TCLP of Chapter 6 and the acidic agitated tests of section 7.5.4.

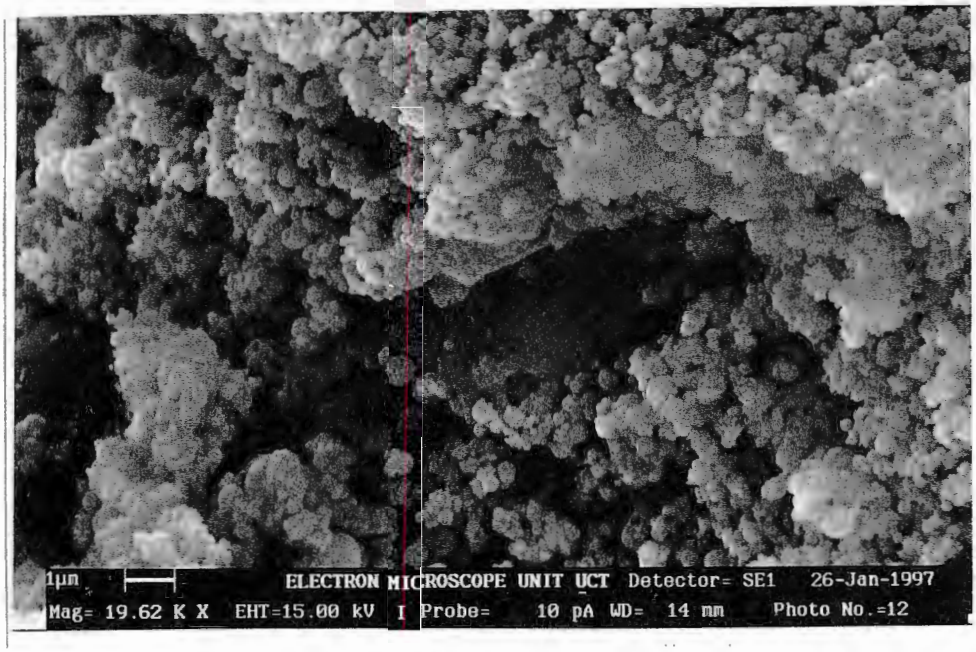

Figure 7-7 - SEM Image of the Leached Layer

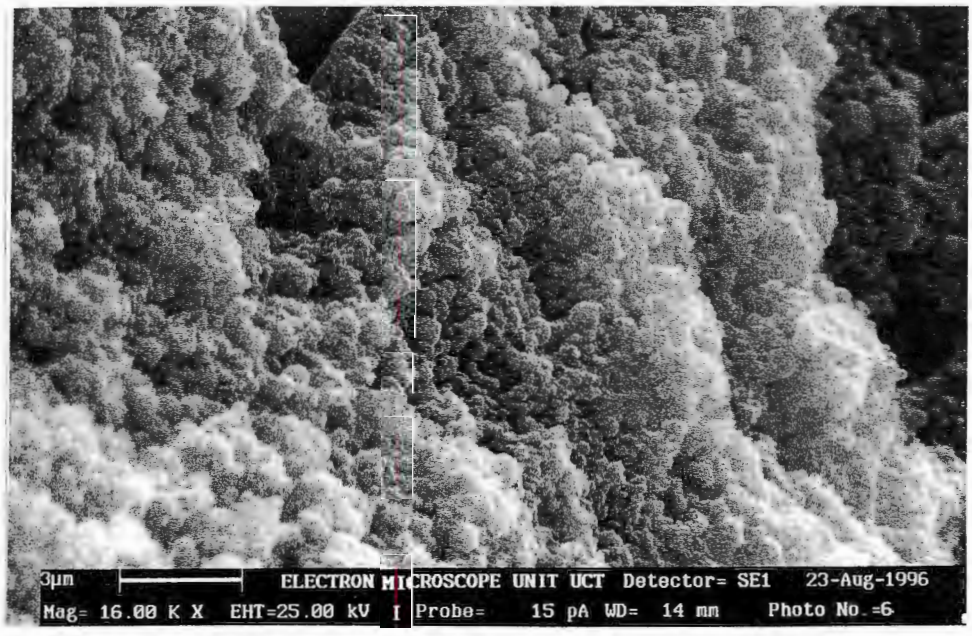

Figure 7-8 - SEM Image of the Unleached Core

7.6.4 Analytical Results from Non-agitated Kinetic Leach Tests

According to the NKLT procedure, the first step of the NKLT is a surface wash-off step, followed by leaching in 10 intervals.

(i) Pre-NKLT Surface Wash-off Step

The NKLT procedure requires a surface wash-off or dissolution step to remove mobile constituents from the surface of the solidified products. A solidified sample is immersed in the leachant solution for 30 seconds, suggested by US EPA (1980) to be sufficient time for the dissolution of such mobile surface constituents. The resulting solution is analysed via Atomic Adsorption Spectroscopy for metals content.

Table 7-4 presents results of the surface washoff step from the solidified products the compositions of which are presented in Table 7-2. The table shows that no Cr is detected in either the distilled water or the acetic acid leachants. From Chapter 6 it would be expected that mobile Cr(VI) contained at the surface of the solidified block would be readily released during the wash-off step. The large volume of leachant, relatively small amount of mobile Cr(VI) in the sample and the short contact period limits the amount of Cr released during the wash-off step. The AA spectrometer used in these analyses can accurately detect concentrations down to 0.1 ppm. Cr in concentrations below this value will not be detected.

The total amount of Zn in the samples is greater than for Cr - the FeCr dust contains a total of 7.14% Zn vs 2.52% Cr on a w/w basis. Furthermore, only a small amount of the Cr is potentially mobile - the Sequential Chemical Extraction of Chapter 6 indicates approximately 95% of the Cr is contained in the stable dust core, compared to approximately half of the zinc in the S/S product being potentially mobile. The large difference in the amount of mobile Cr and Zn in the S/S products explains why a small amount of Zn is detected in the acidic surface wash steps while no Cr is detected.

The acid leachant removes more Ca and Zn than does the distilled water. As discussed in Chapter 2, the hydroxides of these two elements are more soluble in low pH, explaining their higher concentrations in the acidic solutions.

Trace amounts of K are seen in the surface washoff. In Chapter 6 it was found that K is present in high concentrations in the S/S products, and some of the K is readily mobile in

solution. That contained near the surface of the S/S product will be released during the surface wash-off step.

Table 7-4 - Typical Metal Concentrations in the NKLT Surface Wash-off Step of S/S products (all concentrations in ppm, average of two samples)

Leachant	Sample no	pH	Cr	Zn	Ca	K
Distilled	1	8.6	0	0	0.9	0.8
Water	2	8.7	0	0	0.9	0.8
	3	9.7	0	0	0.7	1.1
Acetic Acid	1	3	0	0.7	4.5	1.7
	2	2.9	0	0.7	3.3	1.2
	3	2.9	0	0.8	4.2	5.6

The combination of the short time for which the sample is immersed in the solution and the large liquid to solid ratio does not allow for any other accurate comments to be made about constituents loosely bound at the product surface. These tests were repeated in lower liquid volume to surface area ratios, and for time periods of up to 5 min, but still limited element concentrations were detected. It is thus suggested that, in the case of these S/S products, the surface washoff step of the solidified products prior to conducting the NKLT is superfluous and provides little information with regard to leaching.

Results which are presented in the following sections all relate to the 10 steps in the NKLT which are carried out subsequent to the surface wash step.

(ii) pH of the Leachate Solutions

Figure 7-9 and Figure 7-10 show the pH of the leachate solutions as a function of time for the NKLT performed in the acid and distilled water leachants respectively. The pH of the leachates all lie between 3.7 and 4.1 for the acid tests and between 8.1 and 10.7 for the distilled water tests. For the acid leaches, this is lower than was observed for the TCLP results of Chapter 6 and the acetic acid agitated kinetic tests discussed above (5.3 to 7.3). In the case of distilled water leaching, leachate pH's were once again low compared what is expected from distilled water leaches of Chapter 6 and agitated kinetic tests of section 7.5.1.

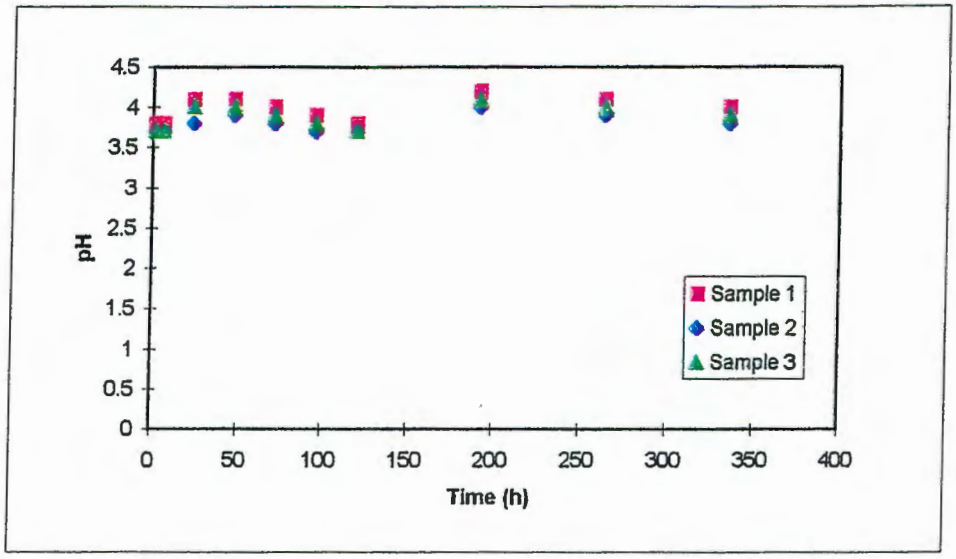

Figure 7-9 - pH - Time Profiles for the Acid Leaches

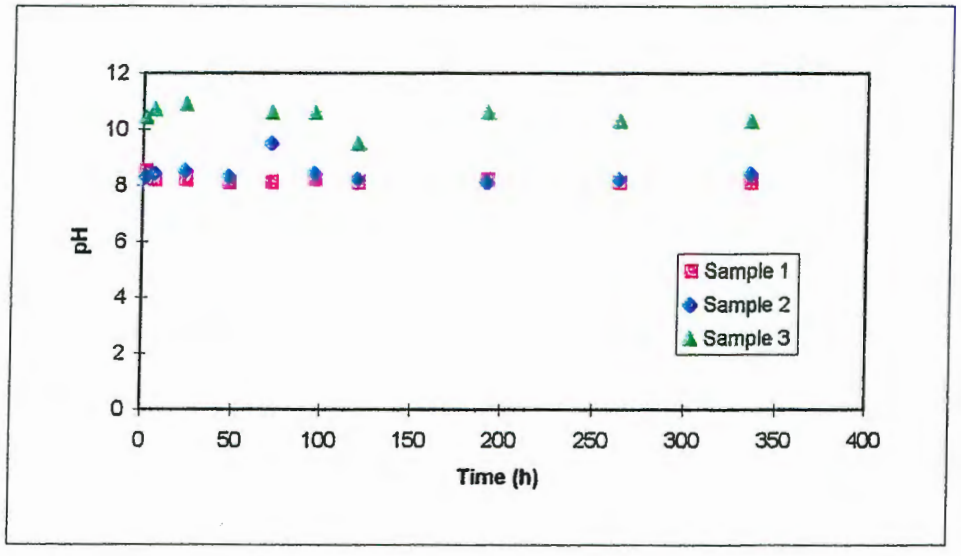

Figure 7-10 - pH - Time Profiles for the Distilled Water Leaches

These observations are explained as follows. The primary factor determining leachate pH was shown in Chapter 6 to be the release of calcium and potassium hydroxide species into solution. Ca contents in TCLP solutions ranged from approximately 1100 to 2200. Those in the individual acidic NKLT leachates were between approximately 90 and 320 ppm. Similarly, K concentrations were 86 to 201 ppm in the TCLP and 14 to 42 in the acidic NKLT. Similar observations may be made by comparing EE results to the distilled water leaches. The lower Ca and K concentrations in the NKLT leachates imply lower release of hydroxide ions and hence lower solution pHs.

Since contact periods were greater in the NKLT than in the agitated tests it would be expected that more Ca and K would be released in the former tests if release were determined by contact time alone. In the agitated tests of Chapter 6 and section 7.5.1, however, crushed material was leached, while in the NKLT a solid slab was leached. It is thus suggested that the smaller exposed surface area in the NKLT limits leaching of Ca and K from the solid over time periods studied here. Leaching of these two components is discussed further in the sections which follow.

(iii) Chromium

Table 7-5 presents the total amount of Cr leached in the NKLT for each of the samples tested.

Table 7-5 - Cumulative Cr Leached in NKLT (mg)

Sample No	Distilled Water	Acetic Acid
1	1.6*	12.6
2	8.7	18.2
3	6.7	18.9

* Cr concentrations in individual leachants were low (0.1 to 0.3 ppm). This value is therefore limited in accuracy

Results are discussed individually for the distilled water and acid leaches.

Distilled Water Leachants

In the distilled water environments the Cr available for leaching is suggested to be that contained in the pore solution. In accordance with the solubility-pH discussions of Chapter 2 and the results of Chapter 6, the solubility of Cr(III) between pH of 6 and 11 is minimal and hence further mobilization will only occur in a higher or lower pH leachate environment. Considering the leachate pHs presented above, no Cr(III) is expected to be mobilized.

UV spectroscopy showed that the majority (>97%) of the Cr in the distilled water leachates to be Cr(VI). The Cr in the pore solution was found to be between 72% and 86% Cr(VI), the rest being Cr(III). At the pH of the pore solution (≈10.5), Cr(III) was not expected based on literature observations. It was, however, observed in Chapter 6 that solubility-pH behaviour

of individual metal species was determined for pure water systems, and the high ionic strengths of the pore solution will affect the solubility. In the NKLT leachate, which has a lower ionic strength than the pore solution, the Cr(III) which was solubilized in the pores will precipitate as $Cr(OH)_3$ and will not be detected by AA analysis.

For sample 1, the high cement sample, Cr concentrations were low in all of the 10 leaching intervals - concentrations ranged between 0.1 and 0.3 ppm. Samples with higher cement addition have lower amounts of potentially mobile Cr(VI) in the pores and hence leach less in the distilled water leach. Due to the error which is expected in the measurement of such low Cr concentrations, no further attempt is made to interpret the results from sample 1 in the distilled water leaches in terms of leaching kinetics.

For samples 2 and 3, the majority of the mobile Cr(VI) found from the pore extrusion results is removed in the 336 hour distilled water NKLT leach. The total amount of Cr leached from sample 2 is greater than sample 3. From the pore solution extracts it was seen that sample 2 contains more mobile Cr(VI) than does sample 3, which explains the greater amount of Cr leached.

The leach profiles are presented for Figure 7-11 for samples 2 and 3. The initial release of Cr is seen to be rapid. As leaching progresses the rate of release of Cr decreases.

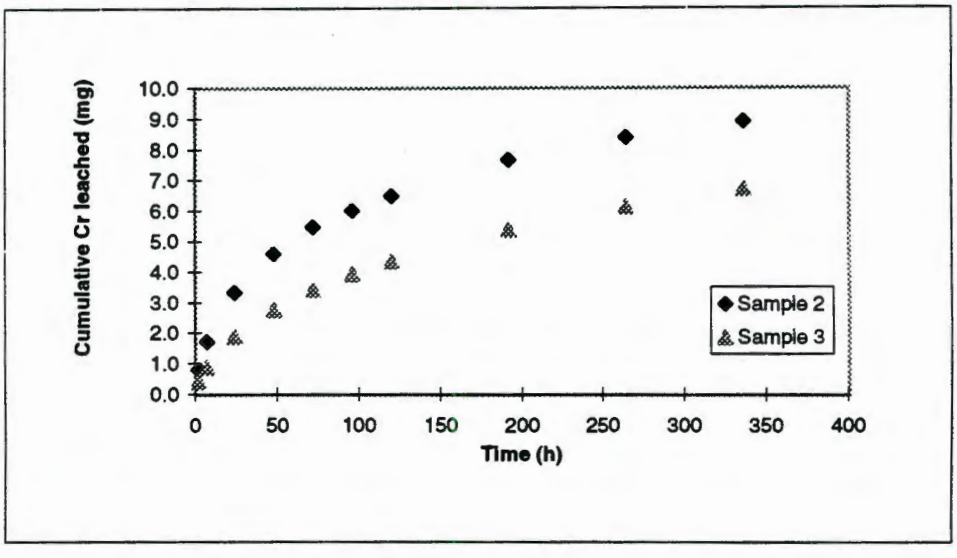

Figure 7-11 - Cumulative Mass of Cr Released as a Function of Time - Distilled Water Leachant

Since a large proportion of the potentially mobile Cr from the S/S products is leached in these tests, the model of Côté (1986) described in section 7.2.5 could not be fitted to the leaching data - this model requires the assumption of a semi-infinite solid to hold.

Diffusion is suggested to be rate limiting in the release of Cr(VI). Since Cr(VI) is already mobile in the pores, reaction cannot be rate limiting. Furthermore, since concentrations in the bulk solutions in each of the ten extractions are low, external mass transfer resistances are also not expected to be significant in determining leaching rate.

Since the semi-infinite solid solution does not hold in this case, it is necessary to turn to analytical solutions such as those presented in Welty et al (1984) for the calculation of diffusion coefficients for Cr in the distilled water leachants. Using graphical solutions as detailed in the above-mentioned text, the following diffusion coefficients were calculated:

Table 7-6 - Calculated Diffusion Coefficients for Cr - Distilled Water Leach

Sample	1	2	3
D_e (cm^2/s)	2E-09	2.4E-09	8.2E-09

These values are discussed further below.

Acid Leachant

Table 7-5 indicates the following. For samples 2 and 3 the amount of Cr ultimately leached is identical. The total amount of Cr leached for sample 1 is lower than for the other two samples - due to the higher cement content, sample 1 contains less total Cr, and hence less mobile Cr.

Figure 7-12 shows the cumulative amount of Cr leached as a function of time. The model presented in Equation (7-21) was fitted to these leaching results using a curve fitting procedure described in Kojovic (1996). Table 7-7 shows the values of the parameters obtained. The curves generated by this model are also shown in Figure 7-12.

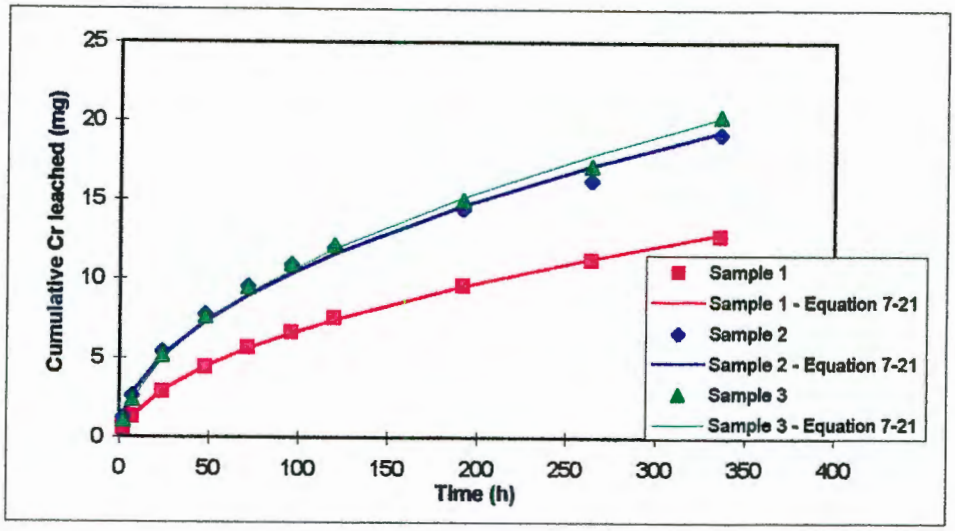

Figure 7-12 - Cumulative mass Cr Leached as a Function of Time - Acid Leaches

Table 7-7- Semi-Empirical Model Parameters for Acid Leach: Cr

Sample No	k_1	k_2	k_3	k_4
1	-0.62	0.64	0.73	0.001
2	-0.02	0.99	1.06	0
3	-0.60	1.07	1.14	0

The constants in this table were calculated with t in hours and cumulative amount leached (M_t) in mg. Table 7-8 shows the relative contributions of the various terms to the cumulative amount of Cr leached for each of the three samples. These values were calculated by substituting the constants in Table 7-7 into Equation (7-21).

Table 7-8 - Contribution of the various terms to Cumulative amount of Cr leached.

	Sample 1				Sample 2				Sample 3			
Time (h)	k_1	$Exp(-k_2t)$	$k_3*t^{1/2}$	k_4*t	k_1	$Exp(-k_2t)$	$k_3*t^{1/2}$	k_4*t	k_1	$Exp(-k_2t)$	$k_3*t^{1/2}$	k_4*t
2	-0.6	0.3	1.0	0.0	-0.02	0.1	1.5	0.0	-0.6	0.1	1.6	0.0
7	-0.6	0.0	1.9	0.0	-0.02	0.0	2.8	0.0	-0.6	0.0	3.0	0.0
24	-0.6	0.0	3.6	0.0	-0.02	0.0	5.2	0.0	-0.6	0.0	5.6	0.0
48	-0.6	0.0	5.0	0.0	-0.02	0.0	7.3	0.0	-0.6	0.0	7.9	0.0
72	-0.6	0.0	6.2	0.0	-0.02	0.0	9.0	0.0	-0.6	0.0	9.7	0.0
96	-0.6	0.0	7.1	0.1	-0.02	0.0	10.4	0.0	-0.6	0.0	11.1	0.0
120	-0.6	0.0	8.0	0.1	-0.02	0.0	11.6	0.0	-0.6	0.0	12.5	0.0
192	-0.6	0.0	10.1	0.1	-0.02	0.0	14.6	0.0	-0.6	0.0	15.8	0.0
264	-0.6	0.0	11.8	0.1	-0.02	0.0	17.2	0.0	-0.6	0.0	18.5	0.0
336	-0.6	0.0	13.3	0.2	-0.02	0.0	19.4	0.0	-0.6	0.0	20.9	0.0

From Table 7-7 and Table 7-8 the following is observed. The exponential term, which represents surface processes rapidly becomes insignificant. The first term of the equation ($k_1*(1-e^{-k2t})$) is thus rate limiting for small values of time and can thus be approximated by the constant k_1 which represents instantaneous surface processes.

A negative value of k_1, which suggests that surface process cause a delay in leaching, is observed. Since diffusion is seen to be the controlling resistance in leaching (see below), there will be a lag before Cr moves from the bulk solid where it is contained into the leachant solution. This lag explains the delay suggested by k_1. The value of k_1 is, however, observed to be small relative to other terms. The first 2 hours of leaching would need to be examined more closely to establish the significance of this delay in leaching. Furthermore, the value of k_1 for sample 2 is higher than for the other samples. No reason could be found for this observation. The observation that the effect of surface processes only dominate at short time periods is in line with those of Andres et al (1995) and Côté (1986).

In Table 7-7 and Table 7-8 it is seen that the k_4, which represents either mobilization reactions or external mass transfer, is ~ zero and thus mobilization reactions are suggested not to play a role in determining leaching kinetics. The diffusion term, represented by $k_3t^{1/2}$, is thus the most significant term in determining the rate of Cr leaching. This is as expected from observations presented in literature (section 7.6.1).

In the acid leachates approximately 50% of the Cr was found by UV spectroscopy to be Cr(VI); the rest is assumed to be Cr(III). In accordance with previous discussions at a pH of 3.7 to 4.1, being those of the acid leaches, Cr(III) is soluble in solution predominantly in the form of $Cr(OH)^{2+}$. The total amount of Cr potentially available for leaching in acidic leachants will thus be the sum of that solubilized in the pore solution, precipitated as $Cr(OH)_3$ within the pore spaces and that adsorbed on to particle surfaces. The pore solution extracts of Chapter 6 identified Cr in the pores to constitute approximately 1% of the total Cr in the sample, while the Sequential Chemical Extraction (SCE) of Chapter 6 indicated the Cr of which mobility is a function of pH to be a further 4% to 5% of the total Cr contained in the sample. In accordance with the results of both the agitated kinetic tests of this current chapter and the characterisations of Chapter 6, the Cr contained in the stable dust core will not be

expected to be mobile in a 1N acetic acid solution. While recognising that the SCE does not provide accurate results, the total Cr mobile in an acidic leachant is suggested to be approximately 5% to 6% of the total Cr in the sample (see also Table 7-1).

Replotting Figure 7-12 as (cumulative Cr leached as a fraction of total *potentially mobile* Cr in the sample) vs square root of time in Figure 7-13 shows the following. For all three samples the plot is linear throughout the leaching period studied here, with a r^2 value of ~ 1.

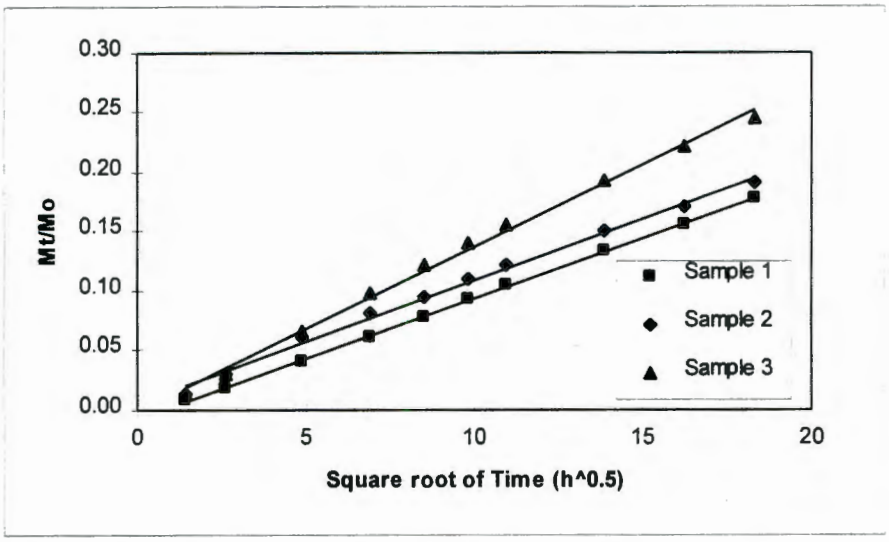

Figure 7-13 – Cumulative Fraction of Cr Leached as a Function of Square Root of Time – Acid Leaches Showing Best Linear Fits to Data

According to equation (7-7) the straight line suggests once again that diffusion is the resistance controlling leaching. Diffusion coefficients calculated from the slope of the plot according to Equation (7-7) are presented in Table 7-9.

Table 7-9 - Values of D_e for Cr from the Acid Leaches

Sample	1	2	3
D_e (cm^2/s)	6.7E-09	7.3E-09	1.3E-08

These values are two orders of magnitude greater than those found by Côté et al (1987) (see section 7.6.1). Two reasons are offered for this observation. Firstly, Côté et al (1987) used cement in combination with fly ash and clay. Furthermore, their samples were made with a low solids containing sludge (~8.2% by weight) with which additive was mixed. In other

words, the primary solid constituent in their samples was cement and pozzolans. Both additives to the product such as fly ash and clay and high cement contents are expected to result in a product with lowered porosities and higher tortuosities than for those presented here, where the cement constitutes 10% to 30% of the solid mass and no additives are used. Porosities are not reported in Côté et al, which is why this explanation is qualitative. According to the preceding discussion, lower porosities and higher tortuosities result in lower values of D_e.

A second observation is that the leachant used in determining the results of Table 7-3 was distilled water, whereas values of D_e in Table 7-9 were determined using acetic acid. As was observed in section 7.6.3, acid causes breakdown of the solid structure, resulting in a layer of increased porosity in which diffusion is faster. This also contributes to the higher observed values of D_e.

The linear regressions do not pass through the origin. This is in line with the results in Table 7-7 which suggest a delay in leaching as discussed.

The initial and boundary conditions used in the development of the diffusion model of section 7.2.2 suggested that the condition of a semi-infinite solid holds provided $X/(4D_et)^{0.5} > 2$ in the case of a finite slab. Using values of D_e presented above for the acid leaches and t=336 hours the condition holds in all three dimensions of the slab leached, with the value of $X/(4D_et)^{0.5}$ being between 7.6 and 10.5 in the shortest dimension of the sample. Hence the condition of 'infinite slab' holds. For the condition of an infinite bath, it is observed that concentrations in the leachates are low. Solubility is not expected to be limiting in the case of these contaminants and hence the condition of infinite bath is suggested to hold.

Diffusion coefficients in distilled water are observed to be slightly lower than those for the acid leaches. Although variabilities in values of D_e have been suggested previously to be as high as one order of magnitude, the following is also suggested. In the acid leaches a leached layer was formed, separated from an unleached core by a leach front (see section 7.6.3). The controlling resistance in the case of the acid leaches is suggested to be diffusion from the leach front through the leached layer to the surface of the solid. In the case of distilled water leaching it was diffusion through the solid (in which no leached layer was formed) to the

surface controls leaching. The solid is more tortuous and less porous than the leached layer. According to Equation (7-6), which says that D_e increases with increased porosity and decreases with increased tortuosity, diffusion coefficients will be greater in the leached layer than in the unleached core.

(iv) Zinc

Distilled Water Leachant

The pH of the leachant solutions for these tests was observed to lie between 8 and 10.6 and, given the solubility constraints discussed previously, the Zn concentrations in the individual leachates were negligible. The leaching of Zn in the distilled water leaches is thus not considered further. In the high pH environments Zn is therefore retained either as the insoluble hydroxide species or else as an immobile species in the original dust core.

Acid Leachant

In acid leachants, where the pH lies between 3.7 and 4.2, the total amount of Zn leached is high compared to Cr; 536 mg, 565 and 610 mg for samples 1, 2 and 3 respectively. At the pH values of the leachants, the solubility of $Zn(OH)_2$ is high. The results of the characterisations of Chapter 6 indicate that approximately half of the Zn is contained as $Zn(OH)_2$ (immobile at high pH) and the remainder is contained in the stable dust core. The latter is not expected to be mobile in the acetic acid leachant solutions during the duration of these tests.

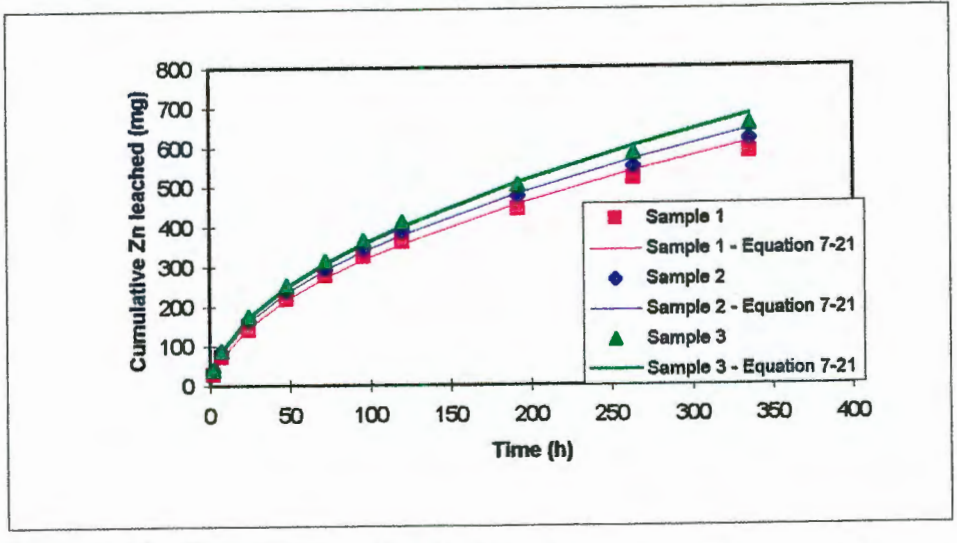

Figure 7-14 - Cumulative Zn Leached as a Function of Time - Acid Leaches

The cumulative mass of Zn leached as a function of time is presented in Figure 7-14. The parameters obtained by fitting the model of Côté from section 7.2.5 are presented in Table 7-10. The curves generated by this model are also shown in Figure 7-14.

Table 7-10 - Coefficients of Semi-Empirical Model: Zn in Acid Leach

Sample	k_1	k_2	k_3	k_4
1	-18.8	19.8	33.9	0
2	-12.4	31.2	35.8	0
3	-13.9	56.6	37.9	0

An analysis similar to that presented in Table 7-8 for Cr is shown in Table 7-11 for Zn.

Table 7-11 - Contribution of the various terms to Cumulative amount of Zn leached.

	Sample 1				Sample 2				Sample 3			
Time (h)	k_1	Exp($-k_2t$)	$k_3*t^{1/2}$	k_4*t	k_1	Exp($-k_2t$)	$k_3*t^{1/2}$	k_4*t	k_1	Exp($-k_2t$)	$k_3*t^{1/2}$	k_4*t
2	-18.8	0	47.9	0	-12.4	0	50.6	0	-13.9	0	53.6	0.1
7	-18.8	0	89.7	0	-12.4	0	94.7	0	-13.9	0	100.3	0.3
24	-18.8	0	166.1	0	-12.4	0	175.4	0	-13.9	0	185.7	1.1
48	-18.8	0	234.9	0	-12.4	0	248.0	0	-13.9	0	262.6	2.2
72	-18.8	0	287.7	0	-12.4	0	303.8	0	-13.9	0	321.6	3.4
96	-18.8	0	332.2	0	-12.4	0	350.8	0	-13.9	0	371.3	4.5
120	-18.8	0	371.4	0	-12.4	0	392.2	0	-13.9	0	415.2	5.6
192	-18.8	0	469.7	0	-12.4	0	496.1	0	-13.9	0	525.2	9.0
264	-18.8	0	550.8	0	-12.4	0	581.7	0	-13.9	0	615.8	12.4
336	-18.8	0	621.4	0	-12.4	0	656.2	0	-13.9	0	694.7	15.7

This Table and the previous indicate once again that a delay or lag in leaching occurs (hence the negative value of k_1) where after diffusion is the resistance controlling leaching. The lag in leaching (k_1) is approximately the same as that for Cr, relative to the total amount leached during the first time period, and is explained as the time required for Zn to move from the bulk solid into the leachant solution. Once again, leaching kinetics during the first two hours needs to be resolved to determine the details of this delay effect. The value of k_2 is large for all three samples, and the term which represents surface reactions (e^{-k2t}) becomes insignificant after very short time periods. Since the Zn is expected to be contained in the pores as the insoluble hydroxide species, these observations confirm the suggestion that solubilization reactions are rapid.

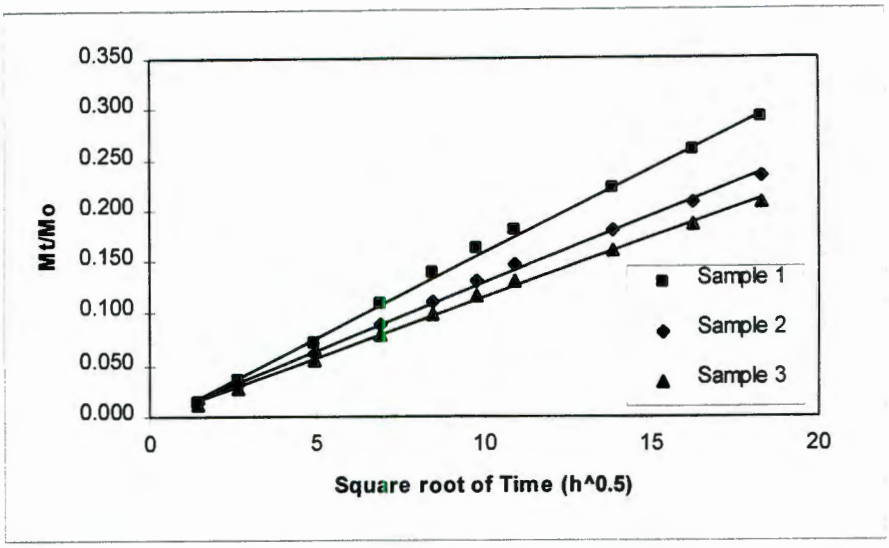

Figure 7-15 - Cumulative Zn Leached as a Function of Square Root of Time - Acid Leach Showing Best Linear Fit to Data

Presenting cumulative fraction Zn leached (based on half the total Zn being mobile) as a function of square root of time shows a straight line relationship (Figure 7-15). This in line with the suggestion of the above model that diffusion is the controlling resistance in the release of Zn (see Equation (7-7)). The values of r^2 for these linear fits are 0.998 for all three plots, confirming a strong linear correlation. The values of D_e calculated from the slopes using Equation (7-7) are presented in Table 7-12.

Table 7-12 - D_e values for Zn Leaching - Acid Leachant

Sample	1	2	3
D_e(cm^2/s)	2.2E-08	1.4E-08	1.1E-08

Since Côté (1986) suggests that the variability in values of D_e determined in tests such as the NKLT is as high as one order of magnitude, it is suggested that the above values of D_e are essentially similar for all three products. As in the case of Cr these results are higher than those of Andres et al (1995) presented in section (iii) above due to the different S/S products and leachants used.

Values of $X/(4D_et)^{1/2}$ are 5.9, 7.4 and 8.4 in the shortest dimension of the sample for samples 1, 2 and 3 respectively. This is well above the required minimum of 2 for the assumption of a semi-infinite solid to hold. Leachate concentrations in the individual leachants are once again

below solubility limits, and thus the approximation of infinite bath is valid. Based on the observation that diffusion through the solid is the resistance controlling leaching, and boundary layer mass transport is insignificant, the assumption of a constant surface concentration equal to the bulk concentration is also valid.

(v) Potassium

The cumulative mass of K leached as a function of time is presented in Figure 7-16 and Figure 7-17 for the distilled water and acid leaches respectively. The parameters obtained by fitting the semi-empirical model which accounts for the various steps of leaching of section 7.2.5 to the K results are presented in Table 7-13.

Table 7-13 - Model Parameters for K Results

	Distilled Water				Acetic Acid			
Sample	k_1	k_2	k_3	k_4	k_1	k_2	k_3	k_4
1	6.8	12.8	6.9	0	29.7	0.4	13.2	0
2	6.8	13.6	7.8	0	36.2	0.1	13.2	0
3	6.9	0.1	6.8	0	32.9	0.1	14.2	0

It is seen that values of k_1 are positive, implying a rapid surface washoff contribution to leaching. In Chapter 6 it was suggested that the S/S products contain a large amount of mobile K, and it is this K released from the surface of the solid blocks which accounts for the observed positive values of k_1. Such behaviour was not observed for the other elements studied as the total amounts thereof which are potentially rapidly mobile are much lower than for K. Contributions of surface release to leaching for other elements are thus negligible.

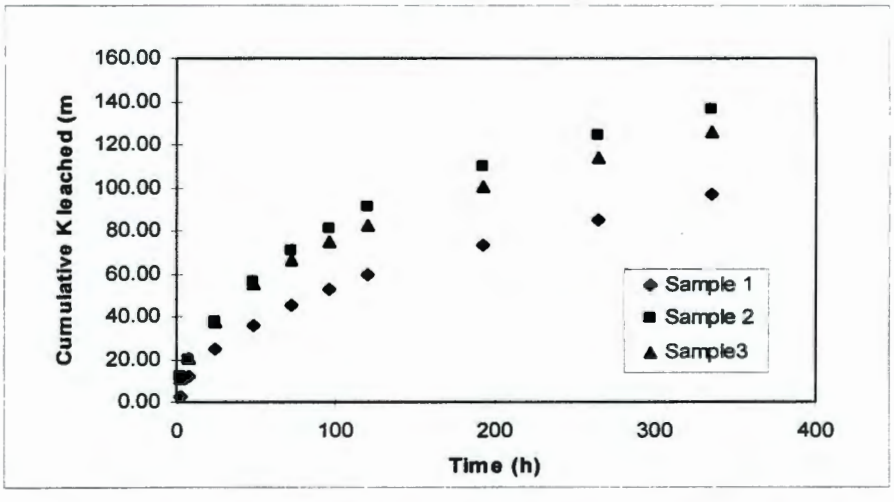

Figure 7-16 - Cumulative K Leached as a Function of Time - Distilled Water

Furthermore, the acid leachants remove more K in surface washoff than the distilled water leaches. This is attributed to rapid acid attack at the surface of the solids.

For both the distilled water and the acid leaches of sample 1 and the distilled water leaches of samples 1 and 2, diffusion is once again seen to be the resistance controlling release of K for time periods of $t>0$. It is observed that the distilled water leach for sample 3 and the acid leaches for samples 2 and 3 have a significant contribution of the exponential term $k_1(1-e^{-k2t})$ for periods of up to approximately 40 hours. This term was suggested in section 7.2.4 to be represent kinetics which are controlled by surface chemical reaction and transfer into the bulk solution. Since a large amount of the K in the solid is expected to be readily mobile, that contained at the surface of the solid will enter the bulk solution during the initial stages of leaching. After a period of 40 hours, and the K bound near the surface has been removed, diffusion is once again seen to be the controlling resistance.

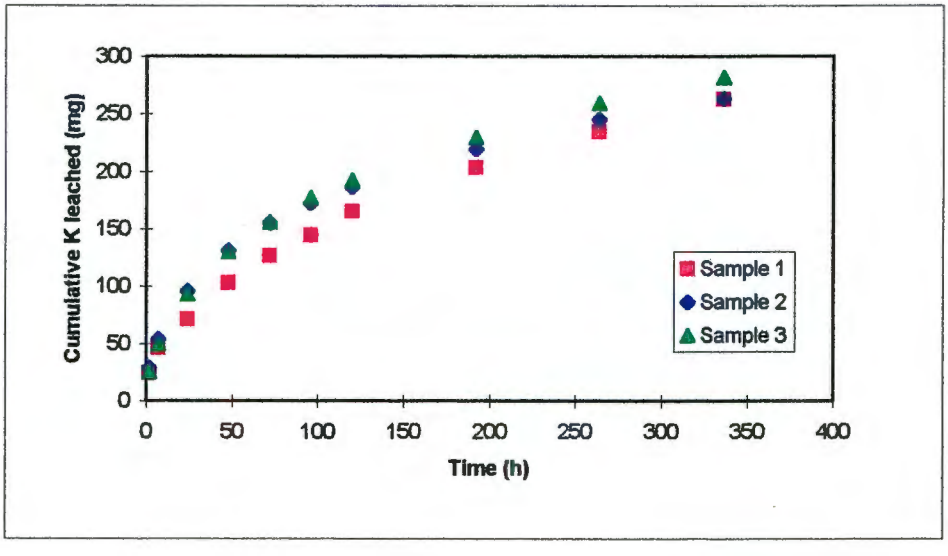

Figure 7-17 - Cumulative K Leached as a Function of Time - Acid Leaches

Of the total K in the S/S products, the SCE of Chapter 6 indicated that approximately 60% is contained in the stable dust core. The other 40% of the K is expected to be mobile. The cumulative fraction of the total *potentially mobile* (ie 40% of the total in the solid) K leached was calculated and plotted as a function of square root of time. For samples where surface processes dominated at earlier times (distilled water for sample 3 and acid leaches for sample 2 and 3), graphs were plotted for periods of more than 40 hours, being that time after which diffusion was suggested to control leaching. Once again the plots were linear, with r^2 values ~

1, suggesting in accordance with Equation (7-7) that diffusion once again controls leaching. Diffusion coefficients, calculated from the slopes of these plots, are presented in Table 7-14.

Table 7-14 - Diffusion Coefficients for K

Sample	1	2	3
D_e(cm^2/s) - Water leach	9.5E-09	5.2E-09	3.9E-09
D_e(cm^2/s) - Acid Leach	5.7E-08	1.2E-08	1.6E-08

Although diffusion was indicated to be the controlling resistance in both distilled water and acid leaches (for some samples after approximately 40 hours), the calculated values of D_e are slightly lower in the former than in the latter. The explanation for this is the same as in the case of Cr. In the acid leaches a leached layer was formed, separated from an unleached core by a leach front (see section 7.6.3). Diffusion from the leach front through the leached layer to the surface of the solid is suggested to be the resistance controlling leaching in the acid leaches. In the case of distilled water leaching diffusion through the solid (in which no leached layer was formed) to the surface controls leaching. The solid is more tortuous and less porous than the leached layer. According to equation (7-6), which says that D_e increases with increased porosity and decreases with increased tortuosity, the diffusion coefficients will be greater in the leached layer than in the unleached core.

Once again the semi-infinite model is seen to hold in the case of K, with $X/(4D_et)^{1/2}$ being between 8.8 and 12.4.

(vi) Calcium

Figure 7-18 and Figure 7-19 present the cumulative amount of calcium leached as a function of time for the distilled water and acid leachants respectively. The coefficients calculated for the model of section 7.2.5 are presented in Table 7-15.

Table 7-15 - Model Coefficients for Ca

	Distilled Water				Acetic Acid			
Sample	k_1	k_2	k_3	k_4	k_1	k_2	k_3	k_4
1	1.0	6	0.1	0.2	-24.4	7.8	122.4	0
2	1.4	0.7	0.8	0.1	-22.6	5.8	83.3	0
3	1.0	1.5	1.7	0.1	-10.2	6.6	87.6	0

The differences in the Ca leaching parameters for distilled water and acetic acid are discussed individually below.

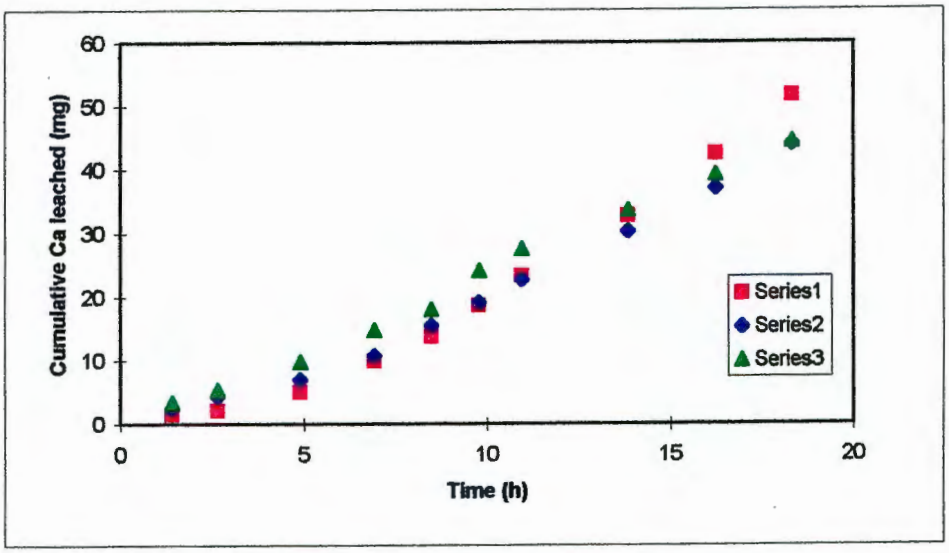

Figure 7-18 - Cumulative Ca Leached as a Function of Time - Distilled Water Leach

Distilled Water Leaches

Table 7-16 presents the contribution of the various terms in Equation (7-21) to leaching as a function of time.

From the table it is observed that, after a rapid initial washoff similar to what was observed for K, both the diffusion and reaction terms contribute to the leaching process. Calcium is expected from literature observations and the results of Chapter 4 to be contained as soluble Ca or insoluble $Ca(OH)_2$ in the pore spaces and as part of the calcium silicate hydrate cement hydration products. The calcium hydroxide which is in the pore spaces is readily mobile: dissolution of insoluble hydroxides has been suggested by Côté (1986) to be rapid compared

to diffusion of the ions through the solid. Diffusion is thus the rate controlling step for leaching for that calcium which is *present in the pore spaces*, either solubilized or as the insoluble hydroxide species.

Table 7-16 - Contribution of various terms to Ca leaching - Distilled Water Leaches

	Sample 1				Sample 2				Sample 3			
Time (h)	k_1	$Exp(-k_2t)$	$k_3*t^{1/2}$	k_4*t	k_1	$Exp(-k_2t)$	$k_3*t^{1/2}$	k_4*t	k_1	$Exp(-k_2t)$	$k_3*t^{1/2}$	k_4*t
2	1.6	0.9	1.9	0.1	1.4	0.2	1.2	0.2	1.0	0	2.3	0.1
7	1.6	0.8	3.6	0.3	1.4	0	2.2	0.6	1.0	0	4.3	0.3
24	1.6	0.4	6.6	1.0	1.4	0	4.1	2.1	1.0	0	7.9	1.1
48	1.6	0.1	9.3	1.9	1.4	0	5.7	4.2	1.0	0	11.2	2.2
72	1.6	0.1	11.4	2.9	1.4	0	7.0	6.3	1.0	0	13.7	3.4
96	1.6	0	13.2	3.9	1.4	0	8.1	8.5	1.0	0	15.9	4.5
120	1.6	0	14.7	4.8	1.4	0	9.1	10.6	1.0	0	17.7	5.6
192	1.6	0	18.7	7.7	1.4	0	11.5	16.9	1.0	0	22.4	9.0
264	1.6	0	21.9	10.6	1.4	0	13.4	23.3	1.0	0	26.3	12.4
336	1.6	0	24.7	13.5	1.4	0	15.2	29.6	1.0	0	29.7	15.7

Ca which is contained in the cementitious products is suggested here to be mobilized more slowly, and for this Ca the slow dissolution of the CSH in water controls the leaching rate. From Table 7-16 it is seen that the contribution of the reaction term to the leaching process becomes more significant in the later time periods (boundary layer mass transfer, which is also included in k_4, is suggested to be insignificant in determining the rate of leaching after short time periods [Levenspiel (1979)]). At longer time periods the calcium hydroxide which was present in the pores has been removed and the Ca which is released from the S/S product is that which is mobilized from the CSH.

The implication of this observation is significant. Even if the S/S product is able to buffer mild acidic solutions with which it comes into contact, and thereby prevent acid attack, slow dissolution of the cementitious products may still occur in water. This ultimately results in physical breakdown of the product and increased release of those metals for which the retention is a function of physical encapsulation. A further study into long-term dissolution in distilled water is thus warranted.

Examples of such plots are presented in Figure 7-21 and Figure 7-22 for a cylinder and a flat slab respectively [US EPA (1980)]. The effect of geometry and the significance of wasteform integrity on leaching is discussed further below and in Chapter 8.

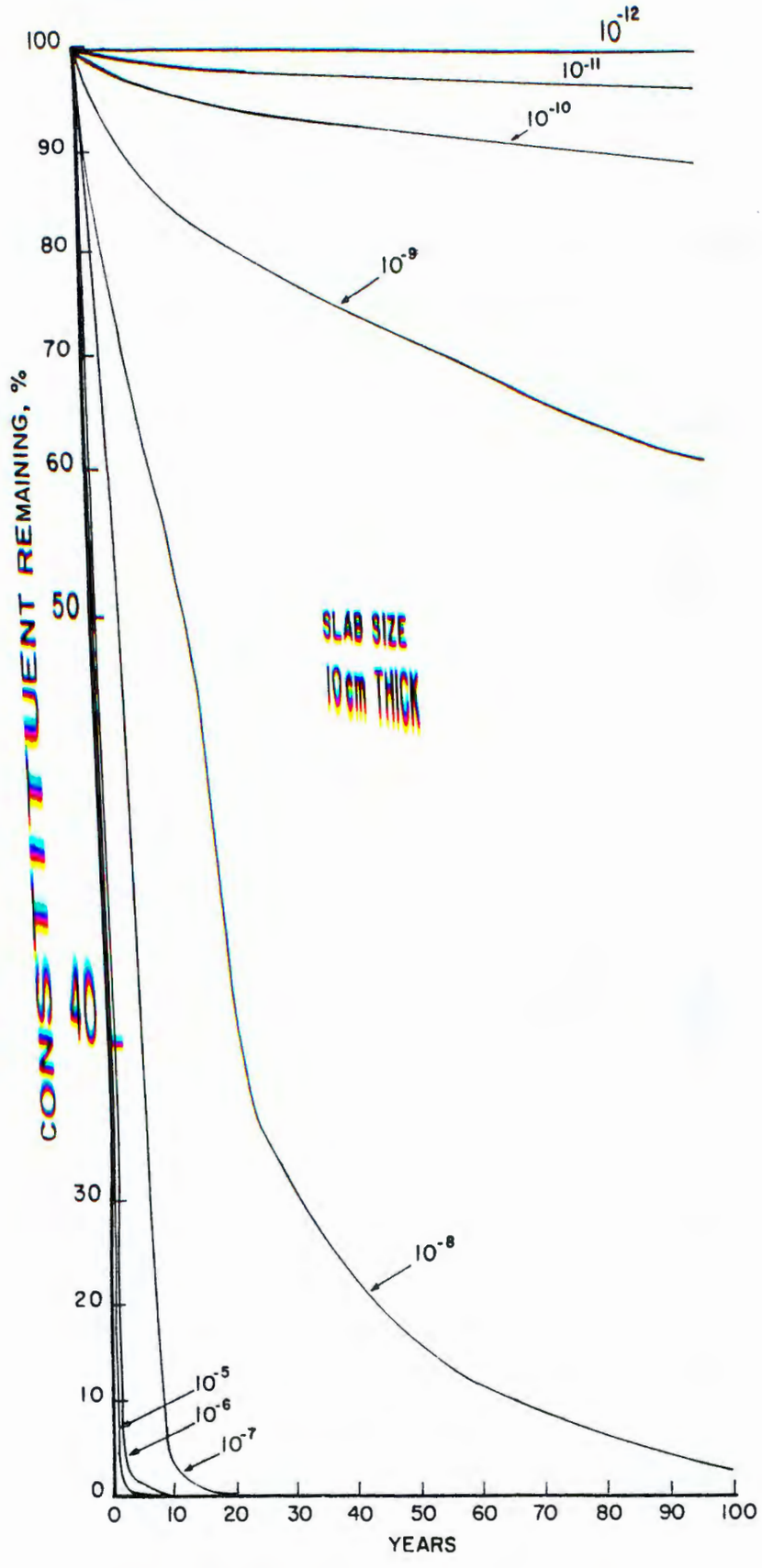

Figure 7-21 - Percent of Constituent Remaining in a Semi-infinite Slab (10 cm Thick) of Solidified Waste for 100 Years of Leaching for wastes having Diffusivities of 10^{-5} to 10^{-11} cm^2/s

to diffusion of the ions through the solid. Diffusion is thus the rate controlling step for leaching for that calcium which is *present in the pore spaces*, either solubilized or as the insoluble hydroxide species.

Table 7-16 - Contribution of various terms to Ca leaching - Distilled Water Leaches

	Sample 1				Sample 2				Sample 3			
Time (h)	k_1	Exp($-k_2t$)	$k_3*t^{1/2}$	k_4*t	k_1	Exp($-k_2t$)	$k_3*t^{1/2}$	k_4*t	k_1	Exp($-k_2t$)	$k_3*t^{1/2}$	k_4*t
2	1.6	0.9	1.9	0.1	1.4	0.2	1.2	0.2	1.0	0	2.3	0.1
7	1.6	0.8	3.6	0.3	1.4	0	2.2	0.6	1.0	0	4.3	0.3
24	1.6	0.4	6.6	1.0	1.4	0	4.1	2.1	1.0	0	7.9	1.1
48	1.6	0.1	9.3	1.9	1.4	0	5.7	4.2	1.0	0	11.2	2.2
72	1.6	0.1	11.4	2.9	1.4	0	7.0	6.3	1.0	0	13.7	3.4
96	1.6	0	13.2	3.9	1.4	0	8.1	8.5	1.0	0	15.9	4.5
120	1.6	0	14.7	4.8	1.4	0	9.1	10.6	1.0	0	17.7	5.6
192	1.6	0	18.7	7.7	1.4	0	11.5	16.9	1.0	0	22.4	9.0
264	1.6	0	21.9	10.6	1.4	0	13.4	23.3	1.0	0	26.3	12.4
336	1.6	0	24.7	13.5	1.4	0	15.2	29.6	1.0	0	29.7	15.7

Ca which is contained in the cementitious products is suggested here to be mobilized more slowly, and for this Ca the slow dissolution of the CSH in water controls the leaching rate. From Table 7-16 it is seen that the contribution of the reaction term to the leaching process becomes more significant in the later time periods (boundary layer mass transfer, which is also included in k_4, is suggested to be insignificant in determining the rate of leaching after short time periods [Levenspiel (1979)]). At longer time periods the calcium hydroxide which was present in the pores has been removed and the Ca which is released from the S/S product is that which is mobilized from the CSH.

The implication of this observation is significant. Even if the S/S product is able to buffer mild acidic solutions with which it comes into contact, and thereby prevent acid attack, slow dissolution of the cementitious products may still occur in water. This ultimately results in physical breakdown of the product and increased release of those metals for which the retention is a function of physical encapsulation. A further study into long-term dissolution in distilled water is thus warranted.

Acid Leaches

In the acid leaches diffusion is once again observed to be the resistance controlling leaching. From the results of Chapter 6 and those of the agitated kinetic tests of section 7.5.1, acidic breakdown of the cement hydration products is rapid. The rate limiting reaction terms observed in the distilled water leaches are thus not seen in the case of acid leaching, and reaction is once again fast compared to the diffusion process.

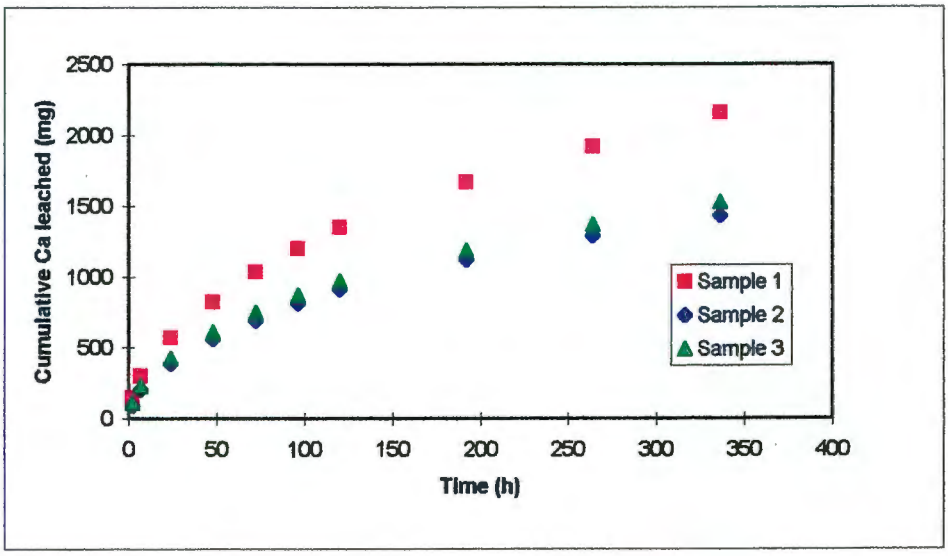

Figure 7-19 - Cumulative Ca Leached as a Function of Time - Acid Leach

In the SCE it was identified that almost all of the Ca in the solid (>92%) is potentially leachable in low pH solutions and hence in the acid NKLT. Taking this figure as the total potentially mobile Ca, the fraction of mobile Ca leached as a function of time was calculated. In Figure 7-20 this fraction is plotted as a function of square root of time. Linear relationships between cumulative fraction of calcium leached and the square root of time are seen for all samples. Thus diffusion is suggested to be the controlling resistance in leaching. Diffusion coefficients calculated from the slopes appear in Table 7-17 below.

Table 7-17 - Diffusion Coefficients for Ca - Acid Leach

Sample	1	2	3
D_e(cm^2/s)	1.5E-08	1.6E-08	2.1E-08

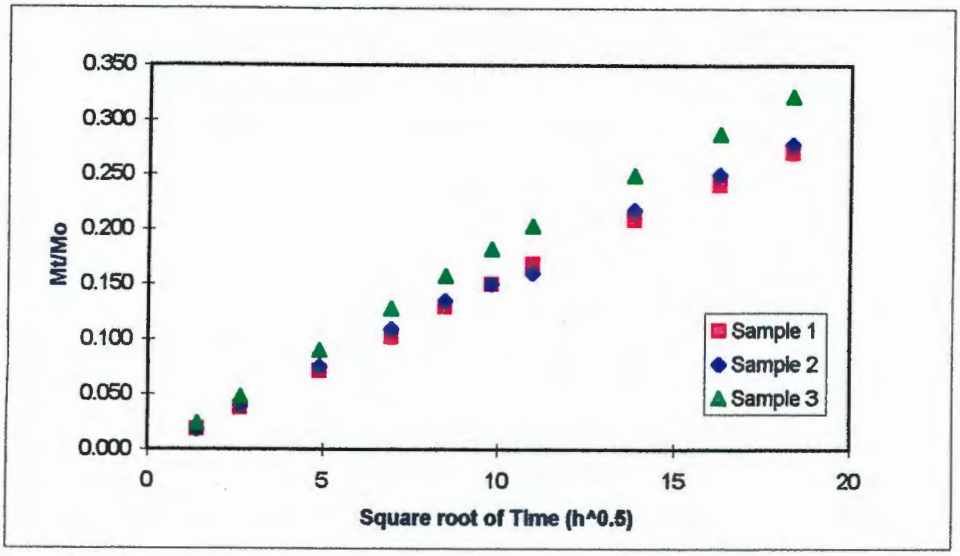

Figure 7-20 - Cumulative Fraction of Ca Leached as a Function of Square Root of Time - Acid Leach

Once again the assumption of semi-infinite solid needs to be assessed to ensure validity of these results. $X/(4D_e t)^2$ are between 5.9 and 7.1 in the shortest dimension of the slab and hence the condition holds.

7.6.5 Closure of the Mass Balance

An attempt was made to close the mass balance between what was left in the solid from the NKLT and what was released into solution. The fusion process which was used to determine solid compositions uses only 0.5 g of material. Given this amount of material and the low concentrations of elements in the leachates results were not found to be accurate enough for closure of the mass balance.

7.6.6 Use of Leaching Data for Long-Term Predictions

The following comments surrounding the use of leaching data for long-term predictions are offered based on literature observations. For situations where diffusion into a dilute solution is the principal transport mechanism out of the solid, Anders et al (1978) present the development of numerical models which describe the percentage of a contaminant remaining in a solid as a function of time and the effective diffusion coefficient. These equations can be used to develop the graphs which describe the amount of a constituent retained in the solid.

Examples of such plots are presented in Figure 7-21 and Figure 7-22 for a cylinder and a flat slab respectively [US EPA (1980)]. The effect of geometry and the significance of wasteform integrity on leaching is discussed further below and in Chapter 8.

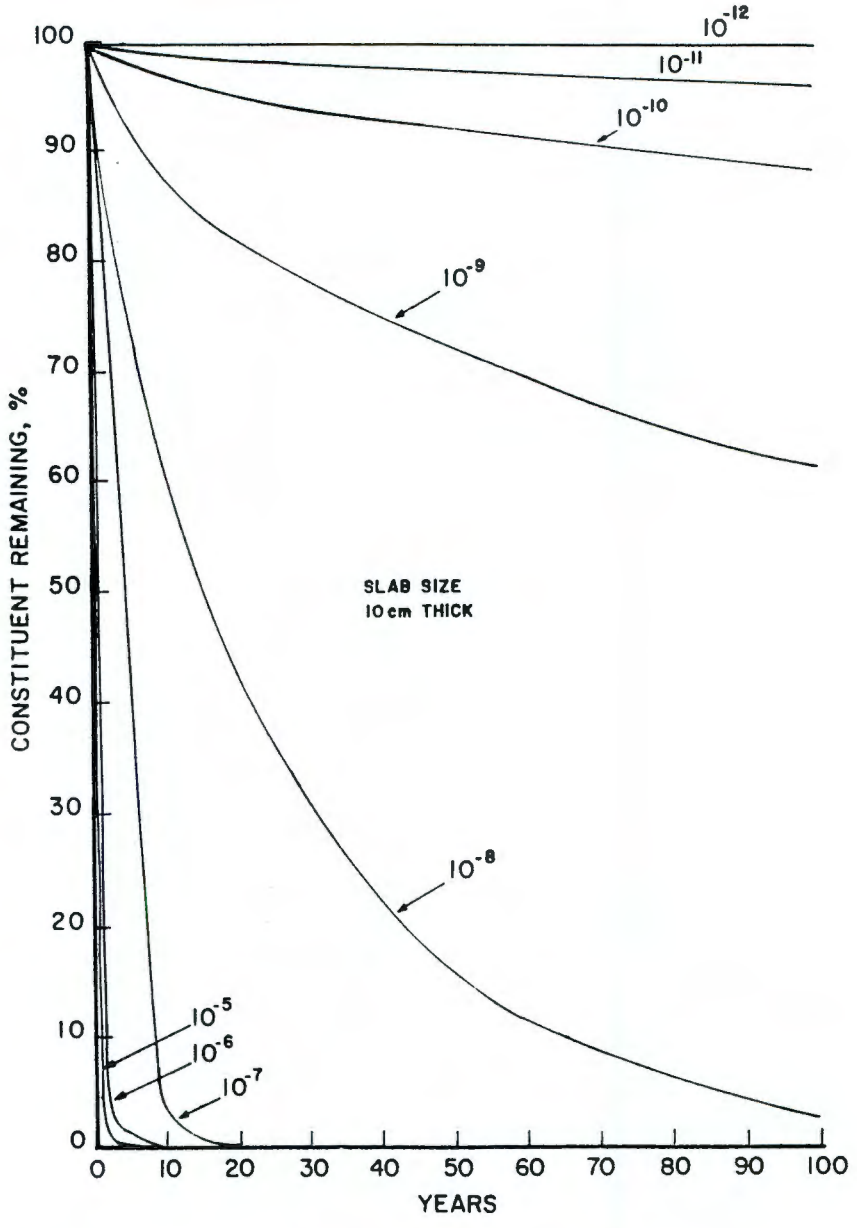

Figure 7-21 - Percent of Constituent Remaining in a Semi-infinite Slab (10 cm Thick) of Solidified Waste for 100 Years of Leaching for wastes having Diffusivities of 10^{-5} to 10^{-11} cm^2/s

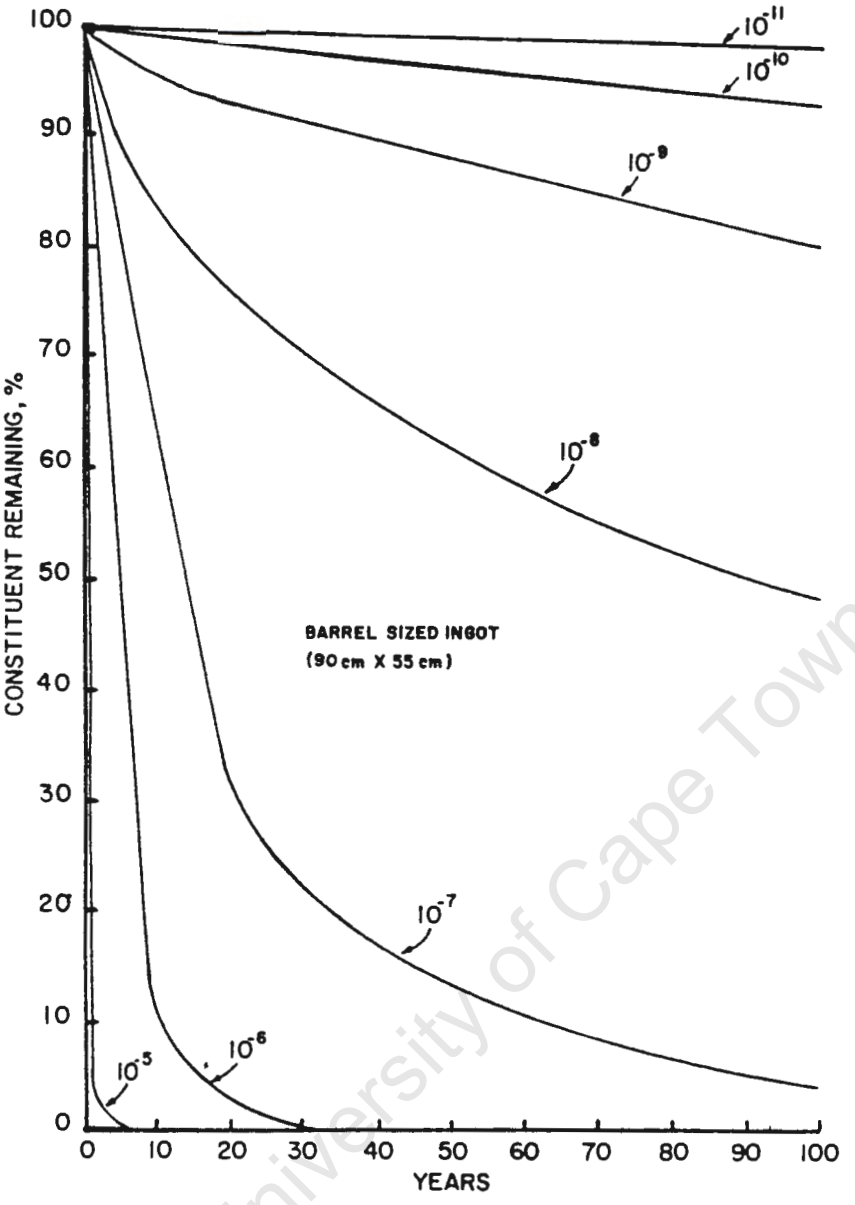

Figure 7-22 - Percent of Constituent Remaining in Barrel Sized, Cylindrical Ingots (90 cm long x 55 cm Diameter) of Solidified Waste for 100 Years of Leaching for wastes having Diffusivities of 10^{-5} to 10^{-11} cm^2/s

Based on the D_e results presented previously in this work, the percentages of the potentially mobile contaminants remaining in the solid after 100 years as predicted by Figure 7-21 and Figure 7-22 are presented in Table 7-18. Since calculated values of D_e were based on that fraction of each element which is predicted to be potentially mobile, and not the total

concentration of an element in the solid, the numbers presented in Table 7-18 refer to the percentage of *mobile* constituents remaining in the solid.

Table 7-18 - Values of D_e and Approximate Percentages of Potentially Mobile Contaminants Remaining after 100 years, as predicted by Figure 7-21 and Figure 7-22

Element	Range of D_e values observed (cm^2/s)	From Figure 7-21	From Figure 7-22
Cr (acid leach)	1.6E-08 to 6.7E-09	50% to 65%	3% to 63%
Zn (acid leach)	1.1E-08 to 2.2E-08	50%	3%

From this table it is seen that the geometry of the waste form makes a large difference to the percentage of constituent removed from a solid when diffusion is the resistance controlling leaching, and that larger samples will have lower rates of release than smaller samples. This reiterates the importance of the maintenance of the physical integrity of the product which was discussed in Chapter 5. If large monoliths are cast in landfill sites, and minimal decripitation occurs, retention levels of mobile constituents will be high. Should breakdown occur, however, release rates will increase.

The predictions presented in Figure 7-21 and Figure 7-22 are thus optimistic. These relationships are based on the assumption that diffusion is the sole release mechanism. A complex model which takes into account chemical and physical breakdown would be worthwhile developing and is one of the avenues for further research in this field.

7.6.7 Summary of the NKLT Results

In the distilled water leaches no distinct leach front was observed. In the acid leaches, however, a leached layer was formed in which material had become paste-like. This was suggested to be due to the removal of the cement hydration products.

The results for the various elements in the two leachants are summarized in Table 7-19 overleaf.

Table 7-19 - Summary of Results from the NKLT

Element	Leachant Solution	Resistance Controlling Leaching	Summary of the Leach Test Observations	Calculated Values of D_e (cm^2/s)
Cr	Distilled Water	Diffusion	The results suggest that Cr(VI) is contained as a mobile species in the pores. This Cr(VI) moves from the pores into the solution via diffusion. A large proportion of the *mobile* Cr(VI) is removed for samples 2 and 3.	2E-09 to 8.2E-09
	Acetic Acid	Diffusion	Cr(VI) and Cr(III) are released in these tests by diffusion. Thus both of these species are readily mobile, and are contained in the pores, either in the soluble or insoluble form. Cr from the core of the dust is not released here. Delay is observed which is attributed to the time required for Cr to begin to move from the solid where it is contained into the bulk solution	6.7E-09 to 1.3E-08 Higher than for water leach since diffusion through leached layer.
Zn	Distilled Water		Once again the immobile Zn hydroxides are not released in high pH distilled water solutions.	
	Acetic Acid	Diffusion	$Zn(OH)_2$ species, insoluble in the high pH pore solutions, are readily released by diffusion in an acid. Stable Zn from the dust core is not released. Initial delay in leaching observed for the same reasons as for Cr.	1.1E-08 to 2.2E-08. Similar magnitude to Cr, indicating size effects do not play a big role in diffusion.
K	Distilled Water	Diffusion	Mobile and immobile K are found in the product. In sample 3 surface mobilization dominates for up to 40 hours. A large amount of mobile K is contained at the surface which is removed during the first hours of leaching. After surface washoff, diffusion controls leaching.	3.9E-09 to 9.5E-09
	Acetic Acid	Diffusion	For samples 2 and 3 surface mobilization dominates for up to 40 hours. Thereafter diffusion controls leaching	1.2E-08 to 5.7E-08. Higher than for water leach since diffusion through leached layer.
Ca	Distilled Water	Reaction and Diffusion	Ca is contained both in the pores and as part of the cement hydration products. Slow dissolution of Ca from the cement hydration products is observed, indicating reaction controls rate of leaching, while diffusion controls leaching of $Ca(OH_2)$ from the pores.	
	Acetic Acid	Diffusion	In acid the dissolution reaction is fast compared to diffusion. Almost all of the Ca is potentially removable in acid, release of which is controlled by diffusion	1.5E-08 to 2.1E-08. Similar magnitude to Cr, K and Zn results

7.7 Lysimeter Test Results

Both the agitated kinetic tests and the NKLT are limited in their potential to predict leaching behaviour of the S/S products in large-scale application. They provide a microscopic or small scale view of the leaching process. In order to provide a macroscopic picture of leaching as it would occur in landfill, and determine how this relates to the observed small scale tests, use is made of flow-through tests. A porous or crushed solid is packed into an open container and the leachant is passed through it either continuously or intermittently. The contaminant removal takes place through advection (removal in the flowing bulk liquid phase). Tests are done in either columns (upflow or downflow) or in lysimeters (downflow).

This current work uses a lysimeter test to simulate a larger scale leaching environment. The lysimeter used consists of a glass column of diameter 225mm into which 7.05 kg of solidified FeCr Dust, crushed to less than 9.5 mm as in the TCLP standard, was packed to a height of 198 mm (see Photograph 7-2). Although the crushing is not strictly representative of a monolithic mass consigned to a landfill, it represents a worst case scenario in which material disintegrates once placed in the landfill site. An attempt was made to cast a monolith in one of the glass columns for comparison to the results observed for the crushed material. Shrinking during curing, and decrepitation and dehydration upon exposure to air, prevented a self-supporting monolith from being cast and sealed effectively in the column. After several unsuccessful attempts this idea was abandoned.

To simulate effectively the situation expected in landfill, the ratio of particle sizes in the column to the column diameter should be sufficiently small that wall effects do not come into play and that the column represents, essentially, finite sized particles in an infinite medium. Since the particles are two orders of magnitude smaller than the column diameter (the particle diameter to column diameter ratio is less than 0.04), it is suggested that the dimensions of the system are appropriate to represent finite particles in an infinite medium, and that wall effects do not come into play in this experimental configuration.

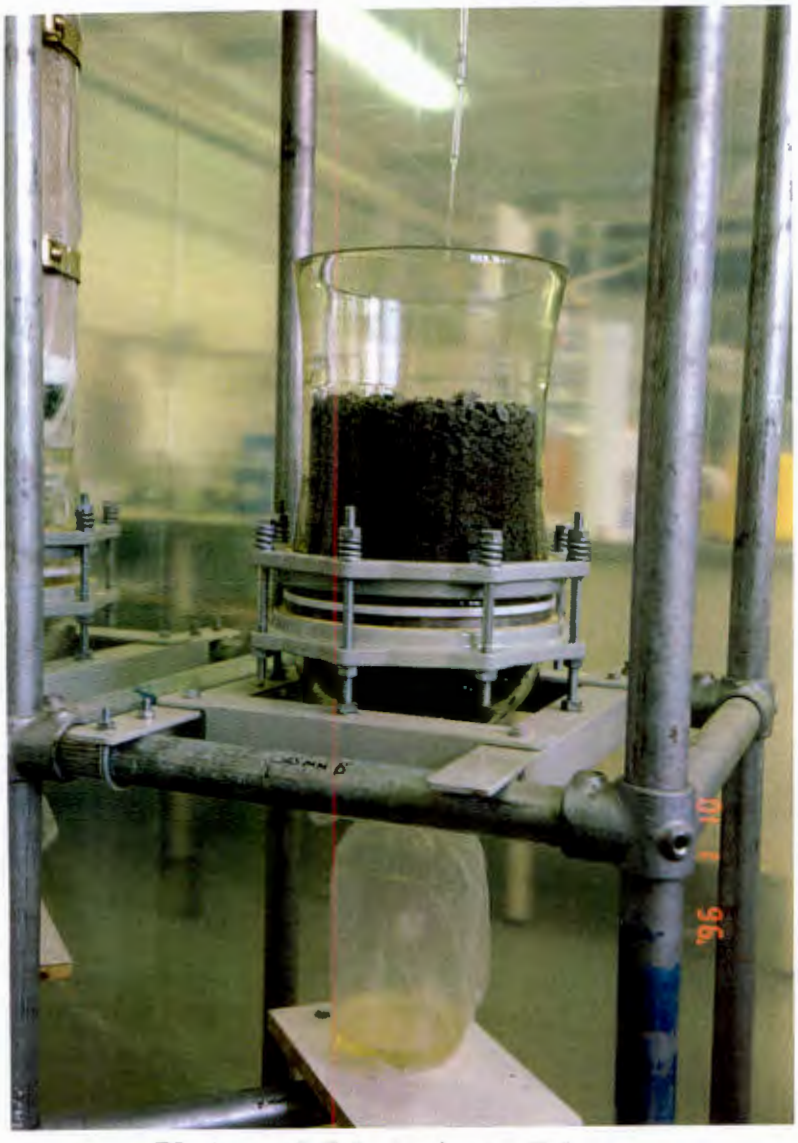

Photograph 7-2 - Lysimeter Column

A leachant solution was sprinkled over the surface of the bed of material for 4 x 2 hour periods each day at a rate of approximately 230 ml of leachant per day. The leachate was collected at the base of the column. Samples were taken on a regular basis for 160 days and contaminants of interest in the leachate determined.

The solution used as leachant in the lysimeter tests approximates the composition of local rainfall. It was made by adding a mixture of concentrated nitric acid (HNO_3) and sulphuric acid (H_2SO_4) in a 1:1.45 molar ratio to well aerated distilled water until the solution had a pH of 4. This "simulated rain" is indicative of natural rainfall in areas where acidic deposition is likely, although further saturation of acid rainfall with CO_2 would be expected in reality. In the long term, this CO_2 will react with Ca from the S/S product to form $CaCO_3$. Since $CaCO_3$ is

insoluble, this may suggest the potential for long-term 'self-healing' of S/S products, which may have begun to decrepitate as a function of time, through the formation of $CaCO_3$.

In the lysimeter tests, S/S product was packed into a column, and a leachant solution allowed to percolate through the column. These tests were the final kinetic tests to be performed in this work, aimed at simulating leaching within the landfill itself. Details of the experimental procedure for the lysimeter work are presented in Appendix A6. The tests were run for a period of 160 days after which no change in release behaviour was observed (see the results which follow) and the test was terminated. The full set of data appears in Appendix D4.

7.7.1 pH

The pH of all of the solutions lie between 11.1 and 12.0 (see Figure 7-23). This is in a similar range to pH values of the pore solutions. The maintenance of a high pH provides an indication of the buffering capacity of the S/S product. The leachant solution is a mild acid of pH of approximately 4. During the course of this work the importance of pH and the buffering capacity of the S/S product on leaching has become clear. In a landfill situation, providing the product can continue to buffer mild acid solutions (such as acid rain passing through it), metals retained owing to their decreased solubility will be held in the solid.

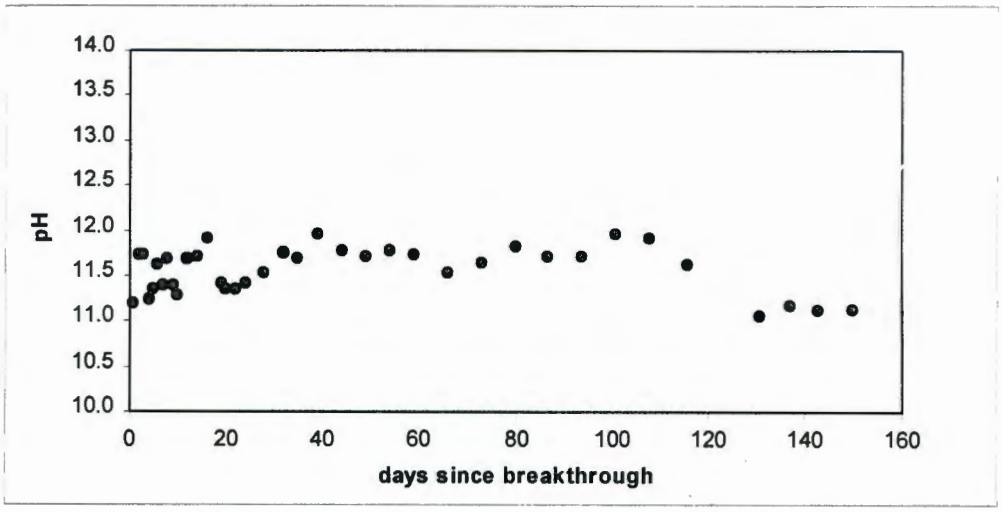

Figure 7-23 - pH Profile from the Lysimeter Column

Ultimately, if all of the buffering capacity of the S/S product is exhausted, the pH of the environment will drop and metals such as Cr(III) and Zn(II) have the potential to be

mobilized and removed from the solid. Due to random errors in results obtained from the pH probe at the time of testing, the apparent drop in pH of 0.5 units after 120 days is suggested to be a consequence of inherent variability in the pH-measuring device.

7.7.2 Chromium

Cr release from the lysimeter column as a function of time is presented in Figure 7-24. Chromium shows an initial high release followed by a drop-off and further low release rates. All the Cr detected is Cr(VI). At the pH of the leachates, Cr(III) solubility is below detection limits. As in previously presented leaching results, Cr(III) is expected to be retained in the solids as the insoluble hydroxide species.

The initial release of Cr is high. In the columns crushed samples are used and, in accordance with the discussions presented previously in this chapter, crushing increases the exposed surface area and leads to a high initial surface washoff of soluble Cr(VI). After the high initial washoff, further release of Cr continued throughout the leaching period. The equilibrium release level was reached after a period of approximately 50 days.

A qualitative attempt was made to see whether the results of the NKLT could be used in the modelling of the column results. In the NKLT it was suggested that, after initial washoff, diffusion controls the rate of leaching for Cr in distilled water.

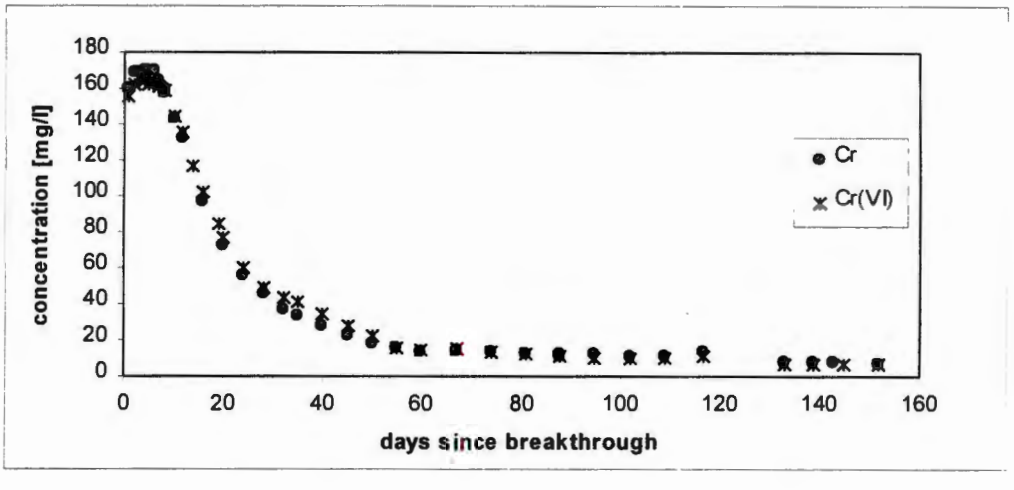

Figure 7-24 – Total Cr and Cr(VI) released from the Column as a Function of Time

The daily amount of liquid sprinkled over the column (diameter 225 mm, height 198 mm) is 230 ml. A liquid hold-up of 5 days is observed - being the time required for the first liquid to be collected at the bottom of the column. The flow rate of the liquid is 198 mm per 5 days or 4.6×10^{-4} mm/s. It is suggested that this flow rate is small enough to discount the effect of bulk advection or hydrodynamics on leaching kinetics. After 5 days, the amount of liquid released on a daily basis is approximately 200 ml, being 86% of that added at the top. The rest is assumed to be lost to evaporation.

The diffusion models used previously in this chapter were developed based on a semi-infinite medium in an infinite bath. Assuming the liquid hold-up within the column to be sufficient to approximate an infinite bath, an attempt was made to fit the semi-infinite diffusion models to column results after surface washoff was taken into account (ie for t>50 days). If these models are appropriate in describing leaching, a linear relationship between fraction of mobile contaminant leached and square root of time would be expected. As in the case of the NKLT, from the pore solution results, the amount of Cr which is potentially mobile in distilled water is suggested to be approximately 1% of the total Cr in the solid. Using this value as the total mobile Cr, M_t, the cumulative fraction of Cr leached is plotted against the square root of time as suggested by Equation (7-7) for t>50 days. This graph is presented in Figure 7-25.

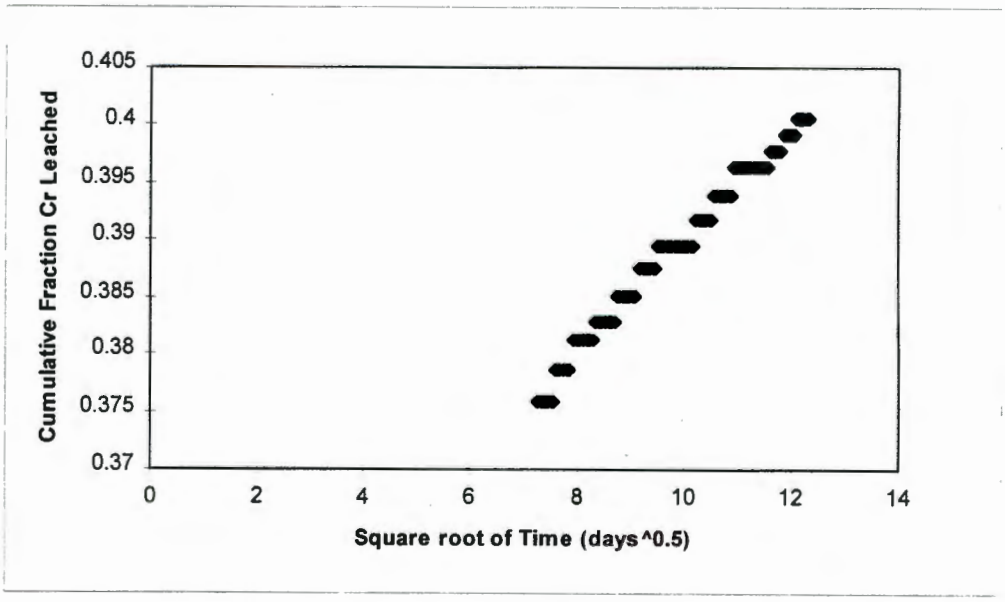

Figure 7-25 – Plot of Cumulative Fraction of Cr Leached from the Column as a Function of Square Root of Time for t>50 days

A straight line relationship is observed, suggesting intra-particle diffusion to be the resistance controlling leaching in the column studies for t>50 days. Assuming the column consists of spheres of an average diameter of 4.5mm, the value of D_e calculated from the slope of the plot is $8.3x10^{-8}$ cm^2/s. Since the pH of the leachate from the columns is to the order of 11.5, it is of significance to compare this value of D_e to that obtained from the distilled water NKLT leaches, which is $1.2x10^{-7}$ cm^2/s. This suggests an acceptable correlation between the two results. Côté (1986) suggests that the variability of calculated values of D_e from tests such as NKLT may be as high as one order of magnitude.

It is suggested here, therefore, that release from the columns is initially due to surface washoff, which is high due to the high exposed surface area. Further leaching can be approximated by simple diffusion models such as those presented in section 7.2.2.

These observations confirm the significance of the maintenance of waste form integrity to ensure the effectiveness of metal retention. This ensures the a reduction in surface area for surface washoff to occur and increased diffusion paths for the removal of Cr to occur.

It is recognised that the approach described above makes a number of simplifications to the system, including ignoring reaction and hydrodynamic effects. Much work has been carried out concurrently with this project to develop detailed mathematical models which describe the long-term modelling of contaminant release from waste dumps based on data from lysimeter columns. This work is not presented here and is explored in Petersen (1997) and Davies (1995). Furthermore, prediction of leach profiles beyond the time periods explored in this work will be significant in performance assessment and in determining landfill design.

7.7.3 Zinc

Zinc concentrations of the leachates from the column were negligible at all times. The amphoteric nature of Zn was discussed in Chapter 2. At the pH values of between 11.1 and 12.0 the solubility of $Zn(OH)_2$ is expected to be low. It is thus expected that Zn mobility is restricted primarily by solubility considerations.

7.7.4 Calcium

Calcium in the leachate shows a sharp initial rise which rapidly drops off after 10 days after which a slow release of Ca is observed (see Figure 7-26). The column contains 7.05 kg of S/S material with a moisture content of 35%. Using the pore solution results of Chapter 6, it is calculated that approximately 310 mg of calcium is contained solubilized in the pores. In the first 12 days from breakthrough, a total of 320 mg of calcium is released. The soluble calcium from the pores is thus released rapidly. After this point calcium contents in the leachates are between 4.5 and 5.3 ppm. In the NKLT it was observed that slow dissolution of Ca contained in the cementitious products occurs. This accounts for the slow continued release of Ca observed in Figure 7-26.

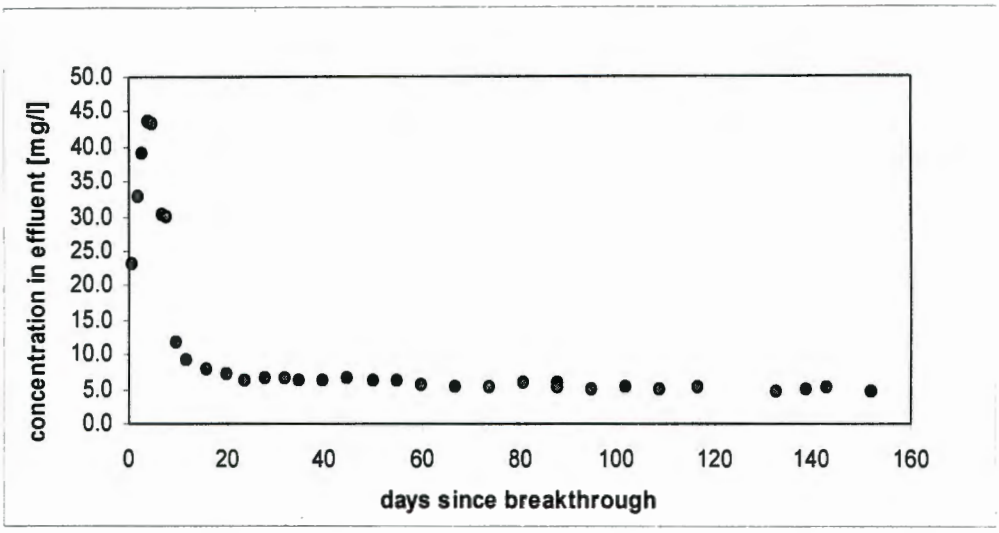

Figure 7-26 - Ca Release from the Column as a Function of Time

7.7.5 Potassium

Potassium release as a function of time is presented in Figure 7-27. As in the case of Cr and Ca, a high initial rate of release is observed. The release once again drops off and continues at a low rate for the full 154 days. This initial high rate of release is suggested to be K bound at the surface of the individual S/S particles which is readily released into the fluid percolating through the column.

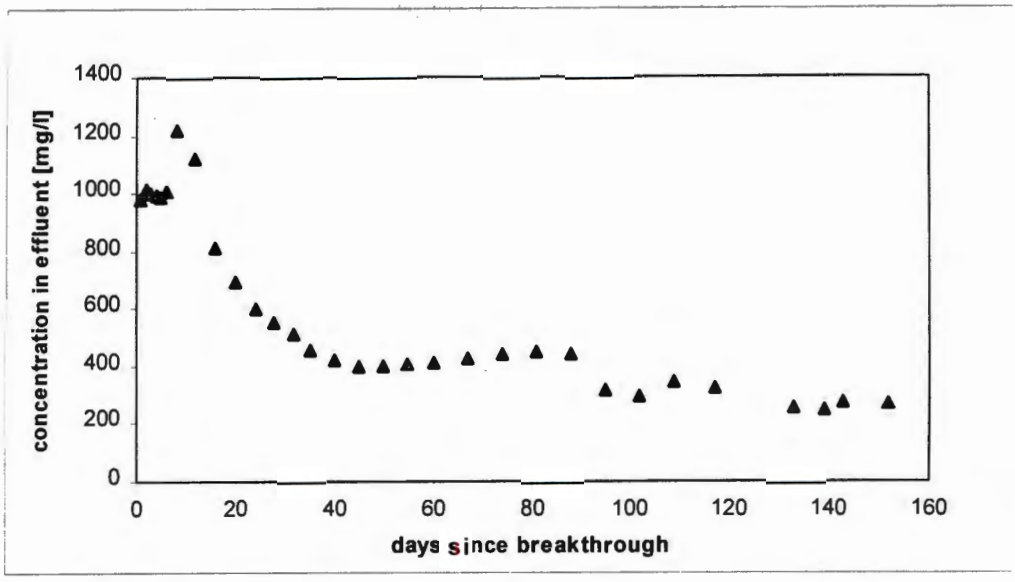

Figure 7-27 - K release from the Column as a Function of Time

The diffusion analysis presented for Cr in section 7.6.2 was applied to K for t>50 days. The NKLT suggests values of D_e for K to the order of 10^{-9}, while the column predicts a value of D_e of 4.5×10^{-8} after t=50 days. Taking into account the inherent error in such calculations [Côté (1986)], this indicates a reasonable correlation between NKLT and column results, and hence once again the NKLT results can be used to approximate the column results after surface wash-off has been accounted for. This suggests once again that intraparticle diffusion is rate limiting even in the column results.

7.8 Summary of Results from Kinetic Leaching Tests

7.8.1 Solid Decripitation

Acetic acid causes a rapid breakdown of the solid structure. In the case of the agitated kinetics tests and TCLP of Chapter 6 this is indicated by a reduction in the particle sizes. In the acid NKLT a distinct leach front is formed as the acid penetrates the monolith. It was suggested that removal of Ca from the cementitious products by the acid is responsible for this observed breakdown. These cementitious products are responsible for maintaining the solid structure. The removal of Ca from the cementitious products was also suggested in the case of distilled water leaching, but this process was observed to be slow and the effect of Ca removal on solid structure over the time periods studied here was observed to be insignificant.

7.8.2 Buffering Capacity of the S/S Products

In distilled water leaches and the column leach tests the buffering capacity of the S/S product was observed to be sufficient to raise the pH of the leachant solutions to the alkaline range - in the case of the NKLT to a pH of between 8 and 10, in the column leach tests to a pH of 11.5. The high pH was suggested to be maintained by calcium and potassium hydroxides released into solution.

In acetic acid leaches the S/S product raised solution pH from 2.9 to above 4 in the NKLT and approximately 5.5 in the agitated kinetic tests. The buffering capacity of the S/S products was not sufficient to raise the acidic pHs to the pH of the pore solutions.

pH plays a significant role in the release of metals from the S/S products. Some metals were observed to be contained as insoluble hydroxides in the alkaline S/S products, which resolubilize if the pH drops. The specific case of Cr(III) and Zn(II) are discussed further below.

7.8.3 Chromium

Cr(VI) is mobilized in both distilled water and acidic leaches. In both leachates it was suggested that the rate of release of Cr(VI) is controlled by diffusion, after washoff of that contained at the surface of the particles occurred. In the model of Chapter 4, Cr(VI) was proposed to be contained in the pore solutions. The fact that reaction did not determine the leaching rates for Cr(VI) indicates either that the Cr(VI) is mobile, as suggested in the model, or that mobilization reactions are fast relative to diffusion. In the column tests release was once again controlled by diffusion after initial surface washoff was accounted for.

In the agitated kinetic tests, it was observed that higher agitation rates give rise to lower rates of Cr(VI) leaching. The potential for adsorption of Cr(VI) onto solid surfaces, with subsequent kinetically controlled desorption, was demonstrated by monitoring the liquid phase reduction of Cr(VI) to Cr(III) using $Fe(SO)_4$ - as time proceeds more Cr(VI) is released into solution, implying that Cr(VI) is slowly desorbing from solid surfaces. Higher agitation

rates result in more attrition, implying a greater surface area for Cr(VI) adsorption and hence less Cr released in the leach tests.

No Cr(III) was detected in the distilled water leachates and the mild acid leachates used in the column test. Cr(III) solubility is at a minimum between a pH of 6 and 11 and hence is not soluble at the pHs of these leachates. Cr(III) is, however, detected in low pH leachates from the acid agitated kinetic tests and acid NKLT. Release of this Cr was also controlled by diffusion, indicating that the solubilization reactions are fast compared to diffusion.

Reaction did not limit the rate of Cr leaching in any of the leaching tests. Mobilization of Cr from the stable dust core would be expected to be observed to be a slow mobilization reaction. Based on these observations it is suggested that the dust core is not mobilized over the leaching periods studied here. Further tests over a number of years would indicate the significance of leaching from this dust core.

7.8.4 Zinc

In the case of high pH leachants, no Zn was mobilized. In acidic leachants, release of Zn is observed. Once again the zinc which is contained in the pores is expected to be present as insoluble $Zn(OH)_2$. In the low pH leachants this is rapidly mobilized and diffuses through the solid and into the bulk. The intra-solid diffusion is rate controlling in the release of zinc. The zinc contained in the stable dust particle is suggested not to be mobilized over the time periods studied here, since no reaction controlled release is observed.

7.8.5 Potassium

Potassium solubility is not a strong function of pH. In some of the materials a surface contribution to the release of K was observed, after which release was controlled by diffusion. In the column tests, after initial surface washoff was accounted for, release was also suggested to be controlled by diffusion.

The calculated values of D_e were lower in distilled water than in acid for K. It was suggested that the controlling resistance in the case of the acid leaches is diffusion from the leach front through the leached layer to the surface of the solid. In the case of distilled water leaching diffusion through the solid (in which no leached layer was formed) to the surface controls the rate of leaching. The leached outer shell is suggested to be more porous and less tortuous than the unleached S/S product and hence the rate of diffusion through the leached layer will be higher than through the S/S product.

Once again no long-term mobilizing reaction was observed, suggesting that the K contained in the dust core remains stable over the time periods studied here.

7.8.6 Calcium

Calcium was identified in Chapters 2 and 4 to form part of the cement hydration product matrix. Furthermore, some of the calcium exists as the hydroxide species in the pore spaces, being a product of the cement hydration reactions. The results presented in this current chapter indicate both a reaction and a diffusion contribution to the rate of Ca leaching from the S/S products in distilled water leaches, and diffusion control of leaching in acidic leachants. Release of that calcium contained in the pore solutions will be controlled by diffusion. In the case of acid attack on the S/S products, the breakdown of the cement products is rapid and hence diffusion will be the resistance controlling leaching. In distilled water leaching, however, this reaction is slow and hence the reaction term is observed for the Ca contained in the cementitious products.

The significance of the release of $Ca(OH)_2$ in determining pH and hence metal solubility which was suggested in Chapter 6 is once again observed in this current Chapter.

7.8.7 Inferences for Large Scale Application of the Technology

This Chapter has shown that two primary considerations must be taken into account during large-scale implementation of the technology with regard to metals retention. Firstly, since diffusion is the primary rate controlling step for all metals, it is essential that waste form

integrity be maintained to ensure long diffusion paths. Secondly, since the release of metals such as Cr(III) and Zn is dependant on pH, the waste which is placed into landfill should be isolated from acidic rain and groundwaters. A high buffering capacity of the waste is advantageous in that it is able to buffer any water with which the waste comes into contact.

Chapter 6 and 7 have presented the results of a number of leaching tests, each of which aims at providing different information on the chemical nature of the S/S product. It is recognised, however, that such a large suite of tests is not practical to carry out each time a new S/S product is to be evaluated. Whilst recognising the limitations of these tests, it is suggested that the TCLP and EE tests of Chapter 6 be used to compare retention potential of different S/S product formulations. For the purposes of predicting long-term leaching performance, the distilled water NKLT is suggested to provide a simple and effective indication of the rate of long-term leaching from the S/S product, provided the buffering capacity of the product is not used up.

In Chapter 8 which follows both leaching and strength behaviour are studied further with reference to practical aspects of laboratory-scale testing of S/S products. This is done using an experimental programme based on a factorial design technique. Chapter 8 concludes with a discussion of considerations surrounding the large-scale implementation of S/S.

8.

Practical Considerations in the Implementation of S/S Processes

In Chapter 4 the chemistry and physical microstructure of the S/S products was explored using fundamental characterisation tools. In Chapter 5, strength attributes of the products were assessed, to provide a fundamental understanding of bonding in- and fracture behaviour of- the products. Chapter 6 and 7 looked at leaching behaviour with the aim of expanding on the understanding of the chemistry of the products gained in Chapter 4.

The discussions presented thus far have all been based on in-depth laboratory scale investigations which use time-consuming and expensive characterisations. In reality, S/S is a practical option for waste treatment. The technology should therefore also be explored with a view towards large-scale implementation. It is based on this observation that work reported in this current chapter was launched. Three aspects of the practical implementation of S/S are discussed here:

(i) A factorial design technique known as the Central Composite Rotational Design (CCRD) is employed here for three purposes. Firstly, to optimize the operational variables presented in previous chapters to create a product which has the combined desirable attributes of minimum leachability and maximum strength. This is investigated for both the FeCr Dust and the ETP products which were discussed in Chapter 3. Secondly, based on the results of Chapters 5, 6 and 7, the design is used to determine the interaction between the operational variables on leaching and strength behaviour. Finally, at the beginning of this thesis it was suggested that, since both strength and containment depend on the extent of formation of cement hydration products, a relationship between strength and leaching behaviour exists. The CCRD is used to explore this hypothesis.

(ii) The use of other additives besides cement in the S/S formulation is qualitatively discussed here.

(iii) Considerations on the practical implementation of cement-based S/S and landfill design are presented.

8.1 Factorial Design

In the context of this thesis factorial design investigation was undertaken to:

(i) Assess the appropriateness of experimental design technique for modelling strength and leaching behaviour of the S/S products to changing operational inputs,

(ii) Investigate the hypothesis of the existence of a relationship between strength and leaching behaviour,

(iii) Optimize process variables values to give maximum strength and minimum leaching behaviour,

The following terms relevant to factorial design are defined in the context of this work:

(i) **System:** the S/S product

(ii) **Input variables:** inputs to the system which may be changed. Three operational variables, **amount of cement added**, **water addition** and **curing time**, were identified in Chapter 3 as being of interest in this work. These were identified as being the operational parameters which have a significant effect on the strength and permeability of cement and S/S products. Although these are not fundamental variables, they are important practical variables for full scale operation in that they are readily measured and easily controlled. The choice of the high and low levels of these variables used here is discussed further in section 8.2.3 below.

(iii) **Responses:** Characteristic outputs of the system. From Chapter 5, 6 and 7, the responses of interest in this work are leaching and strength behaviour.

(iv) **Model:** A quadratic equation which describes the response surface in terms of the input variables. It is recognised at the outset that such models are neither mechanistic nor deterministic. Furthermore, the validity of the quadratic in predicting the response is bounded by the values of the input variables used in development of the expression.

As mentioned above, three operational variables were highlighted to be significant in determining the responses of the S/S products. A *standard* three-level experimental design can be used to explore a system's responses at three levels of each of the three input variables and to develop a quadratic model based on these responses. Such an experimental design has the disadvantage, however, that a large number of tests are required to fully characterise the responses of the system to changing the individual variables, and to identify the interaction between these variables.

Factorial experimental designs in general are designed to reduce the number of tests required to fully characterise the response of a system. When a response can be represented by a second order quadratic expression, a three-level factorial design is often used [Diamond (1989)]. 'Three levels' implies that the effect of each variable is assessed at each of three levels - at the minimum in the range being considered, at some median value and at the maximum value. Using the measured responses at various inputs, a quadratic expression or mathematical model describing the response surface as a function of the input variables is developed.

The 'model order' is defined by the degree of interaction between the significant variables; for example a second order model accounts for first order interactions. Murphy (1977) suggests that where the variables are continuous, a second order model is sufficient to describe most systems and that higher order models give little extra information above what is obtained from a second order model. Such a second order model thus reflects the effect of changing a variable independently of other variables, and can identify any interactions between variables which may occur [Diamond (1989)]. Furthermore, the model can be manipulated to find the required variable values for optimum response; in the context of this work the optimum responses are a product with minimum leaching behaviour and maximum strength. This is discussed further below.

The number of experiments required for any factorial experimental design is given by:

$$\textbf{Number of experiments} = (\textbf{model order} + 1)^{n} \qquad (8\text{-}1)$$

where n is the number of independent input variables.

For a second order model for a system with three variables, 27 tests are thus required to completely characterize the system. This excludes any repeat tests to determine inherent variability in results.

8.1.1 The Central Composite Rotational Design (CCRD)

The Central Composite Rotational Design (CCRD) provides an alternative to a regular three level factorial design, in which considerably fewer experiments are required to develop the model describing the system [Diamond (1989)]. For example, for a three level, three variable design, the

CCRD requires 15 tests versus 27 for the standard three-level design above (excluding repeat tests). The CCRD once again gives rise to a quadratic expression which describes the response in terms of the input variables. Furthermore, by introducing repeat tests, the design allows the statistical error in the responses to be determined. As in the case of the standard factorial design discussed above, the significance of interactions between the variables can be assessed. An interaction implies that the effect of one variable, x_1, on the response is dependant on the level of a second variable x_2. For example, the effect of variable x_1 on the response may be insignificant at a low level of variable x_2 but may be significant at a high level of x_2.

The CCRD has been used successfully in the modelling of a number of different minerals processing systems including hydrocyclones [Cilliers et al (1992)] and flotation operations [Mular and Klimpel (1991)]. No record was found of this design being applied to S/S systems. It was, however, felt that due to the nature of the system and the effectiveness of the CCRD in characterising other multi-variable systems with interactions between the variables, applying this factorial design to modelling responses of S/S products to operational variable inputs had merit.

8.1.2 Implementation of the CCRD

The use of the CCRD proceeds as follows: the significant variables as well as their maximum and minimum values are chosen by preliminary laboratory testing and from literature reports (see Chapter 3 and section 8.2.3 below for a discussion of the choice of significant variables in the context of this current work). The CCRD design procedure is used to calculate the composition of the samples required for the experimental programme. This procedure is detailed in Appendix F1 [Diamond (1989)]. The tests are performed and responses determined. Once testing is complete a regression analysis is carried out to determine the coefficients of the response function given in Equation 8-2 below. Established relationships presented as part of the CCRD design procedure are used in calculating the model's coefficients. These relationships are also presented in Appendix F1.

For a three-variable CCRD the results of experiments are reduced to a regressed function given by:

$$y = a_o + a_1x_1 + a_2x_2 + a_3x_3 + a_{11}x_1^2 + a_{22}x_2^2 + a_{33}x_3^2 + a_{12}x_1x_2 + a_{13}x_1x_3 + a_{23}x_2x_3 \qquad (8\text{-}2)$$

where y is the response being estimated, a_{ij} are constants and x_i are independent process variables.

The general model for a CCRD thus includes three groups of terms in addition to a constant a_0:

(a) Linear terms in each of the variables, $x_1, x_2, x_3, ..., x_n$

(b) Squared terms in each of the variables, $x_1^2, x_2^2, ..., x_n^2$.

(c) First order interaction terms for each paired combination, $x_i x_j$ where $i \neq j$.

Once results have been used to determine the model coefficients, statistical analysis via a simple t-test allows for determining which of the terms in the above equation are significant in determining the response at various confidence limits [Diamond (1989)]. The first terms ((a) above) indicate a linear relationship between the variables and the response. The x_i^2 terms (b) indicate a quadratic relationship between the variables and the response. Finally, interaction terms (c) indicate where the effect of one variable x_i on the response depends on the value of another variable x_j, as discussed previously.

Three types of experimental trials define the CCRD - centre, star and axial trials (see Appendix F1). These points are shown schematically in Figure 8-1 for a design of three variables. Here the *centre point* is given by point 15, surrounded by *factorial* or *star trials* (1-8) and *axial trials* (9-14).

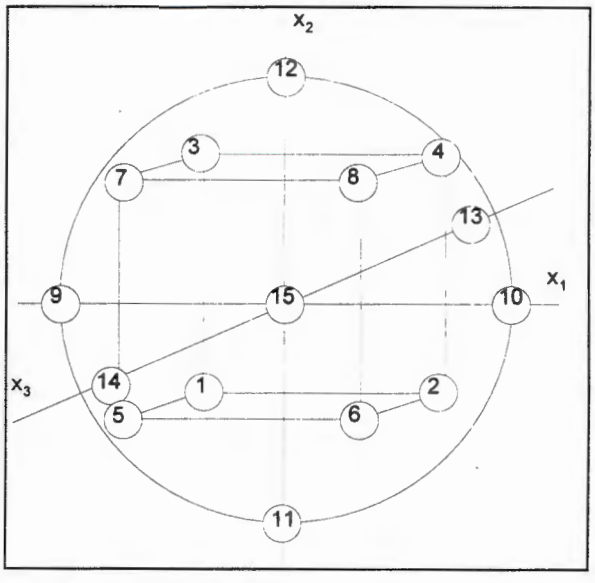

Figure 8-1 - The Central Composite Rotational Design Matrix

The experimental region of interest is defined by the maximum and minimum values for each independent variable (process parameter) being investigated (see section 8.2.3 below). These are the *axial* values. The *centre* of the design is equally spaced between the axial values. Finally, the *star* trials are positioned as discussed in Appendix F1.

To determine the inherent variability in responses, a number of repeat trials are required. Ideally, repeat testing should be carried out at each of the points in the design to provide an accurate measure of the variability in the responses. It is, however, often expensive, time consuming and impractical to perform such a large number of tests. Diamond (1989) and Myers (1971) suggest that if the variables are continuous (ie are not discrete points), a reasonable estimate of the variance for the entire experimental set can be obtained by repeating the tests at the centre of the system. In a CCRD for three variables, six repeats are carried out at the centre point of the design (point 15 on Figure 8-1). Variability in these results is taken to represent the variability for all results in the system.

8.2 Experimental Details and Results

8.2.1 Products Tested

Previous chapters focused primarily on characterisation of the solidified FeCr Dust. It was seen previously that a preliminary water wash step was required to remove soluble components from the surfaces of the dusts to allow for effective solidification. The remaining solution from this washing step is a heavy-metal laden stream which requires treatment prior to discharge. A potential option for treatment of this stream is lime-based neutralization of the stream which results in precipitation of heavy metals in solution. The solution is filtered giving rise to the formation of a metal hydroxide filter cake, the metal content of which indicates that this filter cake will require treatment prior to disposal. This is just one potential origin of metal-laden wastewater streams which may be treated by lime-based neutralisation. The precipitation procedure, and the composition of the resultant solids, was discussed in Chapter 3 for two such streams, with the resultant products called the ETP 1 and ETP 2 filter cakes.

It is recognised that both the chemistry and physical nature of the waste form will affect the ultimate strength and leaching behaviour of the S/S products. The differences between the two wastes are the following. The FeCr Dust has been shown to consist of a central stable core with soluble species surrounding this core. The ETP filter cakes, however, are metal hydroxide precipitates, the solubilities of which depend on the pore solution chemistry and that of the leaching environment. Furthermore, ETP 1 and ETP 2 differ in the concentrations of total Cr (in the form of Cr(III)) and Ca in the filter cakes, with the latter having higher concentrations of these species than the former.

The ETP products were also shown to contain high levels of anions in the pore solutions, including SO_4^{2-}, Cl^-, F^- and NO_3^-. ETP2 contains considerably more F^- and NO_3^- than does ETP 1.

The CCRD is thus used here to assess the potential for using S/S in the treatment of metal hydroxide precipitates. Application of the CCRD to the solidified FeCr Dust products is also discussed.

8.2.2 Parameters Measured using the CCRD

In the context of this work the CCRD was used to explore the responses in strength and leaching behaviour to changes in operational variables.

ITS was used as a strength characterisation parameter (see Chapter 5 for test procedure details). While the results of Chapter 5 identified that ITS is a less sensitive strength measurement than K_{IC}, K_{IC} testing is more time-consuming than ITS measurement. Considering that this chapter focuses on the practical implementation of the S/S technology, it was decided to use the quicker and hence more economical ITS over K_{IC}. Furthermore, since the strength of the solidified FeCr Dust was extensively characterised in Chapter 5, only the solidified ETP products are tested for strength characteristics here.

Both the solidified FeCr Dust and the ETP products were tested for leaching characteristics via the TCLP of Chapter 6. As has been discussed previously, the TCLP provides no information about leaching kinetics or mechanisms, and the leaching media do not simulate conditions which would be expected in reality. Despite these downfalls, and the wide controversy surrounding the use of the TCLP as a waste classification tool, the TCLP is still widely used as a "pass-fail" test for characterising wastes prior to consignment to landfill. In previous chapters it was found that acetic acid causes extensive breakdown of the cement hydration products, and provides an environment where previously insoluble metal species are mobilized. Based on the observations from previous chapters the TCLP is thus used as an evaluation tool in the current chapter to represent a "worst-case" scenario for leaching from the S/S products.

8.2.3 Choice of Values of Operational Variables

In Chapter 3 the selection of maximum and minimum levels of the operational variables as used in this work were presented and discussed. For **cement addition**, literature reports showed that cement to waste ratios ranging from 1%-2% for wastes with pozzolanic properties, to up to 90% for liquid wastes, are commonly used. Based on initial investigation and consultation with waste contractors, it was decided to confine the range of cement additions to between 10% and 30% based on a dry mass of cement to dry solids in the filter cake. 10% was identified to be the minimum to give a product with an acceptable structural strength as observed in initial laboratory investigations, while 30% would be the maximum which would be feasible in terms of costs and bulk increases when consigned to landfill.

Due to the fineness of the waste solids, more water was required to achieve a workable paste than what is normally used in the manufacture of concretes [PCI (1986)]. It was found also that higher water:solids ratios were required to obtain workable pastes in the case of the ETP products than in the FeCr Dust. Although no particle size distribution was obtained for the ETP solids, this is suggested to be due to the smaller particle sizes as discussed in Chapter 3. **Water to dry solid** ratios of between 0.9 and 1.08 for the FeCr Dust and values of 1.1 and 1.26 for the ETP products

were used in sample making. This range of w/s ratios was chosen as being those giving a workable paste which could be effectively cast into moulds.

Finally, in terms of **curing**, it was found that a minimum time of two weeks was required before samples could be removed from their moulds intact , and a further two weeks required prior to being able to carry out the strength tests (see Chapter 5). No tests were therefore carried out before 28 days after mixing. The FeCr Dust were cured for periods of up to 180 days. From observations in previous Chapters it was observed that little change in product properties were observed after curing periods of about 70 days and hence the maximum time for which the ETP products were cured was 70 days.

Table 8-1 summarizes the minimum and maximum values of the operational variables used in the development of the experimental matrix in the CCRD.

Table 8-1 - High and Low values of Variable used for ETP and FeCr Dust Products

Variable	ETP Cakes			FeCr Dust Products		
	Low	**Mean**	**High**	**Low**	**Mean**	**High**
Water/solids	1.1	1.18	1.26	0.9	0.99	1.08
Cement content (%)	10	20	30	10	20	30
Curing time (days)	28	49	70	28	104	180

8.2.4 Development of the Experimental Matrix and Sample Preparation

Using the design technique described in section 8.1.1 and Appendix F1, and the maximum and minimum values presented in Table 8-1, the experimental design matrix was developed. The MSEXCEL spreadsheet which supports the development of the CCRD can be found on the disk which accompanies this thesis. The instructions for use of the spreadsheet appear in Appendix F2. The experimental matrices are presented in Table 8-2 (a) for the ETP products and in Table 8-2 (b) for the FeCr Dust products. Samples were mixed and cured in accordance with the procedures detailed in Chapter 3, using the cylindrical moulds previously used for ITS testing.

Table 8-2 (a) - Experimental Matrix for ETP products

Trial No	Water/ Solids	Cement (%)	Curing (days)	Trial No	Water/ Solids	Cement (%)	Curing (days)
	Factorial	**Trials**			**Centre**	**Trials**	
1	1.23	14.1	37	15	1.18	20.0	49
2	1.23	25.9	37	16	1.18	20.0	49
3	1.23	25.9	61	17	1.18	20.0	49
4	1.13	25.9	61	18	1.18	20.0	49
5	1.23	14.1	61	19	1.18	20.0	49
6	1.13	25.9	37	20	1.18	20.0	49
7	1.13	14.1	61				
8	1.13	14.1	37				
	Axial	**Trials**					
9	1.10	20.0	49				
10	1.26	20.0	49				
11	1.18	10.0	49				
12	1.18	30.0	49				
13	1.18	20.0	28				
14	1.18	20.0	70				

Table 8-2 (b) - Experimental Matrix for FeCr Dust products

Trial No	Water/ Solids	Cement (%)	Curing (days)	Trial No	Water/ Solids	Cement (%)	Curing (days)
	Factorial	**Trials**			**Centre**	**Trials**	
1	1.04	14.1	59	15	0.99	20.0	104
2	1.04	26.0	59	16	0.99	20.0	104
3	1.04	26.0	149	17	0.99	20.0	104
4	0.94	26.0	149	18	0.99	20.0	104
5	1.04	14.1	149	19	0.99	20.0	104
6	0.94	26.0	59	20	0.99	20.0	104
7	0.94	14.1	149				
8	0.94	14.1	59				
	Axial	**Trials**					
9	0.9	20.0	104				
10	1.08	20.0	104				
11	0.99	10.0	104				
12	0.99	30.0	104				
13	0.99	20.0	28				
14	0.99	20.0	180				

8.2.5 Experimental Data Analysis

A full set of experimental results is presented in Appendix D5. Using the CCRD procedure discussed above, the model coefficients for Equation 8-2 were calculated. The spreadsheet designed to do all calculations can be found on the attached disk. Model coefficients for all measured responses are presented in Appendix F3.

Coefficients were substituted into the model equation and used to plot surfaces which provide a graphical representation of the responses as a function of two of the three operational variables. Since on a 3-dimensional plot it is only possible to plot two variables and one response, the third variable is required to be held constant.

The plots and a discussion thereof are presented below. Results are presented for strength and leaching behaviour and analysed in the context of both their relationship to observations from previous chapters and to extending the information presented therein. A simple t-test was conducted to identify the significance of the various terms in the model equation (8-2) in determining the responses at the 90% confidence level.

To determine the accuracy of the model in predicting experimental results, the actual responses were plotted against values predicted by the model equations. Should the model perfectly represent the predicted results, a straight line relationship between predicted and actual results would be observed. In reality, however, inherent variability in results will result in the fit not being perfectly linear. To determine the accuracy of the model in predicting experimental results, the coefficient of correlation, R is calculated from the plot described using:

$$R = \left(\frac{(\Sigma XY) - (\Sigma X)(\Sigma Y)/n}{\sqrt{(\Sigma X^2 - (\Sigma X)^2/n)(\Sigma Y^2 - (\Sigma Y)^2/n)}} \right) \qquad (8\text{-}3)$$

where n is the number of data points, X is the actual experimental result and Y is the predicted result. A simple t-test on this value of R can be carried out to determine the probability or certainty with which predicted results can be taken to represent experimental results. Here t is given by:

$$t = \frac{R\sqrt{n-2}}{\sqrt{1-R^2}} \tag{8-4}$$

where this value of t takes into account the number of data points used to calculate R. Here there are (n-2) degrees of freedom, with n being the number of data points. Probability-t tables can be found in all standard statistics texts [Miller and Freund (1985)]. Table 8-3 summarizes probability points for the t-distribution for 18 degrees of freedom (the factorial design gives 20 data points, hence (n-2) or 18 degrees of freedom).

Table 8-3 - Probability Points for the t-distribution for 18 d.o.f.

t	1.33	1.73	2.10	2.55	2.88
P	0.1	0.05	0.025	0.01	0.005
R*	0.074	0.096	0.116	0.140	0.158

* These values of R were calculated by substituting the above values of t into equation (8-4)

The above table implies that for example, if t = 1.73, or R=0.096, the correlation between predicted results and experimental results is significant within a 95% confidence limit. Due to the high number of data points, the value of R required for 99.5% confidence is low. For this reason a visual inspection of the plot of experimental vs predicted results should be carried out in order to determine whether scatter around the straight line is random or whether results diverge significantly from the straight line plot described previously. Such plots are used further below.

8.2.6 Indirect Tensile Strength (ITS) Results

In Chapter 5 it was observed that strength of the S/S product depends on the strength of the bonds formed between the particles by the cement hydration product. This was in turn found to be dependant on the amount of cement present, the water present in the initial mixture, the curing time and the chemical composition of additives to the cement, in this case the waste products. The strength work in this current chapter aims to further quantify the effect of changing the operational variables on strength using the factorial design.

The response surfaces generated by the model equation for ITS as a function of cement content and curing time are presented in Figure 8-2 and Figure 8-3 for ETP cake 1 and cake 2 respectively, and those for ITS as a function of cement content and water to solids ratio in Figure 8-4 and Figure 8-5. The following observations with regard to the effect of operational variables on strength are made from these figures:

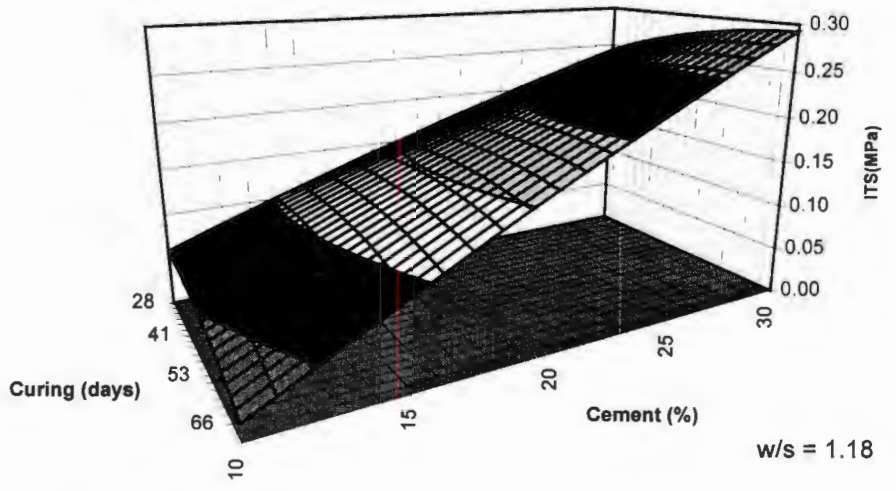

Figure 8-2 - ITS of the Solidified ETP 1 Products as a function of Cement Content and Curing time, w/s constant

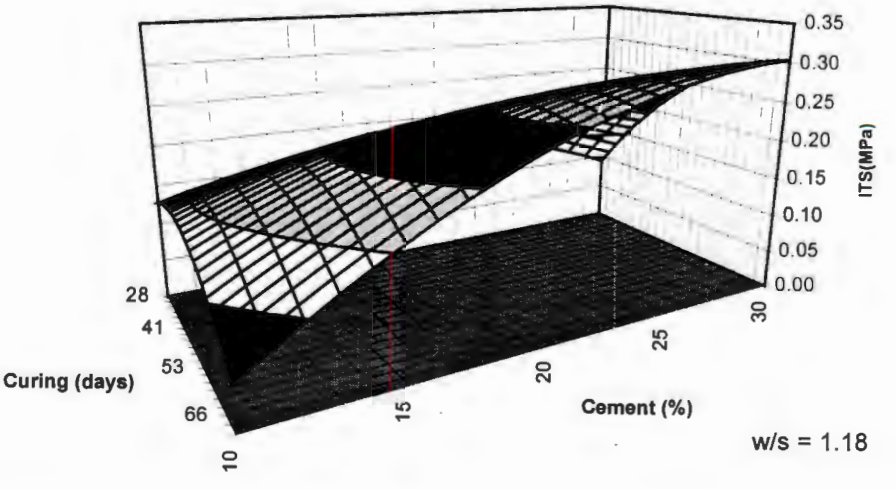

Figure 8-3 - ITS of the Solidified ETP 2 Products as a function of Cement Content and Curing time, w/s constant

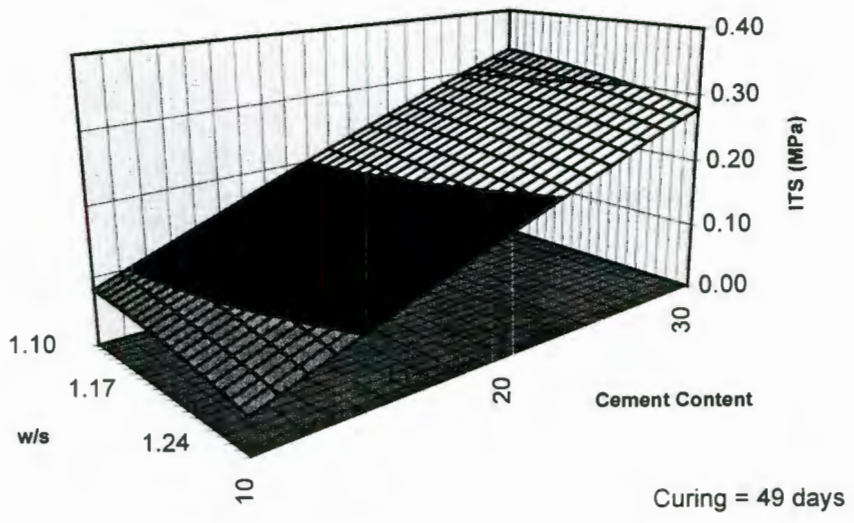

Figure 8-4 - ITS of the Solidified ETP 1 Products as a function of Cement Content and w/s ratio, Curing time constant

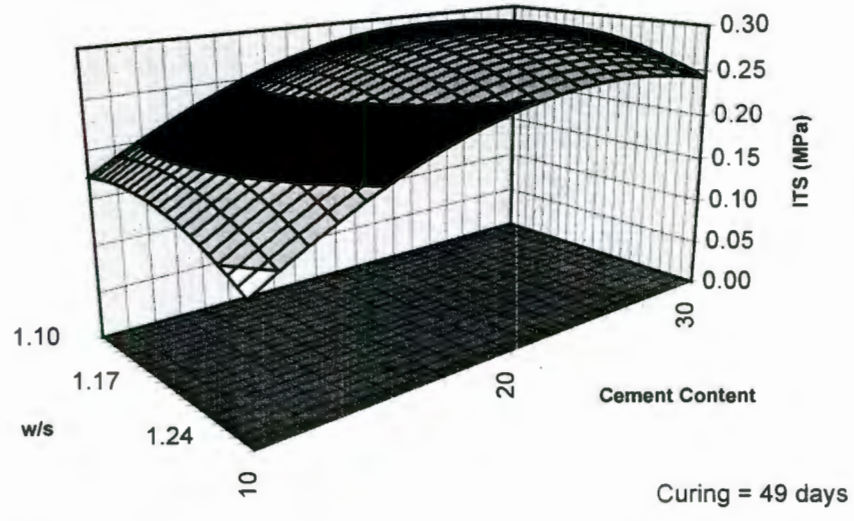

Figure 8-5 - ITS of the Solidified ETP 2 Products as a function of Cement Content and w/s ratio, Curing time constant

(i) **Increased cement content results in an increase in strength.** The results of Chapter 5 indicated that more cement implies the formation of a greater amount of cement hydration product and hence greater strength. This observation is independent of the type of waste.

(ii)**For high cement contents, strength increases with curing time.** The hydration of cement was shown in Chapters 2 and 5 to be a kinetically controlled process. The increased formation of hydration product as time progresses results in an increase in strength.

(iii) **At low cement contents the effect of curing on strength is minimal.** In low cement samples the small amount of cement limits the total amount of cement hydration product formed and consequently low strengths are observed for all samples. Changes in strength as a function of curing time are therefore not as significant as in high cement samples.

(iv) **At short curing times, w/s has a minimal effect on strength.** At short curing times minimal amounts of cement hydration product have formed and hence strength development is limited for all products. The small changes in strength which may occur due to changing the w/s ratio are insignificant.

(v)**At longer curing times, strength decreases as w/s increases.** As the w/s ratio in the initial mixture increases, the void space increases. As the void space in the mixture increases, less extensive infilling occurs during cement hydration. A more porous, and, consequently, weaker product will result. This is in line with the observations in Chapters 4 and 5 and literature observations [PCI (1986)]. The effect of w/s on strength is observed to be less significant than for the other two variables.

The various terms in the model equation were tested via a t-test for the significance of their contribution to ITS. This analysis indicated that the ETP 1 products show a linear relationship between the three process variables and strength, while for the ETP 2 products a second order relationship is observed. This is reflected in Figure 8-2 to Figure 8-5. For low cement contents in the ETP 2 products, a small increase makes a large difference to strength. As cement content increases, however, the effect of cement on strength decreases. The same quadratic relationship is observed for the effect of both curing time (at high cement contents) and w/s on strength of the ETP 2 products. This is explained as follows

The primary differences between ETP 1 and ETP 2 are in the concentrations of Ca, Cr, F^- and NO_3^- contained in the filter cakes, with ETP 2 having higher concentrations of these species in the original waste streams than ETP 1. All of the Cr is Cr(III). For the low cement additions, it is seen that the ETP 2 products have higher strengths than the ETP 1 products. The higher

concentrations of Cr and Ca will result in the precipitation out of solution of more $Ca(OH)_2$, $Ca(SO)_4$ and $Cr(OH)_3$ in the pores of ETP 2 than ETP 1. In accordance with the discussions of Chapter 5, the formation of precipitates in the pore spaces cause an increase in the strength of the final product. This explains the higher strengths. Although F^- and NO_3^- are expected to remain solubilized in the pore solutions, their presence has the potential to affect hydration chemistry [PCI(1986)]. The retention of anions and their effect on the S/S products is, however, not the focus of this work and hence is not studied further here.

The contribution of the cement hydration product to strength is, however, greater than that of the precipitates and as the amount of cement is increased, the significance of the contribution of these precipitates to overall strength decreases. This dual effect explains the second order relationship between strength and cement addition for ETP 2. For ETP 1 the effect of the precipitates on strength is limited, and hence strength is primarily determined by cement addition, explaining the linear relationship.

The significance testing confirms that the effects of both cement and w/s ratio on strength depend on curing time. This is in line with the discussion in points (ii) to (v) above.

Experimental results are plotted against those predicted by the model equation for the ITS in Figure 8-6 for ETP 1 and Figure 8-7 for ETP 2. Using Equation 8-3, values of R = 0.96 for ETP cake 1 and R = 0.91 for ETP cake 2 were calculated. The t-test, as presented in Table 8-3, suggests that the predicted strength results from the CCRD model can be accepted to represent experimental data within a 99.5% confidence limit.

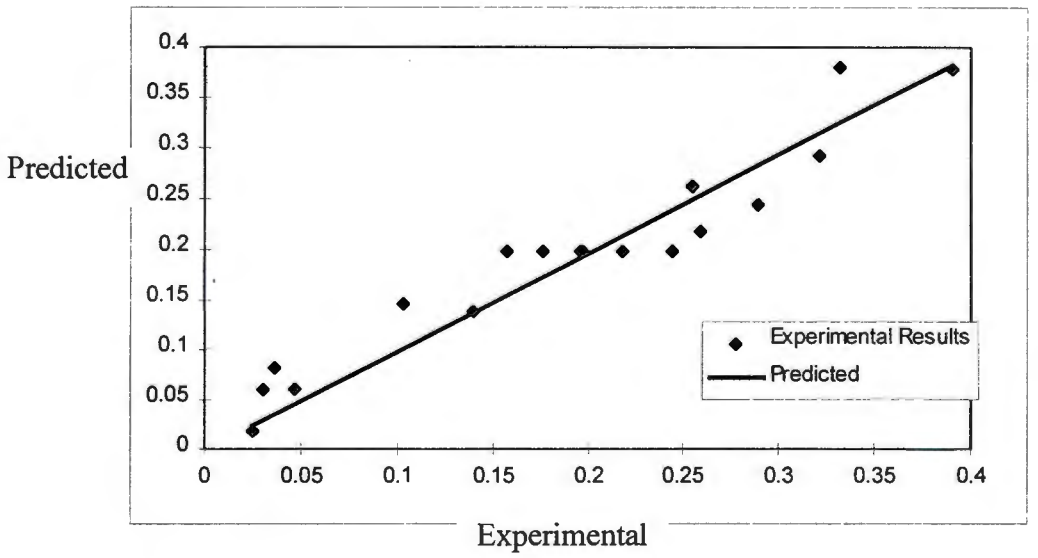

Figure 8-6 - Correlation between Experimental ITS Results and those Predicted from the CCRD Model (indicated by the straight line) for ETP1

Furthermore, inspection of Figure 8-6 and Figure 8-7 suggests that scatter around the straight line is random, implying that the model is accurate in describing experimental results. It is noted that the value of R does not account for inherent variability in strength testing. The inherent variability in ITS is discussed in Chapter 5.

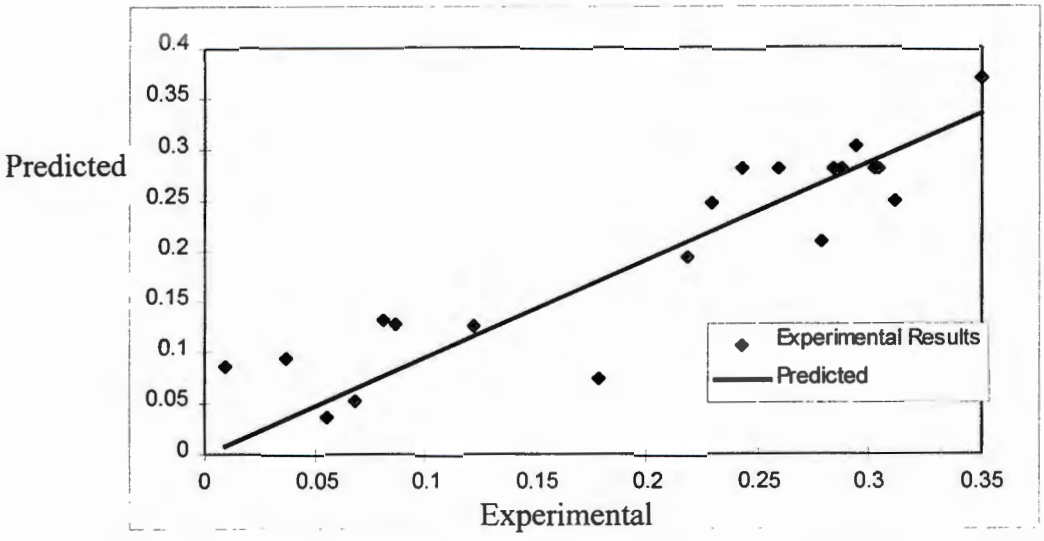

Figure 8-7 - Correlation between Experimental ITS Results and those Predicted from the CCRD Model (indicated by the straight line) for ETP2

8.2.7 Leach Test Results

TCLP results are presented in Appendix D5. For the purposes of the discussion, pH and leaching of Cr, Zn and Ca for the solidified FeCr Dust products is presented, Cr and Zn being the elements of interest in this study and Ca providing an indication of the extent of cement breakdown. Only pH, Cr and Ca leaching are discussed for the ETP products, as no Zn was contained in these products (see Chapter 3). Model parameters for other elements not discussed in detail in the text are presented in Appendix F3.

(i) pH of the TCLP Leachates

pHs of the TCLP leachates are presented in Appendix D5. For all leachates, pHs lie between 5.4 and 7.5. The factorial design indicates that a second order relationship between pH and cement content for all of the products, implying an increase in cement content causes an x^2 increase in pH of the leachate. The cement contains high levels of free alkalis, as discussed in Chapters 6

and 7, and an increase in cement content implies an increase in alkali content. The other two operational variables (w/s and curing time) have an insignificant effect on leachate pH.

(ii) Chromium

The response surfaces generated by the CCRD model for chromium leaching from the solidified ETP 1, ETP 2 and FeCr Dust products are presented in Figure 8-8 to Figure 8-10 as a function of cement content and curing time. No Cr(VI) was present in the ETP filter cakes (see Chapter 3) and the Cr in leachates from the ETP products is all Cr(III). It is furthermore noted that the Cr levels in the ETP 1 leachates are low (between 0.13 and 1.8 ppm). It is noted that the ability of the AA spectrometer to accurately read such low Cr concentrations is limited. The ETP 1 filter cakes contained less Cr(III) than the ETP 2 cakes which explains the lower amounts of Cr leached in the former over the latter. As was seen in Chapter 6, both Cr(III) and Cr(VI) are found in TCLP leachates from the solidified FeCr Dust products.

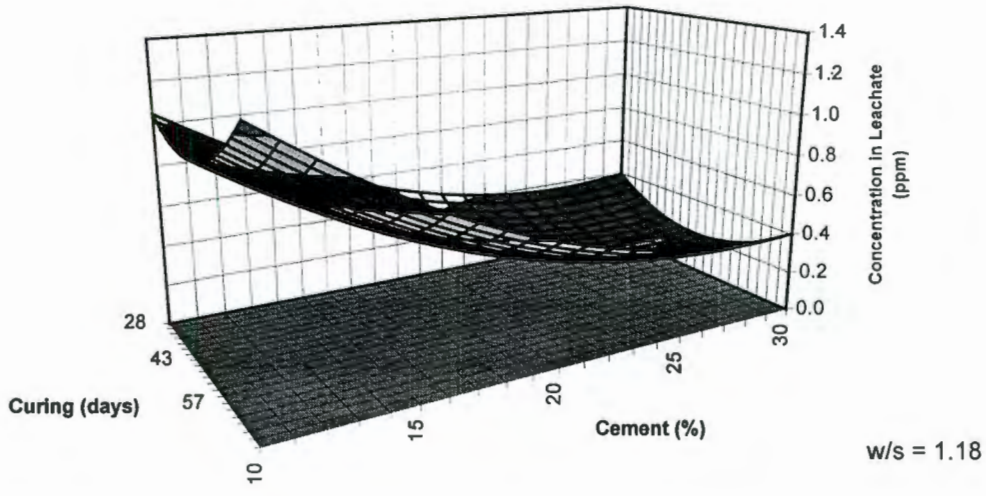

Figure 8-8 - Cr Release from the Solidified ETP 1 Products as a function of Cement Content and Curing Time, w/s constant

Figure 8-8 to Figure 8-10 indicate that Cr leaching as a function of the operational variables depends on the type of S/S product leached. The three products (solidified ETP 1, ETP 2 and FeCr Dust) differ in both physical nature and chemistry. In Chapters 2, 6 and 7 the significance of both waste chemistry and physical form on leaching have become apparent. This observation

is consistent with literature observations. Means et al (1995) highlights one of the limitations of cement-based S/S as being "..small changes in the waste composition or mix proportions can alter the properties, sometimes without the knowledge of those utilizing the waste form". The effect of both waste type and the operational variables on leaching is discussed further below.

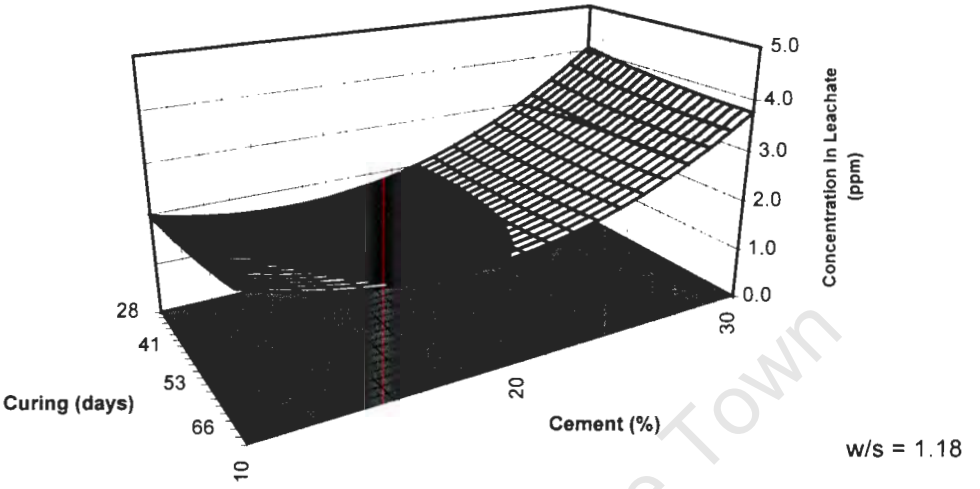

Figure 8-9 - Cr Release from the Solidified ETP 2 Products as a function of Cement Content and Curing Time, w/s constant

The CCRD model indicates that all three of the operational variables, as well as the interaction between the three variables, are significant in determining Cr leaching. The interaction implies that the effect of any one of the operational variables on amount of Cr leached depends on the values of the other two variables at which that test is carried out. The model thus confirms the importance of these three process parameters on the leaching behaviour of the ultimate S/S product, as was suggested in Chapter 3.

The effect of the individual process variables on Cr leaching is observed to be the following:

ETP 1 and ETP 2

The solidified ETP 1 and ETP 2 products show minimum Cr leaching at intermediate *cement* additions. As the cement content is either increased or decreased, Cr release increases. The initial decrease in Cr leaching as cement content is increased is consistent with observations of

previous chapters: as more cement hydration product is produced, physical retention is improved. Furthermore, an increase in pH is observed as cement addition is increased, resulting in lowered Cr(III) solubility.

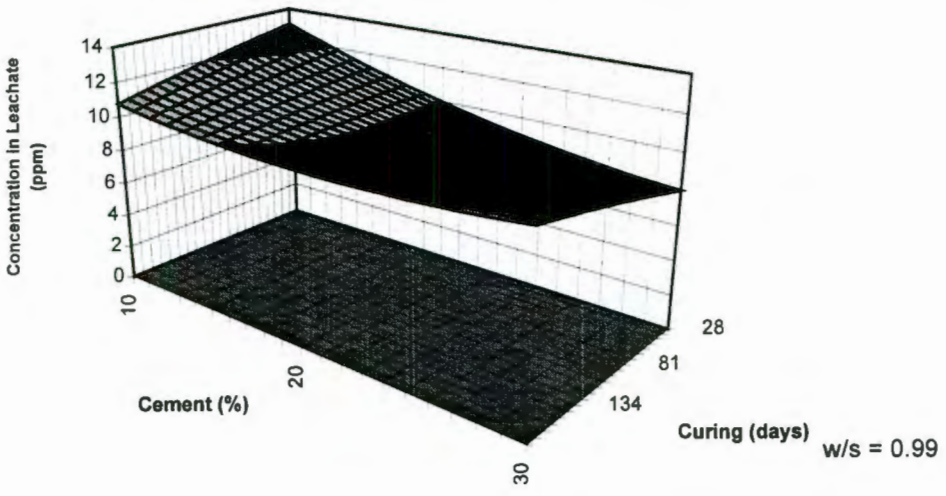

Figure 8-10 - Cr Release from the Solidified FeCr Dust Products as a function of Cement Content and Curing Time, w/s constant

As the amount of cement increases above approximately 18% cement addition, however, the amount of Cr released begins to increase. The ETP cakes were formed by precipitation of metal species from solution using $Ca(OH)_2$. The solid is thus a complex equilibrium between the solid phase and the water entrained in the filter cake. The latter entrained water contains high concentrations of anions, including F, Cl, SO_4, NO_3 and CO_3 (see Chapter 3).

Furthermore, during hydration of cement, large amounts of SO_4 and lesser amounts of Cl, NO_2, PO_4, NO_3 enter the pore solution (see Figure 4-27). It is suggested, therefore, that at high cement additions, the release of high concentrations anionic species from the cement into the pore solution affects the equilibrium between Cr in the liquid and solid phases and results in resolubilization of $Cr(OH)_3$ from the solid, giving rise to increased leaching of Cr(III) at high cement additions. The chemistry which results in this resolubilization is once again complex and resolution thereof requires further study of pure cement-$Cr(OH)_3$ systems.

It is noted that pH increases with cement addition for all cement contents, indicating that pH is not the parameter controlling Cr leaching from the ETP products at high cement additions.

The effect of the other operational variables on Cr leaching from the ETP 1 products is observed from the graphs to be minimal, with any change in w/s and curing resulting in a maximum change of 0.15 ppm in Cr in solution. Once again the low amounts of Cr in the original filter cakes limits the amount of Cr available to be leached, and changing the operational variables thus has little effect on the amount leached.

For the ETP 2 products, at high cement contents, leaching decreases with increased curing and decreased w/s ratios. This observation is consistent with results from Chapters 4, 6 and 7. A more tortuous and less porous product, which results from decreased w/s ratios and increased cement contents, will result in reduced Cr release.

FeCr Dust Products

For the FeCr Dust product an increase in *cement* content results in a decrease in Cr leaching for all values of the other variables. The FeCr Dust products contain both Cr(VI) and Cr(III). Cr(VI) release was found in Chapters 6 and 7 to be related to physical encapsulation effects. In the case of Cr(III), however, release is a function of both physical encapsulation and solubility. The observation that Cr leaching decreases with increased cement addition is thus as a result of two combined effects. Firstly, a greater extent of formation of cement hydration products is expected as more cement was present in the mixture. This leads to a more tortuous and integral structure in which, physically, both Cr(III) and Cr(VI) are contained. Secondly, as was observed above, an increase in the amount of cement in the mixture results in an increase in leachate pH. Higher pH implies a reduction in the solubility of Cr(III).

The effect of *curing* on Cr leaching depends on the amount of *cement* present in the mixture. At low cement contents, leaching decreases with increased curing time. This would be consistent with observations that cement hydration proceeds with time. At high cement contents, however, leaching increases slightly with increased curing time. Two possible explanations are presented for this observation. Firstly, in Chapter 6 it was suggested that slow solubilization of Cr from

the central dust core in the pore solution is possible. This would increase the amount of Cr available for leaching in samples with longer curing periods. Secondly, the potential for oxidation of Cr(III) to more soluble Cr(VI) has been suggested previously [Petersen (1997)]. This phenomenon may explain the observed increase in Cr leaching in samples which have cured for longer.

The effect of *w/s* on Cr leaching for the solidified FeCr Dust is minimal. The maximum effect which a change in w/s has on Cr in solution leaching is to cause a change of 0.5 ppm of Cr leached which, considering the inherent variability in leaching results discussed in Chapter 6, is insignificant.

Correlation between Predicted and Observed Cr Leaching

A plot of experimental values of Cr leached versus those predicted by the model equation appears in Figure 8-11, Figure 8-12 and Figure 8-13 for the solidified ETP 1, ETP 2 and FeCr Dust products. For the solidified ETP 2 and FeCr Dust products predicted results show good correlation with measured results, with R = 0.97 and 0.91 respectively. This implies once again that the model accurately describes Cr leaching within the 99.5% confidence limit. Furthermore, Figure 8-12 and Figure 8-13 indicate that scatter around the straight line appears to be random.

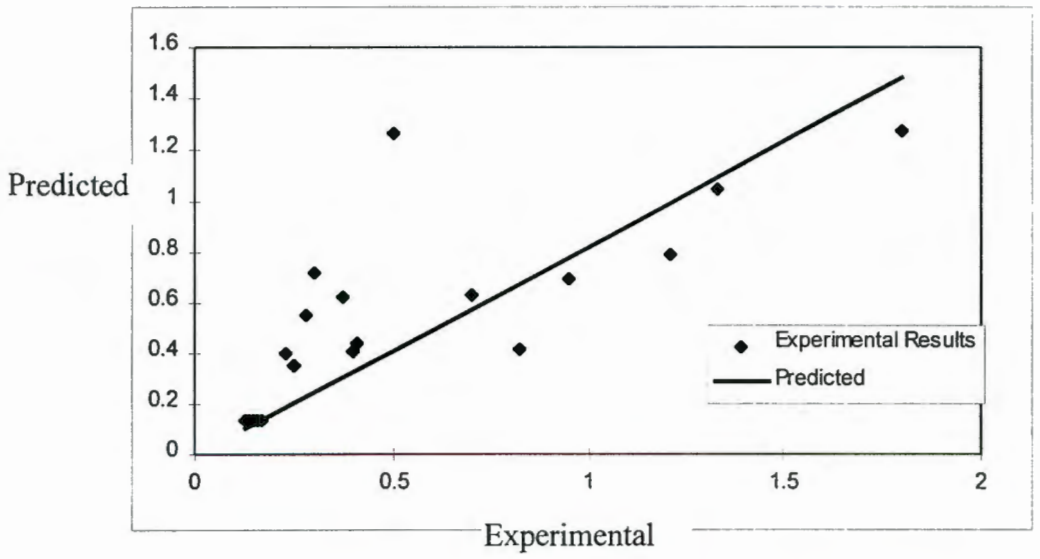

Figure 8-11 - Correlation between Experimental Cr Leaching Results and those Predicted from the CCRD Model (indicated by the straight line) for ETP1

The coefficient of correlation between experimental and predicted data for ETP 1 is 0.77, which is lower than for strength results and other leaching results discussed below (see Figure 8-11). Although the t-test still suggests that the predicted results accurately describe the experimental results, Figure 8-11 indicates a divergence of results from the straight line. Once again, due to the low leachate Cr levels no conclusion can be drawn as to whether observed trends in the responses of the Cr leaching of ETP 1 are as a result of changing operational variables or merely analytical or experimental inconsistencies.

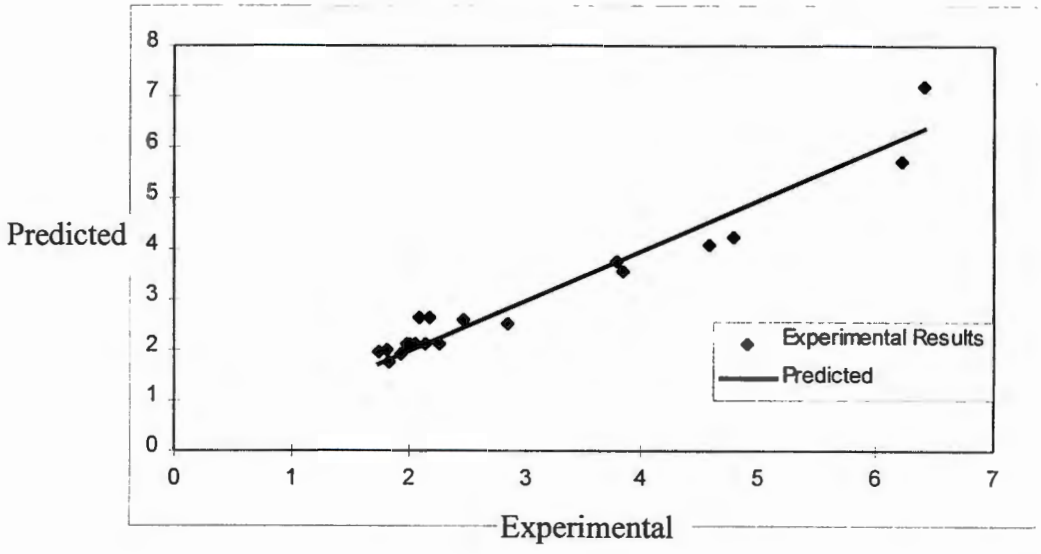

Figure 8-12 - Correlation between Experimental Cr Leaching Results and those Predicted from the CCRD Model (indicated by the straight line) for ETP2

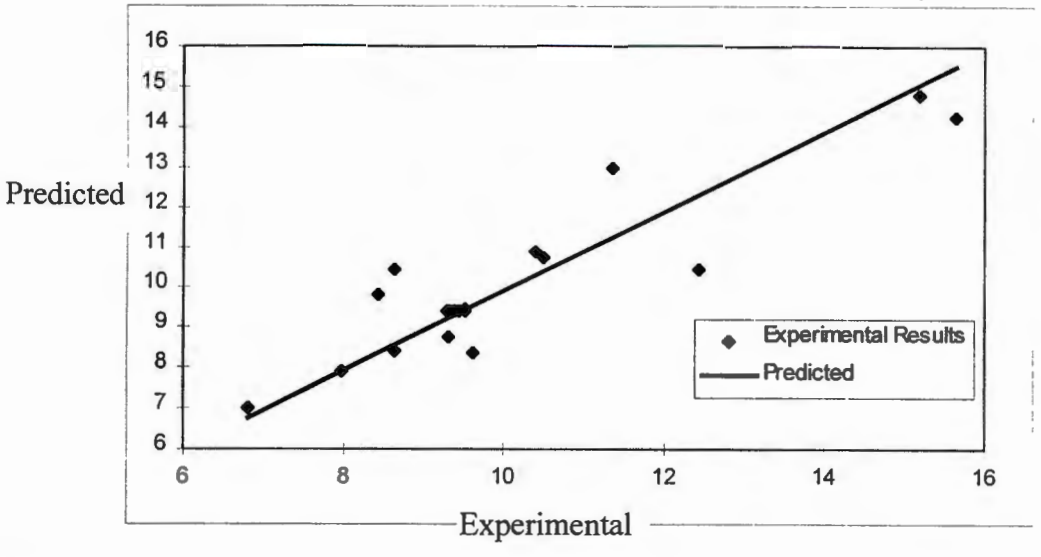

Figure 8-13 - Correlation between Experimental Cr Leaching Results and those Predicted from the CCRD Model (indicated by the straight line) for the FeCr Dusts

(iii) Zinc Leaching

The surface for Zn leaching generated by the model equation is plotted in Figure 8-14 as a function of cement content and curing time for the FeCr Dust products. Zn is not present in the ETP solids. The model equation indicates that cement content is the only significant variable in determining Zn leaching from the solidified FeCr Dust.

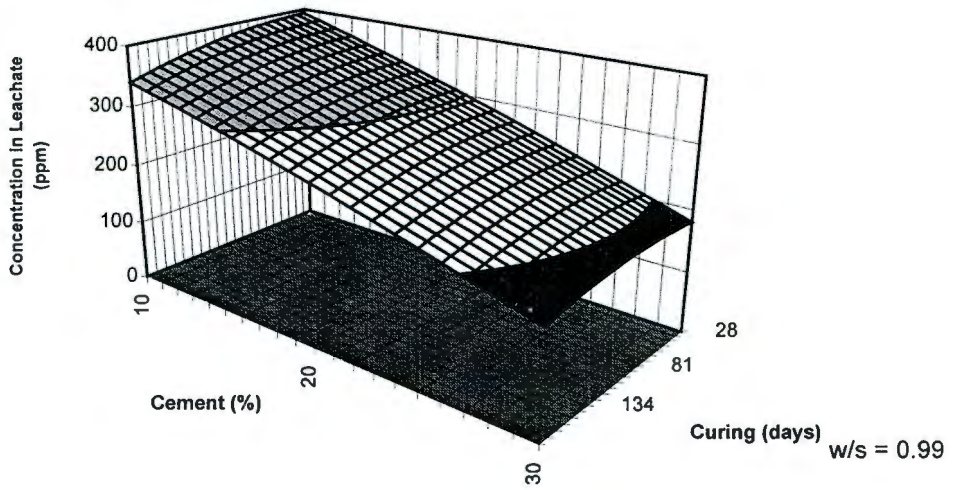

Figure 8-14 - Zn Release from the Solidified FeCr Dust product as a function of Cement Content and Curing Time, w/s constant

Figure 8-14 indicates a reduction in Zn release as the amount of cement added increases. This is as a result of pH effects observed previously: as the amount of cement present in the initial mixture is increased, so the pH of the leachate increases (see point (i) above) and Zn solubility decreases. This is in line with observations from Chapter 6. Once again, Zn contained in the dust core is expected to be immobile in the tests used here.

The effect of w/s and curing time on Zn leaching are observed to be minimal. The coefficient of correlation between predicted and measured results for Zn leaching is R=0.92. This once again suggests acceptable correlation between experimental results and responses predicted by the design model to the 99.5% confidence limit. A plot of experimental vs predicted results once again indicates that scatter around a straight line is random, providing support for the observation that the model is effective in predicting results.

(iv) Calcium

The results of Chapter 6 and 7 showed that Ca is contained in one of three ways in the S/S products. The first is solubilized in the pore solution. The second is as the hydroxide species

which is readily mobile in low pH environments, while the third is as part of the cement hydration product. This latter Ca was found in Chapter 6 and 7 to be readily mobile in acetic acid and may slowly solubilize in distilled water. In the ETP products, $Ca(SO_4)$ is also expected to be formed, due to the high sulphate concentrations in the streams from which these solids were precipitated (see Chapter 3). This Ca is, however, expected to be insoluble in the TCLP test conditions. The response surfaces predicted by the model equation for Ca leaching are presented in Figure 8-15 to Figure 8-17 as a function of cement content and curing time for the three solidified products.

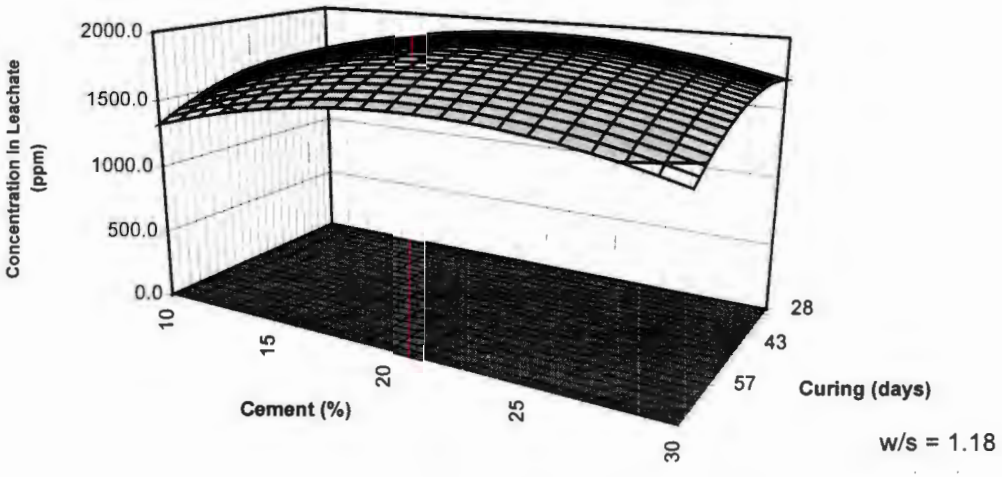

Figure 8-15 - Ca Release from the Solidified ETP 1 product as a function of Cement Content and Curing Time, w/s constant

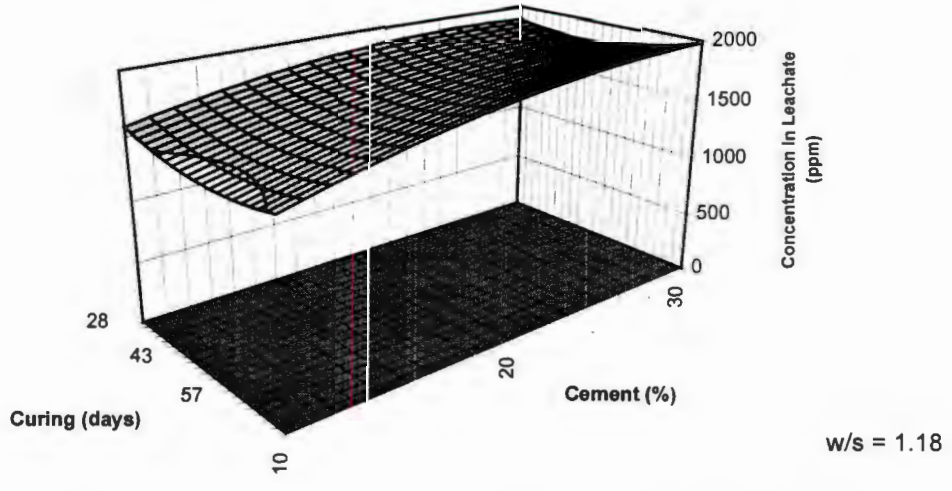

Figure 8-16 - Ca Release from the Solidified ETP 2 product as a function of Cement Content and Curing Time, w/s constant

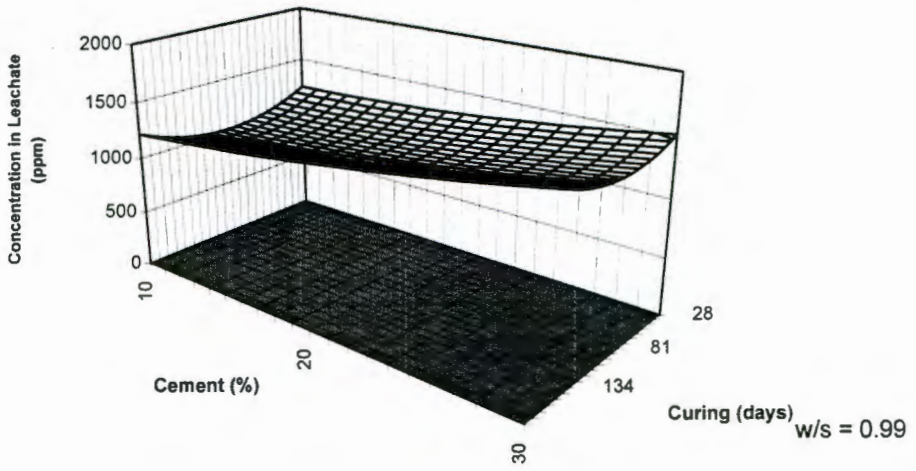

Figure 8-17 - Ca Release from the Solidified FeCr Dust product as a function of Cement Content and Curing Time, w/s constant

The results of the CCRD modelling indicate the following with respect to Ca.

(i) Ca leached increases with increased cement addition. During cement hydration calcium is released into the pores as $Ca(OH)_2$. Higher cement additions thus imply higher amounts of free Ca and consequently greater amounts of Ca released in the TCLP. As mentioned above, in previous chapters it was observed that the S/S agglomerate is readily broken down during the TCLP which was suggested to result in release of Ca from the cement hydration products. This Ca is expected to contribute to calcium leaching here, explaining higher amounts of Ca leached as cement content is increased. The ETP products contain large amounts of $Ca(SO_4)$, but this complex is relatively insoluble and will not contribute significantly to leaching.

(ii)w/s ratio is observed to have an insignificant effect on calcium leaching for all three waste products. The amount of potentially mobile Ca will be independent of w/s, since the amount of cement which hydrates, and hence Ca release, will not be a function of w/s.

(iii) For the ETP 1 products, maximum calcium release is observed at an intermediate cement content and curing time. For the ETP 2 and FeCr Dust products, the minimum amount of calcium leached is at intermediate curing times. At both short and long curing periods release increases. Due to the fact that Ca is released as cement hydration progresses, it would be expected that Ca release increases as a function of time. It is proposed that a kinetically controlled complexation reaction - either in the formation of secondary CSH, or in formation of complexes with anionic and cationic species from the wastes - converts calcium in the pores into an insoluble species. This explains the decrease in Ca leached as curing increases.

The coefficient of correlation between experimental and predicted results for Ca is 0.90 for the ETP 1 products, 0.88 for the ETP 2 products and 0.93 for the FeCr Dust products. Once again, these high values of R indicate prediction of experimental results by the model for all three products at the 99.5% confidence limit. These observations are supported by plots of predicted vs experimental results which indicate that scatter is random around a straight line.

8.2.7 Optimization of the Operational Variables using the Model Equation

One of the aims of the laboratory work was to evaluate the optimum parameters for maximum strength and minimum leaching. To carry this out, the SOLVER routine supplied with the Microsoft EXCEL software package was used. This routine uses the forward difference method for calculating the derivatives of the function and, by iterative calculation, solves for the variable values which give the optimum response. Details of application of this routine using the spreadsheet attached to this thesis are presented in Appendix F2. Optimal values for the objective functions in this work, being maximum strength and minimum leaching, within the constraints of the variable values presented in Table 8-1 are presented in Table 8-4 below. Note that no full factorial design was carried out for the strength of the solidified FeCr Dust products. Optimal operational variable values for the other leaching responses appear in Appendix F3.

Table 8-4 - Optimal variable values for maximum strength and minimum leaching within the range of variables under investigation

Variable	ETP 1		ETP 2		FeCr Dust
	ITS	Cr leaching	ITS	Cr leaching	Cr leaching
Water/solids	1.1	1.2	1.1	1.1	0.9
Cement (%)	30	23	26.5	19	23.1
Curing time (days)	70	49	70	70	180

In industrial application of the technology it is difficult to control the operational variables to achieve the exact values presented in Table 8-4. Prior to discussing the results in Table 8-4, it is significant to identify the sensitivity of the system to variations in the values of the operational variables. Table 8-5 shows the effect of a change in the operational variables

on the ITS and Cr leaching responses for the ETP 2 products. Responses for the other two products were similar and hence are not reported here.

Table 8-5 - Effect of Changing Operational Variables on Responses

Variable	Increase/Decrease in Variable Value	% Deviation from Optimum	Decrease in ITS	Increase in Cr Leaching
w/s Ratio	0.05	4.5%	0.1% - 3.8%	1.3% - 2.6%
Cement	5%	18.8%	3% - 4%	13% - 18%
Curing Time	10 days	14.3%	1.2% - 1.4%	1% - 2.5%

From Table 8-5 it can be seen that strength is relatively insensitive to the changes in the operational variables in the ranges indicated here. Cr leaching is sensitive to a change in cement addition, but is not as sensitive to the other variable values. Control of cement addition in practice is, therefore, important, but fluctuations in the residual water content of the filter cakes will not have as significant an influence on either Cr retention or strength.

Based on the observations of Table 8-4, it is suggested that when implementing the S/S process, the w/s ratio be kept as low as is possible while still allowing for the formation of a workable paste. With regard to the optimal cement contents for maximum strength and minimum leaching presented in Table 8-4, the following is considered. It is seen that high cement contents lead to high strengths, which is in line with observations throughout this work. Intermediate cement contents, however, favour improved retention. Since retention is the primary goal of S/S, with structural implications being of secondary consideration, it is suggested here that cement contents of approximately 20% be used for maximum retention. According to Table 8-5 this implies a reduction in strength of up to 10%. Considering that the strength of the products in this work were well above legislatory requirements, it is suggested that this reduction in strength is insignificant.

Finally, with regard to curing time, it is recognised that the material will ultimately be placed into landfill and left there for unspecified time periods - up to hundreds of years. Table 8-4

indicates that, for ETP 2 and the FeCr Dust products, maximum strength and minimal Cr leaching occurs at maximum curing for the times investigated here. This suggests that as curing proceeds, product performance (indicated by high strength and low leachability) is improved. For the ETP 1 products strength is once again maximum at long curing times. Although it is seen that Cr leaching reaches a minimum at an intermediate curing, it is recognised that Cr concentrations in the ETP 1 leachates were low and hence results were limited in accuracy.

Further practical implications of S/S, including costing of the processes, are discussed further in sections 8.5 and 8.6 below.

8.2.9 Correlation Between Strength and Leaching Behaviour

One of the hypotheses of the work reported in this thesis was the potential existence of a relationship between strength and leaching behaviour. Strength depends on the extent of cement hydration and therefore on the formation of bonds between particles. Leaching, in turn, depends on both the buffering capacity of the S/S products and on the accessibility of the constituents to the leachant, which will be a function of the nature and tortuosity of the pore network - again a function of cement hydration. It was based on these statements that the hypothesis was initially proposed.

In Table 8-4 the optimal variable values for maximum strength and minimum leaching are presented. While taking into account the sensitivity of the responses to the variables as shown in Table 8-5, it would appear that maximum strength and minimum Cr leaching can be achieved at similar operational variable values. Comparison of graphs such as those presented in Figure 8-2 with Figure 8-8 confirms the existence of such a relationship.

The significance of the relationship is the following. The ITS test was observed to be a simple, and economical test compared to the TCLP. It is suggested here that, when assessing S/S technologies for application to other waste products, it is possible to cut down on the number of leach tests required to fully characterise the system. For example, considering the factorial design discussed above, a decision may be made to perform leach tests only at the axial points (being those defining the maximum and minimum values of the operational variables) and strength tests at all of the points. Based on the correlation presented here, the strength results may be used to predict the ultimate effect of changing the operational variables on leaching.

8.3 Summary of Observations from the CCRD

This section of work was performed with three main aims. These were, firstly, to investigate the use of the experimental design technique to characterise S/S systems, secondly to determine values of the operational values which give the combined desirable attributes of maximum strength and minimum leach potential and finally to provide support for the hypothesis of the existence of a relationship between strength and leaching behaviour in S/S matrices.

In support of the former, the experimental design was shown to aid in development of models to predict the strength and leaching behaviour of the S/S products within an acceptable degree of error. All three variables were found to be significant in determining strength properties of the S/S materials. The effect of the operational variables on leaching depends on the type of waste treated and the element of interest.

The fact that different waste products respond to changing the operational variables in different ways reiterates the need for evaluation of the appropriateness of the process for all waste products prior to implementation of the technology. The CCRD was found to provide a useful tool for two aspects of this evaluation. Firstly, the CCRD can be used to develop an experimental matrix which provides a rigorous framework within which laboratory experiments can be planned in order that they will fully characterise the system. Secondly, the results of the experimental design can be used to find the values of operational variables to provide a product with maximum strength and minimal leaching potential.

At the beginning of this thesis the hypothesis of a relationship between strength and leaching potential of the S/S products was discussed. This was based on the fact that both strength and the mobility of metals would be, to some degree, related to the extent of formation of the cement hydration products. The observations presented here, that lower strength products leach more Cr than stronger products, provides support for this hypothesis.

8.4 Effect of Additives on Properties of S/S Products

The work presented in this thesis thus far has focused on the use of cement as the sole treatment agent for the waste products from the ferro-alloy industry. In practice, however, it is

common to use cement in conjunction with other additives for treatment purposes. This is either to improve strength and retention characteristics of the products or to reduce cement requirements and thereby the costs of the treatment process. Furthermore, the additives may be wastes themselves, and thus using them as an additive has the added advantage of co-disposal.

The following sections present qualitative observations with regards to the use of calcium hydroxide and fly ash in the treatment of the FeCr Dust wastes.

8.4.1 Effect of Calcium Hydroxide Content on Leaching

Calcium hydroxide is sometimes added to an S/S process to improve the quality and performance of the technology in practice. This is usually done for one or more of three primary reasons.

(i) To neutralize acidic wastes prior to addition of cement - in the case of the ETP solids this step has already been carried out as part of the process,

(ii) The presence of calcium hydroxide in solution is required for the precipitation of CSH - the cement hydration products. Conner (1993) suggests that if there is insufficient $Ca(OH)_2$ in solution for complete cement hydration, the formation of CSH will be limited and a product with inferior strength and retention properties will occur.

(iii) To increase the buffering capacity of the S/S product against acidic groundwaters.

The effect of the addition of calcium hydroxide on leaching from the solidified FeCr Dust products was assessed using a simulated acid rain type leach solution which was taken to be representative of low pH rainfall. The primary differences between this solution and that used in the TCLP previously are:

(i) The acid rain solution has less buffering capacity than the TCLP solution, and solution pH is quickly raised to the naturally alkaline pH of the S/S products.

(ii) The TCLP solution is an organic acid, while the acid rain solution consists of a nitric/ sulphuric acid mix.

Other leaching conditions including time, temperature, separation methods, leachate analysis, were consistent with those used in the TCLP.

Leach test results are presented in Table 8-6. In this table, $Ca(OH)_2$ additions of 1.6% and 5% are presented, being based on $Ca(OH)_2$ to dry waste solid ratio. Although the cost of lime is low, it is desirable to use the minimum amount of additive to give the maximum benefit. This reduces bulk increases to the waste. The $Ca(OH)_2$ additions in Table 8-6 were identified to be sufficient to neutralize the FeCr Dust wastes, which is desirable for the reasons discussed above, while still being low enough to minimize bulk increases [Richard Paxton Associates (1996)].

Table 8-6 - Leach Test Results from S/S Products made with $Ca(OH)_2$ (results in ppm)

Cement (%)	$Ca(OH)_2$ (%)	Leachate pH	Cr	Ca
7.5	0	11.5	5.1	75.3
	1.6	12.5	1.1	102.5
13.75	0	12.0	1.3	186.2
	5	12.3	0.8	195.2
20	0	12.2	1.4	102.8
	1.6	10.5	0.6	184.3

It is seen that addition of $Ca(OH)_2$ results in a reduction in Cr release. The Cr in the leachates was found by UV spectrometry to be Cr(VI). Cr(III) solubility was shown in Chapter 2 to be below detection limits at the pH values observed here. Since Cr(VI) is soluble across the entire pH range, leaching of Cr(VI) will not be a function of pH. Lime is sometimes added to S/S processes to provide extra calcium for the formation of CSH and hence the improved retention of Cr as a consequence of $Ca(OH)_2$ addition is due to increased physical retention due to a more developed cement hydration matrix [Conner (1993)].

Zn levels in the leachates were below detection limits. At the pH of the leachates, the solubility of Zn is once again negligible. Calcium is observed to increase with increased $Ca(OH)_2$ addition which is as would be expected.

In summary, therefore, the addition of $Ca(OH)_2$ has the potential to contribute to improved Cr retention due to the more extensive formation of the cement hydration products and hence the formation of a stronger, less porous monolith. This is similar to what was seen in the case of

increased cement addition, and is suggested to hold for other species for which retention is dependant on physical encapsulation.

8.3.1 Effect of Fly Ash on Leaching and Strength

In a parallel study, the effect of the addition of coal power station fly ash on strength and leaching of metals from solidified FeCr Dust was determined. Results of this work appear in Barton and Dickason (1994). Samples were made in the same way as in this work, except that various proportions of the cement were replaced by fly ash. The following two main conclusions were drawn in this work:

(i) At low water additions, ITS decreases as the amount of fly ash increases. The opposite is observed at high water contents.
(ii) Substitution of fly ash for some of the cement in the S/S product reduces the retention of Cr. The pH of leachates from an EE-type extraction of samples containing fly ash are to the order of 7, versus 10.5 from the S/S products without flyash. Reduced pH implies greater solubility of Cr(III), and hence greater leach potential.

Two notes should be made about the results obtained in this study. Firstly, due to time constraints, samples were cured only for periods of up to 28 days. It was noted in Chapter 3 of this work that samples could not be demoulded prior to 14 days of curing. Hence testing in the work of Barton and Dickason (1994) reflects the first four weeks of curing, or the two weeks after demoulding. The formation of pozzolanic products such as those from fly ash can continue for periods up to one year. It is not known whether fly ash will improve either ITS or retention over longer curing periods. Secondly, this study was carried out on only one type of fly ash. Different types of fly ash show a variety of chemical compositions and hence differing pozzolanic behaviour. For this reason fly ash from other sources may be more effective in stabilizing the FeCr Dust than that studied here.

8.3.2 Summary

In summary, therefore, it was found that $Ca(OH)_2$ has potential for contributing to improved waste retention in the S/S products. Although no benefit of the addition of fly ash was found in this work, it is reiterated here that many researchers have found benefit in using fly ash as a

waste treatment additive. Results presented here, therefore, do not rule out the use of fly ash in the treatment of other types of waste products.

8.5 Considerations in the Landfill-Scale Implementation of the Technology

What remains at this point is to discuss the practical aspects of implementation of the technology. This section is divided into two parts. Firstly, mixing and transportation issues are discussed, followed by considerations of landfill location and design.

8.5.1 Mixing, Transport and Placement Considerations

The consistency, and subsequent mixing and transport properties of a freshly prepared S/S mixture will be dependant on, amongst other factors, the particle size distribution of the waste material and the water to solids ratio in the mixture. Should coarse additives form part of the S/S mixture, a different material in terms of mixing and pumping characteristics will be obtained over one which contains only a fine, dust-like material.

The work reported in this thesis has been used in the design of a waste treatment plant from which the wastes arise. Consultation with practitioners who have been implementing the S/S process in practice indicate that the consistency of the fresh S/S mixture will determine the equipment required for mixing, transport and placement in the landfill. A stiff paste will require a high shear type mixer, and transport in trucks. A more fluid S/S formulation, however, could be mixed in a simple cement mixer, and could be transported to the final disposal site by conveyer belts or pumping.

In this specific case, therefore, three options were available for transport of the fresh S/S mixture to the placement site (trucking (stiff pastes) and pumping or conveying (fluid mixtures)). In terms of capital investment, conveyer systems cost to the order of R10 million[1], approximately three times what either trucking or pumping systems cost. It was found furthermore that more fluid mixtures would give problems with both flow out of the placement sites and would also blind drainage systems (these are discussed in section 8.5.2 below).

From Table 8-5 it was identified that the effect of water addition on strength and leaching is relatively insignificant. In large-scale application, therefore, it has been decided to formulate the

[1] One South African Rand ≈ US$ 4.6. Values quoted in the text are 1995 prices.

mixture to be as dry as possible and truck it to the placement site. The mixture is placed in cells of approximately 350 m^3, being large enough to hold one day's production of fresh S/S mixture. It is then patted down using a long-reach patter, in an attempt to remove voids, the presence of which have been shown through this work to be conducive to mechanical breakdown and increased leaching [Paxton (1997)].

8.5.2 Considerations in Landfill Location and Design

The selection of the site for the landfill and the design thereof have to be such that the landfill provides the minimum potential for adverse impact on the surrounding environment. The mechanical stability of the deposit should be ensured by choosing areas in which ground movement is limited. Furthermore, factors such as soil type and permeability and situation of groundwater flows which determine the potential environmental risk in the case of contaminant leaking out of a landfill site, should be considered.

The site selection process should thus include a full site characterization, consisting of characterisation of the sub-surface geology, identification of ground-water conditions and flows, determination of the properties of major subsurface zones, including hydraulic conductivity, the potential for geochemical attenuation behavior and the site stability and strength [Sittig (1979)].

Other practical factors may play a role in site selection. These include proximity to the plant producing the waste, current land use and impact on local communities. Most large-scale mining and minerals processing operations deposit their waste materials on their own properties in close proximity to the operations in order to minimize transport of waste materials over long distances.

In accordance with the results presented in this current thesis, reducing contact with a liquid passing through the site is important to minimize leaching. For this reason it is preferable for a liquid, such as rainwater or groundwater, to pass around the mononlith than through it. Côté and Bridle (1987) recommend among others two ways in which the landfill can be designed such that interface exchanges at the surface of the waste mass are favoured rather than advective transport through the solid mass itself. These are, firstly, to avoid a potential build-up of hydraulic gradients, and secondly, to protect the waste mass from weathering and physical breakdown. The latter is in line with discussions presented in the strength results of Chapter 5. In order to minimize leaching

resulting from exchange at the surface of the waste mass three main recommendations are made. The first is to minimize the waste surface area-to-volume ratio, the second is to ensure a low rate of groundwater flow around the waste and the third is the minimization of contact with acidic waters [Côté and Bridle (1987)].

To collect any leachate which invariably does flow through the site, landfills are usually lined with some type of reduced permeability liners. A liner consists of a material of low hydraulic conductivity which forms the base of a waste deposit. Should any leachate percolate through the waste deposit, it will collect above the liner material. If a drainage or leachate collection system is in place the leachate is collected and removed through controlled channels prior to seepage through the liner. Should no leachate collection system be in place, the collected leachate will gradually seep into the underlying sub-soil and potentially enter groundwater. Commonly used linings include naturally-occurring clay liners, compacted soil or composite liners and geosynthetic liners.

Available options for the treatment of collected leachate include:

- Recycle as part of process water - feasible if the water is not too heavily contaminated,
- Treatment in treatment plants, in processes such as lime-based neutralization and precipitation as described in the scope of this current work.
- Evaporation in evaporation ponds - the liquid is evaporated, leaving the salts in solid form. These salts must be disposed of in a manner which ensures long term stability (S/S is one such option) [Sittig (1979)].

The choice of which option to use will be based on practicality and economic viability. In the case of the landfills which have been designed to contain these specific S/S wastes, the landfills are lined with compacted clay. Berms or embankments surround the landfill to divert rainwater runoff. From the results of this current work, the significance of physical encapsulation, and hence the geometry of the waste form, in metals retention has been highlighted.

The landfill designed for retention of these products has been divided into cells, each cell being large enough to contain $350m^3$, which, in this specific case, is enough to contain one day's production of fresh S/S mixture. The wet mixture is cast into these cells and is allowed to set to form a monolith in which, in accordance with the work presented in this thesis, metals will be both

physically retained (due to the large solid block formed) and chemically retained, provided the buffering capacity of the solid is not consumed. The material in cells is allowed to cure for a number of days prior to new material being placed on top of it - times of 14 days were demonstrated here to be required for the material to set into a block which was self-supporting.

The cell is shaped such that all liquid drains toward the centre and is collected into a common drainage system from other cells. This is combined with rainfall runoff collected from the top of the landfill and is fed into a lagoon. Here the liquid is checked for metals content and is released to a second lagoon. Should the metals contents be unacceptably high, the liquid from the lagoon is treated via reverse osmosis prior to discharge [Richard Paxton Associates (1996)].

8.6 Costing of S/S Operations

Costing of S/S operations in a South African context is difficult, since limited information is available from companies who have put this technology into practice. Information must, therefore, be drawn from information available in literature, which refers primarily to the USA.

Table 8-7, extracted from Means et al (1995), shows the costs of treatment per cubic yard of waste for cement-based S/S treatment. For extrapolation to the work presented in this thesis it is significant to look at figures for plant mixing prior to placement in landfill, ie column 3 on the table. It is seen that reagents and mixing materials constitute the largest proportion of the running costs. Optimization of quantities of the required additives, via a technique such as the CCRD presented in this chapter can, therefore, result in a significant reduction in costs. Furthermore, should it be possible to replace some of the cement added to the samples by one of the additives suggested in section 8.4, especially those which are wastes themselves, costs will be further reduced. Further exploration of the use of alternatives to cement in the S/S process is thus warranted.

Although every waste disposal scenario will take cost considerations into account, the following is noted by Means et al (1995). "Cost is an additional binder screening criterion, although this should be applied only after the interference, chemistry, and disposal / reuse ... have been considered. Because economic considerations are secondary to performance considerations, cost should only be used to screen binders that are significantly less economical or whose benefits clearly do not justify

the added expenditure." It is thus recommended that economics is only one of many factors considered when screening potential waste treatment technologies.

Table 8-7 - Comparison of Major Cost Elements of Cement-Based Solidification/ Stabilization with Cement [Means et al (1995)]

	Cost, $/Cubic Yard			
Category	In-Drum Mixing	In Situ	Plant Mixing	Area Mixing
Labor, overhead, and profit	216.30	1.40	1.10	3.00
Equipment and metering	65.40	1.60	0.70	3.00
Conveyance	NA	NA	1.40	
Pretreatment	NA	NA	0.50	NA
Monitoring and testing[a]	115.40	4.00	3.10	5.10
Reagents and mixing materials	31.10	31.10	31.10	31.10
Offsite disposal (nonhazardous waste)	NA	NA	3.10	NA
Supplies	84.60	0.60	0.80	1.30
TOTAL	512.80	38.70	41.80	43.50

[a]Monitoring and testing costs assume that in-drum wastes require sampling of each drum, while the other approaches require representative samples of a large, relatively uniform body of waste. Source: Arniella and Blythe, 1990, p. 101. Excerpted by special permission from *Chemical Engineering*, February 1990.

NOTES:
1. NA = not applicable
2. Not included are costs for mobilization and demobilization, engineering and administration, and health and safety.
3. All mixes are based on 30% Portland cement and 2% sodium silicate.
4. Cost for delivering reagent is not included.
5. Approximate production rates assumed are: in-drum mixing, 5 drums/h; in situ, 500 yd^3/d; plant mixing, 650 yd^3/d; area mixing, 400 yd^3/d.

8.7 Concluding Remarks

In terms of the characterisation of the S/S products, the following points were identified:

(i) The CCRD provides an effective tool for determining the effect of process variables on product responses, and allows for calculation of the optimum variable values for optimum responses.

(ii) The process variables for which give rise to maximum strength and minimum leach potential must be found for each waste product, as responses are affected by the chemical and physical nature of the waste product.

(iii) A relationship between strength and leaching behaviour of the S/S products was identified using the factorial design.

(iv) Addition of $Ca(OH)_2$ to the S/S mixture results in improved Cr retention

(v) The fly ash used in this work had no effect on Cr leaching at short curing periods.

Based on the results presented here, the following comments are offered with regard to the proposed physico-chemical model of the S/S products:

(i) The primary bonding mechanisms between solid particles in the S/S product depends on the amount of cement present in the mixture. In solids with higher cement additions, the products of cement hydration are primarily responsible for the solid structure of the product. In low cement samples, precipitates in the pores may contribute to strength characteristics of the solid.

(ii)Release of Cr(VI) has been confirmed to be controlled by physical encapsulation effects. Cr(III) release is primarily controlled by pH, although ultimate solubility of Cr(III) will be affected by other anions and cations in solution. Cement content plays the biggest role in determining Cr release.

(iii) Zn leaching has once again suggested to be a function of pH, indicating that all potentially mobile Zn is contained as the insoluble $Zn(OH)_2$ form in the S/S products.

(iv) Ca release depends on both the amount and chemical speciation of the Ca in the S/S product. $Ca(SO)_4$ is expected to be insoluble. Ca from $Ca(OH)_2$ is readily released into solution. Ca bound in the cement hydration products may also be released into solution.

These results thus support observations from previous chapters with regard to the validity of the physico-chemical model proposed in Chapter 4.

The following comments were made with regard to practical aspects of the large-scale implementation of the S/S process.

(i) Consistency of the fresh S/S mixtures will determine mixing and transport requirements.

(ii) Location of a landfill site is determined by a number of factors including the mechanical stability of the deposit, soil permeability, situation of groundwater flows, proximity to the plant producing the waste, current land use and impact on local communities.

(iii) The effective design of waste disposal sites is necessary to reduce both infiltration of liquid into the landfill and subsequent transport of toxic contaminants out of the site.

(iv) Leachate collection systems will minimize entry of contaminants into the environment.

(v) Reagents and mixing materials contribute the highest proportion of costs to the S/S operations. The use of cheaper additives, especially if they are wastes in themselves, to replace some of the cement in the S/S mixture can significantly reduce costs and further investigation into this area of S/S is therefore warranted.

9.

Conclusions

In this chapter the results from work presented in this thesis are summarized. The physico-chemical model, proposed at the beginning of this thesis, is re-examined. Recommendations are made for the path for future work, and the overall significance of the study is discussed.

9.1 Summary of the Background to the Study

The Minerals Beneficiation industry was identified to be the largest contributor to both the total and hazardous waste production streams in South Africa. The extensive growth in the industry and the associated increase in waste production has resulted in increased pressure on the industry to look more critically at its production of- and disposal options for- its waste.

Of interest in this study were wastes from the ferroalloy industry, and, in particular, ferrochromium production. A number of process steps result in the production of wastes. Such wastes often contain high levels of metals, including mercury, zinc, cadmium, chromium, boron, lead, arsenic, magnesium, manganese, sodium, potassium and antimony, which preclude the wastes from direct disposal to landfill without some form of pretreatment. Cement-based Solidification/ Stabilization (S/S) was identified to be a potentially appropriate technology for the treatment of wastes prior to consignment to landfill.

In this work a study was made of the application of S/S to the pre-landfill treatment of two different waste products from the ferrochrome industry. The wastes chosen were a ferrochromium smelter dust (designated as FeCr Dust) and two metal-rich precipitates from wastewater streams (designated as ETP 1 and ETP 2). These wastes were shown throughout the thesis to differ both physically and chemically.

Some work has been reported in open literature on the S/S of liquid wastes and slurries with low solids contents. It was identified here, however, that little work has been reported on the

cement-based S/S of wastes containing primarily solid material. In order to ensure effective retention and long-term physical stability of a solidified product once consigned to landfill, a need exists for a complete characterisation of physical and chemical interactions between the waste and the treatment agent, in this case cement, prior to implementation of the process. The study for which the results are presented here was launched on this basis.

9.2 Summary of Results

In Chapter 2 a literature review was presented which provided the reader with an understanding of the chemistry and mechanisms associated with the hydration of cement. A discussion of retention of metal species in cement-based S/S products was presented. It was identified that cement chemistry is complex, and, when considering interactions between metal-laden wastes and cement in an S/S product, isolation of the effect of different metals on cement hydration is not straightforward.

In Chapter 3, the wastes of interest in this study were characterised. It was found that all waste products contained high levels of heavy metals, and specifically Cr, which precludes their direct disposal to landfill. Furthermore, the ferrochrome smelter dusts contain high levels of mobile zinc.

Based on literature observations and preliminary investigations undertaken by the author, three operational variables were chosen as being significant in determining the quality and performance of the S/S products. These are water to solids ratio, cement content and curing time. To ensure effective setting of the cement - FeCr waste product, a preliminary wash of the untreated dust was required to remove much of this soluble chromium and other salts which inhibit cement hydration. Due to the high solids content and fine particle sizes of the dusts, it was observed furthermore that higher water to solids ratios are required to produce a workable paste than has been shown to be required for both cement pastes and in other S/S studies reported in literature (see, for example, Ivey et al (1990) and PCI (1986)).

A fundamental physical and chemical characterisation of the S/S products was presented in Chapter 4. The following observations were made based on these results. The morphology of

the solidified FeCr Dust was identified to be significantly different to that of hardened cement paste (hcp). The 'fibrils' formed during cement hydration are shorter than those found in hcp and form a less continuous matrix. Furthermore, the Ca:Si ratio in these fibrillar structures is lower than for Calcium Silicate Hydrate (CSH) found in hardened cement pastes. This was explained by differing pore solution compositions between hcp and the S/S products which results in the precipitation of different hydration products.

X-Ray Diffraction (XRD) identified the S/S products to be largely amorphous. Two crystalline CSH structures found in hardened cement paste were not isolated in the S/S products. No crystalline $Ca(OH)_2$ or ettringite were found in the S/S products.

No evidence of metal incorporation in cement hydration structures was found using the fundamental characterisation tools presented in Chapter 4. The low cement contents (implying low amounts of cement hydration product formation) suggested that any incorporation which does occur will be below the limits of the analytical equipment used here.

X-Ray maps indicated that Cr is often associated with Fe in the S/S product. Fe-Cr complexes, assumed to be chromites, are suggested to originate from the original ores used in process. Mercury Intrusion Porosimetry indicated a decrease in pore size and pore volume as the amount of cement added to the S/S mixture was increased. This is due to more extensive formation of cement hydration product. Furthermore, higher porosities were obtained as water to solid ratios were increased. Permeabilities of the S/S products were observed to be within regulatory requirements. At the end of Chapter 4 a physical and chemical model of the S/S product was proposed based on observations from literature and the authors own initial experimental. The rest of the thesis was aimed at exploring further the appropriateness of this model.

Chapter 5 investigated physical aspects of the products. The strength characteristics of S/S products were reported and discussed. In terms of meeting regulatory requirements, it was found that the Indirect Tensile Strength (ITS) of the S/S products was significantly higher than that required by statutory requirements for S/S products placed in landfill.

A number of strength parameters were measured in this work. These had two aims. Firstly, to provide an understanding of factors which affect bonding and fracture mechanisms within the product, and secondly, to facilitate the prediction of fundamental strength characteristics from quick and economical tests. The ITS, as well as $K_{IC,}$ the critical strength intensity factor, the yield strength, $\sigma_{YS,}$ and the plastic zone size, r_p, were all observed to be a function of the operational variables investigated in this work. Cement content causes an increase in the amount of hydration product present per unit volume. Furthermore, the extent of hydration of the cement is a function of curing time, as curing can proceed for periods of up to a year. The water to solids ratio (w/s) determines the porosity of the agglomerate. Hence the strength and fracture behaviour are a function of the bonding between the solid particles within- and the porosity of- the agglomerate, which, in turn, are a function of the operational variables.

The stress intensity factor, K_{IC}, and ITS were observed to be strong functions of cement content and water to solids ratio. K_{IC} is a measure of the strength and type of bonds between the individual particles and will thus be related to both the amount of cement hydration product formed and the porosity of the end product.

The yield strength, $\sigma_{YS,}$ which indicates the load required to permanently deform the solid, and the plastic zone size, r_p, which indicates the size of the zone over which this permanent deformation occurs prior to fracture, showed the following. Yield strength decreased with increasing water to solids ratio and increased with increasing cement content. The plastic zone size increased with increasing cement content. As the solids density within the agglomerate increases due to increased amount of cement hydration product, the area over which energy can be spread prior to permanent deformation occurring also increases, and hence the greater is the plastic zone size.

Values of the critical strain energy release rate for crack propagation, G_c, showed a wide scatter in results due to both packing inconsistencies and the fact that errors in calculated values of K_{IC} are carried forward into the calculation of G_c. For this reason no accurate comments could be made about the effect of the operational variables on G_c.

A correlation was identified between ITS and K_{IC}. This is seen to have value in the prediction of fundamental strength characteristics from easy to use and economical tests. It was suggested that this correlation could be used to predict K_{IC}. The maximum number of tests will usually be governed by both time constraints and economic considerations.

Chapter 5 identified strength characteristics to be both a function of amount of water and cement hydration product in the agglomerate.

Chapters 6 and 7 continued the analysis into a chemical characterisation of the S/S products via a number of different leaching tests. These included pore water extrusions, the Toxicity Characteristic Leaching Procedure (TCLP), the Equilibrium Extraction test (EE), the Sequential Chemical Extraction test (SCE), agitated kinetic tests, the Non-Agitated Kinetic Test (NKLT), as well as pilot scale lysimeter tests. Based on these results, the following observations were made with regard to chemical aspects of the S/S products:

9.2.1 Solid Decrepitation

Acetic acid, often used as a leachant to simulate an aerobic environment in which microbial activity is a possibility, was used as lixiviant in a number of the leach tests in this work. The acid was observed to cause rapid breakdown of the solid structure. In the case of the agitated kinetics tests and the TCLP of Chapter 6, this was indicated by a reduction in particle size. In the acid NKLT, a distinct leach front is formed as the acid penetrates the monolith. It was suggested that removal of Ca from the cementitious products by the acid is responsible for this observed breakdown. The cementitious products are responsible for maintaining the solid structure. The removal of Ca from the cementitious products was also suggested in the case of distilled water leaching, but this process was observed to be slow, and the effect of Ca removal on solid structure over the time periods studied here was suggested to be insignificant. In the long-term, however, wastes may remain in a deposit for hundreds of years. The potential for slow dissolution of the product with an associated release of metals warrants further study.

9.2.2 Buffering Capacity of the S/S Products

In both the distilled water leaches and the column leach tests, the buffering capacity of the S/S product was observed to be sufficient to raise the pH of the leachant solutions to the alkaline range - in the case of the NKLT to a pH of between 8 and 10, in the EE and the lysimeter tests to a pH of approximately 11.5. The high pH was suggested to be maintained due to alkalis, including calcium and potassium hydroxide, released into solution.

In acetic acid leaches the S/S product raised the solution pH from 2.9 to above 4 in the NKLT and to approximately 5.5 in the TCLP and the agitated kinetic tests. The buffering capacity of the S/S products was not sufficient to neutralize the acidic leachants.

pH plays a significant role in the release of metals from the S/S products. Some metals were observed to be contained as insoluble hydroxides in the alkaline S/S products, which resolubilize if the pH drops. This is discussed further.

9.2.3 Chromium

A small percentage of the total Cr in the sample is contained solubilized in the pore solution, primarily as Cr(VI). This Cr is readily released into solution when the sample is crushed and agitated with a leachant in agitated tests such as the TCLP and the EE. Furthermore, in both acidic and distilled water kinetic tests, it was suggested that the rate of release of Cr(VI) is controlled by diffusion, after surface washoff occurred. Similar behaviour was observed in lysimeter tests. No Cr(III) was detected in the distilled water leachates and the mild acid leachates from the column test. Cr(III) solubility is at a minimum between a pH of 6 and 11 and hence is not soluble at the pHs of these leachates.

Cr(III) is, however, detected in low pH leachates from the TCLP, the acid agitated kinetic tests and acid NKLT. This indicates that some of the Cr in the S/S product is contained as the insoluble hydroxide species in the pores. This fraction is soluble in acidic environments. The SCE suggests that this Cr constitutes approximately 4-5% of the total Cr in the S/S product.

Kinetic tests indicate that release of Cr(III) is also controlled by diffusion, suggesting that the solubilization reactions are rapid.

In the agitated kinetic tests of Chapter 7 it was observed that higher agitation rates give rise to lower rates of Cr(VI) leaching. The potential for adsorption of Cr(VI) onto solid surfaces, with subsequent kinetically controlled desorption, was demonstrated by monitoring the liquid phase reduction of Cr(VI) to Cr(III) using $Fe(SO)_4$. From a zero concentration of Cr(VI), as time proceeds, more Cr(VI) is released into solution. It was suggested that attrition results in the formation of new, highly active solid surfaces. Cr(VI) from solution adsorbs onto these surfaces and slowly desorbs as Cr(VI) in solution is depleted. Higher agitation rates result in greater attrition, implying a larger surface area for Cr(VI) adsorption and hence less Cr released in the leach tests.

The SCE suggests a large proportion (≈94%) of the Cr is contained as a stable species, presumably as part of the original dust particle. Mobilization of Cr from the stable dust particle would be expected to be observed to be a slow mobilization reaction. Cr from the dust particle was observed not mobilized over the leaching periods studied here and was suggested to be stable in the original dust core.

9.2.4 Zinc

No Zn was found in the pore solution, EE leachate, distilled water NKLT, or leachate from the lysimeter column. In these high pH solutions, Zn will precipitate as the hydroxide species, $Zn(OH)_2$.

Zn was found to be released in the TCLP and the acidic NKLT. This indicates the effect of pH-solubility relationships on the release of Zn. In low pH leachants Zn is mobilized and released into solution. In kinetic tests it was observed that intra-solid diffusion is rate controlling in the release of zinc, suggesting once again that the solubilization reactions are rapid compared to the diffusion process.

The SCE indicated that roughly equal proportions of zinc are contained as a species the release of which is controlled by pH (suggested to be in the $Zn(OH)_2$ form) and that contained as a stable, immobile species. Since no reaction-controlled release is observed in kinetic tests, Zn contained in the stable dust particle is suggested not to be mobilized over the time periods studied here.

9.2.5 Potassium

Potassium, the solubility of which is less dependant on pH than other metals studied here, is found in both the acidic and distilled water leachants. Based on observed results, dissolution of K(OH) is suggested to be significant in determining pore solution pH. Long-term release of K was controlled by diffusion in all tests, after accounting for surface washoff and desorption processes.

The calculated diffusion coefficients for K were lower in distilled water than in acid solutions. It was suggested that the controlling resistance in the case of the acid leaches is diffusion from the leach front through the leached layer to the surface of the solid. In the case of distilled water, diffusion through the solid (in which no leached layer was formed) to the surface controls the rate of leaching.

K was found to be contained in three separate forms:
(i) as species solubilized in the pore solution,
(ii) as that for which release is a function of pH and
(iii)as K which is stable as part of the dust core.
Once again, no long-term mobilizing reaction was observed, suggesting that the K contained in the dust core remains stable over the time periods studied here.

9.2.6 Calcium

Large amounts of Ca are released in the TCLP and acidic NKLT tests. Limited amounts of Ca are present in the pore solutions and EE extracts.

Calcium was identified in Chapters 2 and 4 to form part of the cement hydration product matrix. Furthermore, some of the calcium exists in the pore spaces as $Ca(OH)_2$, a product of the cement hydration reactions. The results presented in the kinetic leaching tests of Chapter 7 indicate both reaction and diffusion contribute to the rate of Ca leaching from the S/S products in distilled water leaches. Release of calcium contained in the pore solutions will be controlled by diffusion, while slow dissolution of Ca from the cement hydration products in the distilled water accounts for the reaction contribution to leaching. In acid leaches, the rate of leaching is controlled by diffusion. Rapid breakdown of the cementitious products is observed during acid leaching due to acid attack.

The SCE and TCLP indicate that a large proportion of the Ca is mobile in low pH environments - that is to say, it is readily removed from the S/S product. These results highlight the fact that the cement hydration products identified in Chapter 4 are readily broken down via acid attack.

9.2.7 Engineering Implementation

In Chapter 8, a factorial design known as the Central Composite Rotational Design (CCRD) was assessed for its applicability to characterizing the S/S processes on a laboratory scale. The CCRD was found to provide an effective tool for determining the effect of process variables on product responses, and could be used to calculate the values of operational variables required for maximum strength of- and minimum leaching from- S/S products.

Using the design, all three operational variables of interest in this work were seen to be significant in determining strength properties of the S/S materials. The effect of the operational variables on leaching depends on the type of waste treated and the constituent of interest. This reiterates the need for evaluation of the process for all waste-binder combinations prior to implementation of the S/S technology on a large scale. The CCRD provides a useful tool for carrying out this evaluation.

Furthermore it was hoped to use the CCRD to provide an indication of the existence of a relationship between strength and leaching behaviour in S/S matrices. Some indication of

such a relationship was found, although further work should be carried out to confirm its existence over a wider range of operational variables and different wastes.

Chapter 8 went further to provide some comments about the extension of the results obtained in this work to large-scale implementation of the technology, and in addition some general comments about the design and operation of landfill sites were made, including:

(i) Addition of $Ca(OH)_2$ to the S/S mixture results in improved Cr retention
(ii) The fly ash used in this work had no effect on Cr leaching at short curing periods.
(iii) Consistency of the fresh S/S mixtures will determine mixing and transport requirements.

9.3 Final Statements on the Model of the S/S Products

In Chapter 4, a model was proposed for the S/S product. It was suggested that the agglomerate material would consist physically of solid waste particles held together by cement hydration products, solids crystallizing out of the pore solution and liquid filling the pore spaces. Both fundamental characterisations of Chapter 4 and strength results of Chapter 5, which indicated the effect of changing process conditions on the agglomerate forming bonds, showed the significance of the contributions of the three bonding products (hydration products, crystallized solids and pore liquid) to overall agglomerate strength.

In the development of the model it was suggested that metal retention in the S/S product could be as a consequence of one or more of the following:

(i) chemical incorporation into cement hydration products,
(ii) precipitation of insoluble hydroxides in the pores,
(iii) in the stable core of the dust products
(iv) adsorption onto solid surfaces
(v) physical encapsulation of solubilized species in the pores due to the tortuous character of the pore network

The following was observations were made with regard to the above proposed retention mechanisms:

(i) Some of the Ca and Mg in the solid was indicated to be found incorporated into the cement hydration product
(ii) The remainder of the Ca and Mg, as well as some of the Zn and Cr(III), is present precipitated as the insoluble hydroxide species
(iii) The remaining Cr, Fe and Zn were indicated to be contained in the stable dust cores of the FeCr Dust
(iv) Cr(VI) and other species found in Chapter 6 to be solubilized in the pore solution were retained physically due only to the tortuous nature of the pore structure of the agglomerate. Some potential for the adsorption of Cr(VI) onto solid surfaces, especially newly created solid surfaces, was identified in Chapter 6.

Based on the results of this work, therefore, the proposed model is suggested to be accurate in describing of the S/S products studied in this work.

When considering the extension of this model to other waste products, the following is suggested. The physical structure of other solid wastes which have been solidified with cement will be similar to that found for the FeCr Dusts. The resultant solids will be agglomerates of fine solids, bound together by the products of cement hydration (short fibrillar Calcium Silicate Hydrate structures). The fineness of the solid, as well as the chemical composition thereof (discussed further below) will affect the extent of formation of these hydration products. Furthermore, the amount of water used in mixing the S/S products (dictated by either the residual water in the wastes or the water required to achieve a workable paste) determines the porosity of the agglomerate and hence affect its inherent strength properties. This latter observation was highlighted by comparing the FeCr Dust products to the solidified ETP wastes.

With regard to the chemical model of other solidified wastes containing similar constituents as the ones studied in this work, similar retention mechanisms to those observed here can be expected. No evidence of chemical incorporation of any of the waste constituents, except Mg

and Ca was found in this work. Metal species which are soluble at the pH of the pore solutions (such as Cr(VI)) are expected to be physically retained as such or sorbed onto solid surfaces. Other metal species (Cr(III), Zn) may precipitated as hydroxides in the pore solutions. In the case of other dust products from the ferroalloy industry, a dust core similar to that observed here, containing stable metal species can be expected. Metals contained in this core are expected to be stable in the S/S product.

Ca and Mg will exist both in the pore solutions and can be incorporated into the products of cement hydration. These are easily leached out during acid attack on the solid.

The fate of anions has not been studied in detail here. It has, however, been suggested that SO_4^{2-} will form insoluble Ca SO_4, while anions such as NO_3^-, Cl^- and F^- will remain solubilized in the pore solutions.

The results presented in this thesis can be used to form a qualitative picture of other solid waste products which have been treated by cement-based S/S. The limitation of the model is recognised, however, to lie in the fact that quantitative analysis of strength and leaching characteristics of other solidified waste products will require individual characterisation, and no predictive statements can be made with respect to these attributes from the results presented here.

9.4 Directions for Future Work

9.4.1 Practical Aspects of the Implementation of S/S

This work has focused on treatment of two specific wastes from the ferroalloy industry. The first is a dust product containing high levels of heavy metals. Many other similar dust products originate from process, all differing primarily with regard to their chemical composition.

The second type of waste studied here is a metal hydroxide precipitate from effluent treatment. The origin of such streams will include processes such as the 1 hour water wash found in this work to be necessary for the treatment of the dusts prior to solidification.

The building and operation of individual solidification processes for each type of waste product described above is an expensive and impractical option. For this reason further work is required to adapt and optimize the solidification process described in this work such that an integrated waste management system is developed which can satisfactorily immobilize all of the wastes from process simultaneously. Such a treatment process would have to be relatively insensitive to variations in the amounts and compositions of the various waste products.

Once an integrated system is developed for waste from a *single* industry, it would be relevant to expand the capabilities of such a system to be able to handle a wide variety of hazardous wastes from a number of industries simultaneously. This would have advantages in improved monitoring of waste disposal practices (in that disposal is centralized) and may also have cost-saving benefits.

One aspect of the treatment which warrants further exploration is the use of additives in the S/S process as a supplement to some of the cement in the process. This is important in three respects. Firstly, additives have the potential to improve performance of the S/S process. Secondly, additives may be wastes themselves, in which case the advantage of co-disposal is found. Finally, since the cost of treatment agents is significant in S/S processes, use of low-cost additives may have cost-saving benefits.

9.4.2 Recommendations for Further Study of the Fundamental Physical and Chemical Properties

The following aspects of the fundamental physical and chemical study presented in this work warrant further investigation:

1. The strength tests used in this work were inconclusive with regard to characterisation of a process zone ahead of the notch tip in the S/S products. Further study to ascertain the size of such a process zone, and the significance thereof on energy dissipation during loading, would provide further fundamental information on bonding within- and strength and fracture of- the S/S products.

2. The strength - leaching relationship proposed and identified in this work indicates that simple strength tests such as the ITS can be used to predict and optimize leaching behaviour, the characterisation of which is more time consuming and expensive to carry out. This suggests potential for reducing costs in the evaluation of waste-binder combinations, and should therefore be explored further.
3. Leaching behaviour was characterised extensively during the course of this work. It is identified, however, that long-term testing, perhaps even in a pilot scale plant, may be warranted to characterise the effect of product breakdown on leaching behaviour. A complex model which takes into account the effect of simultaneous chemical and physical breakdown on leaching behaviour is thus worthwhile developing.
4. The observations of Chapter 7 indicate that long-term dissolution of Ca in distilled water is possible. The extent to which this occurs, and its implications for solid breakdown, warrants further investigation in that it has implications for the long-term breakdown of the product in neutral or alkaline groundwater scenarios.

9.5 Overall Significance of the Study

Results from the study have enabled the development of both a physical and chemical model of the waste products. This model is of benefit in understanding chemical interactions between the waste and the cement and the mechanisms associated with the products physical breakdown. This is suggested to go a long way to predicting the long-term performance of the waste products, measurable by both long-term retention of metal species and physical stability.

The study has further relevance in that results have been suggested to be applicable in the qualitative description of other similar waste products which have been solidified with cement. Results from this work therefore form a basis from which an integrated waste management strategy can be developed whereby the treatment of all hazardous waste outputs from a process may be handled simultaneously.

10.

Bibliography

Abdel-Ghani, M., Petrie, J.G., Seville, J.P.K., Clift, R. and M.J. Adams (1991), 'Mechanical Properties of Cohesive Particulate Solids', *Powder Technology,* 65, pp. 113-123.

Abdel-Ghani, M., Petrie, J.G., Seville, J.P.K. and R. Clift (1990), 'Mechanical Properties of Powder Compacts: A New Experimental Technique to Investigate Scaling Effects in Fracture', Proceedings of Second World Congress, Particle Technology, September, Kyoto, Japan, pp.19-22.

Adams, M. J., Mullier, M.A., Seville, J.P.K. and J.G. Williams (1989a), 'A Fracture Mechanics Approach to the Breakage of Agglomerated Particulate Solids', in *Powders and Grains*, Eds. Biarez and Gourvés, Rotterdam: Balkema, pp. 105-110.

Adams, M. J., Williams, D. and J.G. Williams (1989b), 'The Use of LEFM for Particulate Solids', *Journal of Material Science*, 24, pp. 1772-1776.

Adams, M. J. and B. Edmondson (1987), 'Forces between Particles in Continuous and Discrete Liquid Media', in *Tribology in Particulate Technology*, Bristol: Adam Hilger.

Adams, M. J. (1985), 'The Strength of Particulate Solids', *Journal of Powder and Bulk Solids Technology*, 9, pp. 15-20.

Albanese, J.A. (1990), 'TCLP Rule Promulgated by EPA', *Plating and Surface Finishing*, May, pp. 120-126.

Alexander, M.G., Professor, Department of Civil Engineering, University of Cape Town (1993), *Personal Communication.*

American National Standards Institute (1979), *Standard Testing Methods for the Unconfined Compressive Strength of Cohesive Soils*, Philadelphia: ANSI.

Anders, O.U., Bartel, J.F. and S.J. Altschuler, (1978) 'Determination of the Leachability of Solids', *Analytical Chemistry*, vol 50, no 4, April, pp. 564-569.

Andres, A., Ortiz, I., Viguri, J.R. and A. Irabien (1995), 'Long-Term Behaviour of Toxic Metals in Stabilized Steel Foundry Dusts', *Journal of Hazardous Materials*, 40, pp. 31-42.

Arniella, E.F. and L.J. Blythe (1990), 'Solidifying Traps Hazardous Wastes', *Chemical Engineering*, February 1990, pp. 92-102.

Ashby, M.F. and D.R.H. Jones (1989), *Engineering Materials 1: An Introduction to Their Properties and Applications*, Oxford: Pergammon Press.

Baes, C.F. and R.E. Mesmer (1976), 'Chromium', in *The Hydrolysis of Cations*, Anonymous, New York: John Wiley and Sons, pp. 211-219.

Ballim, Y. (1991), 'A Low Cost, Falling Head Permeameter for Measuring Concrete Gas Permeability', *Concrete Beton*, 11, pp. 13-19.

Barneyback, R.S. Jr and S. Diamond (1981), 'Expression & Analysis of Pore Fluids from Hardened Cement Pastes & Mortars', *Cement and Concrete Research,* 11, pp. 279-285.

Bartlett, R.J. and B. James (1979), 'Behaviour of Chromium in Soils: III Oxidation', *Journal of Environmental Quality*, vol. 8, no. 1, pp. 31-35.

Barton, N. and G. Dickason (1994), *The Effectiveness of Using Fly Ash in the Solidification/ Stabilization of Hazardous Wastes*, Department of Chemical Engineering, University of Cape Town: Internal Report.

Batchelor, B. (1992), 'A Numerical Leaching Model for Solidified/Stabilised Wastes', *Water Science Technology,* 26, 1-2, pp. 107-115.

Batchelor, B. (1990), 'Leach Models: Theory and Application', *Journal of Hazardous Materials,* vol. 24, pp. 255-266.

Batstone, S.T. (1989), *The Safe Disposal of Hazardous Wastes*, vol. 1, Washington D.C: World Bank, pp. 16-18.

Bird, R.B., Stewart, W.E. and E.N. Lightfoot (1960), *Transport Phenomena*, Singapore: John Wiley and Sons.

Bishop, P.L. (1986), *Prediction of Heavy Metal Leaching Rates from Stabilized/Solidified Wastes*, Proceedings of the 18th Mid-Atlantic Industrial Waste Conference, Blacksburg VA.

Boelsing, F. (1988), *Remediation of Toxic Waste Sites: DCR Technology in the Field of Immobilization and Fixation of Hazardous Compounds*, Hanover: Ministry of Economics, Technology and Traffic.

Boynton, R.S. (1970), *Chemistry and Technology of Lime and Limestone*, New York: Wiley and Sons, p. 549.

Bricka, R.M. and L.W. Jones (1989), *An Evaluation of Factors Affecting the Solidification/ Stabilization of Heavy Metal Sludge*, Cincinnati: US Environmental Protection Agency.

British Standard Method BS 7448 (1991), *Fracture Mechanics Toughness Tests: Part 1, Method for Determination of K_{IC}, Critical CTOD and Critical J Values of Metallic Materials.*

British Standard Method BS 5447 (1977), *Test for Plane Strain Fracture Toughness (K_{IC}) of Metallic Materials.*

Brown, W.F. Jr and J.E. Srawley (1966), *Plane Strain Crack Toughness Testing of High Strength Metallic Materials,* ASTM Special Technical Publication, no. 410, Philadelphia: ASTM.

Burns, S.J. and B.R. Lawn (1968), 'A Simulated Crack Experiment illustrating the Energy Balance Criterion', *International Journal of Fracture Mechanics*, vol. 4, no. 3, pp. 339-345.

Brown, W.F. Jr and J.E. Srawley (1966), *Plane Strain Crack Toughness Testing of High Strength Metallic Materials*, Baltimore: ASTM.

Capes, C.E. (1980), 'Particle Size Enlargement', in *Handbook of Powder Technology*, Amsterdam: Elsevier, pp. 23-51.

Carman, P.C. (1956), *Flow of Gases Through Porous Media*, London: Butterworth Publishing.

Cheng, K.Y. and P.L. Bishop (1990), 'Developing a Kinetic Leaching Model for Solidified/Stabilized Hazardous Wastes', *Journal of Hazardous Materials,* 24, pp. 213-224.

Cilliers, J.J., Austin, R.C., and J.P. Tucker (1992), 'An Evaluation of Formal Experimental Design Procedures for Hydrocyclone Modelling', *Fourth International Conference on Hydrocyclones*, Southampton: Anonymous, pp. 31-49.

Claudio, J.R. and A.S. Pedro (1990), 'Solidification of Electroplating Waste Water Sludges with Cement', *Water Science and Technology*, vol. 22, pp. 287-301.

Cocke, D.L. and M.Y.A. Mollah (1993), 'The Chemistry and Leaching Mechanisms of Hazardous Substances in Cementitious Solidification/Stabilization Systems', in *Chemistry and Microstructure of Solidified Waste Forms*, R.D. Spence, Ed., Florida: Lewis, pp. 187-242.

Cocke, D.L., Mollah, M.Y.A., Parga, J.R., Hess, T.R. and J.D. Ortego (1992), 'An XPS and SEM/EDS Characterization of Leaching Effects on Lead- and Zinc- Doped Portland Cement', *Journal of Hazardous Materials*, vol. 30, pp. 83-95.

Cocke, D.L. (1990), 'The Binding Chemistry and Leaching Mechanisms of Hazardous Substances in Cementious Solidifications/Stabilization Systems', *Journal of Hazardous Materials*, vol. 24, pp. 251-253.

Code of Federal Register (1988), 'Toxicity Characteristic Leaching Procedure', Appendix I, vol. 40 (268), Washington DC: Goverment Printing Office.

Code of Federal Register (1980), 'EP Toxicity Test Procedure', Appendix II, Vol. 45 (98), Washington DC: Goverment Printing Office, pp. 33127-33128.

Conner, J.R. (1993), 'Chemistry of Cementitious Solidified/Stabilized Waste Forms', in *Chemistry and Microstructure of Solidified Waste Forms*, R.D. Spence, Ed., Florida: Lewis, pp. 41-82.

Conner, J.R. (1993), 'Stabilising Hazardous Waste', *CHEMTECH*, pp. 35-44.

Conner, J.R. (1986), 'Fixation and Solidification of Wastes', *Chemical Engineering*, November 7, pp. 79-85.

Côté, P.L., Constable, T.W. and A. Moreira (1987), 'An Evaluation of Cement-Based Waste Forms Using the Results of Approximately Two Years of Dynamic Leaching', *Nuclear and Chemical Waste Management,* 7, pp. 129-139.

Côté, P.L. and T.R. Bridle (1987), 'Long-Term Leaching Scenarios for Cement-Based Waste Forms', *Waste Management & Research* 5, pp. 55-66.

Côté, P.L. (1986), *Contaminant Leaching from Cement-Based Waste Forms under Acidic Conditions*, PhD Thesis: McMaster University, Canada.

Côté, P.L. and D. Isabel (1984), 'Application of a Dynamic Leaching Test to Solidified Hazardous Wastes', *Hazardous and Industrial Waste Management,* vol. 851, p. 52.

Cox, X.B., Linton,R.W. and F.E. Butler (1985), 'Determination of Chromium Speciation in Environmental Particles, Multi-Technique Study of Ferrochrome Smelter Dust', *Environmental Science and Technology*, 19, pp. 345-352.

Crank, J.N.R. McFarlane, J.C., Newby, Patterson, G.D. and J.B. Pedley (1981), *Diffusion Processes in Environmental Systems*, Hong Kong: McMillan Press Ltd.

Crank, J. (1970), *The Mathematics of Diffusion*, London: Oxford University Press.

Crosswell, S. (1990), *Lecture Notes on Hydraulic Cements*, Department of Materials Science and Engineering, University of Cape Town.

CSIR (1994), *Saldanha Steel Project Phase 2 - Final Environmental Impact Report* CSIR Report EMAS C94017C.

Cullinane M.J. Jr, Bricka, R.M. and N.R. Francingues Jr (1987), 'An Assessment of Materials that Interfere with S/S Processes', in *Land Disposal, Remedial Action, Incineration and Treatment of Hazardous Waste - Proceedings of the 13th Annual Research Symposium*, pp. 64-71.

Cullinane, M.J., Jones, L.W. and P.G. Malone (1986), *Handbook for Stabilisation and Solidification of Hazardous Wastes*, Cincinnati: US EPA.

Davies, G.M. (1995), *Prediction of Leachate Generation from Minerals Processing Waste Deposits*, Masters Thesis: University of Cape Town.

Davies, R.M. (1949), 'The Determination of Static and Dynamic Yield Stresses Using a Steel Ball', *Proceedings of the Royal Society of London*, A 197, pp. 416-432.

Davis, M.E. (1991), 'Zeolites and Dimolecular Sieves: Not Just Ordinary Catalysts', *Industrial Engineering and Chemical Research*, vol. 30, pp.1675-1683.

De Grood, T. (1991), 'Appeal of Solidification, Stabilisation Grow for Treating Wastes', *Hazmat World*, February, pp. 60-61.

Department of Chemical Engineering (1995), *Final Report on the Solidification/Stabilization of Filter Cakes from the Effluent Treatment Plant,* Department of Chemical Engineering, University of Cape Town: Internal Report.

Department of Chemical Engineering (1993), *Chromium Interconversions in Their Natural Environments*, Department of Chemical Engineering, University of Cape Town: Internal Report.

Department of Water Affairs and Forestry (DWAF) (1994), *Minimum Requirements for the Handling and Disposal of Hazardous Wastes,* Pretoria: Department of Water Affairs and Forestry.

De Percin, P.R. (1989), 'Description of EPA SITE Demonstration of the HAZCON Stabilisation Process at the Douglassville, Pennsylvania Superfund Site', *Journal of Air Pollution Control in America,* vol. 39, p. 283.

Diamond, S. (1975), 'Long-Term Status of Calcium Hydroxide Saturation of Pore Solutions in Hardened Cements', *Cement and Concrete Research,* vol. 5, pp. 607-616.

Diamond, W.J. (1989), *Practical Experimental Design for Engineers and Scientists*, New York: Van Nostrand Reinhold.

Double, D.D. (1983), 'New Developments in Understanding the Chemistry of Cement Hydration', *Philosophical Transactions of the Royal Society of London*, A310, pp. 53-66.

Double, D.D. and A. Helawell (1977), 'The Solidification of Cement', *Scientific American*, vol. 237, no. 1, July, pp. 82-90.

Drews, S.C. and S.I. Mahote (1994), *Laboratory Leach Tests for Modelling Hazardous Waste Containment,* Department of Chemical Engineering, University of Cape Town: Internal Report.

Dustan, A.C., PhD Student, Department of Chemical Engineering, University of Cape Town (1997), *Personal Communication.*

Eary, L.E. and D. Rai (1987), 'Kinetics of Chromium (III) to Chromium (VI) by Reaction with Manganese Dioxide', *Environmental Science and Technology*, vol. 21, no. 12, pp. 1178-1193.

Eaton, C., Zincor (1993), *Personal Communication.*

Echenfelder, W.W. and D.L. Ford (1970), *Water Pollution Control*, New York: Pemberton Press.

Ewalds, H.L. and R.J.H. Wanhill (1984), *Fracture Mechanics*, Delft: Edward Arnold.

Gencor (1996), *Preliminary Characterisation of Tubatse Ferrochrome's East Plant Bag Filter Dust Through the Use of SEM Analysis*, Gencor Process Research - Chromium R&D Department, Technical Note No. Cr96/03.

Glasser, F.P. (1993), 'Chemistry of Cement-Solidified Waste Forms', in *Chemistry and Microstructure of Solidified Waste Forms,* R.D. Spence, Ed., Florida: Lewis, pp. 1-40.

Godbee, H.W., Compere, E.L., Joy, D.S., Kibbey, A.H., Moore, J.G., Nestor, C.W. Jr, Anders, O.U. and R. M. Neilson Jr (1980), 'Application of Mass Transport Theory to the Leaching of Radionuclides from Waste Solids', *Nuclear and Chemical Waste Management*, vol. 1, pp. 29-35.

Godbee, H.W. and D.S. Joy (1974), *Assessment of the Loss of Radioactive Isotopes from Waste Solids to the Environment, Part I: Background and Theory,* Contract No. W-7405-eng-26, Oak Ridge National Laboratory: Oak Ridge, Tenessee.

Gordon, J.E. (1988), *The New Science of Strong Materials*, 2nd ed, London: Penguin.

Goto, S. and Roy, D.Y (1981), 'The Effect of W/C Ratio and Curing Temperature on the Permeability of Hardened Cement Paste', *Cement and Concrete Research,* vol. 11, no. 4, pp. 575-579.

Griffith, A.A. (1920), 'The Phenomena of Rupture and Flow in Solids', *Philosophical Transactions of the Royal Society of London*, A221, p.163.

Grudemo, A. (1979), 'Microcracks, Fracture Mechanism, and the Strength of the Cement Paste Matrix', *Cement and Concrete Research*, vol. 9, pp. 19-34.

Heckroodt, R.O. (1990), *Summary of Lecture Notes on Portland Cement*, Department of Materials Science and Engineering, University of Cape Town.

Hemond, H.F. and E.J Fechner (1994), *Chemical Fate and Transport in the Environment*, San Diego: Academic Press

Heimann, R.B., Conrad, D., Florence, L.Z., Neuwirth, M., Ivey, D.G., Mikula, R.J., and W.W. Lam (1992), 'Leaching of Simulated Heavy Metal Waste Stabilized/Solidified in Different Cement Matrices', *Journal of Hazardous Materials*, 31, pp. 39-57.

Hiemenz, P.C. (1986), *Principles of Colloid and Surface Chemistry*, New York: Marcel Dekker.

Higgins, D.D. and J.E. Bailey (1976), 'Fracture Measurements on Cement Paste', *Journal of Materials Science,* 11, pp. 1995-2003.

Hills, C.D., Sollars, C.J. and R. Perry (1992), 'Poisoning of OPC during Solidification of Toxic Wastes', in *Cement Industry Solutions to Waste Management, Proceedings of the 1st International Symposium*, Calgary, Alberta, Canada. October 7-9, pp. 23-44.

Irwin, G.R. (1957), 'Analysis of Stresses and Strains Near the End of a Crack Traversing a Plate', *Journal of Applied Mechanics,* no. 24, pp. 361-364.

Ivey, D.G., Heimann, R.B., Neuwirth, M, Shumborski, S., Conrad, D, Mikula, R.J. and W.W. Lam (1990), 'Electron Microscopy of Heavy Metal Waste in Cement Matrices', *Journal of Material Science*, 25, pp. 5055-5062.

Ivey, D.G., Neuwirth, M., Conrad, D., Mikula, R.J., Lam, W.W. and R.B. Heimann (1993), 'Electron Microscopy Characterization Techniques for Cement Solidified/Stabilized Metal Wastes', in *Chemistry and Microstructure of Solidified Waste Forms*, R.D. Spence, Ed., Florida: Lewis, pp. 123-150.

Jacobs, J.H. (1992), 'Treatment and Stabilisation of Hexavalent Chromium Containing Waste Material', *Environmental Progress*, vol. 11, no. 2, May, 123-126.

Kindness, A., Macias, A. and F.P. Glasser (1994), 'Immobilization of Chromium in Cement Matrices', *Waste Management*, vol. 14, no. 1, pp. 3-11.

Knott, J.F. (1973), *Fundamentals of Fracture Mechanics*, London: Butterworths.

Kojovic, T. (1996), *Mathematical Techniques for Mineral Processing Analysis, Course Notes: 3rd Edition,* Julius Kruttschnitt Mineral Research Centre, University of Queensland.

Kornelius, G. and N. Boegman (1994), 'Water Soluble Components in Dust from Ferro-Alloy Production', *5th Annual Clean Air Conference*, National Association for Clean Air: Cape Town.

Lawn, B.R. and T.R. Wilshaw (1975), *Fracture of Brittle Solids*, Cambridge: Cambridge University Press.

Laidler, K.J. and J.H. Meiser (1982), *Physical Chemistry*, Menlo Park, California: Benjamin/Cummings Publishing Co. Ltd.

Lee, C., Wang, H., Lin, C., and Yang, G. (1994), 'A Long-Term Leachability Study of Solidified Wastes by the Multiple Toxicity Characteristic Leaching Procedure', *Journal of Hazardous Materials*, 38, pp. 65-74.

Levenspiel, O. (1979), *The Chemical Reactor Omnibook*, Corvallis, OR.: Oregon State University.

Lowell, S. (1979), *Introduction to Powder Surface Area*, Wiley: New York.

Lydon, F.D. (1979), *Developments in Concrete Technology - 1*, London: Applied Science Publishers.

Malone, P.G. and R.J. Larson (1983), 'Scientific Basis of Hazardous Waste Immobilization', in *Hazardous and Industrial Solid Waste Testing: Second Symposium*, ASTM STP 805, Eds. R.A. Conway and W.P. Gulledge, pp. 168-177.

Malone, P.G., Jones, L.W. and J.P. Burkes (1983), 'Application of Solidification/Stabilization Technology to Electroplating Wastes', USAE Waterways Experiment Station.

Means, J.L., Smith, L.A., Nehring, K.W., Brauning, S.E., Gavaskar, A.R., Sass, B.M., Wiles, C.C. and C.I. Mashni (1995), *The Application of Solidification/Stabilization to Waste Materials*, Boca Raton, Florida: CRC Press.

Miller, I. and J.E. Freund (1985), *Probability and Statistics for Engineers* 3rd ed, Englewood Cliffs: Prentice Hall.

Mindess, S. (1983), 'An Application of Fracture Mechanics to Cement and Concrete', in *Developments in Civil Engineering 7, Fracture Mechanics of Concrete*, Amsterdam: Elsevier, pp. 1-30.

Mindess, S. and J.F. Young (1981), *Concrete*, Englewood Cliffs, NJ: Prentice Hall.

Mollah, M.Y.A., Tsai, Y-N, Hess, T.R. and D.L. Cocke (1992), 'An FTIR, SEM and EDS Investigation of Solidification/Stabilization of Chromium using Portland Cement Type V & Type IP', *Journal of Hazardous Materials*, 30, pp. 273-283.

Montgomery, D.M., Sollars, C.J., Perry, R., Tarling, S.E., Barnes, P. and E. Henderson (1991), 'Treatment of Organic-Contaminated Industrial Wastes Using Cement-Based Stabilization/Solidification -1, Microstructural Analysis of Cement - Organic Interactions', *Waste Management and Research*, 9, pp. 103-111.

Moragues, A., Macias, A., Andrade, C. and J. Losada (1988), 'Equilibria of the Chemical Composition of the Pore Concrete Solution. Part II: Calculation of the Equilibria Constants of the Synthetic Solutions', *Cement and Concrete Research*, vol. 18, no. 3, pp. 342-350.

Moragues, A., Macias, A. and C. Andrade (1987), Equilibria of the Chemical Composition of the Concrete Pore Solution, Part 1: Comparative Study of Synthetic and Extracted Solutions', *Cement and Concrete Research*, vol. 17, pp. 173-182.

Mular A.L. and R.R. Klimpel (1991), in *Evaluation and Optimization of Metallurgical Performance*, Eds. Malhotra, R.R. Klimpel, and A.L. Mular Littleton, Colorado: AIME.

Mullier, M.A., Seville, J.P.K. and M.J. Adams (1987), 'A Fracture Mechanics Approach to the Breakage of Agglomerates', *Chemical Engineering Science,* vol. 42, no. 4, pp. 667-677.

Mullier, M.A. (1991), *The Strength of Agglomerates and Their Breakage During Fluidisation*, PhD Thesis: University of Surrey.

Murphy, T.D. (1977), 'Design and Analysis of Industrial Experiments', *Chemical Engineering*, June 6, pp. 168-182.

Myers, R.H. (1971), *Response Surface Methodology,* Boston: Allyn and Bacon.

Myers, T.E. (1986), 'A Simple Procedure for Acceptance Testing of Freshly Prepared Solidified Waste', *Hazardous & Industrial Solid Waste Testing: Fourth Symposium,* Petros, J.K.J., Lacey, W.J. and R.A. Conway, R.A., Philadelphia: Anonymous, pp.263-272.

Paxton, R.G., Richard Paxton Associates Waste Consultants (1997), *Personal Communication.*

Perry, R.H. and D.Green (1984), *Perry's Chemical Engineers' Handbook*, 6th ed, Singapore: McGraw-Hill.

Petersen, J. (1997), *Assessment and Modelling of Chromium Release in Minerals Processing Waste Deposits,* PhD Thesis: University of Cape Town.

Petrie, J.G. and R.G. Paxton (1995), 'Integrated Technologies for Treating Liquid and Solid Wastes from Ferrochrome and Stainless Steel Production', *Pollution Prevention for Process Engineers, Proceedings of Technical Solutions for Pollution Prevention in the Mining and Mineral Processing Industries, January,* Eds. P.E. Richardson, B.J. Scheiner and F. Lanzetta Jr, New York: Engineering Foundation, pp. 22-27.

Plati, E. and J.G. Williams (1975), 'The Determination of the Fracture Parameters for Polymers in Impact', *Polymer Engineering and Science*, vol. 15, no. 6, pp. 470-477.

Poelmann, H., St Auer and H.-J. Kuzel (1993), 'Solid Solution of Ettringites, Part II: Incorporation of $B(OH)_4^-$ and CrO_4^{2-} in $3CaO.Al_2O_3.3CaSO_4.32H_2O$', *Cement and Concrete Research*, no. 23, pp. 422-430.

Pojasek, R.B. (1989), 'Solid Waste Disposal: Solidification', *Chemical Engineering*, 13 August, p. 141.

Poon, C.S., Perry, C.J. and R. Perry (1983), 'Use of Stabilization Processes in the Control of Toxic Wastes', *Effluent and Water Treatment Journal*, November, pp. 451-459.

Poon, C.S., Clarke, A.I., Perry, C.J. and R. Perry (1985a), 'Mechanisms of Metal Fixation and Leaching by Cement-Based Fixation Processes', *Waste Management and Research*, vol. 3, pp. 127-142.

Poon, C.S., Peters, C.J., Perry, R., Barnes, P. and A.P. Barker (1985b), 'Mechanisms of Metal Stabilization by Cement-Based Fixation Processes', *The Science of the Total Environment*, 41, pp. 55-71.

Poon, C.S., Clark, A.I., Perry, R., Barker, A.P. and P. Barnes (1986), 'Permeability Study on the Cement-Based Solidification Process for the Disposal of Hazardous Wastes', *Cement and Concrete Research*, vol. 16, pp. 161-172.

Popovics, S. (1982), *Fundamentals of Portland Cement Concrete: A Quantitative Approach,* vol 1, *Fresh Concrete*, New York: John Wiley and Sons.

Portland Cement Institute (PCI) (1986), *Fulton's Concrete Technology*, Midrand: The Natal Witness (Pty) Ltd.

Pourbaix, M. (1966), *Atlas of Electrochemical Equilibria in Aqueous Solutions*, Bristol: Pergamon.

Public Law (US) 94-580 (1976), *Resource Conservation and Recovery Act.*

Pulles, W. (1993), *Mine Water Quality Management Reference Manual,* Sandton: Pulles, Howard and De Lange, p. 24.

Rai, D., Sass, B.M., and D.A. Moore (1987), 'Chromium(III) Hydrolysis Constants and Solubility of Chromium(III) Hydroxide', *Inorganic Chemistry*, pp. 345-349.

Richard Paxton Associates Ltd. UK (1996), *Review of the BPEO Strategy for Middelburg Site 16/06/96*, Report No: 9207/434/UAR148.

Richardson, G.L. (1981), 'The Phantom Dissolution Leach Model', *Nuclear and Chemical Waste Management*, 2, pp. 237-241.

Rooke, D.P. and D.J. Cartwright (1976), *Compendium of Stress Intensity Factors* HMSO.

Roy, A. and Scheetz (1993), 'The Chemistry of Cementitious Systems for Waste Management: The Penn State Experience', in *Chemistry and Microstructure of Solidified Waste Forms*, R.D. Spence, Ed., Florida: Lewis, pp. 83-103.

Roy, A., Eaton, H.C., Cartledge, F.K. and M.E. Tittlebaum (1992), 'Solidification/Stabilisation of Hazardous Waste: Evidence of Physical Encapsulation', *Environmental Science and Technology*, 26, 7, pp. 1349-1353.

Rumpf, H. (1977), 'Particle Adhesion', in *Agglomeration 77*, Ed. K.V. Sastru, New York: AIME, pp. 97-129.

Rumpf, H. (1962), 'The Strength of Granules and Agglomerates', in *International Symposium on Agglomeration*, Ed. W.A. Knepper, New York: Interscience, pp. 379-418.

Saleh, F.Y. et al (1989), 'Kinetics of Chromium Transformations in the Environment', *Science of the Total Environment*, vol. 86, pp. 25-41.

Sarkar, S L (1992), 'The Importance of Microstructure in Evaluating Concrete', *Advances in Concrete Technology: Proceedings of an International Conference*, Athens, Greece, May, pp. 123-158.

Schubert, H. (1975), 'Tensile Strength in Agglomerates', *Powder Technology* 11, Netherlands: Elsevier, pp. 107-109.

Shively, W., Bishop, P., Gress, D. and T. Brown (1986), 'Leaching Tests of Heavy Metals Stabilized with Portland Cement', *Journal of the Water Pollution Control Federation*, 58, no. 3, 234-241.

Sittig, M. (1979), *Landfill of Hazardous Wastes and Sludges*. Park Ridge: Noyes Data Corporation.

Smith, J M (1981), *Chemical Engineering Kinetics*, Singapore: McGraw-Hill.

Sollars, C.J. and R. Perry (1989), 'Cement-Based Stabilisation of Wastes: Practical and Theoretical Considerations', *Journal of Industrial Water and Environmental Management*, vol. 3, p.125.

Stegman, J.A., Environment Canada, Wastewater Technology Centre (1996), *Personal Communication.*

Struble, L.J., Stutzman, P.E. and E.R. Fuller Jr (1989), 'Microstructural Aspects of the Fracture of Hardened Cement Paste', *Journal of the American Ceramic Society*, vol. 72, no.12, pp. 2295-2299.

Stumm, W. and J.J. Morgan (1981), *Aquatic Chemistry* 2nd ed, New York: John Wiley and Sons.

Sujata, K. and H.M. Jennings, (1992), 'Formation of a Protective Layer During the Hydration of Cement', *Journal of the American Ceramic Soceity*, 75, 6, pp. 1669-1673.

Tabor, D. (1948), 'A Simple Theory of Static and Dynamic Hardness', *Proceedings of the Royal Soceity of London* A192, pp. 247-274.

Tabor, D. (1987), 'Adhesion of Solids', in *Tribology in Particulate Technology*, Briscoe, B.J. and M.J. Adams, Bristol: Adam Hilger, pp. 206-219.

Tada, H., Paris, P. and G. Irwin (1973), *The Stress Analysis of Cracks Handbook*, St Louis: Del Research Corporation.

Tashiro, C, Takashi, H., Kanaya, M., Hirakida, I. and R. Yoshida (1977), 'Hardening Property of Cement Mortar Adding Heavy Metal Compound and Solubility of Heavy Metal From Hardened Mortar', *Cement and Concrete Research*, vol. 7, pp. 283-290.

Telles, R.W. (1984), *Review of Fixation Processes to Manage Hazardous Organic Wastes*, Cincinnati: US EPA.

Tessier, A., Campbell, P.G.C. and M. Bisson (1979), 'Sequential Extraction Procedure for the Speciation of Particulate Trace Metals', *Analytical Chemistry*, vol. 51, no. 7, pp. 844-851.

Topping, J. (1965), *Errors of Observation and Their Treatment*, London: Chapman and Hall Ltd.

Treybal, R.E. (1981), *Mass Transfer Operations*, Singapore: McGraw Hill, p.566.

US Environmental Protection Agency (EPA) (1985), *Critical Characteristics and Properties of Hazardous Waste Solidification/Stabilization*, EPA Contract No. 68-03-3186, Cincinatti: US EPA.

US Environmental Protection Agency (EPA) (1987), *Interference Mechanisms in Waste Solidification/Stabilization Processes*, Interagency Agreement No. DW219306080-01-0, Cincinatti: US EPA.

US Environmental Protection Agency (EPA) (1980), *Guide to the Disposal of Chemically Stabilized and Solidified Waste*, Cincinatti: US EPA Report no SW-872.

US Government Printing Office (1988), *Code of Federal Register*, Appendix I, vol. 40 (268).

US Government Printing Office (1980), *Code of Federal Register*, Appendix II, vol. 45 (98).

Van der Sloot, H.A. (1990), 'Leaching Behaviour of Waste and Stabilized Waste Materials; Characterisation for Environmental Assessment Purposes', *Waste Management and Research*, vol. 8, pp. 215-228.

Van Niekerk, G., PPC Riebeek West Plant (1994), *Personal Communication.*

Von Blottnitz, H.B. (1994), *Development and Assessment of a Hydrometallurgical Process to Treat Chromium-Containing Dusts*, PhD Thesis: University of Cape Town.

Von Mises, R. (1913), 'Gottinger Nachrichten', *Math-Phys Klasse*, p. 582.

Wastewater Technology Centre (1990), *Compendium of Waste Leaching Tests*, Environment Canada, Report EPS 3/HA/7.

Weitzman, L. (1990), 'Factors for Selecting Appropriate S/S Methods', *Journal of Hazardous Materials,* vol. 24, pp.157-168.

Welty, J.R., Wicks, C.E. and R.E. Wilson (1984), *Fundamentals of Momentum, Heat and Mass Transfer*, 2nd ed, Singapore: John Wiley and Sons.

Westergaard, H.M. (1939), *Journal of Applied Mechanics*, A 49, June.

Western Cape Environmental Monitoring Group (1993), *Clean Production*, Cape Town: Western Cape Environmental Monitoring Group.

Wiles, C.C. and M. Lynn Apel (1985), 'Critical Characteristics and Properties of Hazardous Waste Solidification/Stabilization', *US EPA Report No. 68-03-3186*, Cincinnati: US Environmental Protection Agency.

Wiles, C.C. (1987), 'A Review of Solidification/Stabilisation Technology', *Journal of Hazardous Materials*, vol. 14, pp 5-21.

Wiles, C.C.(1988), 'S/S Technology', in *Standard Handbook of Hazardous Waste Treatment and Disposal*, New York: McGraw Hill, pp.7, 85-7, 101.

Williams, J.G. (1973), *Stress Analysis of Polymers*, New York: John Wiley and Sons.

Williams, J.G. (1984), *Fracture Mechanics of Polymers*, Chichester: Ellis Horwood.

Winslow, D.N. and S. Diamond (1970), 'A Mercury Porosimetry Study of the Evolution of Porosity in Portland Cement', *Journal of Materials*, JMLSA, vol. 5, no. 3, September, pp. 564-585.

Wright, P.J.F. (1955), 'Comments on an Indirect Tensile Test on Concrete Cylinders', *Magazine of Concrete Research*, July, pp. 87-96.

Xu, L., Helstroom, R., Scott, O.J. and A.J. Chambers (1995), 'Fracture Characteristics of Powder Compacts', *Powder Technology*, 83, pp. 193-199.

Zamorani, E., Sheikh, I.A. and G. Serrini (1988), 'Physical Properties Measurements and Leaching Behaviour of Chromium Compounds Solidified in a Cement Matrix', *Nuclear and Chemical Waste Management*, 8, pp. 239-245.

APPENDICES

Appendix A1 - Procedure for fusion of samples

1. Weigh 0.5g of dry sample with 5 g sodium peroxide (solid).

2. Mix well

3. Samples are placed in a zirconium crucible over a bunsen burner in a fume cupboard and heated until it is a cherry red liquid.

4. Allow to cool and place the entire crucible in a beaker with 50 ml deionized water to remove the solid from the crucible.

5. Add 20ml concentrated HCl.

6. Heat the beaker to boiling point and remove the crucible from the beaker and rinse well with water.

7. Wash the solution into a 100 ml flask and fill to the mark with deionized water and analyse using AA spectroscopy.

8. Concentration metal in dust = ppm in solution * 200

Appendix A2 - The Toxicity Characteristics Leaching Procedure (TCLP)

Procedure

The following is the TCLP procedure as used in the context of this work. It is based on the TCLP method of the United States Environmental Protection Agency [Code of Federal Register (1988)].

The materials to be studied must be dry and the particle size must not exceed 9mm.

If the sample is of a type not previously tested, so that its acidity/alkalinity is unknown, the following test is performed:

1. A 10 g sample is mixed with twenty times its weight of deionised water.

2. The mixture is placed on a magnetic stirrer for two minutes and the pH is measured.

   2.1 If pH of a solution is < 5.0, the extraction fluid is made by adding 5.7 ml of glacial acetic acid to 500ml deionised water, then adding 64.3ml 1.0 N NaOH and diluting to 1 litre with deionised water.

   2.2 If pH of the solution is > 5.0, 3.5ml 1.0 N HC1 is added to the mixture. This is then slurried for 30s, covered with a watchglass, heated to 50°C and held for 10 minutes. After cooling, the pH is measured.

3. If pH < 5.0, the extraction fluid is made as described in 3.1 above.

4. If pH > 5.0, the extraction fluid is made by diluting 5.7 ml glacial acetic acid with deionised water to a volume of 1 litre.

Samples for which the acidity/alkalinity can be expected to be similar to that of previously tested materials are immediately subjected to the main part of the TCLP, as described below.

1. A fresh sample to be extracted is placed with 20 times its weight of the extraction fluid into a *Schott 21* borosilicate glass bottle which is then agitated by end-over-end rotation for eighteen hours.

2. The slurry is filtered through Whatman's no 1 filter paper using vaccum filtration. A sample is further cleaned by filtration through a 0.45 μm Millipore filter.

3. The pH of the filtrate is recorded.

4. If necessary, the filtrate is refrigerated before further analysis.

5. Samples are analysed for metal concentrations using Atomic Absorption Spectroscopy.

Maximum Limits of Contaminants in TCLP Leachants

The Table below presents the maximum allowable concentrations of metal species in TCLP leachates before wastes required disposal to landfill [Albanese (1990)].

Element	Regulatory Limit, mg/l
Cadmium	1.0
Chromium	5.0
Lead	5.0
Mercury	0.2

Appendix A3 - The Sequential Chemical Extraction Procedure

The SCE, as carried out in the context of this work, requires the following procedure:

Chemicals

1. 0.75 M LiCl with 0.25M CsCl in 60% CH_3OH (v/v)
2. Distilled water
3. 1 M CH_3COONa adjusted to pH 5 with CH_3COOH
4. 1 M $NH_2OH.HCl$ in 25%CH_3COOH (v/v)
5. 0.02 M HNO_3
6. 30% H_2O_2
7. 1.2 M CH_3COONH_4 in 20% HNO_3 (v/v)

Procedure

The sample is dried to constant weight at 60±3°C. The dried sample is ground to pass an ASTM No. 325 sieve. 0.50g is weighed into a 50ml centrifuge tube.

The different steps are carried out as follows:

1. **Extraction of the Ion Exhangeable Fraction (A)**

The sample is agitated with 8.0 ml of Solution 1 for 10 minutes and then centrifuged at approximately 14 000 rcf for 20 minutes. 7.0 ml of the supernatant is decanted and made up to 25 ml with distilled water. This is acidified to pH 2 and stored in a polyethylene bottle at 4°C.

Add 15 ml distilled water to the test tube to wash the residue. Mix thorougly and discard the wash water taking care not to lose any of the residue.

2. Extraction of Surface Oxide and Carbonate Bound Metal Ions

Add 8.0 ml of solution 3 to the test tube containing the residue. Agitate constantly for 5 hours at room temperature. Centrifuge for 20 minutes at approximately 14 000 rcf. Decant 7.0 ml of the supernatant, make this up to 25 ml with distilled water, acidify to pH 2 and store at 4°C. Add 15 ml distilled water to the test tube to wash the residue. Mix thorougly and discard the wash water taking care not to lose any of the residue.

3. Extraction of Metal Ions Bound to Fe and Mn Oxides

Add 20 ml of solution 4 to the tube containing the residue. Agitate continuously for 2 hours at room temperature. Centrifuge for 20 minutes at approximately 14 000 rcf. Decant 19.0 ml of the supernatant and make it up to 50.0 ml with distilled water to be stored at 4°C. Repeat the washing step in section 2.

4. Extraction of Metal Ions Bound to Organic Matter and Sulfides

Add 3.0 ml of 0.02 M HNO_3 and 5.0 ml of 30% H_2O_2 to the residue. Heat the mixture slowly in a water bath to 90±5°C. Agitate periodically. After 2 hours add 3.0ml of 30% H_2O_2 taking care to avoid excessive foaming and continue heating. After 3 hours add 5.0ml of solution 7 and dilute to 15.0 ml with distilled water. Agitate continuously for 30 minutes. Centrifuge at approximately 14 000 rcf for 20 minutes. Decant 14 ml of the supernatant and dilute with distilled water to make 50.0 ml which are stored at 4°C. Rinse as above.

5. Extraction of Residual Metal Ions

This is carried out using the fusion procedure detailed previously in Appendix...

Appendix A4 - Details of the Agitated Kinetic Tests

The S/S product to be tested is mechanically crushed and sieved. Three different particle size fractions are tested in the scope of this work:

+8 mm -11.2 mm
+4.6 mm -5.7 mm
fines fraction of <0.5 /mm.

50 g of the material is weighed out on a top-loading balance and is placed in a two litre borosilicate bottle. One litre of extraction fluid is added to the bottle. The bottle is sealed and agitated on a tumbling device. 5 ml samples of the liquid are extracted using a pipette at various time intervals. The liquid is filtered through a 0.45 μm filter paper and refrigerated prior to metals analysis via AA spectroscopy. Cr, Ca and Zn were the only metals explored in this work.

The two leachants investigated in this work were a 1.0N acetic acid solution and distilled water. The former was made by diluting 5.7 ml of glacial acetic acid to one litre.

Initially three agitation rates were explored; 15 rpm, 25 rpm,30 rpm. For further testing an agitation rate of 30 rpm was used.

Appendix A5 - Procedure for the Non-Agitated Kinetic Leach Tests (NKLT)

The Non-Agitated Kinetic Leach Test (NKLT) is based on that presented in US EPA (1980). In the scope of this work rectangular samples were used for the tests, being those remaining from the three point bend tests of Chapter 5. Sample dimensions were measured using a vernier. Leachant volumes were calculated based on a liquid volume to surface area ratio of 10:1. In the present work two leachants were investigated: 1.0 N acetic acid and distilled water.

The first step in the test is to measure surface washoff. The sample is immersed in the leachant of interest for 30 s. The pH of the solutions are measured and the concentrations of contaminants of interest determined. Cr, Zn, Mg, Ca, K and Na concentrations are determined by AA spectroscopy, while Cr(VI) is measured by UV spectroscopy.

Leachants are placed into borosilicate glass bottles. The samples are suspended in the solution using a string harness, and the bottles covered. The bottles are placed in a temperature controlled room with the temperature set at 25°C. Leachants are changed at the following time intervals:

Interval	1	2	3	4	5	6	7	8	9	10
Time (h)	2	7	24	48	72	96	120	192	264	336

Leachant renewal is performed as follows: a second bottle is filled with the correct volume of leachant solution. The sample is removed from the old leachant solution and transferred directly into the new solution. The old solution is mixed to ensure even distribution of elements in the solution and an aliquot is extracted and placed in a glass vial. The pH of the solution is determined and the sample refrigerated prior to analysis. Cr, Zn, Ca, K and Na are once again determined by AA spectroscopy while Cr(VI) is determined by UV spectroscopy.

Appendix A6 - Details of the Lysimeter Work

Lysimeter tests were carried out in the glass column presented in Photograph 7-2. Material for the lysimeter was made with 26% cement and a 0.94 w/s ratio. The material was cured for approximately 40 days and then crushed to less than 9.5 mm using a hammer.

The leachant solution used in this work was a mild acid made by adding a mixture of concentrated nitric acid (HNO_3) and sulphuric acid (H_2SO_4) in a 1:1.45 molar ratio to well aerated distilled water until the solution had a pH of 4.

The material to be tested was packed into the glass column to approximately 190 mm in height. The solution was sprinkled on at a rate of 230 ml/day pumped in 4 intervals of 2 hours each with a 4 hour interval between intervals. Although the rate of leachant addition was observed to be much lower than the average rainfall in the area where the material was expected to be consigned to landfill, the rate of sprinking was kept low in order to prevent a flooding scenario occuring. The effluent liquid was collected on a daily basis and the volume recorded. The effluents were analysed for pH, Cr, Na, K, Ca, Mg, Si, and Al.

Appendix B - Sample Preparation Technique

(i) In the case of dusts, these are washed in distilled water with a water to solids ratio of 10:1. Agitation is via an overhead stirrer at 2000 rpm for one hour at 25°C. The slurry is filtered using a pressure filter to 32 ± 1% moisture (w/w) and the filter cake stored in a sealed container to prevent water loss.

(ii) The water content of the filter cakes is determined by drying a representative sample in an oven at 60°C until constant mass.

(iii) The required cement addition is calculated based on the dry mass of the filter cake used (see section 3.2.3).

(iv) The cement and filter cake are mixed in a paddle mixer for a minimum of 5 minutes. The extent of mixing required depends on the consistency of the mixture. The amount of water present in the mixture determines the fluidity of the paste and hence the time required to ensure effective mixing.

(v) During mixing, distilled water is added to make the water content up to the desired water to solids ratio (see section 3.2.3). It was suggested that there would be no added benefit in using deionized water over distilled water as the former quickly equilibrates with air.

(vi) The mixture is placed into moulds in which the sample sets to form an aggregate of dimensions which allow for meaningful characterisation via strength tests (see Chapter 5 for details of different sample dimensions used in this work).

(vii) The moulds are vibrated on a vibrating table for a minimum of three minutes to remove entrapped air.

(viii) Moulds are placed in sealed buckets which contain an open beaker of water to ensure constant humidity. Curing takes place at room temperature. After 2 weeks samples are removed from the moulds and left in the buckets for the required curing time prior to testing.

Appendix C1 - Derivation of Equation (5-26)

From equation 5-24, for unstable crack propagation,

$$\frac{dG}{da} > 0$$

and, equation 5-25 gives:

$$G = \frac{1}{2B}\left(\frac{x}{C}\right)^2 \frac{dC}{da}$$

Substituting 5-25 into 5-24 gives:

$$\frac{d\left(\frac{1}{2B}\left(\frac{x}{C}\right)^2 \frac{dC}{da}\right)}{da} > 0$$

At failure, the deflection is not a function of a. Hence x and B are constants (>0), and can be removed from the equation, giving:

$$\frac{d\left(C^{-2}\frac{dC}{da}\right)}{da} > 0$$

By the chain rule this becomes:

$$\frac{dC}{da}.\frac{dC^{-2}}{da} + C^{-2}.\frac{d\left(dC/da\right)}{da} > 0$$

or:

$$-2\frac{dC}{da}C^{-3}.\frac{dC}{da} + C^{-2}\frac{d^2C}{da^2} > 0$$

Rearranging gives:

$$C\frac{d^2C}{da^2} > 2\left(\frac{dC}{da}\right)^2$$

which is equation 5-26.

Appendix C2 - Derivation of Equation (5-27)

Equation (5-21) gives

$$\phi = \frac{C}{dC/d(a/W)} = C.\left(\frac{dC}{d(a/W)}\right)^{-1} \tag{5-21}$$

taking the derivative with respect to a/W gives:

$$\begin{aligned}\frac{d\phi}{d(a/W)} &= \frac{dC}{d(a/W)}.\left(\frac{dC}{d(a/W)}\right)^{-1} - 1.C.\left(\frac{dC}{d(a/W)}\right)^{-2}.\frac{d^2C}{d(a/W)^2} \\ &= 1 - C.\left(\frac{dC}{d(a/W)}\right)^{-2}.\frac{d^2C}{d(a/W)^2}\end{aligned} \tag{I}$$

Now,

$$\frac{dC}{da} = \frac{dC}{d(a/W)}.\frac{d(a/W)}{da} \quad \text{or} \quad \frac{dC}{d(a/W)} = \frac{dC}{da}.\left(\frac{d(a/W)}{da}\right)^{-1} \tag{II}$$

This gives

$$\frac{dC}{d(a/W)} = \frac{dC}{da}.\frac{1}{(1/W)} = W\frac{dC}{da} \tag{III}$$

and

$$\begin{aligned}\frac{d^2C}{d(a/W)^2} &= \frac{d}{da}\left(\frac{dC}{d(a/W)}.\frac{d(a/W)}{da}\right) \\ &= \frac{d(a/W)}{da}.\frac{d}{da}\frac{d^2C}{d(a/W)^2} + \frac{dC}{d(a/W)}.\frac{d^2(a/W)}{da^2}\end{aligned} \tag{IV}$$

From (III), and that $d^2(a/W)/da^2 = 0$, (IV) becomes:

$$\frac{d^2C}{d(a/W)^2} = \frac{1}{W}.W.\frac{d^2C}{da^2} = \frac{d^2C}{da^2} \qquad (V)$$

Substituting (III) and (V) into (I) above gives:

$$\frac{d\phi}{d(a/W)} = 1 - C.\left(W\frac{dC}{da}\right)^{-2}.\frac{d^2C}{da^2} \qquad (VI)$$

Now, from equation (5-26),

$$C\frac{d^2C}{da^2} > 2\left(\frac{dC}{da}\right)^2 \qquad (5\text{-}26)$$

Equation (VI) gives:

$$\frac{d\phi}{d(a/W)} < 1 - 2.\left(\frac{dC}{da}\right)^2\left(W\frac{dC}{da}\right)^{-2} \qquad (VII)$$

$$< 1 - 2.W^{-2}$$

Since $2W^{-2}$ is always greater than zero,

$$-\frac{d\phi}{d(a/W)} > 1 \qquad (5\text{-}27)$$

Which is equation (5-27). Note that W cannot be zero, a condition that will always hold since a sample W *must* be greater than nothing.

Appendix C3 - Derivation of Equation (7-7)

The initial and boundary conditions[1] used in this development were discussed in the main body of the text and are given as:

(i) *The sample being tested is infinite or* $c_A=c_{A0}$ ***as*** $x\rightarrow\infty$ ***for all t***, where c_A is the concentration of contaminant A at position x measured inwards from the surface of the solid and c_{A0} is the initial concentration of A in the sample.

(ii) *Concentration at the surface of the slab is constant and equal to the concentration in the bulk, or* $c_A=c_{A,S}=c_b$ ***at*** $x=0$ ***for all t***. Transport from the solid surface to the bulk liquid is assumed to be rapid compared to transport through the solid to its surface. This assumption is valid for any materials in which diffusion through the solid material occurs [Levenspiel (1979)].

(iii) *The contaminant is distributed homogeneously in the solid to be tested at the start of the leaching period or* $c_A=c_{A0}$ ***at*** $t=0$ ***for all*** x. This can be achieved by effectively mixing the waste-cement combination during sample making.

The following development is based on Welty et al (1984). Consider a rectangular slab of material. Using the initial and boundary conditions above, equation (7-5) can be solved to give the concentration profile across the slab. Assume one-dimensional mass transfer in the x-direction of a component from the slab into the bulk solution. One dimensional transfer can be pictured as sealing the y and z faces of the slab with an impermeable membrane.

With no reaction term, equation (7-5) gives in one dimension:

$$\frac{\partial c_A}{\partial t} = D_e \frac{\partial c_A}{\partial x} \qquad \text{(I)}$$

with initial and boundary conditions:

$c=c_{A0}$	at $t=0$	for all x
$c_A=c_{A,S}$	at $x=0$	for all t
$c_A=c_{A0}$	as $x\rightarrow\infty$	for all t

The variables in equation (I) may be expressed in dimensionless form as follows:

[1] Note that this development is for cartesian coordinates, since samples used in testing are rectangular slabs. These initial and boundary conditions, and the subsequent development, can be altered for other geometries.

$$\frac{(c_A - c_{A0})}{(c_{A,S} - c_{A0})} = f(\frac{X}{x_1}, \frac{D_e t}{x_1^2}) \qquad \text{(II)}$$

where X is the distance from the surface of the slab and x_1 is a characteristic dimension. Since there is no finite characteristic dimension in a semi-infinite solid, the equation becomes $(c_A - c_{A0})/(c_{A,S} - c_{A0}) = f(D_e t/X^2)$, or with equal validity, $(c_A - c_{A0})/(c_{A,S} - c_{A0}) = f(X/(D_e t)^{0.5})$. Now, selecting $\eta = X/(2(D_e t)^{0.5})$ as the independent variable and $Y = (c_A - c_{A0})/(c_{A,S} - c_{A0})$ as the dependant variable, equation (I) above gives:

$$d^2Y/d\eta^2 + 2\eta dY/d\eta = 0 \qquad \text{(III)}$$

with the revised boundary and initial conditions as:

$Y \rightarrow 0$ as $\eta \rightarrow \infty$

and $Y=1$ at $\eta=0$

Integrating equation (III) once gives:

$$\ln (dY/d\eta) = c_1 - \eta^2 \qquad \text{(IV)}$$

or

$$dY/d\eta = c_2 e^{-\eta^2} \qquad \text{(V)}$$

Integrating again gives:

$$Y = c_3 + c_2 \int e^{-\eta^2} d\eta \qquad \text{(VI)}$$

The integral is commonly known as the error function, erf, where

$$\text{erf}(\phi) = \frac{2}{\sqrt{\pi}} \int_0^{\phi} e^{-\eta^2} d\eta \qquad \text{(VII)}$$

Values of erf ϕ for various values of ϕ are presented in standard texts. Now, applying the boundary conditions to equation (III) gives:

$$Y = 1 - \text{erf}\left(\frac{X}{2\sqrt{D_e t}}\right) \qquad \text{(IX)}$$

or

$$\frac{c_A - c_{A0}}{c_{A,S} - c_{A0}} = 1 - \text{erf}\left(\frac{X}{(4D_e t)^{0.5}}\right) \quad \text{or} \quad \frac{c_{A,S} - c_A}{c_{A,S} - c_{A0}} = \text{erf}\left(\frac{X}{(4D_e t)^{0.5}}\right) \tag{X}$$

Here X is the distance from the edge of the slab, c_A is the concentration of A at point X, c_{A0} is the initial concentration of A in the sample, $c_{A,S}$ is the concentration of A at the surface of the slab, t is the time from the start of the leaching test and erf is the error function.

To express the leaching in terms of the fraction of the contaminant leached out of the slab, the above concentration profile is integrated across the entire slab. Still considering 1-directional mass transfer, the fraction of contaminant leached is then given by [Batchelor (1990)]:

$$\frac{M_t}{M_0} = \frac{1}{Lc_0}\int_0^L (c_{A0} - c_A)dX \tag{XI}$$

where M_t/M_0 is the fraction of contaminant leached at time t. Substituting in equation (X) and solving gives:

$$\frac{M_t}{M_0} = \left(\frac{4D_e}{\pi L^2}\right)^{0.5} t^{0.5} \tag{XII}$$

where M_t/M_0 is the fraction of contaminant leached at time t and L is the distance from the edge of the slab to its centre. In order to evaluate D_e from an experimental results the fraction of a contaminant leached is plotted as a function of square root of time. Provided the above diffusion analysis is appropriate to describe leaching, and the above initial and boundary conditions hold, a straight line should be observed. The slope can be used determine the value of D_e using the above equation.

The above development is for one-directional leaching. In practice, however, tests are carried out on rectangular, spherical or cylindrical samples in which leaching occurs from all sample faces. To account for leaching from more than one face, the length parameter L in the above equation can be replaced by the ratio of volume to surface area of solid, V/S [Bishop (1986), Côté and Isabel (1984), Godbee et al (1980)].

$$\frac{M_t}{M_0} = \frac{S}{V}\left(\frac{4D_e}{\pi}\right)^{0.5} t^{0.5} \tag{7-7}$$

Appendix D1 - Results from the Three Point Bend Test

Notches of above approximately 5 mm and above were used in Calculations																										
Cement content %	w/s	Curing (days)	Notch length (mm)	Fracture load (kN)	L (mm)	B (mm)	W (mm)	Y	a/W	sigma*Y	1/a	(sigma* Y)^2	Predict	di^2	Klc Calculations											
															sum x2	91762.7	Slope	1257								
20	0.9	104	4.57	0.1552	118.9	20.2	44.5	0.968	0.103	561.615	218.6	295550	294640	827779	sumx	577.993	Int	19825								
			7.10	0.1217	119.6	20.5	43.4	0.955	0.164	456.222	140.8	189895	196868	4.9E+07	r2	0.99044	No points	4								
			8.30	0.1108	119.5	20.6	42	0.960	0.198	441.36	120.5	179683	171271	7.1E+07	alph a	87.3229	Sum di2	1.3E+08								
			10.20	0.0967	119.7	20.4	42.3	0.978	0.241	383.472	98.0	140712	143061	5514115	Klc	62.841	Alpha 2	6.3E+07								
															Fr Error Klc	0.01106	Delta	32974.6								
20	1.08	104	5.11	0.0855	118.7	20	42	0.961	0.122	350.797	195.7	113556	112613	888797	sum x2	97407.9	Slope	490.371								
			6.20	0.0821	119.1	20.4	42.8	0.956	0.145	318.012	161.3	92400.3	95742.5	1.1E+07	sumx	613.812	Int	16650.4								
			7.35	0.0795	118.6	20	43.1	0.956	0.171	309.743	136.1	87606.8	83367.5	1.8E+07	r2	0.95859	No points	4								
			8.28	0.0728	118.8	19.9	43.2	0.959	0.192	283.746	120.8	74034	75873.9	3385225	alph a	72.0728	Sum di2	3.3E+07								
															Klc	39.2498	Alpha 2	1.7E+07								
															Fr Error Klc	0.02339	Delta	12865.9								
20	0.99	28	4.65	0.0881	118	20.1	43.7	0.966	0.106	332.227	215.1	103071	102326	554274	sum x2	90165.8	Slope	336.807								
			6.75	0.079	119.2	20.1	44.1	0.955	0.153	292.531	148.1	78082.9	79760.9	2815812	sumx	572.321	Int	29863.6								
			9.01	0.073	118.8	20.2	44.1	0.962	0.204	268.976	111.0	67005.6	67245.1	57355.4	R^2	0.99491	No points	4								
			10.20	0.063	118.7	20	42	0.979	0.243	258.482	98.0	64056.9	62883.9	1376004	alph a	17.0335	Sum di2	4803445								
															Klc	32.5286	Alpha 2	2401723								
															Fr Error Klc	0.00805	Delta	33111.3								
20	0.99	89	5.10	0.1118	117.9	20.1	43.6	0.962	0.117	423.537	196.1	166059	163446	6827599												
			10.00	0.0788	117.9	20.2	43.9	0.971	0.228	292.998	100.0	81022.6	86311.6	2.8E+07	sum x2	63763.9	Slope	802.827								
			14.90	0.0553	118.1	20.3	43.1	1.070	0.346	212.272	67.1	51621.6	59909.9	6.9E+07	sumx	612.918	Int	6028.92								
			19.10	0.0466	118.6	20.2	43.4	1.230	0.440	177.286	52.4	47523.4	48061.7	289809	R2	0.94598	No points	9								
			20.50	0.0446	117.6	19.8	43.9	1.294	0.467	169.184	48.8	47912.4	45191.2	7404795	alph a	72.5129	Sum di2	8.1E+08								
			21.60	0.0388	119.1	20.1	43.6	1.373	0.495	146.988	46.3	40753.1	43196.8	5971809	Klc	50.2211	Alpha 2	1.2E+08								
			25.00	0.0375	118.1	20.2	43.1	1.701	0.580	144.658	40.0	60582	38142	5E+08	Fr Error Klc	0.01438	Delta	198207								
			30.10	0.0204	119	20.1	43.6	2.423	0.690	77.2822	33.2	35061.9	32700.9	5574429												
			34.40	0.0099	119	20	44	3.395	0.782	37.0099	29.1	15791	29366.9	1.8E+08												
20	0.99	104	5.12	0.1288	118.6	19.9	44.5	0.963	0.115	473.109	195.3	207500	223303	2.5E+08	sum x2	70240	Slope	1126.41								
			8.98	0.1132	118.5	20	43.6	0.963	0.206	430.985	111.4	172221	128736	1.9E+09	sumx	548.021	Int	3300.75								
			10.90	0.0974	118.3	20.3	43.8	0.983	0.249	362.021	91.7	126538	106641	4E+08	R2	0.77845	No points	5								
			12.30	0.0702	118.7	20	44	1.004	0.280	262.434	81.3	69382.1	94878.8	6.5E+08	alph a	346.946	Sum di2	3.7E+09								
			14.64	0.0582	118.3	20.1	43	1.064	0.340	226.678	68.3	58160	80241.4	4.9E+08	Klc	59.4872	Alpha 2	1.2E+09								
															Fr Error Klc	0.04902	Delta	50873.2								
20	0.99	180	4.55	0.1756	118.8	20	44.4	0.968	0.102	644.684	219.8	389566	387474	4373661	sum x2	57515	Slope	2016.02								
			15.12	0.0654	118.7	20.2	44.5	1.063	0.340	236.66	66.1	63296.3	77727.3	2.1E+08	sumx	383.957	Int	-5560.76								
			18.87	0.0463	119.1	20	44	1.206	0.429	173.087	53.0	43550.6	51229.9	5.9E+07	R^2	0.99206	No points	4								
			22.20	0.0423	118.7	20.3	43	1.441	0.516	163.127	45.0	55223.2	35204.3	4E+08	alph a	127.564	Sum di2	6.7E+08								
															Klc	79.5834	Alpha 2	3.4E+08								
															Fr Error Klc	0.01007	Delta	82636.9								

Appendix D1 - Continued

Cement content %	w/s	Curing (days)	Notch length (mm)	Fracture load (kN)	L (mm)	B (mm)	W (mm)	Y	a/W	sigma*Y	1/a	(sigma* Y)^2	Predict	di^2	Klc Calculations			
50	1.12	104	10.66	0.1053	117.5	19.9	43.1	0.982	0.247	412.3247	93.8	163847.5	168212.8	19055608	sum x2	17550.03	Slope	1603.3
			14.92	0.0952	118.1	20.1	43.9	1.063	0.340	355.7381	67.0	143046.1	125269.2	3.16E+08	sumx	252.6973	Int	17809.42
			19.88	0.0543	118	19.8	43.3	1.274	0.459	211.7276	50.3	72762.4	98458.3	6.6E+08	R2	0.780549	No points	4
			24.06	0.0508	118.2	19.9	43.4	1.585	0.554	196.1778	41.6	96731.21	84446.98	1.51E+08	alph a	601.13	Sum di2	1.15E+09
															Klc	70.97122	Alpha 2	5.73E+08
															Fr Error Klc	0.059672	Delta	6344.172
75	0.86	104	15.44	0.1321	118.5	19.9	43.3	1.084	0.357	512.4984	64.8	308857.5	306267	6710675	sum x2	9924.703	Slope	4873.675
			20.00	0.096	118.5	19.9	43.3	1.281	0.462	372.444	50.0	227589.5	234298.2	45006208	sumx	195.0694	Int	9385.58
			23.90	0.0713	119.1	20	43	1.591	0.556	279.088	41.8	197275.1	194533.9	7514336	r2	0.993788	No points	4
			26.00	0.06	118.7	20.1	43.1	1.821	0.603	232.6051	38.5	179440.4	178063.5	1895966	alph a	272.4699	Sum di2	61127185
															Klc	123.738	Alpha 2	30563592
															Fr Error Klc	0.008898	Delta	1646.748
100	0.36	104	10.18	0.6102	119.6	20.3	42.8	0.976	0.238	2375.238	98.2	5379205	5665230	8.18E+10	sum x2	18363.72	Slope	55680.28
			14.62	0.5367	119.6	20.5	43.4	1.060	0.337	2011.948	68.4	4544942	4004155	2.92E+11	sumx	256.2479	Int	195655.1
			20.84	0.3232	119.5	20.6	42	1.376	0.496	1287.431	48.0	3137182	2867453	7.28E+10	r2	0.893202	No points	4
			24.02	0.2163	119.7	20.4	42.3	1.644	0.568	857.7568	41.6	1989245	2513735	2.75E+11	alph a	13614.22	Sum di2	7.22E+11
															Klc	418.2401	Alpha 2	3.61E+11
															Fr Error Klc	0.038915	Delta	7791.912
25.9	0.94	59	4.92	0.1479	119.2	20.1	43.7	0.964	0.113	557.73	203.3	288926.3	362143.3	5.36E+09	sum x2	52619.54	Slope	1614.224
			6.82	0.1467	118.4	20.1	44.7	0.955	0.153	528.73	146.6	255098	270738.7	2.45E+08	sumx	492.7441	Int	34048.91
			8.94	0.1432	118.5	20.1	44	0.962	0.203	532.67	111.9	262597.3	214610.9	2.3E+09	R^2	0.687679	No points	5
			10.88	0.1084	118.3	20	44.2	0.981	0.246	401.58	91.9	155204.3	182415.1	7.4E+08	alph a	628.075	Sum di2	4.8E+09
			13.34	0.09	118	20	43.5	1.027	0.307	344.23	75.0	125064.9	155055.2	8.99E+08	Klc	71.21261	Alpha 2	1.6E+09
			14.84	0.1005	119.1	20.1	43.4	1.066	0.342	384.25	67.4	167679.6	142824.1	6.18E+08	Fr Error Klc	0.061925	Delta	20300.94
25.9	0.9	149	4.90	0.153	119.5	20	44.2	0.965	0.111	566.81	204.5	298876.2	393898.9	9.03E+09	sum x2	184050.3	Slope	1548.73
			6.90	0.1514	118.9	20.1	43.6	0.955	0.158	573.56	144.9	300083.6	301703.8	2624964	sumx	842.5198	Int	77250.79
			10.10	0.1448	117.7	20.1	43.5	0.974	0.232	551.08	99.0	287852.3	230590	3.28E+09	R^2	0.88	No points	5
			14.90	0.1018	118.6	20.3	43	1.071	0.347	392.58	67.1	176900.2	181192.1	18420459	alph a	335.81	Sum di2	1.42E+10
															Klc	69.75	Alpha 2	4.75E+09
															Fr Error Klc	0.03	Delta	2104116

Appendix D2 – Full Set of Results from the TCLP on the Solidified FeCr Dust

Cement Content	W/S	Curing (days)	pH	Cr	Zn	Ca	K	Si	Na	Mg	Fe
10.0	1.0	104	5.3	15.2	350	832	95	286	79	181	8.6
14.1	0.9	59	6.1	15.6	407	1261	107	477	76	157	12.7
14.1	0.9	149	5.9	10.4	366	1319	151	291	89	166	5.2
14.1	1.0	59	6.2	11.4	421	1279	89	292	122	257	5.1
14.1	1.0	149	5.8	10.5	360	1286	142	303	51	159	5.4
14.1	1.0	434	5.7	13.0	320	1078	nm	142	nm	223	nm
20.0	0.9	54	6.6	9.7	196	1303	nm	185	nm	137.5	nm
20.0	0.9	89	6.5	13.7	216	1313	nm	160	nm	174.5	nm
20.0	0.9	104	6.3	8.4	212	1534	139	57	76	178	6.7
20.0	0.9	111	6.4	9.9	238	1215	nm	202	nm	137	nm
20.0	0.9	131	6.5	10.6	247	1206	nm	224	nm	133.5	nm
20.0	0.9	295	6.4	8.7	225	1208	nm	151	nm	135.5	nm
20.0	1.0	20	6.5	6.6	163	1406	nm	119	nm	73	nm
20.0	1.0	28	6.7	9.5	178	1380	79	446	75	185	4.6
20.0	1.0	104	6.7	9.4	303	1100	87	154	82	183	1.9
20.0	1.0	104	6.6	9.3	316	980	82	208	77	179	2.8
20.0	1.0	104	6.7	9.3	288	1050	77	228	66	157	3.8
20.0	1.0	180	7.3	9.3	257	1612	91	253	101	201	3.8
20.0	1.0	196	6.5	8.4	226	1163	nm	162	nm	133.5	nm
20.0	1.0	419	6.3	8.7	230	1145	nm	166	nm	138.5	nm
20.0	1.0	451	6.3	10.6	206	1351	nm	112	nm	183.5	nm
20.0	1.0	493	6.3	8.5	239	1168	nm	163	nm	140	nm
20.0	1.1	104	6.1	12.4	297	1436	140	77	69	174	10.8
25.9	1.0	149	6.6	8.6	131	1726	117	62	100	159	0.0
25.9	0.9	59	7	6.8	144	1278	125	68	70	136	0.8
25.9	0.9	149	6.7	9.6	193	1552	189	75	59	131	5.1
25.9	1.0	59	6.9	8.0	201	1550	114	nm	107	130	1.4
26.0	0.9	116	6.6	11.2	155	1385	nm	95	nm	202.7	nm
30.0	1.0	104	6.9	8.6	111	1392	127	273	125	162	0.3
30.0	1.0	230	6.6	10.8	140	1375	nm	103	nm	202	nm

Appendix D3 - Results from the Sequential Chemical Extraction

Results are presented as the metal extracted in each step as a percentage of the total in the original sample.

20% cement, 1.5 w/s, 104 days curing

Stage	Cr	Zn	Si	K	Fe	Mg	Mn	Ca
Step 1	0.2%	0.0%	0.1%	14.7%	0.0%	0.2%	0.2%	2.2%
Step 2	4.7%	32.3%	6.1%	6.8%	37.6%	28.9%	16.6%	98.4%
Step 3	0.4%	1.7%	0.9%	2.4%	5.3%	5.0%	2.8%	1.1%
Step 4	1.1%	2.5%	0.9%	3.1%	1.2%	3.4%	2.2%	0.1%
Step 5	37.9%	28.8%		48.5%		26.0%	29.3%	0.3%
Total Rec	**44.3%**	**65.3%**	**7.9%**	**75.6%**	**44.1%**	**63.5%**	**51.0%**	**102.2%**

30% cement, 1.4 w/s, 104 days curing

Stage	Cr	Zn	Si	K	Fe	Mg	Mn	Ca
Step 1	0.2%	0.0%	0.1%	13.1%	0.0%	0.1%	0.2%	2.1%
Step 2	4.9%	37.5%	8.5%	8.0%	40.0%	33.4%	19.9%	90.2%
Step 3	0.5%	2.1%	1.0%	2.1%	5.2%	6.1%	3.3%	1.1%
Step 4	1.0%	2.6%	1.1%	3.1%	0.9%	3.3%	2.0%	0.1%
Step 5	38.7%	29.0%		42.9%		16.4%	26.0%	0.2%
Total Rec	**45.3%**	**71.2%**	**10.7%**	**69.2%**	**46.2%**	**59.4%**	**51.5%**	**93.6%**

50% cement, 1.1 w/s. 104 days curing

Stage	Cr	Zn	Si	K	Fe	Mg	Mn	Ca
Step 1	0.2%	0.0%	0.1%	34.8%	0.0%	0.1%	0.2%	1.2%
Step 2	6.3%	48.2%	15.8%	12.6%	60.0%	52.5%	32.8%	88.6%
Step 3	0.4%	1.9%	0.7%	1.4%	6.2%	5.8%	5.0%	1.1%
Step 4	0.9%	1.8%	1.1%	2.9%	1.0%	3.8%	2.2%	0.5%
Step 5	36.1%	29%		46%				0.0%
Total Rec	**43.9%**	**80.9%**	**17.8%**	**97.7%**	**67.2%**	**62.2%**	**40.1%**	**91.5%**

75% cement, 0.9 w/s, 104 days curing

Stage	Cr	Zn	Si	K	Fe	Mg	Mn	Ca
Step 1	0.1%	0.0%	0.1%	35.1%	0.0%	0.1%	2.4%	0.8%
Step 2	6.8%	50.8%	24.4%	14.9%	65.9%	54.4%	376.2%	94.5%
Step 3	0.5%	1.6%	0.8%	1.1%	6.0%	5.1%	56.2%	1.1%
Step 4	0.9%	1.9%	1.3%	2.6%	1.0%	3.0%	2.1%	0.1%
Step 5	34.2%	16.0%		24.0%		6.8%	177.2%	0.1%
Total Rec	**42.5%**	**70.4%**	**26.6%**	**77.7%**	**72.9%**	**69.5%**	**614.2%**	**96.5%**

Appendix D4 - Experimental Results from the Lysimeter Column

(all days since breakthrough)

pH		Cr		Cr(VI)	
day	pH	day	mg/l	day	mg/l
1	11.2	1	160	1	156
2	11.7	2	169	2	162
3	11.7	3	169	3	166
4	11.2	4	170	4	165
5	11.4	5	170	5	162
6	11.6	6	171	6	163
7	11.4	7	165	7	161
8	11.7	8	160	8	159
9	11.4	8	158	10	145
10	11.3	10	143	12	135
12	11.7	12	132	14	117
14	11.7	16	96.9	16	102
16	11.9	20	72.6	19	84.8
19	11.4	24	56.1	20	76.9
20	11.3	28	45.8	24	60.4
22	11.4	32	37.1	28	48.7
24	11.4	35	32.8	32	43.1
28	11.5	40	28.3	35	40.9
32	11.8	45	22.1	40	34.5
35	11.7	50	17.9	45	27.8
39	12.0	55	15.2	50	22.7
44	11.8	60	13.6	55	16.0
49	11.7	67	14.3	60	14.2
54	11.8	74	13.1	67	15.2
59	11.7	81	12.0	74	13.3
66	11.5	88	10.7	81	12.3
73	11.6	88	12.6	88	10.7
80	11.8	95	12.0	95	10.4
87	11.7	102	11.4	102	10.1
94	11.7	109	11.2	109	9.72
101	11.9	117	13.3	117	11.5
108	11.9	133	7.40	117	11.4
116	11.6	139	7.47	133	6.56
131	11.1	143	7.54	139	6.95
137	11.2	152	7.04	145	7.03
143	11.1			152	6.60
150	11.1				

Appendix D4 - Continued

(all days since breakthrough)

K		Ca		Si		Zn
day	mg/l	day	mg/l	day	mg/l	
1	980	1	23.1	1	69.5	
2	1018	2	32.8	2	67.8	negligible at
3	1002	3	38.9	3	66.6	all times
4	994	4	43.5	4	65.8	
5	988	5	43.2	5	67.4	
6	1006	7	30.1	6	67.7	
8	1221	8	30.0	7	69.4	
12	1122	10	11.6	8	71.6	
16	810	12	9.20	8	77.4	
20	691	16	7.86	10	90.8	
24	601	20	7.14	12	105	
28	554	24	6.27	16	136	
32	512	28	6.56	20	176	
35	456	32	6.46	24	199	
40	422	35	6.20	28	222	
45	399	40	6.22	32	233	
50	399	45	6.47	35	248	
55	408	50	6.28	40	254	
60	413	55	6.26	45	260	
67	430	60	5.65	50	270	
74	443	67	5.07	55	272	
81	447	74	5.22	60	286	
88	440	81	5.78	67	281	
95	318	88	5.71	74	297	
102	294	88	5.12	81	288	
109	344	95	5.02	88	294	
117	325	102	5.12	88	294	
133	253	109	5.03	95	296	
139	245	117	5.30	102	292	
143	276	133	4.45	109	291	
152	267	139	4.75	117	281	
		143	5.25	132	265	
		152	4.55	139	263	
				143	260	
				152	261	

Appendix D5 - Results from the Experimental Design

Waste	Trial No	ITS (MPa)	pH	Cr	Mg	Ca	Zn
ETP 1	1	0.05	5.40	1.33	69.2	1496	nd
ETP 1	2	0.29	7.30	0.23	48.8	1778	nd
ETP 1	3	0.32	7.00	0.4	30.4	1407	nd
ETP 1	4	0.39	7.40	0.41	30.4	1374	nd
ETP 1	5	0.02	5.40	1.8	44.8	1125	nd
ETP 1	6	0.26	7.60	0.28	47.9	1785	nd
ETP 1	7	0.04	5.50	1.21	42	1176	nd
ETP 1	8	0.03	5.50	0.95	65.6	1508	nd
ETP 1	9	0.26	6.40	0.25	36.3	2018	nd
ETP 1	10	0.10	5.80	0.37	35.1	1827	nd
ETP 1	11	0.03	5.30	0.5	54.5	1521	nd
ETP 1	12	0.33	8.30	0.82	18.6	1237	nd
ETP 1	13	0.14	6.20	0.7	47.9	1832	nd
ETP 1	14	0.20	6.20	0.3	40.9	1568	nd
ETP 1	15	0.24	6.40	0.14	34.9	2064	nd
ETP 1	16	0.20	6.30	0.16	35.3	2124	nd
ETP 1	17	0.16	6.10	0.17	34.6	1952	nd
ETP 1	18	0.20	6.20	0.13	34.9	1970	nd
ETP 1	19	0.18	6.20	0.15	35	1940	nd
ETP 1	20	0.22	6.30	0.13	35.3	1983	nd

Waste	Trial No	ITS (MPa)	pH	Cr	Mg	Ca	Zn
ETP 2	1	0.09	5.6	1.75	40.2	1751	nd
ETP 2	2	0.04	7.5	4.58	29.8	1943	nd
ETP 2	3	0.29	7.4	3.79	33.5	1843	nd
ETP 2	4	0.35	7.5	4.79	31.8	1821	nd
ETP 2	5	0.07	5.5	2.47	43.1	1505	nd
ETP 2	6	0.01	7.9	6.22	28.7	1937	nd
ETP 2	7	0.12	5.8	1.82	45.4	1476	nd
ETP 2	8	0.08	5.7	2.86	41.5	1773	nd
ETP 2	9	0.31	6.7	2.09	37.6	1833	nd
ETP 2	10	0.22	6.4	1.83	38	1823	nd
ETP 2	11	0.06	5.5	3.83	55.5	888	nd
ETP 2	12	0.28	8.2	6.42	27.9	1793	nd
ETP 2	13	0.18	6.9	2.17	49.5	1726	nd
ETP 2	14	0.23	6.5	1.94	33.9	2192	nd
ETP 2	15	0.26	6.7	2.06	37.6	1682	nd
ETP 2	16	0.30	6.8	2.26	37.1	1726	nd
ETP 2	17	0.29	6.7	2	38.4	1756	nd
ETP 2	18	0.24	6.6	1.98	37.2	1671	nd
ETP 2	19	0.30	6.5	2.26	37.3	1643	nd
ETP 2	20	0.28	6.6	2.14	37.7	1716	nd

Appendix D5 - Continued

Waste	Trial No	pH	Cr	Mg	Ca	Zn	Na
FeCr Dust	1	6.2	11.36	257	1279	421	122
FeCr Dust	2	6.9	7.97	130	1550	201	107
FeCr Dust	3	6.6	8.62	159	1726	131	100
FeCr Dust	4	6.7	9.6	130.9	1552	193	59
FeCr Dust	5	5.8	10.5	158.95	1286	360	51
FeCr Dust	6	7	6.8	136.4	1278	144	70
FeCr Dust	7	5.9	10.4	165.75	1319	366	89
FeCr Dust	8	6.1	15.64	157	1261	407	76
FeCr Dust	9	6.3	8.415	177.5	1534	212	76
FeCr Dust	10	6.1	12.435	173.5	1436	297	69
FeCr Dust	11	5.3	15.204	180.5	832	350	79
FeCr Dust	12	6.9	8.636	161.5	1392	111	125
FeCr Dust	13	6.7	9.498	185	1380	178	75
FeCr Dust	14	7.3	9.3	201.4	1612	257	101
FeCr Dust	15	6.7	9.3755	146.2	1120	251	64
FeCr Dust	16	6.7	9.4435	158.03	647	261	112
FeCr Dust	17	6.8	9.52	124.95	757	271	75
FeCr Dust	18	6.7	9.36	183	1100	303	82
FeCr Dust	19	6.6	9.28	179	980	316	77
FeCr Dust	20	6.7	9.32	157	1050	288	66

It is noted that these are the same results as presented in Ch 6 for the solidified FeCr Dust. They have been repeated here to show their position in the CCRD matrix

Appendix E - Values of Z as a Function of r

[Miller and Freund (1985)]

r	0.00	0.01	0.02	0.03	0.04	0.05	0.06	0.07	0.08	0.09
0.0	0.000	0.010	0.020	0.030	0.040	0.050	0.060	0.070	0.080	0.090
0.1	0.100	0.110	0.121	0.131	0.141	0.151	0.161	0.172	0.182	0.192
0.2	0.203	0.213	0.224	0.234	0.245	0.255	0.266	0.277	0.288	0.299
0.3	0.310	0.321	0.332	0.343	0.354	0.365	0.377	0.388	0.400	0.412
0.4	0.424	0.436	0.448	0.460	0.472	0.485	0.497	0.510	0.523	0.536
0.5	0.549	0.563	0.576	0.590	0.604	0.618	0.633	0.648	0.662	0.678
0.6	0.693	0.709	0.725	0.741	0.758	0.775	0.793	0.811	0.829	0.848
0.7	0.867	0.887	0.908	0.929	0.950	0.973	0.996	1.020	1.045	1.071
0.8	1.099	1.127	1.157	1.188	1.221	1.256	1.293	1.333	1.376	1.422
0.9	1.472	1.528	1.589	1.658	1.738	1.832	1.946	2.092	2.298	2.647

*For negative values of r put a minus sign in front of the corresponding Z's, and vice versa.

Appendix F1 - Development of the CCRD Matrix

1. The variables (x_1,x_2,x_3) and the maximum and minimum values of interest are defined. The following matrix is set up, whereby each of the variables is tested at a high and a low value while keeping the other two variables at their intermediate values. These tests are known as the 'axial' tests of the design and define the space of interest.

Variable	Ax 1	Ax 2	Ax 3	Ax 4	Ax 5	Ax 6
x_1	low	high	med	med	med	med
x_2	med	med	low	high	med	med
x_3	med	med	med	med	low	high

2. A factor ψ is now introduced. Any value may be used for ψ, but if ψ is set to 1.682, the design will be most practical to implement [Diamond (1989)]. The high, medium and low values of the above variables (the axial trials) are now defined as being at ψ, 0 and $-\psi$ respectively, being known as the 'coded' variables. The above table now looks like this in coded form:

Variable	Ax 1	Ax 2	Ax 3	Ax 4	Ax 5	Ax 6
x_1	$-\psi$	ψ	0	0	0	0
x_2	0	0	$-\psi$	ψ	0	0
x_3	0	0	0	0	$-\psi$	ψ

3. The next trials to be defined in the factorial design are the 'Hadamard Matrix' trials (for a full discussion of Hadamard Matrices see Diamond (1989)). Still using coded coefficients, by definition the star experiments are at variable values of -1, 0 and +1. The star trials look as follows:

Variable	St 1	St 2	St 3	St 4	St 5	St 6	St 7	St 8
x_1	1	1	1	-1	1	-1	-1	-1
x_2	-1	1	1	1	-1	1	-1	-1
x_3	-1	-1	1	1	1	-1	1	-1

4. In order to get the actual values of the variables in the star trials from the coded variables, ψ is set to half the ranges of the variables. Take for argument variable x_1. A scaling factor is obtained as follows:

$$\text{Scale of } x_1\text{: } 1.682\, x_1 = (x_{1,max} - x_{1,min})/2$$

This gives:

$$x_1 = (x_{1,max} - x_{1,min})/(2*1.682) \text{ actual units per coded unit}$$

The actual value of x_1 calculated from the coded units in the above table is thus given by:

$$x_{1,actual} = x_{1,coded}\left[\frac{(x_{1,max} - x_{1,min})}{2*1.682}\right] + x_{1,median}$$

5. The final tests in the experimental design are the 'centre point' trials. For a 3-variable, 3-level design, Diamond (1989) recommends carrying out 6 centre trials at values of x_1, x_2 and x_3 of med, med, med (or 0, 0, 0 in coded terms). The factorial design matrix is now given by the following table, with the Hadamard matrix trials as 1-8, the star trials as 9-14 and the centrepoint trials being 15 - 20. The trials are represented schematically in Figure 8-1.

Trial No	x_1	x_2	x_3	Trial No	x_1	x_2	x_3
1	1	-1	-1	11	0	$-\psi$	0
2	1	1	-1	12	0	ψ	0
3	1	1	1	13	0	0	$-\psi$
4	-1	1	1	14	0	0	ψ
5	1	-1	1	15	0	0	0
6	-1	1	-1	16	0	0	0
7	-1	-1	1	17	0	0	0
8	-1	-1	-1	18	0	0	0
9	$-\psi$	0	0	19	0	0	0
10	ψ	0	0	20	0	0	0

6. The actual values of the variables are calculated for each of the trials, the experiments are performed. The following matrix is set up with R1 to R20 being the results from the 20 experiments above:

TRIAL	T	x_1	x_2	x_3	x_1^2	x_2^2	x_3^2	$x_1 x_2$	$x_1 x_3$	$x_2 x_3$	Result
		HADAMARD MATRIX TRIALS									
1	1	1	-1	-1	1	1	1	-1	-1	1	R1
2	1	1	1	-1	1	1	1	1	-1	-1	R2
3	1	1	1	1	1	1	1	1	1	1	R3
4	1	-1	1	1	1	1	1	-1	-1	1	R4
5	1	1	-1	1	1	1	1	-1	1	-1	R5
6	1	-1	1	-1	1	1	1	-1	1	-1	R6
7	1	-1	-1	1	1	1	1	1	-1	-1	R7
8	1	-1	-1	-1	1	1	1	1	1	1	R8
		STAR TRIALS									
9	1	-1.682	0	0	2.828	0	0	0	0	0	R9
10	1	1.682	0	0	2.828	0	0	0	0	0	R10
11	1	0	-1.682	0	0	2.828	0	0	0	0	R11
12	1	0	1.682	0	0	2.828	0	0	0	0	R12
13	1	0	0	-1.682	0	0	2.828	0	0	0	R13
14	1	0	0	1.682	0	0	2.828	0	0	0	R14
		CENTER TRIALS									
15	1	0	0	0	0	0	0	0	0	0	R15
16	1	0	0	0	0	0	0	0	0	0	R16
17	1	0	0	0	0	0	0	0	0	0	R17
18	1	0	0	0	0	0	0	0	0	0	R18
19	1	0	0	0	0	0	0	0	0	0	R19
20	1	0	0	0	0	0	0	0	0	0	R20

7. The terms in each column are multiplied by the result and each column is summed. Finally, the coefficients in the model equation are calculated using:

$a_0 = 0.1663402267\ \Sigma T - 0.05679210581\ (\Sigma x_1^2 + \Sigma x_2^2 + \Sigma x_3^2)$

$a_i = 0.0732233047\ (\Sigma i)$

$a_{ii} = 0.062500\ (\Sigma ii) + 0.00689003779\ (\Sigma x_1^2 + \Sigma x_2^2 + \Sigma x_3^2) - 0.05679210581\ \Sigma T$

$a_{ij} = 0.125000\ (\Sigma ij)$

where $i = x_1, x_2$ or x_3; $ii = x_1^2$ or x_2^2 or x_3^2, T = total; $ij = x_1 x_2, x_2 x_3$ or $x_1 x_3$

Summing these terms thus gives equation (8-2).

Appendix F2 - Use of the Factorial Design Spreadsheet

The MS - EXCEL (ver. 5) spreadsheet is found on the attached disk, saved under the filename CCRD.XLS.

Design and model calculations appear on the sheet named **CCRD model**

Variable names and high and low variable values are entered in cells R5 to U7 (hotkey for getting to these cells is CTRL D). The median value is calculated automatically.

The experimental design matrix (described in Appendix F1) appears in cells Q25 to T50 (hotkey CTRL E). The tests are run according to this matrix.

Results are entered in cells V25 to V50 (CTRL R).

The model equation coefficients are calculated and appear in cells AQ5 to AQ14 (CTRL M).

The significances of each of the variables on the response is calculated at three different confidence limits : 0.9, 0.95 and 0.99. These appear in cells AU6 to AW 14.

Three plots are presented in the workbook, each with one variable held constant. These are on **Gra cur cons**, **Gra cem cons** and **Gra w-s cons** respectively. The constant variable value is specified in cell A15 of the sheet titled **Grcalcs** for the appropriate graph. If variables other than w/s, cement content and curing time are used, the graph texts must be updated manually.

Use of the SOLVER Routine for Optimization of the Variables

1. Go to sheet entitled **Optimiz**
2. Select TOOLS, SOLVER from the menu
3. Set Target Cell = $C$7
4. Select Max for Strength or Min for leaching
5. By changing Cells $B$3:$B$5
6. Subject to the Constraints
   $B$3 < = $G$6
   $B$3 > = $H$6
   $B$4 < = $G$7
   $B$4 > = $H$7
   $B$5 < = $G$8
   $B$5 > = $H$8

7. Select SOLVE
8. The optimal variable values are given in cell B3:B5, the response variable at that value is given in cell C7.
9. It is noted that the ultimate solution depends on the initial values in cells B3:B5. A number of different first approximations should be used in these cells to determine the true optimum.

Appendix F3 - Model Coefficients and Optimal Variable Values established from the CCRD

	COEFFICIENTS										R^2	Optimal Values of Variables		
	a0	a1	a2	a3	a11	a22	a33	a12	a13	a23		W/S	Cement	Curing
ETP 1														
ITS	-5.376	7.4968	0.033186	0.0345	-2.647	-0.0002	-7E-05	-0.017	-0.028	3E-04	0.92	1.1	30.0	70.0
Cr	72.6992	-121.41	0.249708	-0.166	54.937	0.00702	0.001	-0.455	0.0526	-0	0.60	1.2	23.0	49.0
Ca	-44152	71190	263.1031	84.259	-30737	-7.4021	-0.951	39.333	0.2104	-0.13	0.82	1.1	10.0	28 and 70
Mg	1355.21	-2003.7	-2.25698	-3.732	880.51	0.06485	0.033	-2.431	-0.358	0.02	0.83	1.2	30.0	55.0
ETP 2														
ITS	-14.819	23.419	0.014471	0.0474	-9.529	-0.0016	-3E-04	0.009	-0.03	1E-03	0.83	1.1	27.0	70.0
Cr	45.1813	-48.217	0.169838	-0.593	15.802	0.03266	4E-04	-0.963	0.5051	-0	0.94	1.1	19.0	28 and 70
Ca	36926.5	-58617	125.9467	-91.43	24478	-3.3084	0.652	9.2808	14.1	0.551	0.78	1.2	10.0	53.0
Mg	-298.11	696.57	-5.22786	-0.39	-317.5	0.01868	0.004	2.8284	-0.084	0	0.77	1.1	30	57
FSD														
Cr	162.78	-218.01	-3.36636	-0.197	88.627	0.02213	-5E-05	1.7167	0.1153	0.004	0.82	0.9	23.1	28 and 180
Zn	-444.61	877.14	-4.91109	7.6574	90.076	-0.2337	-0.006	-5.559	-7.151	0.038	0.85	1.1	30	180
Ca	46394.1	-88256	-165.68	-7.519	43333	-0.22	0.063	181.1	-7.702	0.179	0.86	1	10	108
K	7406.86	-15210	10.04222	2.8988	7969.5	0.35548	0.002	-21.76	-2.719	-0.01	0.81	1	16.4	28